University of Alberta

Numerical Study of Sleeve Repair of Wrinkled Energy Pipelines

By

Xuejun Song ©

A thesis submitted to the Faculty of Graduate Studies and Research in partial fulfillment of the requirements for the degree of Doctor of Philosophy

in

Structural Engineering

Department of Civil and Environmental Engineering

Edmonton, Alberta

Fall 2008

Canada

ABSTRACT

Because of the harsh environment in the Canadian north, wrinkles were detected in a buried pipeline, which passes through challenge terrain with unstable slopes. It is pipeline operating company's interests that the field wrinkles were taken care of with minimum cost. Field observations and pipe full-scale laboratory tests show that the pipe buckling behavior is highly ductile and the actual displacement at rupture is quite large. An economical and promising technique to repair the local wrinkles using steel sleeves without cutting out and replacement work is attracting the pipeline operating company's attention. This research is designed to study the behavior and effectiveness of wrinkled pipes repaired using steel sleeves. The project includes development of numerical models for wrinkled repaired pipes, a field case field study, a parametric study, and recommendations of repair procedures.

After describing the numerical modeling technique for the pipe, the repairing sleeve and the collars, a new modeling technique using the FEA package ABAQUS in simulating the pipe wrinkle sleeve repair process is presented and validated. The validation process of this new modeling technique, the Results Transfer technique between ABAQUS products, includes the comparison with another pipe wrinkle sleeve repair modeling technique in ABAQUS, the Element Removal/Reactivation technique.

A case history study of a pipeline field wrinkle sleeve repair work through the numerical simulations is presented thereafter. The numerical simulations of the pipeline field wrinkle sleeve repair case are also treated as part of the validation process of the Results Transfer technique in ABAQUS. In conducting the numerical simulations, the pipeline field profile measurements, which were recorded through the yearly GEOPIG tool run for the past 17 years, are used in creating the numerical models for the pipe, the repairing sleeves and the collars. After the completion of the numerical model validations, a parametric study is carried out as part of the project to expand the field data to more general cases of pipes of different D/t ratios and of different material properties. The effects of the length of the repairing sleeve, the material properties of the repairing sleeve, the thickness of the repairing sleeve and the effect of the thickness of the collar are investigated in the parametric study. Conclusions are drawn and recommendations for future field wrinkle sleeve repair design and future wrinkle sleeve repair study are given based on the results of the parametric study.

ACKNOWLEDGEMENTS

TABLE OF CONTENTS

LIST OF TABLES

LIST OF FIGURES

LIST OF SYMBOLS

Latin Characters

A	Cross sectional area of the pipeline
A_s	the area of the cross section of the steel
D_0	Outside diameter of the pipeline
D_i	pipe internal diameter
D/t	Diameter-to-thickness ratio of pipe
e_{ij}	component of linear or engineering strain tensor in global coordinate system
E	Modulus of elasticity of the pipeline material
f^B_i	component of externally applied forces of per unit volume
f^S_i	component of externally applied surface traction of per unit area
F	design factor
I	Moment of inertia
J	joint factor
K	the global stiffness matrix
L	location factor
L_{SLV}	length of the repairing sleeve
$M^p_{\sigma_\theta,P_e}$	Plastic moment capacity assuming a hoop stress for σ_θ and an axial load of P_e
M_y	yield moment
p	design pressure
p_i	internal pressure
P_e	net axial force acting on a pipe cross section
P_s	the axial force due to the relative movement in the longitudinal direction between the soil and the pipe
p_y	Pressure at which the hoop stress induced equals the yield strength of pipe steel
P_y	pipe yield force (= $A\sigma_y$)
r_{av}	average of the external and internal radii of pipe cross section

R	the external force vector
ΔR	an increment of the external forces during an iteration
S	specified minimum yield strength
S_f	surface on which external tractions are applied
t	pseudo-time indicating the progress of a nonlinear solution
t	thickness of a pipe wall
t_C	the thickness of the collar
t_{SLV}	the thickness of the repairing sleeve
ΔT	the temperature differential between pipeline construction and pipeline operation
ΔT	the temperature differential
u	the nodal displacement vector
Δu	an increment of the nodal displacements during an iteration
u_i	component of displacement vector in global coordinate system (i = 1, 2, 3 referring to global direction)
V	volume of pipe body

Greek Characters

α	Coefficient of thermal expansion of the pipeline material
ε_{ln}	the logarithmic strain
ε_{ln}^{pl}	the true plastic strain
ε_{nom}	the nominal (engineering) strain
ε_{true}	the true strain
ϕ_y	yield curvature
ν	Poisson's Ratio
π_1	Pi-parameter number 1 (D/t)
π_2	Pi-parameter number 2 (σ_y/E)
π_3	Pi-parameter number 3 (p/p_y)
π_4	Pi-parameter number 4 (L_{SLV}/D)
π_5	Pi-parameter number 5 (t_{SLV}/t)

π_6	Pi-parameter number 6 (σ_{ySLV}/E)
π_7	Pi-parameter number 7 (t_C/t)
σ	Stress due to welding
σ_h	hoop stress
σ_{ij}	components of the Cauchy stress tensor
σ_L	the longitudinal stress within the pipe wall
σ_{nom}	the nominal (engineering) stress
σ_θ	Circumferential stress
σ_{true}	the true stress
σ_y	yield stress of the pipe material (stress corresponding to 0.5% strain)
σ_{ySLV}	yield stress of the sleeve material

SYMBOLS IN APPENDIX
APPENDIX A
Latin Characters

A	a positive proportionality factor in the Ziegler hardening rule
C	work-hardening constant in the Prager hardening rule
C_j	curvature of the jth element of pipe used in developing global response
C_{ijkl}	elastic constitutive tensor
C^*_{ijkl}	elastic-plastic constitutive tensor
$d\lambda$	positive factor of proportionality in the flow rule
$d\mu$	a positive proportionality factor in the Ziegler hardening rule
$\{d\varepsilon\}$	vector of principal strain increment
$\{d\sigma\}$	vector of principal stress increment
D_o	outside diameter of the pipe
D_i	inside diameter of the pipe
e	engineering longitudinal strain at an arbitrary point around the cross-section
e_0	engineering longitudinal strain of cross-section at the start of bending

E	Modulus of elasticity of the pipe material
[E]	elastic constitutive matrix
$f()$	yield function
$g()$	plastic potential function
G	shear modulus
H_p	plastic modulus
$\overline{H}_p$	reduced plastic modulus
k	hardening parameter
$\overline{k}$	reduced hardening parameter
ℓ	length of an arbitrary small length of pipe
L	length of the pipe
M	parameter of mixed hardening
M_0	moment required to initiate yielding
M_{end}	average of the two end moments
M_k	moment at the kth element of pipe used in developing global response
N_C	prescribed number of curvature increments used in developing local response
p	internal pressure of pipe
p_0	pressure at the first occurrence of the proportional limit
P	applied axial force
P^*	prescribed external axial load
P_0	axial load required to reach the proportional limit
P_{cal}	calculated external axial load
P_i	tensile axial force in the pipe wall due to internal pressure
$\overline{P}$	initial axial load in Step 3 of the algorithm for developing local response
Q	a constant in terms of Lame's constant, $Q = \dfrac{\lambda_E^{\,2}}{2G + \lambda_E}$
R_i	inside radius of pipe

R_m	average of inside and outside radii
S	cross-section modulus
S_{ij}	deviatoric stress tensor (generic)
$\bar{S}_{ij}$	reduced deviatoric stress tensor (generic)
$\bar{S}_x$	reduced deviatoric longitudinal stress (generic), $\bar{S}_x = \bar{S}_1 = \bar{S}_{11}$
$\{\bar{S}\}$	vector of reduced principal deviatoric stresses (generic)
t	thickness of a pipe wall
ΔT	the temperature differential
u	Pipe slip relative to the soil
y	ordinate of an arbitrary point around the cross-section measured from the bending neutral axis
y_k	deflection of the kth element of pipe used in developing global response

Greek Characters

α	Coefficient of thermal expansion of the pipeline material
α_{ij}	coordinate of the yield surface center in the stress space
β	prescribed tolerance in determining the position of the bending neutral axis
β_C	prescribed tolerance in determining deformed configuration of pipe
δ_{ij}	Kronecker delta
$\{\delta\sigma\}$	stress correction vector
$\Delta\varepsilon_x$	longitudinal strain increment for a small element of cross-section
$\Delta\varepsilon_x^*$	strain increment that moves the stress state onto the yield surface
ε^c	longitudinal strain at the compressive gage location
ε^t	longitudinal strain at the tensile gage location
ε_{ij}	strain tensor (generic)
ε_{ij}^e	elastic strain tensor (generic)
ε_{ij}^p	plastic strain tensor (generic)
ε_p	effective strain

$\bar{\varepsilon}_p$	reduced effective strain
ϕ_0	curvature at the first yield during bending
ϕ^*	prescribed upper limit of curvature used in developing local response
$\bar{\varphi}$	initial curvature in Step 4 of the algorithm for developing local response
γ	a proportionality factor used in correction vector
λ_E	Lame's constant, $\lambda_E = \dfrac{\mu E}{(1+\mu)(1-2\mu\mu)}$
ν	Poisson's ratio
θ_{end}	rotation at each end of pipe used in developing global response
$\sigma 0$	longitudinal stress in a thin-walled, closed-ended pipe that is elastic and subjected to internal pressure only, $\sigma_0 = \dfrac{pR_i}{2t}$
σ_e	effective stress
$\bar{\sigma}_e$	reduced effective stress
σ_i	principal stress (generic)
σ_{ij}	engineering stress tensor
σ_{ij}	stress tensor (generic)
σ_p	proportional limit of the pipe material
σ_x	longitudinal stress (generic), $\sigma_x = \sigma_1 = \sigma_{11}$
σ_θ	hoop stress (generic), $\sigma_\theta = \sigma_2 = \sigma_{22}$
$\bar{\sigma}_{ij}$	Reduced stress tensor (generic)
ζ	a positive constant in terms of Lame's constant, $\zeta = \dfrac{4G(G + \lambda_E - Q)}{2G + \lambda_E - Q}$

APPENDIX B

Latin Characters

a_i	coordinate in global coordinate system for undeformed configuration
$\bar{a}$	longitudinal ordinate after the application of internal pressure and axial load

A	area of the pipe cross-section
A_0	original area of the pipe cross-section
e	engineering longitudinal strain at an arbitrary point around the cross-section
e_0	engineering longitudinal strain of cross-section at the start of bending
e_i	engineering principal strains
E_x	Green-Lagrange longitudinal strain, $E_x = E_1$
R	radius of bending neutral axis
s_i	2nd Piola-Kirchhoff principal stresses
T_1	longitudinal force acting on the cross-section
$T_i^{(k)}$	virtual force used to define 2nd Piola-Kirchhoff stress
u_i	displacement in the ith direction of the coordinate system (x_1, x_2, x_3)
x	ordinate of pipe cross-section measured from the bottom end of centerline
x_i	coordinates in global coordinate system
y	ordinate of an arbitrary point around the cross-section measured from the bending neutral axis

Greek Characters

α	rotation of the centerline of pipe
ε_i	true (logarithmic) principal strains
ϕ	curvature
σ_i	engineering principal stresses
τ_i	true (Cauchy) principal stresses

CHAPTER 1 INTRODUCTION

1.1 INTRODUCTION

In the last few decades, long distance pipelines have proven to be the most economical way of transporting oil and gas from the oil and gas fields to downstream facilities such as refineries and industrial consumers. As the oil and gas resources become exploited in more remote regions with harsh environments, such as those located in areas of discontinuous permafrost in the Canadian Arctic and sub-Arctic regions, pipelines are being exposed to new and more severe loading conditions. If the loading conditions are severe enough, the forces developed in the pipeline may cause the pipeline to buckle, or wrinkle locally, particularly for pipelines buried in areas subjected to large differential ground movements.

Research projects were conducted in the past 15 years to study the behavior of the line pipes under different loading conditions through full scale pipe laboratory tests in the Civil and Environmental Engineering Department of the University of Alberta. A detailed review of these projects is listed in Chapter 2. Two of the most significant observations found in these projects are (i) pipes do not fracture due to the formation of the wrinkle in the pipe wall if they undergo monotonic loads and (ii) Post buckling behavior is highly ductile and the actual displacement at rupture was up as high as 20 times of those under which the wrinkle just initiated.

1.2 WRINKLE DETECTION IN THE PIPELINE FIELD

Research shows that the safety management has taken a dramatic increase in the past 15 years and has become the leading issue and the top priority of the pipeline operating companies (Sandovall, 2001), as shown in Figure 1. With the development of modernized electronic and computer technologies, it has become possible for the pipeline operating companies to monitor their pipelines more accurately and efficiently. Currently, two kinds of in-line inspection tools are commonly used in the pipeline industry to help the pipeline operating companies

1

maintain the integrity of the pipelines, i.e., the Magnetic Flux Leakage (MFL) tool and the GEOPIG tool. Figures 2 and 3 show the pictures of a typical MFL tool and a typical GEOPIG tool, respectively (Westwood and Hektner, 2003). When the MFL tool travels along the pipeline, a magnetic flux path is created between the bristles, magnets, and pipe wall, creating a return path. This magnetic flux is used to saturate the pipe wall. Any defect that causes a reduction in area in the direction of the magnetic field will cause magnetic flux to leak out. This leakage is measured by a ring of sensors mounted on the tool between the magnets, and is recorded using the onboard data storage system. This way, the features of the pipeline such as girth welds, seam welds, tees, valves, buckles and dents can be detected due to a combination of magnetic, geometric or sensor ride effects associated with that feature (Westwood and Hektner, 2003).

During an MFL inspection, the pipe is magnetized in the axial direction (along the pipe). The magnetic field generated from the interaction of the tool with the pipe is measured in all three components. These are the axial component, which is responsive to change in the pipe wall thickness as well as defects, the radial component (into the pipe) and the circumferential component (around the pipe). These latter two components allow defects to be detected and sized with greater accuracy. These MFL tools also contain an inertial navigation unit that allows the exact pipeline coordinates to be determined in relation to a particular feature such as a buckle or a dent. Combining with the MFL tool in pipeline inspection is the modern caliper tool with high resolution, the GEOPIG tool. The GEOPIG tool is a geometry tool, which is used to digitally map the internal diameter of the pipeline using a number of sensors, and allows an accurate determination of the size and shape of any dent, wrinkle or buckle along the pipeline if they exist.

As described above, not only the geometry of the pipe itself but also the pipeline overall profile along the whole pipeline route can be measured and recorded during the combination of the MFL run and the GEOPIG run. This means that the size and the shape of the wrinkle as well as the exact location of the wrinkle

can be determined through the MFL tool run and through the GEOPIG tool run if the wrinkle formed in the pipeline.

One immediate question following the detection of the wrinkles in the pipeline field is that "Does a buckled or wrinkled pipe segment need to be necessarily cut out and removed from the main line system and be replaced by a new segment following the wrinkle detection?" The answer appears to be "no". Firstly, the formation of a wrinkle in the pipes does not necessarily lead to the fracture of the pipe as shown in the pipe full scale laboratory tests (see, for example, Bouwkamp and Stephen, 1973 and Das, 2002). Field observations also showed that the pipeline did not fracture even with a wrinkle of significant magnitude (see, for example, Wilkie et al, 2000 and Yoosef-Ghodsi, et al, 2000). For pipelines in the field, they may experience significant loading as a result of large differential ground movements caused by events such as slope failure, seismic faulting, mining subsidence, frost heave and thaw subsidence. Although the field loadings can induce stresses and strains beyond the original limits contemplated by the pipeline designer, it is possible for the pipeline to survive such events by utilizing its ability to deform well into the inelastic range in order to conform to ground movements without producing rupture.

Secondly, it is expected that the cost of cutting out the wrinkled segments in the pipeline field and replacing them with new segments will be high, considering the revenue loss due to the pipeline shut-down period, the cost for the engineering design of the pipe replacement project, the expense of the necessary equipment, facilities and the crew members for completing the pipe cutout and replacement work during the winter season in the Canadian north (the pipelines buried in the Canadian north are not accessible during other seasons of the year). According to an unofficial estimate, the cost for replacing one relative short piece of pipe segment along the pipeline in the northern Alberta could be as high as several million dollars.

3

Consequently, a more attractive and economical alternative to the pipe segment cutout, remedying the winkled pipe segment externally by encasing it in a sleeve, attracted the pipeline operating company's attention. This type of repair work is expected to reduce the cost dramatically. There is no need to shut down the pipeline. The engineering design work scope is reduced significantly and the time duration for the field repair work can also be reduced, compared with the time line to complete the pipe segment cut out work. More importantly, the residual life of the original pipeline is extended and can be more fully utilized. The sleeve type of remedial method has been used extensively in the pipeline industry to remedy dents, cracks or corrosion damages in the pipeline field and it is one of the permanent repair methods recognized by the pipeline codes and standards such as CAN/CSA Z662 – 03. Although sleeve repair is a promising technique for the wrinkle repair, but it does not appear to have been widely used in the pipeline industry. One of the reasons for this is that the behavior of the wrinkled pipe segment under sleeve repair has not been fully understood yet.

1.3 OBJECTIVES

The main objective of this project is to study the behavior of the wrinkled pipe segment under sleeve repair through a case study of the wrinkle sleeve repair in a pipeline field in the northern Alberta. Parametric study is carried out thereafter to expand the field specific case to more general cases, which cover the most commonly used pipe parameters in the pipeline industry. These include the different D/t ratios of the pipe and different material properties of the pipe. Conclusions are drawn and guidelines for future field pipe wrinkle sleeve repair work are given based on the studies carried out. At the same time, a newly attempted FEA modeling technique in the FEA package ABAQUS, the results transfer between ABAQUS products, which is particularly useful in doing the pipe wrinkle sleeve repair simulations, is validated first.

1.4 LAYOUT OF THE THESIS

This thesis consists of 6 chapters and Appendix A and Appendix B. The main subjects of each of the following chapters are summarized as follows.

Chapter 2 contains the review of the literature regarding the wrinkling behavior of pipes, including the review of the research projects carried out in the Civil and Environmental Engineering Department of the University of Alberta. Considering the similarity between the sleeve repair for corrosion damage and the sleeve repair for the wrinkles, the studies on the behavior of the pipe segment under sleeve repair for corrosion damage were review. This is also due to the fact that limited researches have been carried out to study the behavior of wrinkled pipes under sleeve repair.

Chapter 3 describes the validation of the new technique attempted in this project for use in simulating the pipe wrinkle sleeve repair process, i.e., the results transfer technique between ABAQUS products. This finite element analytical technique in ABAQUS version 6.4 is particularly useful in doing the pipe wrinkle sleeve repair simulations. As part of the validation of this new technique, comparison between two different techniques in modeling the pipe wrinkle sleeve repair process is presented, one using Element Removal/Reactivation technique and one using Results Transfer technique in the FEA package ABAQUS.

Chapter 4 presents the case study of the re-enactment of the Double Sleeve Repair System (DSRS), which was installed to repair local wrinkles occurred in the Norman Wells to Zama pipeline of Enbridge Pipelines Inc. in Northern Alberta. The newly attempted results transfer technique in ABAQUS is used in doing the numerical simulations of the field pipe wrinkle sleeve repair work. The case study of this pipeline field wrinkle sleeve repair work is also treated as part of the validation process for the results transfer technique in ABAQUS.

Chapter 5 outlines the details of the parametric study as part of this project. The effects of different pipe D/t ratios, different material properties, different sleeve lengths and thicknesses, different collar thicknesses to the behavior of the wrinkled pipe segment under sleeve repair are investigated. The parameters used in the parametric study for the pipes cover the most commonly used parameters in the pipeline industry. A brief discussion of the results of the parametric study is given thereafter.

Chapter 6 presents the conclusions based on the studies described in Chapters 3, 4 and 5 and recommendations for future pipe wrinkle sleeve repair study and for future pipeline field wrinkle sleeve repair work.
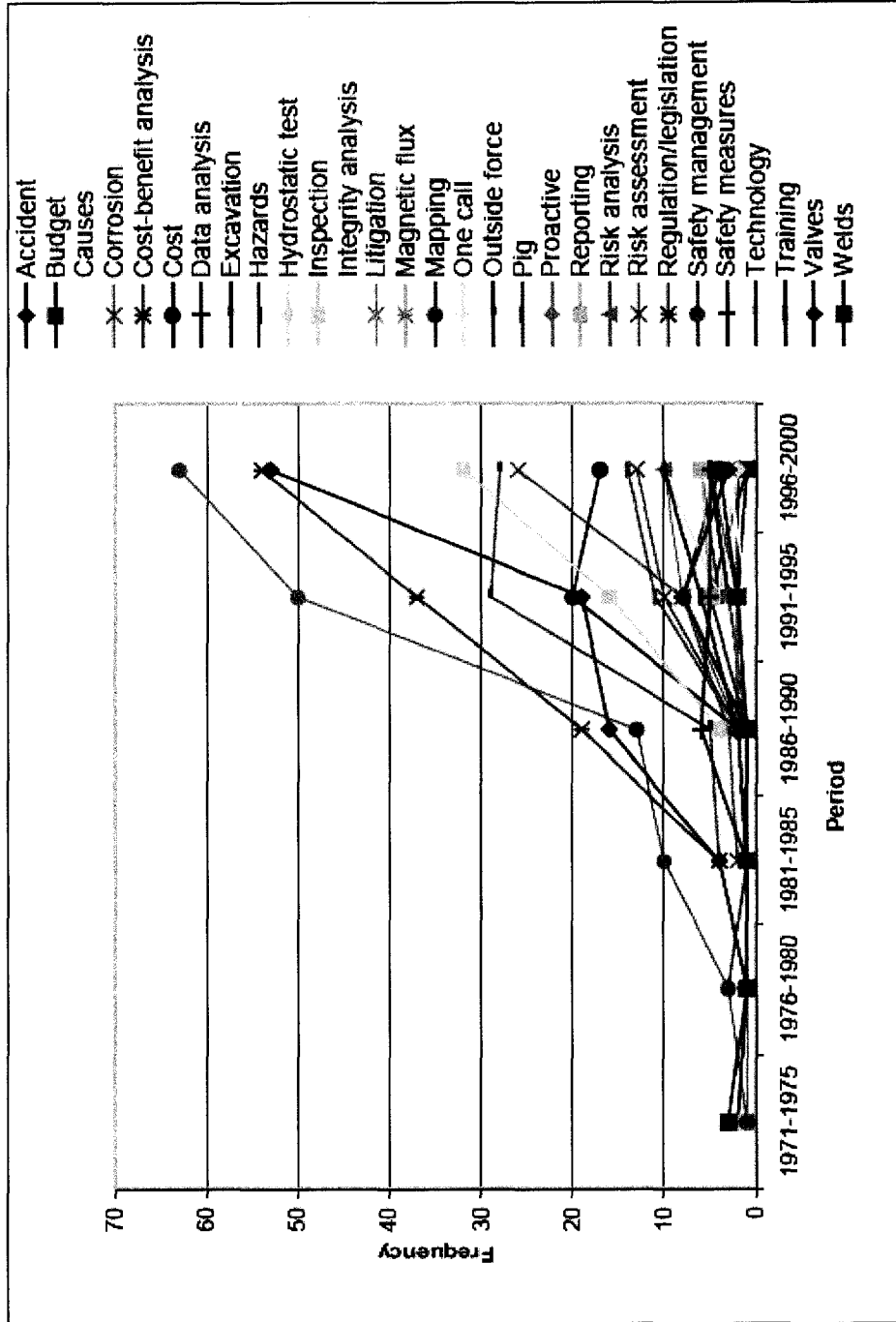
Figure 1.1 Historical Pipeline Key Issues (Sandoval, 2001)
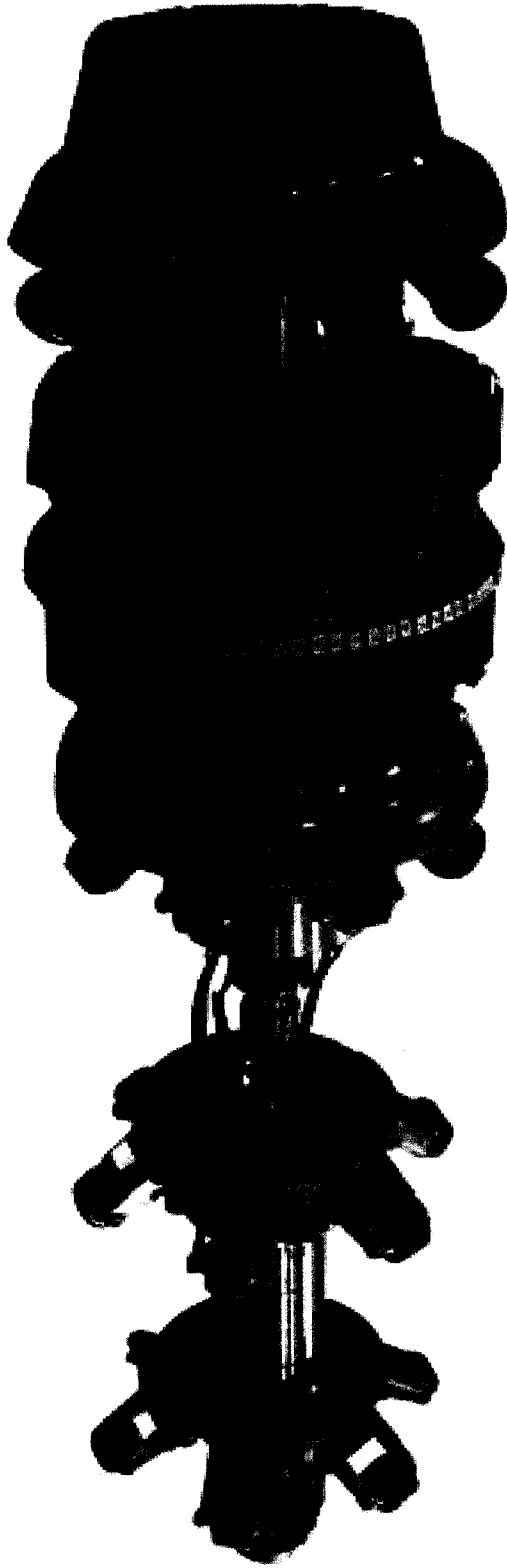
Figure 1.2 Picture of a typical Magnetic Flux Leakage (MFL) Tool
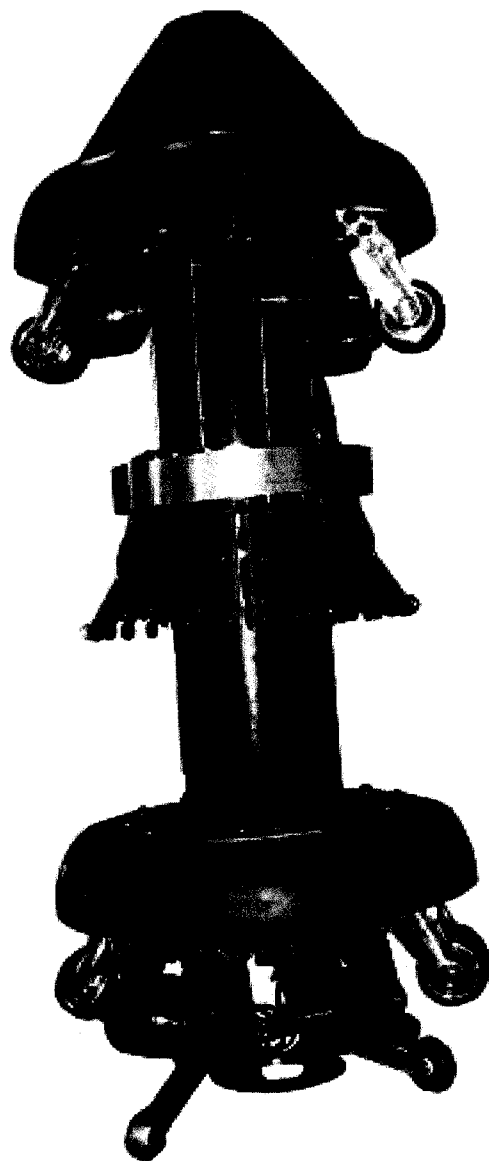
Figure 1.3 Picture of a GEOPIG Tool

CHAPTER 2 LITERATURE REVIEW

The purpose of this chapter is to review the literature that helps understand the failure behavior of onshore pipelines, i.e., the buckling or wrinkling of the pipelines and the behavior of pipes under sleeve repair. Numerous research projects have been carried out to study the buckling behavior of pipelines for the past several decades. Only few projects were carried out to study the behavior of the wrinkled pipe segment under sleeve repair. Consequently, the sleeve repair for corrosion damage of the pipeline in the current pipeline design practice and some research projects conducted in this area are reviewed for reference purpose. The research projects of the buckling behavior of the pipes under different loading combinations carried out in the Civil and Environmental Engineering Department of the University of Alberta during the past 15 years are also reviewed.

2.1 RESEARCH PROGRAMS ON BEHAVIOR OF SLEEVE REPAIR OF CORRODED PIPE

2.1.1 EXPERIEMTS CARRIED OUT BY SCHNEIDER (1998)

Schneider (1998) carried out two large-scale experiments using the pressurized pipes to investigate the flexure capacity of the fully welded sleeve repair on a pressurized pipeline. The purpose of the project carried out by Schneider (1998) is to study the behavior of damaged or corroded pipe segment under fully welded sleeve repair. Each specimen was subjected to a constant axial load combined with the deformation of a four-point bend test to simulate the flexural behavior of the buried pipeline. Internal pressure, which produced hoop stress of 72% of SMYS, was also applied to the pipe specimens. Sleeve was fully welded in the midspan around the pipe circumference. The only test parameter was the length of the sleeve used for the pipe repair: one specimen having a sleeve length equal to one pipe diameter, and the second pipe having a sleeve length that was two pipe diameters in length. A simple theoretical model is discussed to predict the inelastic flexural strength and ductility of the pipes subjected to above mentioned conditions. The conclusions from the research program by Schneider (1998) are:

1. The failure mode of these pipes was by local, outward buckling of the wall of the carrier pipe adjacent to the sleeve region. No damage occurred in the sleeve or the girth weld around the carrier pipe circumference.

2. The pressurized pipe had significant ductility under these conditions without a reduction of the ability to resist the internal pressure. These tests demonstrated that no loss of pressure occurred even for displacements over twice the deformation needed to cause the onset of the local wall buckling.

3. Using the Tresca yield theory produced a reasonably accurate estimate of the yield strength of the pipe and resulted in a conservative estimate of the inelastic deformation capacity compared to the experimental results.

4. Prior to the onset of the local wall buckling, the pipe sustained a deformation ductility of approximately 2.9 times the initial yield displacement. This results in a curvature ductility of approximately 3.3 according to the Tresca yield criterion.

2.1.2 EXPERIEMTS CARRIED OUT BY HART ET AL. (1995)

Two full scale pipe buckling experiments were conducted by Hart et al. (1995) to study the behavior of the corroded pipe segment under sleeve repair. The tests included the application of the internal pressure and the axial force to simulate fully restrained conditions, followed by the application of four-point bending loads up to and beyond wrinkling of the specimens. Split sleeve was welded to the pipe specimen according to field installation procedures. Analytical correlation studies were also carried out using PIPLIN program, in which the tests were simulated using beam bending model. The comparisons show close agreement between the analyses and the experiments, provided that (a) anisotropy of the steel properties is accounted for and (b) a special wrinkling segment is included in the bending models. The main conclusions from this project are:

1. The tests indicted that sleeved pipe behaved in a ductile manner. The test specimens wrinkled locally, with a single large wrinkle. Under the action of

imposed displacement well into the post-wrinkling regime, no distressful conditions occurred in the specimen.

2. The midspan deflection can be very large at wrinkling. Test 1 has a midspan deflection approximately 4 inches and Test 2 has a midspan deflection approximately 6 inches.

3. Close agreement can be obtained between the results of the PIPLIN analyses and the experiments, provided that (a) anisotropy of the steel properties is accounted for in the PIPLIN model, and (b) a wrinkling segment of the correct length is included. The comparisons showed that PIPLIN program can be used, with a substantial degree of confidence, to analyze the behavior of pipeline configuration up to the stage of incipient wrinkling.

2.2 SLEEVE REPAIR IN CSA STANDARD

CSA Z662 – 03 (CSA, 2003) does not state the repair of buckled or wrinkled pipe segments. It does provide the methods for repairing commonly existed imperfections, such as corrosions, dents, gouge and cracks in the pipeline field. Consequently, the repairing of imperfections of the pipelines using sleeves are presented here as a reference.

According to Clause 10.8.5 of CSA Z662 – 03 (CSA, 2003), several permanent repair methods are available for the imperfections that exist in the pipeline such as corrosions or cracks. As one of the permanent repair methods for these imperfections, Clause 10.8.5.4.1 of CSA Z662 – 03 (CSA, 2003) states that:

Repair sleeves shall be permissible as permanent repairs, provided that the following is applicable:

a) The repair sleeves extend longitudinally at least 50 mm beyond the ends of the defects.

c) Consideration is given to the following:

i) concentration of bending stresses in the pipe at the ends of repair sleeves and between closely spaced repaired sleeves;

ii) design compatibility of repair sleeves and piping materials;

Clause 10.8.5.4.2 (a) of CSA Z662 – 03 (CSA, 2003) provides the requirements for the Steel Pressure-Containment Repair Sleeves: repair sleeves shall have a nominal load-carrying capacity at least equal to that of the originally installed pipe.

As mentioned earlier, the above requirements in CSA Z662 – 03 are for repairing the imperfections such as corrosion, dents, gouge and cracks in the pipelines when using the pressure-containment repair sleeves. Similar considerations are also given to the wrinkle repair using collars and sleeves in pipeline practice by the pipeline operating companies.

2.3 RESEARCH PROJECTS ON BEHAVIOR OF PIPE BUCKLING CARRIED OUT IN THE UNIVERSITY OF ALBERTA

The buckling behavior of pipelines under different loading combinations have been studied in the Civil and Environmental Engineering Department of the University of Alberta for the past 15 years, including full scale pipe laboratory tests and finite element analysis. The pipe buckling research projects carried out in the University of Alberta are reviewed in this section considering that the research on the behavior of wrinkled pipelines under sleeve repair is an extension of the research project studying the behavior of the pipe buckling or wrinkling.

2.3.1 STUDY OF DEFORMATIONAL BEHAVIOR OF LINE PIPE CARRIED OUT BY MOHAREB (1994)

Mohareb (1994) studied the deformational behavior of buried pipelines under the action of axial loads, internal pressure and deformation-controlled imposed bending. In total, 7 full scale pipe laboratory tests were conducted using two sizes of pipe, i.e., four 508 mm OD and three 324 mm OD, with D/t ratios of 64 and 51, respectively. Four internal pressure values were used during the full scale pipe laboratory tests, i.e., 0%

13

SMYS, 36% SMYS, 72% SMYS and 80% SMYS. Finite element analysis and parametric study were carried out using finite element package ABAQUS as part of the project. Design equations were provided based on the parametric study, which included the major factors influencing the deformational behavior of the pipes. The following observations and conclusions were obtained by Mohareb (1994):

1) two distinct buckling modes were observed, i.e., diamond shape buckle and outward bulge buckle, which correspond to unpressurized and pressurized pipe specimens, respectively.

2) the highest moment capacity was obtained for unpressurized specimens and the least moment capacity was observed in a fully pressurized specimen. The longest plateau observed in moment vs. curvature curve was obtained for highly pressurized specimen. The length of the plateau decreases as the internal pressure decreases. The final longitudinal compressive strain during the tests can be reached as high as 19% for pressurized pipe specimens without rupture.

3) an equation for calculating the plastic moment capacity of the pipes under combined internal pressure, axial load and bending moment was developed as follows:

$$
\frac{M^{p}_{\sigma\theta,Pe}}{2r^{2}_{av}t\sigma_{y}} = \pm\sqrt{4-3\left(\frac{\sigma_{\theta}}{\sigma_{y}}\right)^{2}}\,\cos\left\{\frac{\pi\left[\frac{P_{e}}{P_{y}}-\frac{1}{2}\left(\frac{\sigma_{\theta}}{\sigma_{y}}\right)\right]}{\sqrt{4-3\left(\frac{\sigma_{\theta}}{\sigma_{y}}\right)^{2}}}\right\}
$$

The results calculated using above developed equation are compared with the results from the pipe full scale laboratory tests conducted in this project. Excellent agreement between the measured moment capacity from full scale laboratory tests and those predicted by the equation was obtained for

unpressurized specimens. For highly pressurized specimens, the equation tends to underestimate the plastic moment capacity due to higher strains.

4) an interaction diagram was developed based on the results from the pipe laboratory tests, which provided an envelop for all possible combinations of applied moment and axial load for a given internal pressure.

2.3.2 PROJECT ON BEHAVIOR OF GIRTH-WELDED LINE PIPE CARRIED OUT BY YOOSEF - GHODSI (1994)

Yoosef-Ghodsi (1994) carried out a project to study the structural behavior of girth-welded line pipe under loading conditions similar to those in the pipeline field. In total, 7 full scale pipe laboratory tests were conducted by Yoosef-Ghodsi (1994), which included four 508 mm × 7.9 mm pipe specimens (D/t = 63) and three 324 mm × 6.35 mm (D/t = 50). Five different internal pressure values were used during the full scale pipe laboratory tests, i.e., 0% SMYS, 36% SMYS, 40% SMYS, 72% SMYS and 80% SMYS. A computational program was developed as part of the project to describe and estimate the moment vs. curvature response of the pipes. The results calculated by this computer program were compared with the results from the full scale pipe laboratory test. The following observations and conclusions were obtained by Yoosef-Ghodsi (1994):

1.) Non-pressurized specimens wrinkled suddenly in a diamond shape (inward wrinkle). In the case of pressurized specimens, the wrinkle formed as a single outward bulge. The final compressive strain during the tests for pressurized pipe specimens can be reached as high as 20% without rupture.

2.) when the internal pressure was increased, the rotation capacity increased as well, but the ultimate moment decreased. The global moment vs. curvature responses showed that the ultimate end moments for the pipes with and without girth weld were almost equal. The pressurized girth-welded pipes showed less rotation capacity than did the plain counterparts.

15

3.) a numerical model was developed to simulate the moment vs. curvature responses for line pipes up to local buckling. The model is based on the incremental theory of plasticity and employs several types of strain hardening models. Different stress vs. strain measures were provided in the numerical model. Analytical results using the model were obtained for the test specimens and compared with the test results. It was concluded that the UL (Updated Lagrangian) formulation with isotropic hardening is the most appropriate model for the analysis of line pipes under combined loads.

2.3.3 PROJECT OF BEHAVIOR OF LARGE DIAMETER LINE PIPE UNDER COMBINED LOADS BY DEL COL (1998)

Del Col (1998) carried out a project to study the behavior of pipelines with large D/t ratios subjected to combined loads. Four full size specimens of NPS30 pipes with X70 steel and a D/t ratio of 92 were tested under the combinations of axial compression, internal pressure and bending. The deformational characteristics of the pipes, particularly the behavior of local buckling, was investigated for the pre- and post-buckling ranges in order to expand the database of experimental results of buckling of pipes to higher D/t ratios. Finite element analysis using FEA package ABAQUS was also carried out as part of the project. Another objective of this project was to investigate the internal pressure value at which the buckling mode changed from the "diamond shape" to the outward "bulge shape". Four internal pressure values were used during the tests, i.e., 0% SMYS, 20% SMYS, 40% SMYS and 80% SMYS. In order to investigate the effect of the initial imperfections on the behavior of the line pipes with large D/t ratios, initial imperfections were measured prior to the laboratory tests. Finite element analyses were also carried out as part of the project to conduct the parametric study. The measured initial imperfections were incorporated into the numerical models. Some typical observations and conclusions were obtained by Del Col (1998) as follows:

1.) Two local buckling modes were observed during the test program. The "diamond shape" configuration occurred for the non-pressurized specimen

16

and the "outward bulge" configuration occurred in all the pressurized specimens.

2.) Moment versus curvature response of the test specimens demonstrated the stabilizing effect of the internal pressure in the post-buckling range. The global curvatures at local buckling and the critical compressive strains also showed a general increase with an increase in the internal pressure.

3.) The presence of the initial imperfections was found to cause important reductions in the limit point curvature and a modest reduction in moment capacity.

4.) The predicted moment capacity using the FE method reached an excellent agreement with the experimental results. The predicted curvature and critical compressive strains were high compared with the test results.

2.3.4 DETERMINATION OF THE CRITICAL BUCKLING STRAIN FOR ENERGY PIPELINES (DOREY ET AL., 2001)

Dorey et al. (2001) carried out a project to determine the critical buckling strain values for the energy pipelines. A total of 15 full-scale pipe laboratory tests on NPS30 pipe with X70 grade steel and a D/t ratio of approximately 92 were conducted. The test specimens were subjected to load cases that are representative of 'typical' load cases the pipe may experience in the field under normal operational conditions, i.e., a combination of axial load, internal pressure and monotonically increasing curvature. A series of numerical analyses were also carried out by using ABAQUS Version 5.7-1 as part of the project. Good agreement between the test results and analytical results were reached. Four important parameters, which influence the development of load capacity and the critical buckling strain of the pipe segment, were identified. They are: Diameter-to-thickness (D/t) ratio, internal pressure ratio (p/p_y), material properties and initial imperfections. Based on the test and analytical results, the following observations and conclusions were obtained by Dorey at al. (2001):

1. Initial imperfections are an important feature in the buckling response of segments of line pipe. Inclusion of an appropriate initial imperfection pattern in an FEA model is crucial in predicting the experimental behavior. An assumed 'blister-type' initial imperfection pattern provided excellent correlation with the experimental data for the plain pipe specimens. An assumed 'offset-type' initial imperfection pattern provided excellent correlation for the girth-welded specimens.

2. The results of the experimental phase of this project show that there are two dominant characteristic buckling modes for segments of line pipe subjected to combined loads. These two modes are dependent on the level of internal pressure in the test specimen. For the unpressurized specimens, the wrinkle develops into a 'diamond-shape' buckle. For the specimens with an internal pressure equal to or greater than that required to produce a circumferential stress of 20% SMYS, the wrinkle develops into a 'bulge' buckle.

3. The local and global response of a test specimen is highly dependent on the grade of the material. For specimen groups in which the only variable was the material strength, an increase in material strength resulted in an increase in peak moment capacity and a reduction in the critical buckling strain.

4. The global and local behaviors of segments of line pipe subjected to combined load cases can be accurately predicted using FEA modeling techniques provided accurate initial imperfection, material property and boundary condition criteria are incorporated into the model.

2.3.5 PROJECT ON FRACTURE OF WRINKLED ENERGY PIPELINES CARRIED OUT BY DAS (2002)

Das (2002) carried out a project to study the fracture behavior of the wrinkle pipelines. The primary objectives of this project was to determine the load conditions/histories that can produce fractures in the wrinkled pipes, to determine the

limiting strain values at the wrinkle location and to develop the limiting fracture criteria that can be used for the assessment of the remaining/residual life of the wrinkled pipelines. A total of twelve full scale laboratory tests using NPS12 pipe with X52 grade steel and a D/t ratio of 50 were conducted. The numerical simulations of the full scale pipe laboratory tests under cyclic loads using ABAQUS were also carried out as part of the project. A simplified fracture model was developed, which could be used to predict the remaining life of wrinkled pipelines. The following observations and conclusions were obtained by Das (2002):

1.) The pipe specimens are highly ductile and do not fail in fracture when they are subjected to monotonically increased axisymmetric compressive axial strain. Rather, an accordion type failure with multiple wrinkles would be expected to occur.

2.) If the pipe is subjected to strain reversals because of loading and unloading of primary loads, the fracture can occur in the wrinkled region in a very few cycles, due to low cycle fatigue.

3.) The maximum strain values that occurred in these tests are much greater than permissible strain values in the design standards and current practice in pipeline industry.

4.) Cycling of the loads at an early stage (just after initiation of the wrinkle) does not result in much strain reversal in plastic strain.

5.) The fracture assessment model proposed in this project works well and provides a conservative prediction for the residual life of the test specimens.

2.3.6 PROJECT OF BEHAVIOR OF COLD BEND PIPES UNDER COMBINED LOADS BY SEN (2005)

Sen (2005) carried out full scale laboratory tests and finite element analysis to study the buckling behavior of cold bend pipes under combined axial load, bending and internal pressure. Seven large diameter cold bend pipes and one straight pipe were tested. The specimens were tested until local buckling occurred, and the curvature of several of the pipes was increased until they fractured at the wrinkle location. A finite element model was also created to validate the behavior of the test specimens. The model incorporated the geometry, imperfections and the material properties that were measured from the cold bends. The following conclusions were obtained by Sen (2005):

1.) The extent of wall thinning/thickening as well as ovalization was insignificant for the cold bend specimens.

2.) Under applied bending loads, pressurized cold bend specimens will develop a bulge shaped buckle, while unpressurized specimens will form a diamond shaped buckle. This behavior is similar to that observed for straight pipes.

3.) The critical strain of a cold bend pipe is somewhat lower than that of a straight pipe. Also, the maximum moment and critical strain of unpressurized cold bends are significantly less than that of similar pressurized specimens.

4.) Cold bends are susceptible to very low cycle fatigue. However, considerable deformation prior to fracture is attainable as these fractures occurred only after a central bend angle of 35 degrees was achieved.

5.) Work hardening in the tension side bend material of the cold bends caused an increase in yield stress. The ultimate stress of the material is nearly unchanged during cold bending.

6.) The finite element model that was developed in this research program was able to reasonably simulate both the global and local response of the specimens during testing. The global behavior of the model developed for this research was relatively similar to that of the model incorporated the cold bending procedures, which demonstrates that residual stresses from cold bending do not significantly affect the pipes global load-deformation response.

2.4 REMAINING LIFE OF BUCKLED PIPELINES BY GRESNIGT ET AL. (2003)

Gresnigt et al. (2003) carried out a research project to study the remaining life of buckled pipelines through full scale laboratory tests and finite element simulations. Three pipes with the outside diameter of 609.6 mm and the pipe wall thickness of 7.925 mm were tested. All pipes were bent until local buckles occurred with certain magnitude. Upon local buckle formation, strain gages were installed at the locations where the greatest strains and strain variations were expected. Then different loading scenarios were applied to the three pipe specimens until cracking of the pipe wall occurred. In addition to the experimental testing, finite element calculations were performed using general purpose finite element program ABAQUS. The analysis included geometric nonlinearities (large displacements), as well as inelastic effects with isotropic hardening for large strains. The numerical calculations were aimed at determining stress and strain distribution at the buckled area, so the experimental measurements are verified and confidence is built on the fatigue calculations. A good agreement was observed between test measurements and the finite element results. Both experimental and numerical results have indicated that, if the depth and the shape of the buckles are not too severe and the pipe wall is sufficiently ductile, then fatigue failure at the buckled area is not a critical issue, provided that the repeated load amplitude (internal pressure) is within a certain operational level.

CHAPTER 3 THE FINITE ELEMENT MODELING
TECHNIQUE

3.1 INTRODUCTION

With the modernization and industrialization in the late 19th century and the early 20th century, many practical structural engineering problems could no longer be solved by the classical mathematical techniques such as those using a closed form solution to the partial differential equations, because of the complexity of the geometry of the structures and the loading history the structures experienced. Consequently, the development of new solution techniques, such as the finite element method (FEM), to solve these complex engineering problems became necessary. The research on the FEM can be traced back to 1940s. The name "finite element" was first coined by Clough (1960). A large amount of research has been devoted to advance this technique since the early 1960s. The development of the digital computers made it possible for this process to achieve effectiveness and general applicability in engineering analysis. The FEM in engineering was initially developed for the analysis of problems in structural mechanics. However, it was soon recognized that this technique could be applied equally well to the solution of many other classes of problems (Bathe, 1996).

The application of the FEM to stress/displacement analysis of solids and structures is based on the principle of virtual work (PVW). A general expression for the PVW used by Bathe (1996) is:

$$\int_{t+\Delta t_V} {}^{t+\Delta t}\sigma_{ij}\ \delta_{t+\Delta t}e_{ij}\ d^{t+\Delta t}V = \int_{t+\Delta t_V} {}^{t+\Delta t}f_i^B\ \delta u_i\ d^{t+\Delta t}V + \int_{t+\Delta t_{S_f}} {}^{t+\Delta t}f_i^S\ \delta u_i^S\ d^{t+\Delta t}S \qquad (3.1)$$

where

$\quad {}^{t+\Delta t}\sigma_{ij}$ = Cartesian components of the *Cauchy stress* tensor (force per unit areas in the deformed geometry)

$\quad \delta_{t+\Delta t}e_{ij} = \dfrac{1}{2}\left(\dfrac{\partial \delta u_i}{\partial^{t+\Delta t}x_j} + \dfrac{\partial \delta u_j}{\partial^{t+\Delta t}x_i}\right)$ = Strain tensor corresponding to virtual displacements

δu_i = Components of virtual displacement vector imposed on configuration at time $t + \Delta t$, a function of $^{t+\Delta t}x_j$, $j = 1, 2, 3$

$^{t+\Delta t}x_i$ = Cartesian coordinates of material point at time $t + \Delta t$

$^{t+\Delta t}V$ = Volume at time $t + \Delta t$

$^{t+\Delta t}f_i^B$ = Components of externally applied forces per unit volume at time $t + \Delta t$

$^{t+\Delta t}f_i^S$ = Components of externally applied surface traction per unit surface area at time $t + \Delta t$

$^{t+\Delta t}S_f$ = Surface area at time $t + \Delta t$ on which external tractions are applied

$\delta u_i^S = \delta u_i$ evaluated on the surface $^{t+\Delta t}S_f$ (the δu_i components are zero on $^{t+\Delta t}S_u$, where displacements are prescribed)

In Equation (3.1), the left-hand side is the internal virtual work and the right-hand side is the external virtual work. In the FE method, the whole structure is discretized into a series of small pieces called elements. The corners of the elements are identified as a set of points in space called nodes. The implementation of the PVW is based upon the structural stiffness method. First, the stiffness matrix of each individual element is formulated. Then, the global structure stiffness matrix is formulated by grouping the individual element stiffness matrices together. After applying the boundary conditions and through the force-displacement relationship, the unknown nodal displacements can be determined for any given loading of the structure. A complete description of the FEM is beyond the scope of this report, but can be readily found elsewhere (see, for example, Bathe, 1996). The details of the solution strategies used in this project will be presented in Section 3.5. In the following subsections, the finite element analytical tool used in this project and the details of the numerical models used in this study are presented. A new technique in the finite element formulations available in the up-to-date FEA package ABAQUS and particularly useful in modeling the pipe wrinkle sleeve repair process is presented and validated.

3.2 THE PIPE NUMERICAL MODEL USED IN THIS PROJECT

3.2.1 The Finite Element Analytical Tool Used in This Project

The finite element analyses carried out in this project were conducted by using the commercially available finite element analysis (FEA) package ABAQUS/Standard (ABAQUS Inc., 2003). The ABAQUS package has been used in the Civil and Environmental Engineering Department of the University of Alberta for more than a decade. Its applications cover a variety of ranges of problems, including static stress/displacement analysis, dynamic stress/displacement analysis, tire and vehicle analysis, electrical analysis and ABAQUS/Aqua analysis etc. Extensive analytical problem solving has proven that FEA package ABAQUS is a versatile, reliable and effective FE tool in doing the analytical work (ABAQUS Inc., 2003). Several features make the ABAQUS package suitable for doing the pipe wrinkle sleeve repair simulations. These features are as follows:

1. ABAQUS can deal with large non-linear deformations by using non-linear geometry and large (finite) strain formulations.

2. ABAQUS offers a variety of shell modeling options, including general purpose shell elements as well as elements especially suitable for the analysis of "thick" or "thin" shells.

3. The ABAQUS material library includes several models of inelastic behavior, including the Classical metal plasticity, which is suitable for modeling pipe buckling behavior when using isotropic hardening rule.

4. ABAQUS has an automated increment size control feature. Once the user specifies the maximum and the minimum of the increment, ABAQUS automatically adjusts the actual increment size during the solution process.

5. ABAQUS offers both load control and displacement control solution scheme. The displacement control scheme is essential for large non-linear deformation analysis when passing through the limit point.

The version of the ABAQUS FEA package used in the Structures Group of the University of Alberta has been upgraded from version 5.3, the first time use in the year of 1994, to the most recent version of 6.4 in 2005.

3.2.2 Loading Consideration in the FEA Model

For pipelines in the field, there exist three basic loads to which the buried pipe is subjected. They are: the internal pressure, the axial load and the monotonically increased curvature. A free body diagram of a short piece of straight pipe in the field is shown in Figure 3.1.

3.2.2.1 Internal Pressure

Pumping stations are arranged along the pipeline in the field at certain intervals to maintain the flow of the fluid or gas inside the pipeline. The presence of the internal pressure in the pipeline induces hoop stress or circumferential stress, σ_h, i.e., stress existing in the pipe wall along hoop direction, according to the free body diagram of a half-cylindrical portion of the pipe, as shown in Figure 3.2. Using statics, the force developed in the steel pipe wall and the force caused by the fluid acting against the pipe internal surface is in equilibrium. Equilibrating these two forces produces the expression for the hoop stress as follows:

$$\sigma_h = \frac{p_i D_i}{2t} \tag{3.1}$$

where

σ_h = Hoop stress

p_i = internal pressure

D_i = Pipe internal diameter

t = the thickness of the pipe wall

25

Because of the Poisson's ratio effect, longitudinal stress is developed in the pipe wall. According to Lay (1982), for open-ended pipe in the field, the longitudinal stress in the pipe wall, σ_L, can be expressed as

$$\sigma_L = \nu\sigma_h \qquad (3.2)$$

where

σ_L = the longitudinal stress within the pipe wall

σ_h = Hoop stress

ν = the Poisson's ratio, assume to be 0.3 in this study

3.2.2.2 Axial Load

For pipelines in the field, axial load is developed primarily due to three primary components. These three components are: (1) the effect of temperature differential between the pipeline construction and pipeline operation, (2) Poisson's ratio effect due to the internal pressure and (3) the imposed axial force due to the relative movement between the soil and the pipeline.

For pipelines buried in the Canadian north, a typical value for the temperature differential would be 40 °C, which accounts for a pipeline construction temperature of –20 °C and a pipeline operating temperature of +20 °C. Because of the restraint between the pumping stations (or compressor stations), a compressive axial force is developed in the pipeline due to the temperature differential.

As described in Section 3.2.2.1, hoop stress is developed due to the internal pressure (Equation 3.1), which tries to expand the pipe in the circumferential direction. Consequently, the pipe attempts to shorten in the longitudinal direction due to the Poisson's ratio effect (Equation 3.2). Long distance pipelines in the field may be considered to be in a plane strain condition. Consequently, the longitudinal shortening of the pipeline is restrained and this results in an axial tensile force in the pipeline.

For pipelines buried in unstable slope, axial load is induced due to the relative movement between the pipe and the soil. In the top portion of the unstable slope, an axial tensile force will be induced in the pipeline. In the bottom portion of the unstable slope, an axial compressive force will be developed in the pipeline. However, this force is difficult to evaluate accurately due to the complexity of the geometry associated with the pipeline field conditions.

A general expression of the axial force, N, developed in the field pipeline is as follows:

$$N = A_s \left(E\alpha\Delta T - \nu\sigma_\theta \right) + P_s \tag{3.3}$$

where

N = axial force developed in the pipe wall

A_s = the area of the cross section of the steel

E = Modulus of elasticity, 200 000 MPa

α = the coefficient of thermal expansion of steel, 11.7×10^{-6} /°C

ΔT = the temperature differential between pipeline construction and pipeline operation

ν = the Poisson's ratio, assumed to be 0.3 in this study

σ_θ = the hoop stress (circumferential stress) in the pipe wall

P_s = the axial force due to the relative movement in the longitudinal direction between the soil and the pipe

3.2.2.3 Monotonically Increased Curvature

Pipelines buried in the field are often subjected to monotonically increased curvature due to differential ground movement caused by settlement or slope instability conditions, especially for pipelines buried in the Canadian north. If the ground movement is large enough, local wrinkle can be developed at a critical location along the pipeline. Some observations of such phenomenon that have occurred in pipeline field are reported by Wilkie et al. (2000) and Yoosef-Ghodsi et al. (2000).

The above are the three basic loads to be carried by pipelines in the field. In doing the numerical analyses, the load combinations of the three basic loads, i.e., internal pressure, axial load and monotonically increased curvatures, are considered. The behavior of the pipe segment under different load combinations is studied further, subsequently.

3.2.3 Elements Used for Modeling the Pipe Segment

Considering the particular cylindrical shape of the pipe segment and by referring to the ABAQUS/Standard User's Manual (ABAQUS Inc., 2003), the S4R shell element is used in creating the pipe model. The S4R shell element is a general purpose 4-node doubly-curved shell element using reduced integration with hourglass control, intended for both thin and thick shell applications (ABAQUS Inc., 2003). It has six independent degrees of freedom per node, namely three translations (u_1, u_2 and u_3) and three rotations (θ_1, θ_2 and θ_3). The details about the element selection in the numerical analyses can also be found elsewhere (see, for example, Dorey (2001) and Das (2002)). The selection of S4R shell elements is based on the following features it possesses.

The S4R element is a general purpose shell element and can be used for both thin and thick shell modeling. This element can provide solutions to shell problems adequately described by classical (Kirchhoff) thin shell theory and also provide solutions to structures that are best described by flexible (Mindlin) shell theory (ABAQUS Inc., 2003). Thick shells are needed where transverse shear flexibility is important. If the shell is thin, as is the case with pipe wrinkling analysis, the shear deformation in the through thickness direction is negligible. Thin shells are used for most pipeline structures.

The S4R element accounts for finite membrane strains. Membrane strains are those strains that exist in thin shells and are not due to bending. The derivatives of the position vector of a point on the deformed reference surface with respect to the same point on the undeformed reference surface gives the membrane strain on the surface.

This allows for a variation in the thickness of the shell element at different load increments.

The S4R element has an iso-parametric formulation, which means that the element displacements are interpolated in the same way as the initial geometry. Therefore, it is assumed that to each nodal point coordinate necessary to describe the geometry of the element, there exists a corresponding nodal point displacement (Bathe, 1996).

The S4R element uses reduced integration. There is only one integration point in the mid-surface (full integration has four integration points). This means that it uses lower-order integration to form the element stiffness. But the mass matrix and distributed loadings are still integrated exactly. Reduced integration usually provides more accurate results (provided that the elements are not distorted), because, for reduced integration elements, the strains and stresses are calculated at locations that provide the optimal accuracy, the so called Barlow points (Barlow, 1976) (ABAQUS Inc., 2003). In addition, the reduced number of integration points decreases the CPU processing time and storage requirements significantly, especially in three dimensional models. In the through thickness direction, the numerical integration is done by using Simpon's rule and the default number of integration points used in the through thickness direction is five. However, it is possible to change the number of integration points in the through thickness direction for calculations involved in more complex non-linearity.

On the other hand, the reduced integration procedure can admit deformation modes that cause no straining at the integration points. These zero-energy modes cause a phenomenon called "hourglassing," where the zero energy mode starts propagating through the mesh, leading to inaccurate solutions (ABAQUS Inc., 2003). The hourglass mode can be associated with in-plane displacements or it may be due to rotational modes. Element S4R formulation provides control to both of the modes by adding an additional artificial stiffness associated with the zero-energy deformation modes to the element. The default values for the stiffness are given in ABAQUS, which are sufficiently small

such that the artificial energy content is negligible. However, the default values can also be modified when necessary.

3.2.4 The Length and the Symmetry of the Pipe Numerical Model

A pipe segment is a cylindrical shell structure. If a pipe segment, with or without internal pressure, is subjected to a monotonically increased curvature, sooner or later, a local buckle or wrinkle will form within the pipe segment, provided that the pipe segment does not fracture first. A typical load vs. deformation curve for a shell buckle is illustrated in Figure 3.3. Point A corresponds to the limit point in the load vs. deformation, i.e., the maximum load the structure can sustain. The curve beyond the limit point is in the post-buckling region. In the post-buckling region, the load that the pipe segment can sustain reduces with further increased curvature. Consequently, plastic deformation concentrates at a critical location where a local buckle or wrinkle is developed due to the strain localization. These are observed in numerous pipe full scale laboratory tests (Mohareb, et al (1994), Yoosef-Ghodsi (1994), Del Col (1998), Dorey (2001) and Das (2003)). Similar wrinkles are also observed in the field (see, for example, Wilkie, et al. (2000) and Yoosef-Ghodsi, et al. (2000) and Song et al. (2003)). Souza and Murray (1996) defined a wrinkle as follows:

"A wrinkle is a local buckle of large magnitude that is clearly visible to the naked eye and possesses the following attributes:

(i)   Its wave form is localized and restricted to approximately a single half-wave, or similar primitive shape,

(ii)   It is formed from plastic deformations,

(iii)   The amplification (and growth) of the single primitive wave-form occurs coincidentally with softening"

It has been observed from the pipe full scale laboratory tests (Mohareb et al (1994), Yoosef-Ghodsi (1994), DelCol (1998), Dorey (2001) and Das (2003)) that there exist two types of buckling modes, i.e., "bulge" buckles and "diamond-shape" buckles. "The magnitude of the internal pressure appears to be the most significant factor in

30

determining which of these two buckling modes would develop" (Dorey, 2001). The diamond-shape buckle is exclusive to very low or non-pressurized pipes. A typical "diamond-shape" buckle and a typical "bulge" buckle from pipe full scale laboratory tests are shown in Figures 3.4 and 3.5, respectively. Similar buckles are also observed in the pipeline field. Figures 3.6 and 3.7 show these two types buckling modes observed from the pipeline field.

Because of the localization characteristics of the pipe wrinkles as mentioned above and considering the validity of St. Venant's principle, a length of approximately 6D long pipe segment is used for the numerical model in doing the FE analysis. That is, there is a 3D length from the middle to either end of the model, where stress concentrations occur due to the prescribed boundary conditions at the ends. This minimizes the disturbance to the stress distribution at the mid-span of the pipe model, where the wrinkle develops.

Because of the symmetric nature of the pipe configuration and the loading conditions as mentioned in Section 3.2.2, the symmetry is utilized in doing the numerical analyses by modeling only half of the pipe. The total nodal numbers and the total degrees of freedom of the numerical model are, therefore, dropped by half and the CPU processing time is reduced dramatically.

3.2.5 Boundary Conditions Used in the Pipe Model

As mentioned in Section 3.2.4, symmetry is utilized in creating the pipe model. Consequently, only half of the pipe segment needs to be modeled. Considering the symmetric characteristics of the loading conditions as mentioned in Section 3.2.2, the model and boundary conditions used in doing the numerical analyses are shown in Figure 3.8.

As shown in Figure 3.8, there are two pivot points at the two ends of the pipe model located at the center of the pipe end cross sections, where the prescribed boundary conditions are applied. The left pivot point is on a pin-ended support and the right pivot

point is on a roller. The nodes at the pipe end cross sections are connected to the pivot points through Multiple Point Constraint (MPC) BEAM options, which is a built-in feature of the ABAQUS package. This ensures that the degrees of freedom of the nodes on the pipe end cross sections are constrained to be the same as those of the pivot points.

3.2.6 End Segment Modeling of the Pipe Model in This Project

By referring to Figure 3.1, the axial force induced into the pipe segment is always perpendicular to the pipe cross section, in both undeformed configurations and deformed configurations. So is the internal pressure, which is always perpendicular to the pipe internal surface at the point it is acting. In ABAQUS formulations, the pressure loads and distributed loads are treated as a follower loads in large-displacement analysis, as in the case of pipe buckling analysis. A follower load means that the direction in which the pressure load or distributed load acts on the pipe numerical model, changes with the deformation of the pipe model. That is, the loading direction is changed in the global coordinate system but is fixed in the local coordinate system. In order to simulate the directional change of the axial load in the pipe segment, the axial load is converted to a distributed load acting on the pipe wall. This distributed load is applied to the pipe numerical model as a follower load in ABAQUS/Standard.

In order to apply the distributed load at the end of pipe model, end caps are used at the two ends of the pipe model. Shell element S3R is selected among the ABAQUS shell element library to model the end caps. Shell element S3R is a general purpose 3-node triangular shell element with 6 degrees of freedom per node. It is fully compatible with shell element S4R. Like the S4R shell element, the S3R element can also be used for both thin and thick shell modeling. It uses thick shell theory as the shell thickness increases and becomes a discrete Kirchhoff thin shell element as the thickness decreases (ABAQUS Inc., 2003).

In order to ease the influence due to the end conditions in the pipe numerical model, where sudden discontinuity and change in geometry occur and the boundary conditions are prescribed, elastic material properties are applied to a very short segment

of the pipe model at the two ends. Because the elastic materials are not permitted to yield, this reduces the possibility that wrinkles will form in the end regions where plastic flow in the supports could introduce significant perturbations in the stress distributions within the model. As only a very short length of pipe segment is modeled using elastic material properties, the influence induced to the overall buckling behavior of the pipe model is expected to be insignificant.

3.2.7 Material Properties

The constitutive relationship used in the numerical analyses was based upon the stress vs. strain curves obtained from tension coupon tests. The material properties determined from the coupon tests are expressed in terms of the engineering stress and engineering strain. As the constitutive relationship for defining plasticity used in ABAQUS is based on true stress vs. true strain (logarithmic strain) formulations, the conversion from the engineering stress and the engineering strain values to the true stress and the true strain values is determined by the following equations (ABAQUS Inc., 2003). See also Lay, 1980:

$$\sigma_{true} = \sigma_{nom} (1 + \varepsilon_{nom}) \qquad (3.4)$$

$$\varepsilon_{true} \text{ or } \varepsilon_{ln} = \ln(1 + \varepsilon_{nom}) \qquad (3.5)$$

where

σ_{true} = the true stress,

σ_{nom} = the nominal (engineering) stress,

ε_{nom} = the nominal (engineering) strain,

ε_{true} or ε_{ln} = the true (or logarithmic) strain

The stress vs. strain curve determined through the tension coupon tests conducted by Mohareb et al (1994) is used in this study as the pipe specimens used by Mohareb et al (1993) were from the same pipeline as that in this project. Figure 3.9 shows the true stress vs. true strain relation of the pipe steel obtained by Mohareb et al (1994), which was converted from engineering stress vs. engineering strain curve from coupon tests.

For defining the plastic behavior in the ABAQUS input, the plastic strain components are used in creating the ABAQUS input files and they are calculated by the following expression (ABAQUS Inc, 2003):

$$\varepsilon_{ln}{}^{pl} = \ln(1 + \varepsilon_{nom}) - \sigma_{true} / E \qquad (3.6)$$

where

$\varepsilon_{ln}{}^{pl}$ = the true plastic strain, and

ε_{nom} = the nominal (engineering) strain,

σ_{true} = the true stress,

E = the Young's modulus

The Von Mises yield criterion is used in the numerical simulations. This criterion is based on the determination of the distortion energy in a given material. It is the default yield criterion in ABAQUS. The Von Mises yield surface is a cylinder centered at the hydrostatic axis in three-dimensional principal stress space and is independent of the equivalent pressure stress. The Von Mises yield criterion is commonly used for isotropic metals like the steel material used for the pipe structure. Detailed discussion of the Von Mises yield criterion can be readily found in literatures such as Chen and Han (1988).

A hardening parameter, which specifies how the yield surface is modified during plastic flow, is also used in doing the numerical analyses considering the fact that steel materials always exhibit work hardening phenomena during the tension coupon tests. The isotropic hardening model is used in this project as the loading conditions are essentially monotonic. Isotropic hardening means that the yield surface expands uniformly about the hydrostatic axis as plastic flow takes place (i.e., it is assumed that the material properties are the same in both tension and compression). It is acknowledged that a kinematic hardening model is more representative of the true behavior of the steel material. As the loadings in the numerical models are only monotonic ones, this eliminates the necessity to consider the Bauschinger effect. Consequently, the more complex kinematic hardening is omitted and an isotropic hardening model is used.

3.3 THE MODELING TECHNIQUE ATTEMPTED IN THIS PROJECT

As mentioned in Section 1.2 of Chapter 1, one of the objectives of this project is to study the behavior of wrinkled pipe segment under sleeve repair, namely, first a wrinkle being formed in a plain pipe segment, then the collars and sleeve being installed to the wrinkled pipe segment to encase the local wrinkle, and then curvature along the pipe segment being further increased and the possible response of the pipe and sleeve assembly being studied. In other words, the modeling of the behavior of the wrinkled pipe segment under sleeve repair is a sequential process.

An implication above is that at the moment of installing the collars and the sleeve, the stress and strain states are not zero in the pipe segment. There exists a stress pattern and a corresponding strain pattern in the wrinkled pipe segment due to the formation of the local wrinkle. Upon the formation of the wrinkle, the pipe segment yields. The collar and sleeve elements must be installed under this current stress and strain states. The pipe, collar and sleeve assembly start to carry further applied loading together. The most important consideration and the key issue in doing the wrinkle sleeve repair numerical simulations are how to add collar and sleeve elements to the "pipe only" model under the current stress state, which the wrinkled pipe segment is carrying. In order to genuinely simulate this sequential behavior of the wrinkle sleeve repair to a pipe segment, a new modeling technique has been adapted in this study, and is described in the following subsection 3.3.1.

3.3.1 The "Results Transfer Technique" in the ABAQUS/Standard 6.4

With the development of new technology and in order to meet the new needs from both research and industrial areas, the version of the FEA package ABAQUS has been upgraded on a nearly yearly basis. The version of ABAQUS currently being used in the Structures Group of the University of Alberta is version 6.4. With the upgrading of the ABAQUS package, some additional features are also updated so that they become more fully integrated and established. Among these, one important feature that has been continually upgraded is the transfer of results between ABAQUS analysis products. That is, transferring the results from one ABAQUS/Standard analysis to a new

ABAQUS/Standard analysis. Also included in this feature is transferring the results from ABAQUS/Standard analysis to ABAQUS/Explicit analysis and vice versa. The results transfer technique in ABAQUS/Standard is fully integrated and established in the current version of 6.4 and becomes the core method for the numerical simulations of the sleeve repair to the wrinkled pipe segment.

The feature of transferring results from one ABAQUS/Standard analysis to a new ABAQUS/Standard analysis in the FEA ABAQUS package was developed in particular for use in simulating assembly processes (ABAQUS Inc., 2003). During an assembly process, the local behavior of a particular component may be of interest to the analyst. But later, the behavior of the assembled product is the main concern. In this case, the local behavior of the particular component is first analyzed in an ABAQUS/Standard analysis. Subsequently, the model information and results from this analysis are transferred to a second ABAQUS/Standard analysis, where additional model definitions for the other components can be specified and the behavior of the entire product is then analyzed.

There exists a close similarity between the pipe wrinkle sleeve repair process and the assembly process. At the beginning, the formation of the local wrinkle in a plain pipe (the local behavior of a particular component) is the main interest. However, later on, the sleeve and collar components are added to the wrinkled pipe segment and the behavior of the collar, sleeve and the wrinkled pipe segment assembly (the assembled product) becomes the main interest. Due to the close similarity between the pipe wrinkle sleeve repair process and the assembly process, the "results transferring feature" in ABAQUS/Standard 6.4 is attempted in this study.

3.3.2 A Brief Description of the "Results Transfer" Technique in the ABAQUS/Standard 6.4

The results from any step and increment of one ABAQUS/Standard analysis can be transferred to a new ABAQUS/Standard analysis, providing that the increment and the

36

step (i.e., the stage in which the results are intended to transfer) have been specified. Other attractive features of the "results transfer technique" include:

(i)   The nodes and the elements in one ABAQUS/Standard analysis can be transferred to a new ABAQUS/Standard analysis, either wholly or partially;

(ii)   New nodes and elements can be added along with the new material property definition;

(iii)   The reference configuration can be specified, either using the updated configuration or the original configuration;

(iv)   The material state such as the stress state and strain state can be transferred from one ABAQUS/Standard analysis to a new ABAQUS/Standard analysis.

The above features make the ABAQUS package much more powerful in conducting numerical analysis. But there are still some limitations in using the "results transfer technique" in the current version of ABAQUS/Standard 6.4. The limitations of the results transfer technique in ABAQUS/Standard 6.4 include:

(a) Not all types of elements can be transferred. Among all the element types used in ABAQUS package, those that can be transferred include: the three-dimensional continuum element C3D8R; the three-dimensional shell element S4R; and the shell element S3R(the complete list of the element types that can be transferred from one ABAQUS/Standard analysis to another is given in Table 7.7.3-2 of ABAQUS/Standard user's manual).

(b) If the current state is set to be transferred, only the material state for the linear elastic, hyperelastic, hyperfoam and Mises plasticity models or materials

37

defined in user subroutines UMAT and VUMAT are imported correctly for further analysis.

(c) The boundary conditions and multi-point constraint specified in the original analysis are not imported. They must be defined again in the new analysis.

(d) Loads defined in the original analysis are not transferred to the new analysis. Consequently, loads need to be redefined in the new analysis.

3.4 MODELING THE COLLAR AND THE SLEEVE

The modeling of the pipe segment in this project has been presented in Section 3.2. As one of the objectives of this project is to study the behavior of wrinkled pipe segment under sleeve repair, the modeling of the collar and sleeve components in the collar, the sleeve and the wrinkled pipe assembly are described in this section.

As mentioned in Section 3.2.4, it is observed during the pipe buckling behavior study that there exist two types of buckling modes, "bulge" buckles and "diamond-shape" buckles. The pipe wrinkle sleeve study will focus on the outward "bulge" buckles. Firstly, in the main line system, the internal pressure is maintained at a specific level through the pump stations along the pipeline. The possibility of forming an inward "diamond-shape" buckle in the main line system is very low. Secondly, the formation of inward "diamond-shape" buckles interrupts the normal operations of the line such as the impact to the flow capacity and blockage of the cleaning or measurement pig passage. Once inward "diamond-shape" buckle develops in the pipeline, they have to be removed from the main line system. Consequently, only the formation of outward "bulge" buckles and the corresponding sleeve repair to this type of buckles are studied in this project.

Due to the formation of a "bulge" buckle in the pipe segment in the field, as shown in Figure 3.7, collars are needed to fit in the gap between the internal surface of the sleeve and the external surface of the pipe. Figures 3.10 and 3.11 are the pictures of the sleeve repair taken from the pipeline field, showing the way of installing the collar

and the sleeve. A schematic of the collar, the sleeve and the pipe assembly is shown in Figure 3.12.

The sleeve and the collar are made from flat plate through the U-ing process to form a half ring called a split sleeve or split collar. The sequence of installing the collar and the sleeve to encase the local wrinkle in a pipe segment is as follows:

1. Butt weld the split collars together to form a whole collar (Figure 3.10).

2. Weld the ring of collar to the pipe external surface using fillet welds (Figure 3.10). The location of the collar depends on the length of the sleeve used.

3. Butt weld the split sleeve together to form a stub pipe segment. Then weld the sleeve to the external surface of the collars using fillet welds (Figure 3.11).

For the length of the sleeve, a common practice used in the pipeline industry is 3 times the pipe diameter. By referring to the features of shell element S4R as mentioned in Section 3.2.3 and considering the geometry of the sleeve, S4R shell elements are used to model the sleeve.

The common practice used in the pipeline industry for the length of the collar is about 150 mm (approximately 6 in) long in the pipe longitudinal direction, i.e., a ring of pipe when butt welded together. Consequently, the three-dimensional solid element C3D8R is used to model the collars in the numerical simulations considering the nature of the collars.

Element C3D8R is an 8-node general purpose solid element with reduced integration. The solid element C3D8R is not sensitive to the mesh orientation and has a better performance if the shape is approximately rectangular. The convergence rate for solid element C3D8R is fast. Similar to shell element S4R, reduced integration is used in solid element C3D8R in forming the element stiffness. The CPU processing time reduces

39

significantly in carrying out the numerical analysis, especially in three dimensions. Hourglass control is also included in solid element C3D8R to eliminate the hourglassing problem caused by the reduced integration procedure (ABAQUS Inc., 2003).

Normally, the sleeve is made from steel plate with the same SMYS as that of the carrier pipe segment. The collar is made from steel plate with SMYS lower than that of the carrier pipe steel. This is the current practice used by the pipeline operating company in repairing field wrinkles using collars and sleeves or other types of defects in the pipeline system where collar and sleeve are also used. In carrying out welding process on different grade of steels, different residual stress pattern will be induced with that when welding the same grade steel. As the wrinkle is always developed outside the weld affected zone, the effect that is due to the welding of the lower grade steel for the collar with the higher grade steel of the pipe and the sleeve is believed to be insignificant. Because there are no test coupons available for the sleeve and the collar in this project, the same stress vs. strain curve obtained from test coupon cut from the pipe specimen is used for the sleeve in doing the numerical modeling. An assumed stress vs. strain curve is used for the collar in the numerical modeling, which is factored from the stress vs. strain curve of the pipe steel. The assumed true stress vs. true strain curve used for the collar is shown in Figure 3.13, which is based on the true stress vs. true strain curve as described in Section 3.2.7. It is acknowledged that residual stresses were induced to the split sleeve and the split collar due to the U-ing process. As no attempt was made to measure the residual stresses due to the sleeve and the collar forming process, the residual stresses induced by the sleeve and the collar forming process are not included in the finite element models.

So far, the model technique for the pipe, the collar and the sleeve in this study has been presented. Table 3.1 lists the summary of the components of the numerical model used in doing the wrinkle sleeve repair simulation in this study.

3.5 SOLUTION STRATEGIES IN ABAQUS/STANDARD

Because of the nonlinear nature of the buckling behavior of solids and structures such as the buckling behavior of the pipe structure, nonlinear solution strategies for solving the equilibrium equations in the FEM are necessary. Several solution strategies for solving the nonlinear equilibrium equations in the FEM are available. A detailed review of these methods can be found elsewhere (see, for example, Crisfield, 1997).

Table 3.1 the Components of Numerical Model Used for the Wrinkle Sleeve Repair Simulation

Element	Pipe Body	Shell Element S4R
	End Plate	Shell Element S3R
	Collar	3D Solid Element C3D8R
	Sleeve	Shell Element S4R
Symmetry	Yes	
Material Properties	Yield Criterion	Von Mises
	Hardening Rule	Isotropic
Boundary Conditions	As shown in Figure 3.8	

As mentioned in Section 3.1, the application of the FEM to stress/displacement analysis of solids and structures is based on the principle of virtual work (PVW). In matrix form, the PVW expression of Equation 3.1 is written as

$$[K]\{u\} = \{R\} \tag{3.7}$$

where

$[K]$ = the stiffness matrix

$\{u\}$ = the nodal displacement vector

$\{R\}$ = the external force vector

In incremental form, the equation (3.7) can be expressed as:

$$[K]\{\Delta u\} = \{\Delta R\} \tag{3.8}$$

where

$[K]$ = the stiffness matrix

$\{\Delta u\}$ = an increment of the nodal displacements during an iteration

$\{\Delta R\}$ = an increment of the external forces during an iteration

As mentioned in Section 3.2.1, the FEA package ABAQUS can handle geometrical nonlinearities as well as material nonlinearities because the ABAQUS package incorporates several nonlinear solution methods in its nonlinear formulations. In ABAQUS analysis, the problem history is divided into steps, and the analysis procedures can be defined within steps. A step is any convenient phase of the history. For example, the simplest form of the step in ABAQUS/Standard is just a load change from one magnitude to another in a static analysis. For the problems analyzed by the ABAQUS package, involving nonlinearities, such as the wrinkle sleeve repair of a pipe segment, the indication is that the problems are history dependent. Consequently, a number of increments are divided within one step and iteration solution schemes are used in solving the nonlinear equilibrium equations in ABAQUS package.

There are three nonlinear solution methods available in ABAQUS/Standard, namely: full Newton's method or standard Newton's method; quasi-Newton method; and modified Riks method (ABAQUS Inc., 2003).

In the full Newton's method or standard Newton's method, the tangent stiffness matrix [K] is updated during every iteration. The advantage of the standard Newton's method is that it exhibits a much faster convergence rate, attributed to the updating of the tangent stiffness matrix [K]. The disadvantage of the standard Newton's method is that the method is expensive per iteration, because the stiffness matrix [K] needs to be reformulated and triangularized during every iteration.

An alternative to the standard Newton's method is the quasi-Newton method, also implemented in ABAQUS/Standard. A detailed description of the quasi-Newton method was made by Matthies and Strang (1979).

In the quasi-Newton method, the tangent stiffness matrix [K] is reformulated whenever a specified number of iterations have been done without obtaining a convergent solution. The default value for the number of iteration in ABAQUS/Standard is 8. In general, the rate of convergence of the quasi-Newton method is slower than the quadratic rate of the standard Newton's method.

The third method incorporated into ABAQUS includes the nonlinear solution method designated as the modified Riks method, and it is intended to deal with the unstable problems typically known as – snap through or snap back problems. That is, during periods of the response of a structure, the load and/or displacement may decrease as the solution evolves. For the modified Riks method, the basic algorithm for iteration is the same as that of Newton's method.

The difference between the Newton's method and the modified Riks method is the way to limit the increment size. ABAQUS provides both automatic and user defined time steps, in the standard Newton's method as well as the quasi-Newton method. The direct user step control can be used only when the behavior is well understood. In most cases, the automatic time step is used in ABAQUS. For static problems, ABAQUS/Standard uses maximum force residuals following each iteration to determine whether convergence is likely in a reasonable number of iterations. If convergence is deemed unlikely, ABAQUS/Standard adjusts the load increment; if convergence is deemed likely, ABAQUS/Standard continues with the iteration process. In the modified Riks method, the increment size is limited by moving a given distance along the tangent line to the current solution point and then searching for equilibrium in the plane that passes through the point and is orthogonal to the same tangent line. By default, ABAQUS/Standard used the standard Newton's method. A detailed review of these methods can also be found in Das (2003).

As mentioned earlier, problems involving nonlinearities in ABAQUS are history dependent. The incremental, iterative procedures are required to solve nonlinear problems in ABAQUS analysis. In using the three nonlinear solution methods mentioned

above during ABAQUS numerical analysis, the state of the model (stresses, strains, etc) is updated throughout the analysis steps, and the effects of previous history are always included in the response of each new step (ABAQUS Inc., 2003). ABAQUS provides "state storage" strategy during the numerical calculations to store the state at a material calculation point for every increment in any analysis step. Because of this feature in ABAQUS, not only the problem can be updated throughout the history, but also the state at any increment of any step can be referred to by a new analysis and can be transferred to a new analysis. This makes the results transfer technique in ABAQUS possible.

3.6 VALIDATION OF THE RESULTS TRANSFER TECHNIQUE IN ABAQUS/STANDARD 6.4

There are no laboratory tests conducted in this project. To the writer's knowledge, up to date no full scale laboratory tests have been carried out to study the behavior of wrinkled pipe segments under sleeve repair. As presented in Chapter 2 of the literature review, Yao et al (2000) carried out a series of numerical analyses to study the behavior of wrinkled pipe segment under sleeve repair using FEA package ABAQUS/Standard and a solution technique called "Element Removal/Reactivation Technique". Consequently, the analytical results obtained by Yao et al (2000) are used here, against which the newly attempted results transfer technique is compared and validated. The parameters studied by Yao et al (2000) included the length of the sleeve and the magnitude of the wrinkle at which the sleeve was installed. It should be noted that collars were not modeled by Yao et al (2000).

In doing the comparisons with Yao et al (2000), the analytical results corresponding to the mature wrinkle configurations (wrinkle with certain magnitude) with 2D long sleeve are used. The pipe parameters used are as follows: outside diameter (OD) 323.85 mm (12.75 in), wall thickness, t, 6.35 mm (0.25 in) and X52 pipe steel grade. The outside diameter of the sleeve is 355.6 mm and the wall thickness of the sleeve is 6.35 mm. The steel grade of the sleeve is the same as that of the pipe, X52. The S4R Shell element is used in modeling the pipe and the sleeve. The length of the pipe model is 1828 mm (72 in), which is approximately 6D long.

For the boundary conditions used by Yao et al (2000), the left pivot of the pipe model is on a pin ended support and the right pivot of the pipe model is on a roller. The length of the model for the sleeve is 2D, i.e., approximately 610 mm (24 in). Based on the consideration that the wrinkle sleeve repair is a sequential behavior, a technique called Element Removal/Reactivation technique in ABAQUS/Standard was used by Yao et al (2000). As collars were not modeled by Yao et al (2000), collars are not modeled also in the current validation process for consistency purpose.

In Element Removal/Reactivation technique of ABAQUS/Standard, all elements including the pipe elements and the sleeve elements are defined at the model definition part of the data input during the creation of the numerical model. The element set for the sleeve is removed before applying any loads. After the formation of a wrinkle in the pipe model, the element set for the sleeve is reactivated when the wrinkle reaches a certain magnitude. The analysis is continued with sleeve and wrinkled pipe assembly carrying further applied load together. The nodes at the sleeve end cross sections are connected to the corresponding nodes in the pipe model through the Multiple Point Constraint (MPC) BEAM feature in ABAQUS/Standard. This ensures that the degrees of the freedom of the nodes on the sleeve end cross sections are constrained to be the same as that of corresponding pipe nodes.

The deformed configurations of sleeve and wrinkled pipe assembly using element removal/reactivation technique by Yao et al (2000) and using the results transfer technique in current study are shown in Figures 3.14 and 3.15, respectively. In order to show that in results transfer technique the results from one analysis are truly transferred to the next analysis, comparisons were also made between the final stress state of one analysis and the initial stress state of the next analysis. Figure 3.16 shows that stress state at the end of 'pipe only' buckling analysis, i.e., before the installation of the sleeve. Figure 3.17 displays the stress state at the beginning of the sleeve and pipe assembly buckling analysis. Clearly, the stress states are exactly the same as shown in Figures 3.16 and Figure 3.17. The moment vs. curvature curves obtained by using element

45

removal/reactivation technique and the results transfer technique are shown in Figure 3.18.

As shown in Figures 3.14 and 3.15, the deformed configurations from ABAQUS numerical analysis using element removal/reactivation technique and using the results transfer technique are exactly the same. Figures 3.14 and 3.15 also display the characteristics of the buckling behavior of sleeve repair to wrinkled pipe segment. The sleeve inhibits further increase of the magnitude of the wrinkle it encases. But another wrinkle begins to develop at the location offset from the end of the sleeve with increased rotations. Similar phenomenon was also observed in the pipeline field wrinkle sleeve repair work, which will be presented in Chapter 4. Comparing the stress state in Figure 3.16 with that in Figure 3.17 shows that the results from 'pipe only' buckling analysis do have been transferred to the next buckling analysis for the wrinkled pipe and sleeve assembly. Figure 3.18 displays the characteristic moment-curvature response of the buckling behavior of a wrinkled pipe segment under sleeve repair. The moment reaches first limit point at point A. With further increased curvature, the moment carrying capacity starts to drop due to the initiation of the local wrinkle until point B, at which the sleeve is installed. With even further increased curvature values, the moment carrying capacity starts to increase due to the installation of the sleeve until point C, which corresponds to the second limit point. Because of the formation of the second wrinkle in the sleeve and pipe assembly, the moment carrying capacity reduces again with increased curvature values. Consequently, second wrinkle develops at the location offset from the end of the sleeve.

The moment vs. curvature curves obtained from two different solution techniques in ABAQUS/Standard, i.e., element removal/reactivation technique and results transfer technique, provide quite similar characteristic behavior of the pipe wrinkle sleeve repair process. The moment vs. curvature curves are essentially the same until point B, i.e., the point at which the sleeve is installed. Because of the different techniques used in doing the numerical simulations, the moment vs. curvature curves are slightly different from the two techniques after the installation of the sleeve. The moment carrying capacity of the

pipe segment is similar as shown in these two curves but the results obtained using element removal/reactivation technique displays a relative larger rotational capacity. The difference between the rotational capacity increases from these two different techniques is approximately 7%.
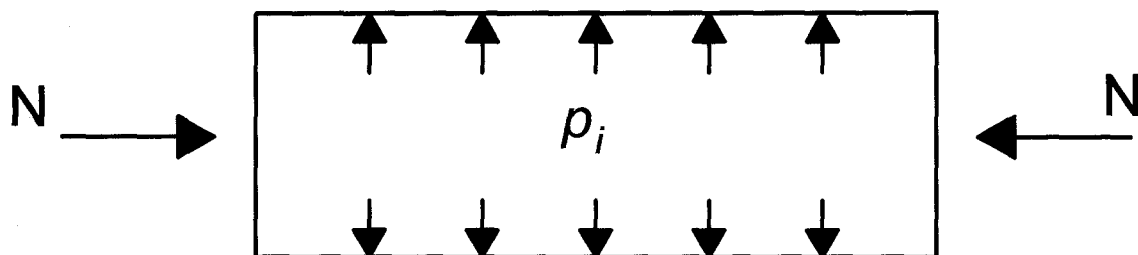
Figure 3.1a Free Body Diagram of A Pipe Segment before Deformation
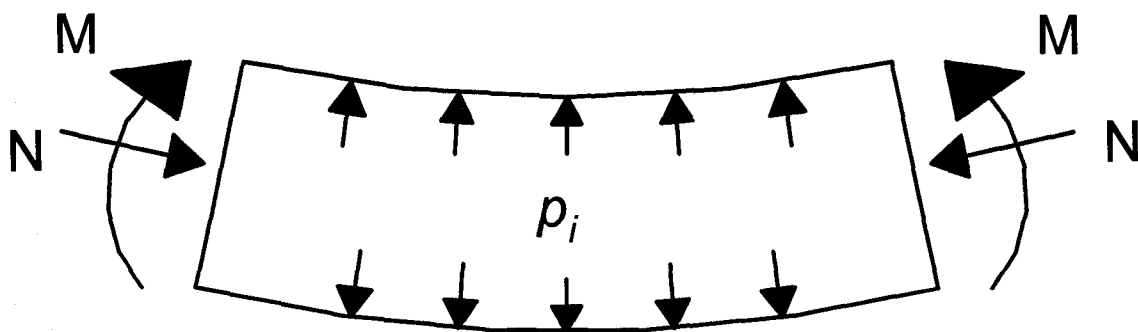
Figure 3.1b Free Body Diagram of A Pipe Segment after Deformation

Figure 3.1 Free Body Diagrams of A Pipe Segment in Undeformed Configuration and Deformed Configuration
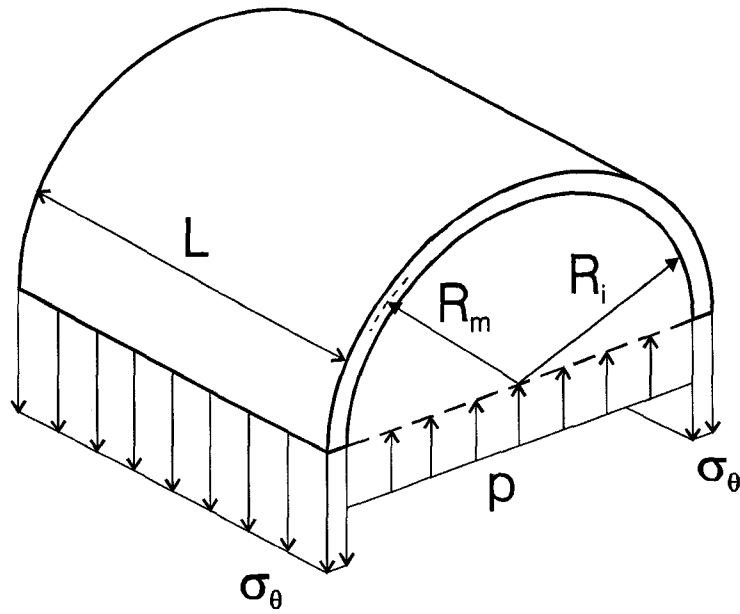
Figure 3.2 Free Body Diagram of a Half Cylindrical Portion of Pipe Segment
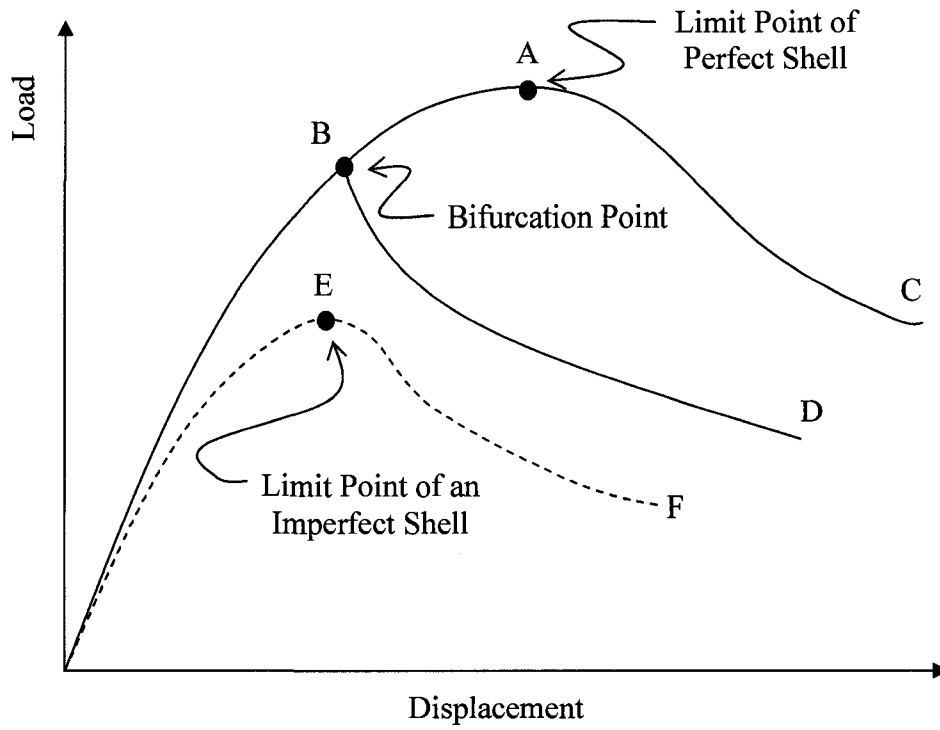
Figure 3.3 Typical Load-Displacement Response of Shell Structures

| Front View | profile |
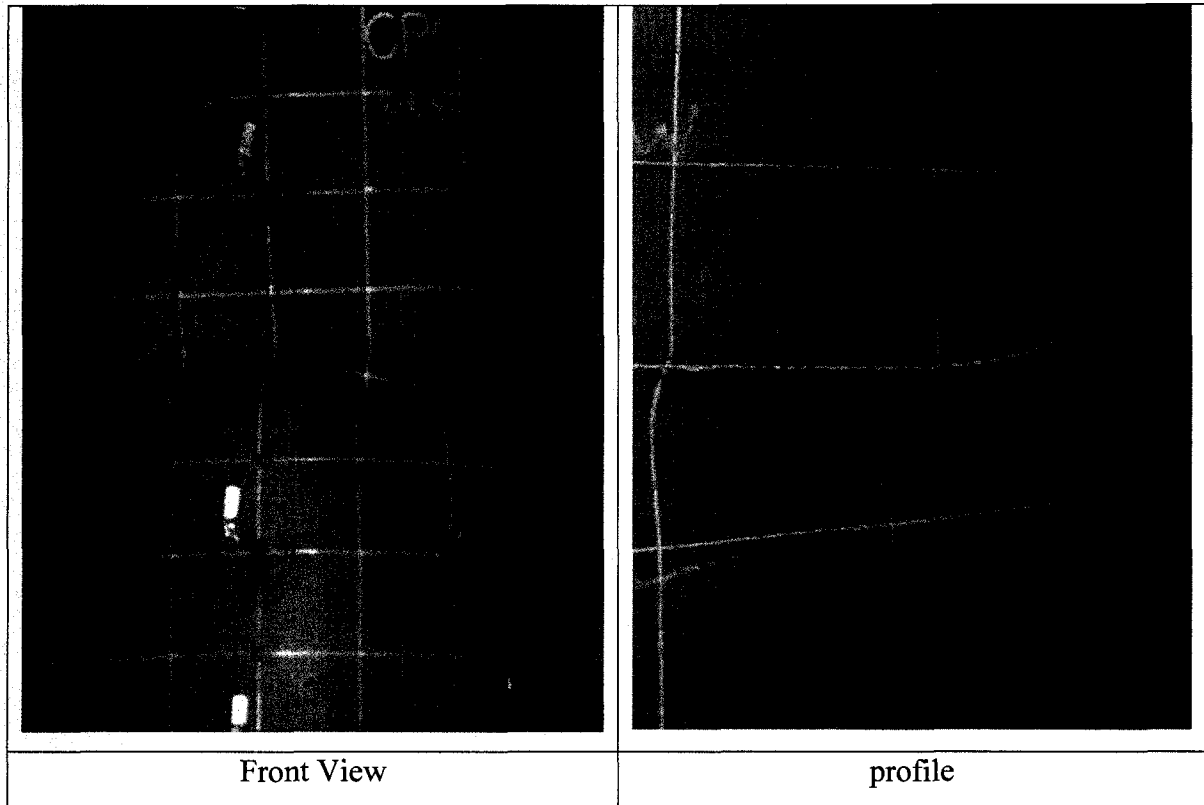
Figure 3.4 Diamond Shape Buckle Observed in Pipe Laboratory Test (Dorey, 2001)

| Front View | profile |
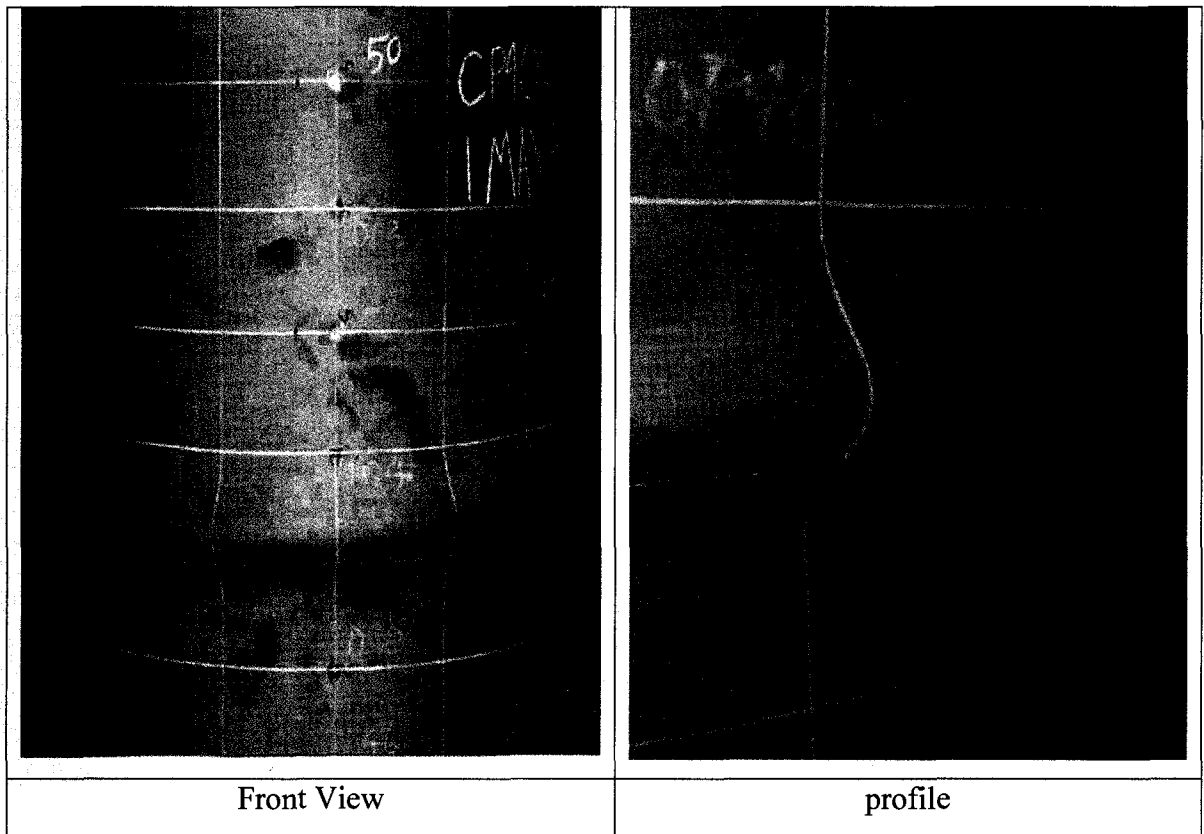
Figure 3.5 Bugle Buckle Observed in Pipe Laboratory Test (Dorey, 2001)

Figure 3.6 Diamond Shape Buckle Occurred in Pipe Segment from the Field (Baumgard, 2005)
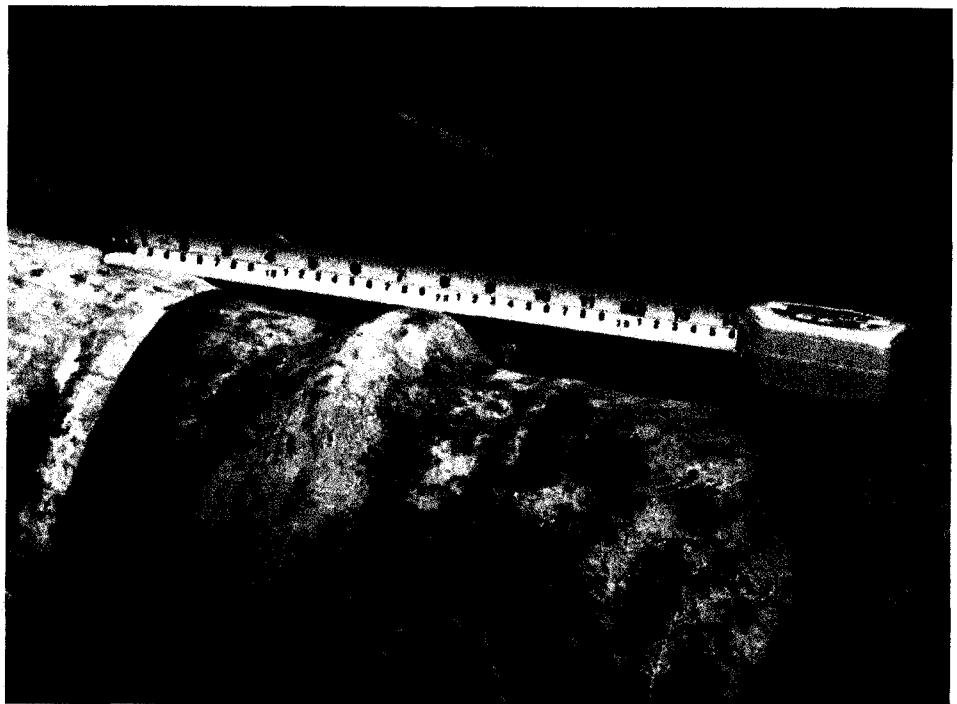
Figure 3.7 Bugle Buckle Observed in Pipeline Field (Yoosef-Ghodsi, 2000)

Right Pivot Point
$u_2=u_3=\theta_2=\theta_3=0$

Plane of Symmetry
$u_3=\theta_1=\theta_2=0$

Left Pivot Point
$u_1=u_2=u_3=\theta_2=\theta_3=0$
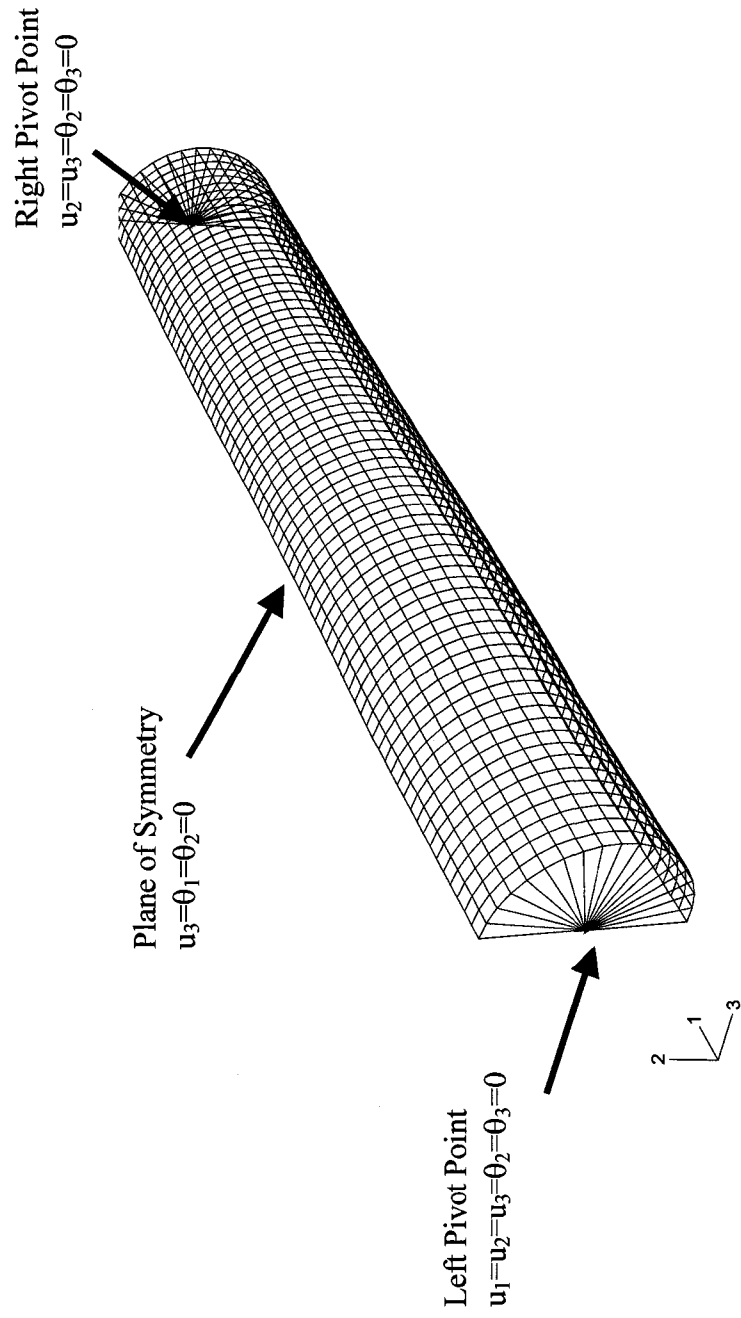
Figure 3.8 Numerical Model for the Pipe Segment and the Boundary Conditions

53
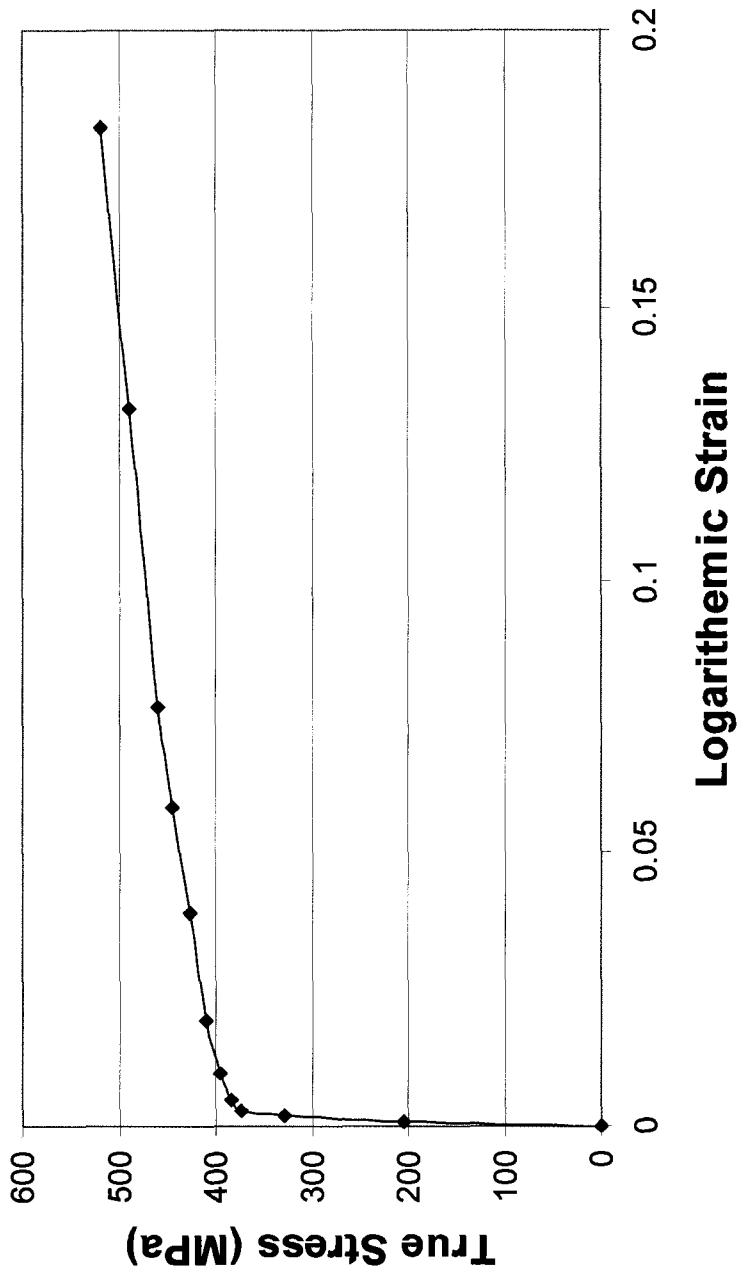
Figure 3.9 The True Stress vs. True Strain Curve for Pipe Steel and Sleeve Steel
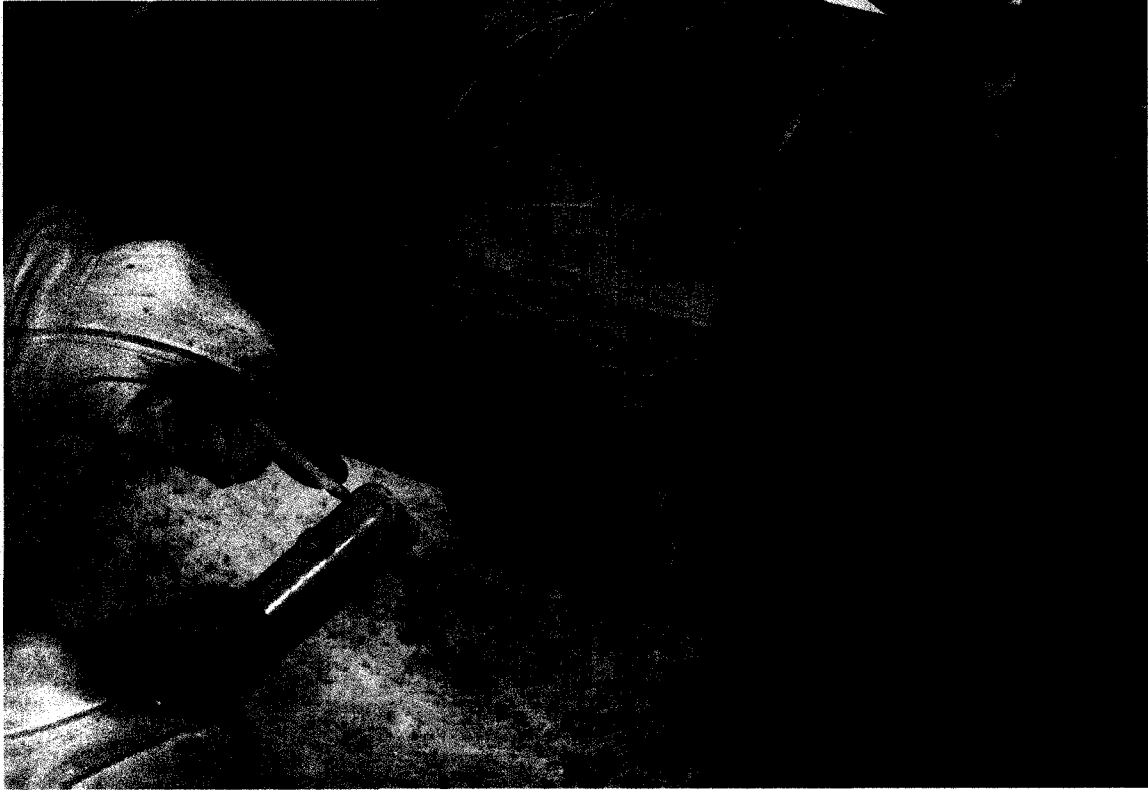
Figure 3.10 Installation of the Collar in the Field
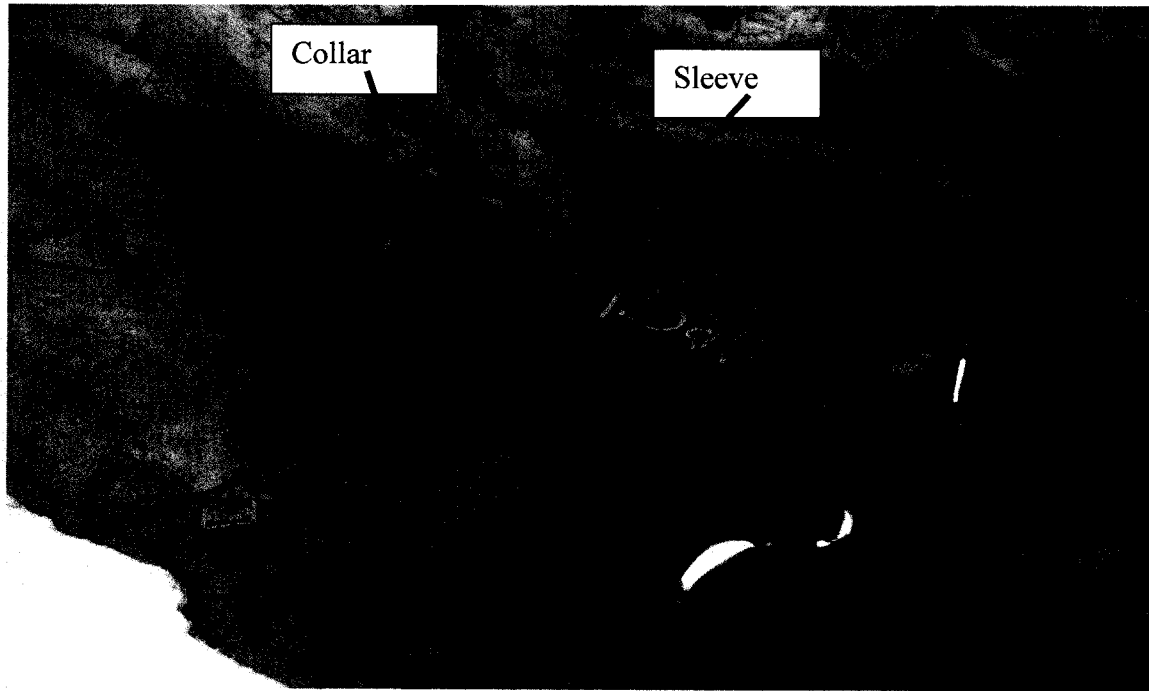
Figure 3.11 Installation of the Sleeve in the Field
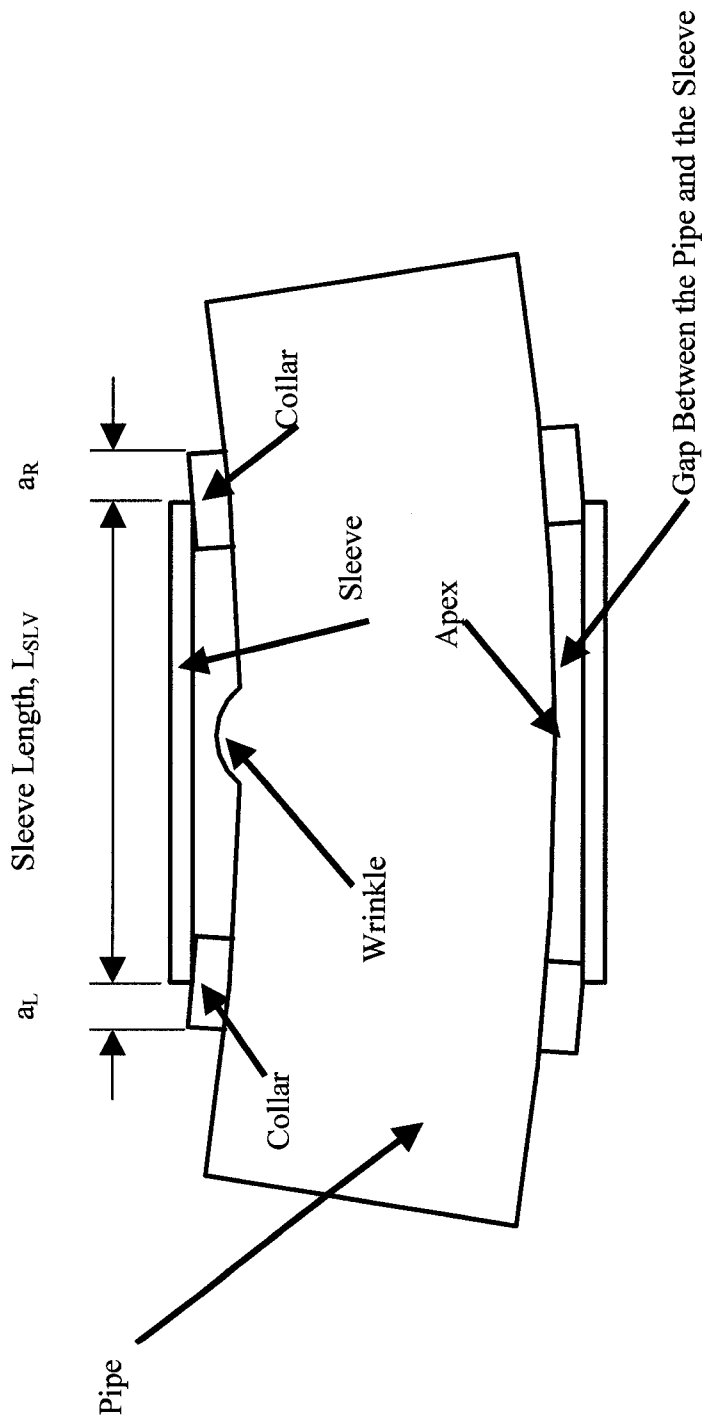
Figure 3.12 Schematic of the Collar, the Sleeve and the Wrinkled Pipe Assembly
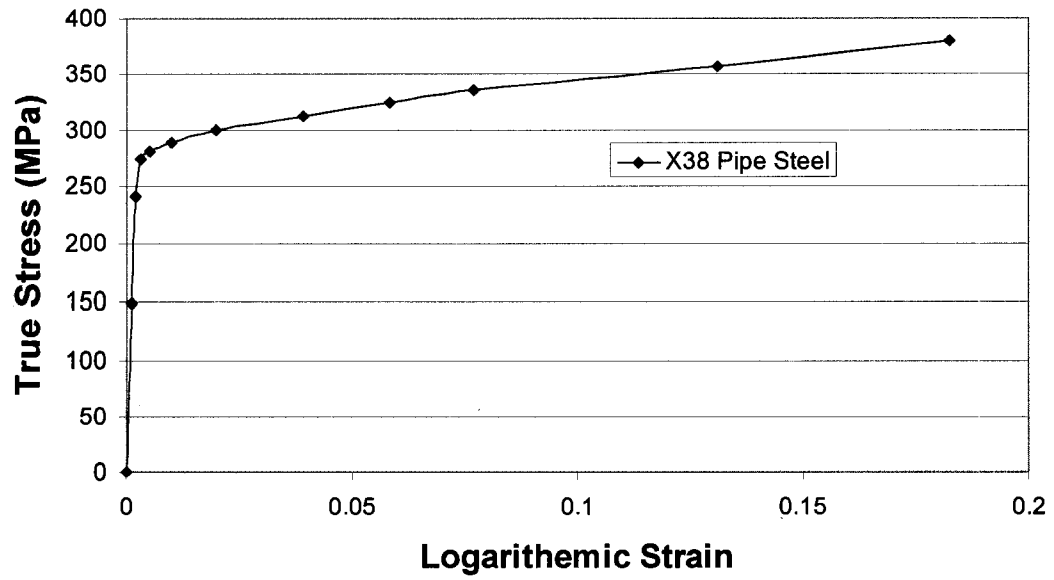
Figure 3.13 Assumed True Stress vs. True Strain Curve for Collar Steel
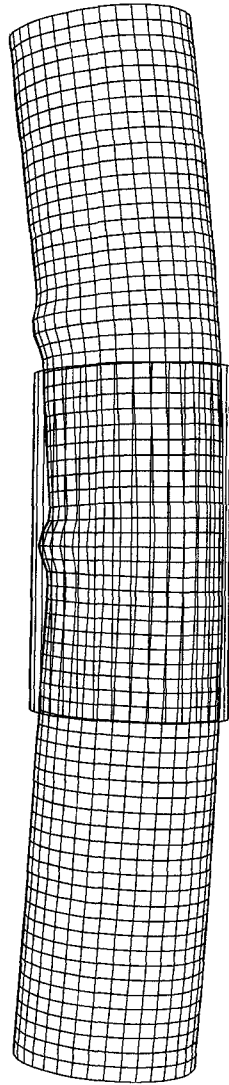
12" pipe; 72" long with one sleeve (24")   Thu May 18 17:06:53 Mountain Daylight Tim
ODB: 2ds72in_React.odb   ABAQUS/Standard 6.4-1

Figure 3.14 Deformed Configuration of the Pipe Model Using Element Removal/Reactivation Technique in ABAQUS/Standard

Transfer results from 2DSV Valida
ODB: 2ds7/2in_Trans_Impor.odb   ABAQUS/Standard 6.4-1   Thu May 18 19:32:00 Mountain Daylight Tim

Figure 3.15 Deformed Configuration of the Pipe Model Using Results Transfer Technique in ABAQUS/Standard

Figure 3.16 Stress State at the End of 'Pipe Only' Buckling Analysis

Figure 3.17 Stress State at the Beginning of Sleeve Pipe Assembly Buckling Analysis
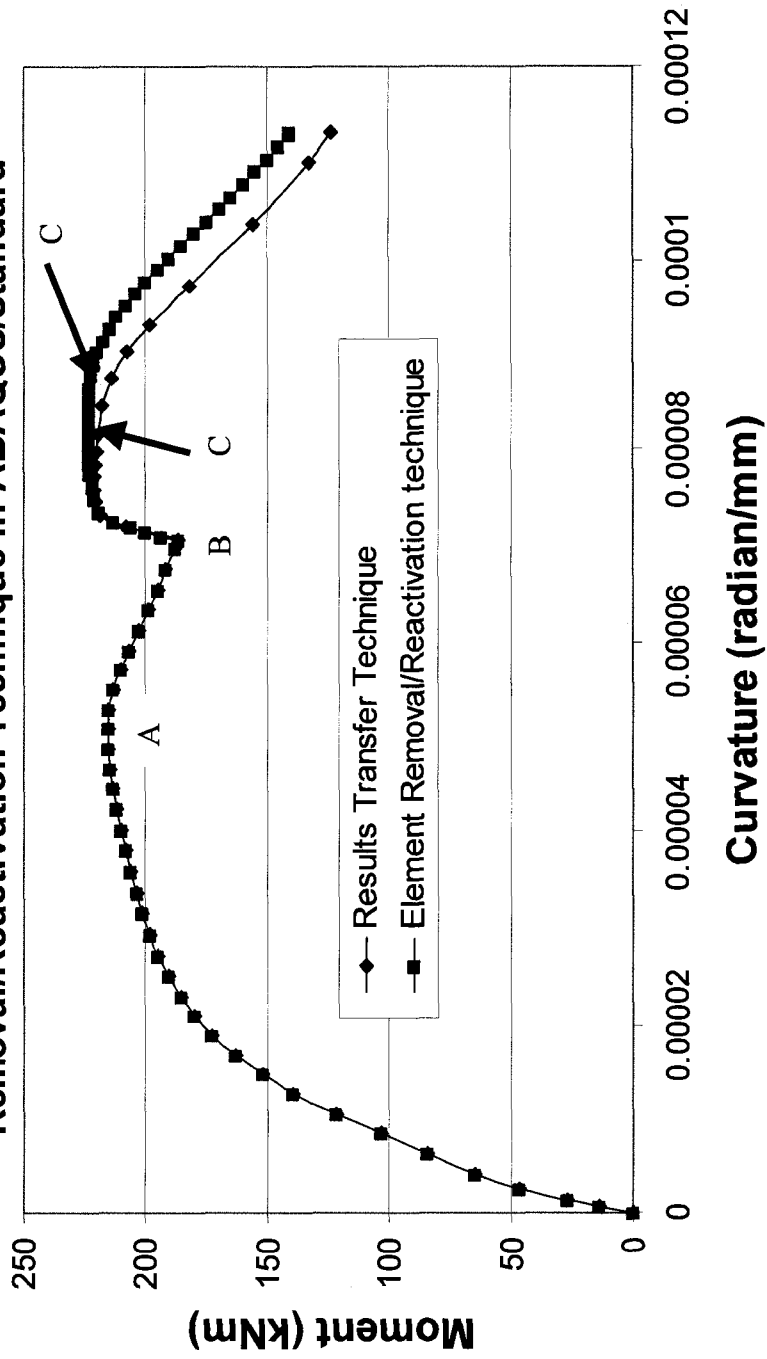
Figure 3.18 Comparison of the Moment vs. Curvature Curve from Two Different Techniques in ABAQUS/Standard

CHAPTER 4 CASE HISTORY OF WRINKLE SLEEVE REPAIR AND NUMERICAL SIMULATIONS

4.1 INTRODUCTION

Following the set up of the new FE model for the pipe wrinkle sleeve repair process as presented in Chapter 3, this technique is used to do a re-enactment of a wrinkle sleeve repairing that occurred at a pipeline field. Since no laboratory testing was carried out in this project for the validation of the FEA model used for the pipe wrinkle sleeve repair process, this pipeline field wrinkle sleeve repair re-enactment based on the data from the field measurements is treated as part of the validation of the numerical model.

As mentioned in Chapter 1, two significant observations are found in the pipe buckling behavior research projects carried out in the University of Alberta. These are (i) pipes do not fracture due to the formation of the wrinkle in the pipe wall if they undergo monotonic loads and (ii) post buckling behavior is highly ductile and the actual displacement at rupture was up as high as 20 times of those under which the wrinkle just initiated.

For pipelines in the field, although they may experience significant loading as a result of large differential ground movements such as slope failure, frost heave and thaw subsidence etc. and the stresses and strains induced could be beyond the original limits contemplated by the pipeline designer, it is possible for the pipeline to survive such events by utilizing its ability to deform well into the inelastic range in order to conform to ground movements without producing rupture.

Enbridge Pipelines Inc. operates an NPS 12 pipeline in the Canadian north that ships crude oil from Norman Wells, NWT to Zama, Alberta, which traverses a geotechnically challenging terrain. One location along the pipeline has experienced slope instability resulting in the deformation of the pipe into a "wrinkled"

configuration. Because of the huge budget to replace the wrinkled pipe segment in the field, repairing sleeves were installed over the wrinkled pipe segment in the critical location. This critical location has been monitored for a number of years using GEOPIG tool (a brief introduction of the GEOPIG is presented in Chapter 1), resulting in a large database of information available.

This chapter describes the numerical analyses of the wrinkle sleeve repair process that was carried out in the University of Alberta at this critical location. The numerical studies include the "re-enactment" of two wrinkles detected in the years of 1998 and 2004, followed by the steel sleeve repair after each wrinkle detection. The results transfer technique as described in Chapter 3 in FEA package ABAQUS/Standard is used here in doing the "re-enactment" of the DSRS. In doing the numerical analyses, data recorded through the yearly GEOPIG run along this line are used in creating the numerical model so that the loading history the critical pipe segment might undergo could be traced from the year of the line vintage up to date. Through the re-enactment of the pipe wrinkle sleeve repair process, the results transfer technique in FEA package ABAQUS/Standard can be further validated through the field case study. In addition, the possible behavior of the pipe segment under a "double sleeve repair" system, denoted by DSRS could also be investigated. This could provide an estimate of the time span for the next repairing sleeve installation.

4.2 BACKGROUND OF THE WRINKLE SLEEVE REPAIR

Norman Wells to Zama pipeline is the first buried oil pipeline that was ever built in the Canadian north. Because of the geotechnically challenging terrain this pipeline traverses, the GEOPIG tool is run on a yearly basis to monitor any abnormal change in curvature plot or in pipe internal diameter plot that may occur along this line. The first GEOPIG run on this pipeline took place in 1989, which was four years after the pipeline was first put into operation. Figure 4.1 shows the 1989 GEOPIG plot around the wrinkle location at chainage of 311 + 745 m (hereinafter, referred to as KP 311) on Slope 84. Although the first GEOPIG run

was carried out four years after the beginning operation of this line, it can be seen that no severe local spikes are observed in either the curvature or the internal diameter plots. Accordingly, the configuration of the pipe segment at KP 311 from the 1989 GEOPIG run is used as the initial configuration of the pipe numerical model in doing the numerical simulations of the DSRS. The following observations are also noticed from the 1989 GEOPIG data:

(i) The pipe segment containing the local wrinkles is not straight and is within a cold bend.

(ii) The wrinkles did not occur in the vicinity of girth welds (this will be seen in Figures 4.2 and 4.3. The first wrinkle is 2.3 m away from the closest girth weld and the second wrinkle is 1.7 m away from the closest girth weld.)

After the GEOPIG run that was carried out in September 1998, high local curvature in the curvature plot and severe local spike in the internal diameter plot were observed from the GEOPIG plot at the bottom portion of Slope 84. Based on the engineering judgment, it is believed that a local wrinkle (Wrinkle 1) was developed at this location. Figure 4.2 displays the 1998 GEOPIG plot at KP 311. Wrinkle 1 was repaired in February 1999 using a steel sleeve. That is five months after the wrinkle detection. After the 2004 GEOPIG run, it was observed, from the 2004 GEOPIG plot as shown in Figure 4.3, that a new severe local spike occurred in the internal diameter plot just adjacent to the first severe local spike measured through 1998 GEOPIG run. This means that a new wrinkle (Wrinkle 2) was developed just beside the first wrinkle (Wrinkle 1). Based on the distance between the two spikes as measured by the GEOPIG tool, it is believed that Wrinkle 2 was formed just beside the end of the sleeve. Figure 4.3 shows the 2004 GEOPIG plot at KP 311. Wrinkle 2 was repaired in February 2005, i.e., five months after the wrinkle detection, using another sleeve. It should be noted that the observations in Figure 4.3 are consistent with those observed in the numerical simulations of wrinkle sleeve repair process as described in Chapter 3. That is, a new wrinkle will

develop offset from the end of the sleeve if keeping increasing the end displacements.

4.3 LAYOUT OF THE "RE-ENACTMENT" OF DSRS BY USING THE FINITE ELEMENT METHOD

Numerical simulations of the wrinkling and sleeving of the deformed pipe segment at this critical location (KP 311), tracing the loading history that the critical pipe segment might undergo, have been carried out in the Civil and Environmental Engineering Department of the University of Alberta based on the recorded GEOPIG information database.

The "re-enactment" of the pipe deformation history is composed of a number of three-dimensional shell buckling analyses. This "re-enactment" describes the development of the first wrinkle, which was repaired in 1999, the development of the second wrinkle which was repaired in 2005, and the development of a possible third wrinkle assuming that the loading conditions do not have significant change. The re-enactment of the first and the second wrinkles could be used as the validations of the new FE modeling technique for pipe wrinkle sleeve repair process. The prediction of the possible third wrinkle could provide Enbridge the approximate time span for next sleeve repair. Because of the sequence of the wrinkling and sleeving activities that occurred in the pipeline field, sequential analytical procedures, as described in Chapter 3, are required to be used in the numerical simulations in order to closely simulate the loading history of this pipe segment.

Based on the recorded GEOPIG data, the dimension of the numerical model used in doing the "re-enactment" of the DSRS is determined at the first step. The maximum axial force (P_{max}) the pipe model can sustain is estimated using the FE method. Subsequently, three stages, as shown in the schematic of Figure 4.4, are used to describe the "re-enactment" of the sequential pipeline field wrinkle sleeve repair process.

In Stage One, the difference of the rotational values, which are based on the recorded GEOPIG data between the year of 1989 and the year of 1999 (the reason for using 1999 GEOPIG data instead of the wrinkle detection year 1998 will be presented in Section 4.5), at the two ends of the selected pipe segment due to soil movement are calculated. These values were applied at the two ends of the pipe numerical model. The possible loading conditions including the possible internal pressure and the possible secondary axial force as a fraction of P_{max} are determined, which should provide the closest match to the first wrinkle as detected and measured by the GEOPIG tool in September 1999. Figure 4.5 shows the profile of Wrinkle 1 that was measured using GEOPIG tool in 1999.

In Stage Two, two collars and one sleeve (Sleeve 1) were added to the wrinkled pipe model. The new model, which includes the wrinkled pipe, two collars and one sleeve, is further loaded with increased rotation values. The increased rotation values are due to further soil movement between the year of 1999 and the year of 2005 and calculated based on the 1989 GEOPIG data and the 2005 GEOPIG data. The deformed configuration of the assembled model (pipe, collars and sleeve) will have similar configuration with that in Figure 4.6, a picture taken at KP 311 just before the installation of the second sleeve.

In Stage Three, another collar (the third collar) and another sleeve (Sleeve 2) were added to the single sleeved pipe model (pipe, collar and sleeve assembly). The new assembly, which includes the double wrinkled pipe, three collars and two sleeves, is further loaded with further increased rotational values at the two ends of the pipe model. Hence the possible behavior of pipe segment under the Double Sleeve Repair System (DSRS) could be predicted by the finite element analysis.

It should be noted that the rotation values applied at the two ends of the numerical model in Stage One and Stage Two are calculated based on the GEOPIG records. Therefore, Stage One and Stage Two could be treated as part of the validations of the numerical model used for the pipe wrinkle sleeve repair process. The rotation values applied to the numerical model in Stage Three are hypothetical

as no GEOPIG measurement has been conducted at the time the project was conducted. But the rotations used in Stage Three are based on the assumption that the loading conditions do not have significant change and are based on the trends of the rotational displacement as observed from Stage One and Stage Two.

4.4 DOING THE "RE-ENACTMENT" OF WRINKLE SLEEVE REPAIR USING THE FEA PACKAGE ABAQUS/STANDARD

For the purposes of simulating the characteristics of sleeved pipelines, the numerical analyses were carried out using 3D shell models in the FEA package ABAQUS/Standard 6.4. The FEA package ABAQUS is commercially available in the Civil and Environmental Engineering Department of the University of Alberta and has been used in the Structures Group for more than 12 years. The applications of the FEA package ABAQUS cover a variety of ranges of problems, including static stress/displacement analysis, dynamic stress/displacement analysis, tire and vehicle analysis, electrical analysis and ABAQUS/Aqua analysis etc. Extensive analytical problem solving has proven that FEA package ABAQUS is a versatile, reliable and effective FE tool in doing the analytical work (ABAQUS Inc., 2003). The details for selecting the FEA package ABAQUS/Standard 6.4 to do the pipe buckling numerical analyses were presented in Section 3.2 of Chapter 3.

Shell elements S4R are used to model the pipe segment and the sleeves because of the cylindrical shapes of the pipe segment and the sleeves and because of the features the shell element S4R possesses. The details for selecting shell element S4R to model the pipe and the sleeves have been presented in Section 3.2 of Chapter 3. By referring to the free body diagram of a pipe segment in the pipeline field as shown in Figure 3.1 and the free body diagram of half cylindrical portion of a pipe segment as shown in Figure 3.2, end caps are used at the two ends of the pipe model in order that the follower load for the axial load can be applied to the numerical model. Follower load means the direction of the load changes with the deformation of the structure in the global coordinate system but is fixed in the local coordinate system. The details have been presented in Section 3.2.6 of Chapter 3. Shell

elements S3R are used to model the end caps. The details of selecting shell element S3R can also be found in Section 3.2.6 of Chapter 3. The solid elements C3D8R are used to model the collars. The details of choosing the element type in modeling the collars have also been presented in Chapter 3. As the pipeline field wrinkles occurred within a cold bend, some special considerations are given in the numerical modeling of the pipe segment under the DSRS. These are described in the following subsections.

4.4.1 The Length of the Numerical Model

As mentioned in Section 4.2, the earliest available field data about the pipe configuration at the KP 311 wrinkle location is from the first GEOPIG run, which was carried out in the year of 1989. Consequently, the pipe configuration from the 1989 GEOPIG run is used as the initial configuration for the numerical simulations of the DSRS. Based on the recorded GEOPIG data and the pipeline field sleeve repair data, the length of the numerical model used in the re-enactment of the DSRS is determined in such a way that two sleeves are accommodated as shown in the schematic of Figure 4.4c. Additional segments at the two ends of the numerical model are included in order to avoid the end effect due to the consideration of validity of Saint-Venant's Principle but with minimized model length.

The total length of the pipe model used in doing the numerical simulation of the DSRS is 3910 mm, which accommodates one 925 mm long sleeve (Sleeve 1) and one 1219 mm long sleeve (Sleeve 2) in the middle portion of the pipe model and two additional segments of approximately 900 mm at each end of the pipe model. A schematic of the numerical model mentioned above is shown in Figure 4.7. The length of the additional segment at each end of the pipe model is about 3 times that of the pipe diameter. It is believed that this is a reasonable length due to the consideration of the validity of Saint-Venant's Principle. The recorded GEOPIG data is interpolated at 10 mm interval for every cross section along the pipeline when they are received from Enbridge. Consequently, no attempt is made to change the intervals between the pipe cross section in creating the pipe numerical model. In

addition, fine mesh can provide a smooth profile for the local wrinkle. Due to the consideration that the element aspect ratio, the ratio between the element length and the width, is as close to 1.0 as possible, uniform mesh is used for the whole pipe model with 10 mm by 10 mm element size. The same element sizes are also used for the collar elements and sleeve elements.

Because of the symmetry of the pipe, the collar and the sleeve, symmetry is utilized in creating the numerical model by only modeling half of the pipe segment, the collar and the sleeve. Consequently, the buckling behavior of the pipe itself and the buckling behavior of the pipe, collar and sleeve assembly are modeled with significantly reduced CPU running time.

4.4.2 Finite Element Mesh for the Pipe, Collars and Sleeves

As mentioned in Section 4.2, the pipe segment containing the local wrinkles is within a cold bend. After checking the 1989 GEOPIG data, i.e., the first run of the GEOPIG along Norman Wells to Zama pipeline, it was found that the curvature of the cold bend is not constant, but varies along the cold bend. Consequently, the initial configuration of the finite element mesh for the pipe segment is also curved and the coordinates of the nodes of the numerical are calculated based on the recorded 1989 GEOPIG data in order to truly replicate the pipe configuration. Recall from Section 4.2 that the wrinkles did not occur in the vicinity of girth welds. Consequently, a plain pipe model, i.e., pipe model without girth weld, is used in doing the numerical simulations of the DSRS. The finite element mesh for the pipe alone that was used in this study is shown in Figure 4.8. A three–dimensional view of the pipe model is shown in Figure 4.9.

From the detection of the first wrinkle (Wrinkle 1) in 1998 till finishing the repair for the second wrinkle (Wrinkle 2) in 2005, three collars and two sleeves have been added to the wrinkled pipe segment. Based on the field records of the collars and sleeves used to repair the two wrinkles, the numerical models for the collars and sleeves are established. Figures 4.10, 4.11, 4.12 and 4.13 show the mesh

of the collar used for the first sleeve, the mesh for the first sleeve itself, the mesh for the collar used for the second sleeve and the mesh for the second sleeve itself, respectively.

Eight hundred 3D solid elements for the first two collars and 4550 S4R shell elements for the first sleeve are added to the pipe model after the formation of the first wrinkle. Four hundred 3D solid elements for the third collar and 6050 S4R shell elements for the second sleeve are added to the pipe, collar and sleeve assembly after the formation of the second wrinkle. A summary of the element types and the number of each element type used in doing the "re-enactment of the DSRS" are listed in Table 4.1.

4.4.3 Boundary Conditions Used in the Re-enactment of the DSRS

As for the boundary conditions used for the numerical model of the DSRS, a hinge is used at the left end support and a roller is used at the right end support. Built-in feature MPC BEAM in FEA package ABAQUS/Standard is used to constrain the degrees of freedom of the nodes on the pipe end cross section to be the same as that of the end supports (pivot points). In this way, all degrees of freedom of the nodes on the pipe end cross section are exactly the same as those of the end supports (pivot points). This facilitates the application of axial and rotational displacements and forces at the model ends.

Two ends of the pipe numerical model are regions where the loads are applied, and displacements and rotations are prescribed. It is possible that local buckling could be triggered at the pipe end regions when applying the loads and the displacements. In order to avoid the plastic deformation occurring at the ends of the numerical model, the elements in the pipe end regions are modeled using elastic material properties rather than elastic-plastic material properties are used for a short segment. Similar technique was described in section 3.2.6 of Chapter 3.

Table 4.1 Summary of the Element Types and the Number of Each Element Type
Used in the Numerical Simulations of the DSRS

Element name	Element type	Component Used for	Number of Element Used
Shell	S4R	Pipe	19650
		1st sleeve	4550
		2nd sleeve	6050
shell	S3R	Caps	100
3D Solid	C3D8R	Collars for the 1st sleeve	800
	C3D8R	Collar for the 2nd Sleeve	400

The prescribed rotational displacements are applied at the pipe end supports as the boundary conditions. The prescribed rotation values are calculated based on the GEOPIG data during the critical year span period, i.e., between the year of 1989 and the year of 1999 to simulate the formation of Wrinkle 1, between the year of 1989 and the year of 2005 to simulate the formation of Wrinkle 2 under SSRS, respectively. In this way, the wrinkling and sleeving response of the pipe segment to geotechnical movements can be closely simulated. The success of the "re-enactment" of the DSRS can be measured against the known data sets including the periodic GEOPIG inspections and the field assessments of the pipeline. The loads applied to the numerical model will be described in Section 4.5 below.

4.4.4 Material Properties Used in the Re-enactment of the DSRS

Mohareb et al. (1994) studied the buckling behavior of pipes under combined loads. The pipe test specimens used by Mohareb et al. (1994) were also from Norman Wells to Zama pipeline, in which the wrinkle sleeve repair work was carried out. The parameters for this line are as follows: pipe outside diameter OD = 323.85 mm, pipe wall thickness t = 6.35 mm and X52 pipe steel with SMYS = 359 MPa. The full scale pipe specimens used by Mohareb et al. (1994) were straight

ones. It is acknowledged that the material behavior of the cold bent pipe segment is slightly different from that of the straight pipe segment due to work hardening effect. As there are no test coupons available and for simplicity purpose, it was decided that the true stress vs. true strain curve obtained by Mohareb et al. (1994) is used here in doing the numerical simulations of the DSRS in the project. Figure 4.14 shows the true stress vs. logarithmic strain curve used for the pipe steel in this project, which is from Mohareb et al. (1994).

In doing the field wrinkle repair work, the steel grade used for the sleeve is the same as that of the carrier pipe, i.e., X52 steel. The steel grade used for the collar is X38 steel, whose SMYS is lower than that of the carrier pipe. No coupon tests are conducted for the sleeve material and for the collar material. The same stress vs. strain curve of the pipe steel is used for the sleeve material in doing the numerical simulations. The stress vs. strain curve for the collar material is obtained by scaling the stress vs. strain curve of the pipe material. The stress vs. strain curves for the sleeves is shown in Figure 4.14. The stress vs. strain curve for the collar material is shown in Figure 4.15.

4.4.5 Residual Stresses in Doing the Re-enactment of the DSRS

4.4.5.1 Residual Stress Induced to the Cold Bend

As the field wrinkles are formed within a cold bend pipe segment, the residual stresses and effective plastic strain values due to the forming process of the cold bend are considered in the numerical simulations of the DSRS. Because of the complexity of the pipe cold bend forming process in the pipeline field, the stress pattern and effective plastic strain pattern are also complex. Because of the human factors involved in the cold bend forming process, no two cold bends are exactly the same. There are no general methods to accurately determine the stress pattern and effective plastic strain pattern in pipes subject to cold bending process. As mentioned in Section 4.4.2, the curvature in the cold bend region containing the field wrinkles varies along the length of the cold bend. This makes the stress and effective plastic strain distribution even more complicated.

An in-house computer program called PAPS (standing for Plastic Analysis of Pipe Sections) is used to determine the residual stress distributions and effective plastic strain distributions for each given cross section along the pipe segment due to the cold bending process. The PAPS program was developed as part of the project in studying buckling behavior of line pipes by Yoosef-Ghodsi et al. (1994). It uses a mathematical formulation to compute the moment vs. curvature response of a pipe section. The output of the program contains stress and strain values around the cross section of the pipe for each curvature. This means that after each PAPS program run, the stress and corresponding strain values can be obtained for every element along the circumferential direction of the pipe segment. A complete description of the PAPS program is given in Appendix A, which is from Yoosef-Ghodsi, et al. (1994). It is believed that the PAPS program could give a reasonable estimate of residual stress distribution and effective plastic strain distribution in the cold bend region. Consequently, the output results obtained from the PAPS program are applied to the pipe numerical model in the simulations of the DSRS as the initial conditions for the stresses and strain values. Because of the variance of the curvature along the length of the cold bend and because the results calculated by PAPS are along the pipe circumferential direction for each curvature value, a number of runs were carried out using the PAPS program to get the residual stresses and effective plastic strain values along the whole length of the cold bend. A typical example of the distribution of the longitudinal residual stresses calculated by PAPS for a given curvature is shown in Figure 4.16.

As mentioned in Section 4.4.1, the total length of the pipe model is 3910 mm and the element size is 10 mm by 10 mm. Consequently, there are 391 elements in the longitudinal direction of the pipe model and 50 elements in the circumferential direction of the pipe model. It is impractical to input the residual stress and the effective plastic strain values for each element individually. Consequently, FORTRAN subroutines for initial stress and initial strain inputs are used in ABAQUS/Standard to read in these values for every element of the pipe model.

4.4.5.2 Residual Stresses Due to Welding of the Collar and Sleeve onto the Pipe Segment

As mentioned in Section 3.4 of Chapter 3, the sequence of installing the collar and the sleeve to encase the local wrinkle in a pipe segment (which can be referred to Figures 3.10 and 3.11) is as follows:

1. Butt weld the split collars together to form a whole collar.
2. Weld the ring of collar to the pipe external surface using fillet welds. The location of the collar depends on the length of the sleeve used.
3. Butt weld the split sleeve together to form a whole sleeve. Then weld the sleeve to the external surface of the collars using fillet welds.

Bang et al. (2002) conducted a research project to do the numerical simulation of sleeve repair welding process onto in-service pipelines using FEA software ABAQUS. Results based on the study by Bang et al. (2002) show that the residual stress distributions in the pipe axial direction and in the hoop direction are very similar and the peak values are approximately equal to the yield strength of the pipe material. As the welding process of the collars and the sleeve is not the main interests of this project and for simplicity purpose, the installation process of the collar and the sleeve is not modeled. But the residual stresses induced due to the welding of the collar and the sleeve are included in the numerical model by referring to the results by Bang et al. (2002). The modeling of the residual stresses due to the welding process was referred to the modeling technique used by Wu and Grondin (2001), who studied the behavior of steel column reinforced by welded plates. The stress due to temperature change induced by the welding process can be expressed as:

$$\sigma = E\alpha\Delta T \tag{4.1}$$

Where σ = Stress due to welding

E = Modulus of elasticity of the pipe steel (200 000 MPa)

α = Coefficient of thermal expansion for steel (11.7×10^{-6} /°C)

ΔT = Temperature differential

For a given stress value, the corresponding temperature change can be calculated. In doing the numerical analysis using FEA package ABAQUS, Wu and Grondin (2001) input a series of temperature changes required by Equation (4.1) to the nodes along the welding path in the numerical models. By self-equilibriting, the stress distribution in the structure can be automatically calculated by ABAQUS. Similar technique is also used here in applying the residual stresses due to the welding process of the collars and the sleeves to the pipe segment in the simulations of the DSRS.

4.5 LOADING CONDITIONS CONSIDERED IN THE NUMERICAL MODEL

As described in Section 3.2.2 of Chapter 3, for pipelines in the field, there exist three basic loads to which the buried pipeline is subjected. These basic loads are: the internal pressure, the axial load and the monotonically increased curvature. The loads applied to the numerical models in doing the numerical simulations of the DSRS are described in the following subsections.

4.5.1 Internal Pressures Used in the Numerical Simulations of the DSRS

The local wrinkles studied in this project occurred in the pipeline field. During the normal operations of the pipeline, the operating pressure of the pipeline fluctuates all the time. In order to find out the most likely internal operating pressure under which the wrinkles were developed, several different operating pressure values, which are all within the fluctuating range as recorded by Enbridge SCADA system, are tested.

Based on the information provided by Enbridge, it was found that at most of the time the internal operating pressure at KP 311 wrinkle location is around 4.0

MPa. Consequently, six internal pressure values, all around 4.0 MPa, are tested here. These values are 2.3 MPa, 3.3 MPa, 3.8 MPa, 4.3 MPa, 4.5 MPa and 4.8 MPa. The effects of the internal pressure to the formation of the local wrinkles can be studied.

4.5.2 Axial Load Applied to the Numerical Model

The axial load applied to a pipe segment in the pipeline field is composed of three components: (1) the axial load due to the temperature differential between the pipeline construction and operation; (2) the axial load due to Poisson's ratio effect associated with hoop stress induced by the internal pressure; and (3) the secondary axial force due to the soil movement. Details of the axial forces developed in the pipeline field are also presented in Section 3.2.2.2 of Chapter 3. The expression for the axial force induced to the pipe segment in the pipeline field, N, is as follows:

$$N = A_s \left(E\alpha\Delta T - \nu\sigma_\theta \right) + P_s \qquad (4.2)$$

Where A_s = the area of steel in the pipe cross section, $(D_o^2 - D_i^2)\pi/4$

E = Modulus of elasticity of the pipe steel, 200 000 MPa

α = Coefficient of thermal expansion for steel, $11.7 \times 10^{-6} /°C$

ΔT = Temperature differential between the pipeline construction and pipeline operation, assumed to be 40 °C

ν = Poisson's ratio, 0.3

σ_θ = Hoop stress due to the internal pressure, $pD_i/(2t)$, t is the thickness of pipe wall

P_s = Secondary axial force due to soil movement, expressed as a fraction of the P_{max}, which will be described in Sections 4.6.

4.5.3 Computation of the Angle Changes between the Critical Year Spans Different Years as Prescribed Boundary Conditions

The occurrence of local wrinkles in a pipe segment involves buckling and plastic deformation. Buckling of the pipe segment requires that the limit point have been passed in the force vs. displacement curve or moment vs. rotation curve. The force or moment starts to decrease with further increased displacement beyond the limit point. As presented in Chapter 3, the FEA package ABAQUS has the capability of tracing the whole force vs. displacement path beyond the limit point even into the post-buckling region.

As mentioned earlier, the GEOPIG tool has been running along Norman Wells to Zama pipeline on a yearly basis for a number of years. The pipe profile is closely monitored through the GEOPIG run and a large amount of information database is accumulated through all the runs. Because of the yearly collected GEOPIG tool run data, the angle change between different years can be calculated at the two ends of a given segment based on the recorded GEOPIG. The calculated angle changes between different years based on the GEOPIG measurements are applied to the ends of the numerical models as prescribed rotational displacement boundary conditions in the re-enactment of the pipe wrinkle sleeve repair system.

Information from Enbridge shows that the first wrinkle (i.e., Wrinkle 1) at KP 311 was detected in September 1998through the GEOPIG run. The sleeve repair work for Wrinkle 1 was carried out in February 1999. The second wrinkle (i.e., Wrinkle 2) was detected in September 2004 after the GEOPIG run. The sleeve repair work for Wrinkle 2 was carried out in February 2005. Because of the time lag between the wrinkle detection and the sleeve repair, the wrinkles were still growing during this time period.

Figure 4.17 shows the screen shot around KP 311 wrinkle location from the 1998 GEOPIG run, which is a duplication of Figure 4.2. Figure 4.18 shows the

screen shot at the same location from the 1999 GEOPIG run. By comparing the changes in the internal diameter plot from these two figures, it can be seen that the spike in the internal diameter plot changed dramatically from 1998 GEOPIG run to 1999 GEOPIG run. This indicates that the magnitude of the wrinkle grew significantly during these two GEOPIG runs. The same phenomenon is also observed in the 2004 GEOPIG plot and the 2005 GEOPIG plot at KP 311, as shown in Figure 4.19 and Figure 4.20, respectively. Consequently, the GEOPIG data from the year of 1999 instead of the wrinkle detection year of 1998 is used in calculating the angle changes with respect to the original pipe configuration, i.e., 1989 pipe configuration, for use in Stage One, i.e., the simulation of Wrinkle One. Similarly, the GEOPIG data from the year of 2005 instead of the wrinkle detection year of 2004 is used in calculating the angle changes with respect to the 1989 pipe original configuration for use in Stage Two, i.e., the simulation of Wrinkle Two. One important observation from Figures 4.18 and 4.20 is that the magnitude of Wrinkle 1 keeps unchanged after it is encased by the sleeve. The effectiveness of using sleeve to repair the local wrinkles is proven and supported by these GEOPIG plots from the pipeline field.

As mentioned in Section 4.4.1, the length used in the pipe wrinkle sleeve repair study for the pipe numerical model is 3910 mm. Accordingly, a segment of pipe of 3910 mm is isolated at the wrinkle location from the GEOPIG records to set up the pipe numerical model. Because of the continuing soil movement from one year to another, the configuration of the pipe in the field also changes. If the configurations of the isolated pipe segment in the wrinkle location from different years of GEOPIG data records are put together into one graph, the angle change at the two ends of the segment between these years can be calculated. These calculated angle changes at the two ends of the pipe segment are applied to the numerical model as prescribed rotational displacement boundary conditions in doing the re-enactment of the DSRS.

Figure 4.21 shows the configuration of the isolated pipe segment at KP 311 wrinkle location based on the 1999 GEOPIG run with respect to the original pipe profile from the 1989 GEOPIG run. The calculated relative angle changes for the two pipe configurations as shown in Figure 4.21 are approximately 0.064 radians at the left end and approximately 0.03 radians at the right end. Figure 4.22 shows the configuration of the same pipe segment based on the 2005 GEOPIG record with respect to the original pipe profile from the 1989 GEOPIG run. The calculated relative angle changes between the year of 2005 and the year of 1989 as shown in Figure 4.22 are approximately 0.0865 radians at the left end and approximately 0.051 radians at the right end. These calculated values are applied to the pipe numerical model at the left and right ends in Stage One and Stage Two of the re-enactment of the DSRS to simulate the behavior of the pipe segment between the critical year span periods in the field.

4.6 DETERMINATION OF AXIAL FORCE APPLIED TO THE NUMERICAL MODEL DUE TO THE SOIL MOVEMENT

One aspect of the re-enactment of the double sleeve repair system (DSRS) of the wrinkled pipe segment using FEM is to determine the possible loading conditions the segment might undergo as stated in Section 4.3. As described in Section 3.2.2.2 of Chapter 3 and Section 4.5.2, for pipeline buried in the field, axial load is developed due to three primary components. These three primary components are: (1) the effect of temperature differential between the pipeline construction and the pipeline operation, (2) Poisson's ratio effect due to the internal pressure and (3) the imposed axial force due to the relative movement between the soil and the pipeline.

The temperature differential exists between the construction of the pipeline, which occurred at about -20°C for this line and the operation of the pipeline, at which the temperature rises to about +20°C for this line. Consequently, compressive internal axial force is induced to the pipeline due to about 40°C temperature increases. Internal pressure also induces internal axial force to the

pipeline due to Poisson's ratio effect. The axial force induced by the temperature differential and the internal pressure is defined as the Primary Axial Force (PAF). The parameters for the pipeline such as the diameter, the pipe wall thickness and the pipe steel grade are all known values. The temperature differential and pipeline operating pressure can be obtained from the data records of the operating company. The PAF can be calculated using the first portion of Equation (4.2) as follows:

$$N = A_s \left(E\alpha\Delta T - \nu\sigma_\theta \right) \tag{4.3}$$

For the pipelines located on unstable slopes, soil movement will induce additional axial force in the pipeline (compressive at the bottom portion of the slope and tensile at the top portion of the slope). We define the axial force caused by the soil movement as the Secondary Axial Force (SAF) and denote it as P_s.

Because there is no field data available from which the actual SAF can be inferred, the following method was used to estimate the SAF, which was applied to the pipe model in the numerical simulations of the DSRS.

(i) First, using the finite element method to obtain P_{max}, the maximum axial force the pipe model can sustain.

(ii) Second, applying a fraction of the maximum axial force, P_{max}, as the SAF along with the axial force due to temperature differential and Poisson's ratio effects to the pipe model to carry out the re-enactment of the DSRS.

For a pipe segment, either straight or cold bent, a local wrinkle can be developed under axially applied load only provided that the pipe segment does not fracture first. The peak load that the pipe segment can sustain is the maximum axial load, P_{max}, which can be applied to the pipe segment before softening occurs due to local wrinkling. It is expected that the values for P_{max} will be slightly different for

different internal pressure values. Since the difference between the maximum internal pressure tested in this project and minimum internal pressure tested in this project is only 2.5 MPa as described in Section 4.5.1, the difference between the P_{max} values obtained under different internal pressures will be small.

Consequently, the average of the six internal pressure values is used in calculating P_{max} of the pipe segment. Figure 4.23 shows the axial force vs. axial displacement response of the pipe model through the FE method by ABAQUS/Standard. The peak value, P_{max}, is about 1000 kN, as shown in Figure 4.23, which is the maximum axial load this pipe segment could sustain.

After the estimate of the P_{max}, different values of SAF were tested as part of the P_{max}. Three values are used for the SAF as the fraction of P_{max}, which correspond to 0%, 4.3% and 12% of Pmax and are applied to the pipe model in the numerical simulations of the DSRS. The details of the determination of the SAF are presented in the following section.

4.7 DESCRIPTION OF THE RE-ENACTMENT OF THE DSRS

As described in Section 4.3, three stages were used in doing the re-enactment of the DSRS at KP 311, the wrinkle location, which include the formation of Wrinkle One (Stage One), the formation of Wrinkle Two (Stage Two) and the possible development of the third wrinkle (Stage Three) provided that the loading conditions in the pipeline field does not change significantly. The simulations of the formations of Wrinkle 1 and Wrinkle 2 are part of the validation process of the numerical model used for the pipe wrinkle sleeve repair process. The details of these three stages are presented in the following subsections.

4.7.1 Stage One: Simulation of the Formation of Wrinkle 1 (1999 Wrinkle)

In Stage One, the objective is to determine the possible loading conditions, including the possible internal pressure and the SAF (Secondary Axial Force), which led to the formation of the first wrinkle and the final pipe configuration as measured from the 1999 GEOPIG run. Because of the uncertainty of the pipeline field conditions and the fluctuating nature of the pipeline operating pressure, different loading regimes are tested in order to find the mostly likely combinations of the internal pressure and SAF, under which the wrinkle obtained from the numerical analysis most closely matches the field wrinkle (i.e., Wrinkle 1), both pictorially and numerically against the 1999 GEOPIG measurements. The wrinkle profile based on the 1999 GEOPIG measurements forms the criteria for Stage One in carrying out the numerical analysis.

Because the internal operating pressure of a pipeline fluctuates all the time, the axial force developed due to the internal pressure in the pipeline varies accordingly. Consequently, different loading regimes were tested in Stage One of the re-enactment of the DSRS to determine the one that provides the closest match to the 1999 GEOPIG measurements. As mentioned in Section 4.5.1, six different values for the internal operating pressure were tested. These values are 2.3 MPa, 3.3 MPa, 3.8 MPa, 4.3 MPa, 4.5 MPa and 4.8 MPa. For the SAF, three values are studied as the percentage of P_{max}. They are 0% of P_{max}, 4.3% of P_{max} and 12% of P_{max}.

A regime loading notation is designated as $P\alpha C\beta$, where P = Internal Pressure, α = Values used for the internal pressure, C = Secondary Axial Force and β = Percentage value of the P_{max} for the Secondary Axial Force. For example, notation P4.8C4.3 means that the numerical solution is based on the internal pressure value of 4.8 MPa with the Secondary Axial Force of 4.3% of P_{max}. Based

on Equation (4.2), the axial force for P4.8C4.3 has a value of 412.39 kN. Table 4.2 lists all the loading regimes tested in Stage One of the study as well as the corresponding axial forces as the results of the combinations of the temperature differential (assumed to be 40 °C), the internal pressure and the SAF due to the soil movement.

Table 4.2 Loading Regimes Tested and the Corresponding Axial Forces

Loading Regime	Axial Force (kN)	Loading Regime	Axial Force (kN)	Loading Regime	Axial Force (kN)
P2.3C0	486	P2.3C4.3	529	P2.3C12	606
P3.3C0	439	P3.3C4.3	482	P3.3C12	559
P3.8C0	416	P3.8C4.3	459	P3.8C12	536
P4.3C0	393	P4.3C4.3	436	P4.3C12	513
P4.5C0	383	P4.5C4.3	426	P4.5C12	503
P4.8C0	369	P4.8C4.3	412	P4.8P12	489

The comparisons of the variation of the pipe internal diameter between the FEA results from different solution sets and the 1999 GEOPIG measurements are shown in Figures 4.24, 4.25 and 4.26, respectively. Comparing the plots in the three figures shows that the wrinkle profile based on the loading regime P4.8C4.3 gives the closest match to the 1999 field GEOPIG measurement as shown in Figure 4.25. Consequently, the loading regime P4.8C4.3, which included the internal pressure of 4.8 MPa and the axial force of 412 kN, is believed to be the one that the pipe segment might most likely experience.

Comparison of the configuration of the local wrinkle is made between the 1999 field GEOPIG measurements and the FE simulations. Figure 4.27 shows the comparison of the wrinkle profile, one from the 1999 GEOPIG measurements and

one from the FE simulations. A further comparison of the variations of the pipe internal diameter are also plotted, one measured by 1999 GEOPIG tool run and the other from FE analysis, as shown in Figures 4.28. The comparisons made in Figures 4.27 and 4.28 clearly show that an excellent match is reached between the numerical analysis and the field observation for the 1999 wrinkle, Wrinkle 1.

4.7.2 Stage Two: Simulation of Wrinkle 2 (Single Sleeve Repair System, SSRS)

In Stage Two, the objective is to simulate the formation of Wrinkle 2, which is based on the loading regime determined in Stage One, as close as possible to the 2005 GEOPIG measurements. The final configuration of the pipe numerical model from Stage One forms the initial configuration of Stage Two. One of the main considerations of the numerical analysis in Stage Two in doing the FEA is how to genuinely simulate the actual situation occurred in the wrinkled pipe segment after Stage One. As mentioned earlier, pipe wrinkling means the occurrence of local buckling and plastic deformation in the pipe segment. There exist a stress pattern and a corresponding strain pattern due to the formation of the local wrinkle. The collars and the sleeve (Sleeve 1) were installed onto the wrinkled pipe segment under the current stress state. This has to be truly simulated in doing the numerical analysis of the wrinkle sleeve repair process. Consequently, the results transfer technique in ABAQUS/Standard is used here in doing the simulations of the field sleeve repair process. The details of the results transfer technique in ABAQUS/Standard was presented in Section 3.3 of Chapter 3.

In the pipeline field, the pipe wrinkled under combined internal pressure, axial force and bending moment. The collars and sleeve were installed to the wrinkled pipe segment thereafter. The pipe, collar and sleeve assembly start to carry any further induced loads together. The assembly in Stage Two is denoted as Single Sleeve Repair System (SSRS) as there was only one sleeve installed so far. The angle change between the 2005 GEOPIG measurements and the 1989 GEOPIG measurements (the original pipe configuration) is applied to the SSRS along with

the internal pressure and the axial load as determined in Stage One. The angle changes at the two ends of the pipe model were calculated in Section 4.5. These values are 0.0865 radians at the left end clockwise and 0.051 radians at the right end counterclockwise.

Again, similar phenomenon as that described in Chapter 3 is observed that a new wrinkle always develops adjacent to the collar, which is used for repairing the first wrinkle, if the rotations keep increasing. Similar to that in Stage One, comparisons are also made between the GEOPIG measurements and the FEA results. Shown in Figure 4.29 are the plots of the variation of the pipe internal diameter due to the formation of Wrinkle 1 and Wrinkle 2, i.e., the 1999 wrinkle and the 2005 wrinkle, one from the 2005 GEOPIG measurements and one from the FE analysis. One picture for Wrinkle 2, which was taken at the pipeline field immediately before the installation of the second sleeve is shown in Figure 4.30a. Figure 4.30b shows the profile of Wrinkle 2 obtained from the numerical simulations using FEA package ABAQUS/Standard. Good agreement is reached between the field observations and the FEA results as shown in Figures 4.29 and 4.30. This also further validates the results transfer technique in ABAQUS/Standard in doing the numerical simulation of the wrinkle sleeve repair process through the numerical simulations carried out in Stage One and Stage Two of this study.

4.7.3 Stage Three: Prediction of Possible Behavior of the Pipe Segment Under the Double Sleeve Repair System (DSRS)

Following the detection of the 2nd wrinkle (i.e., Wrinkle 2) at KP 311 of Norman Wells to Zama pipeline in the fall of 2004 through the GEOPIG run, field wrinkle repair work was carried out using collar and sleeve in February 2005. Figure 4.30a is the picture of Wrinkle 2, which was taken before the repair work was undertaken. It can be observed from Figure 4.30a that the crest of Wrinkle 2 is higher than that of the collar used in installing Sleeve 1. This indicates that the amplitude of Wrinkle 2 grew quite large. This also means that the collar used for

repairing Wrinkle 1 can not be utilized in installing the new sleeve (i.e., Sleeve 2). Consequently, at left hand side of Wrinkle 2 as shown in Figure 4.30a, Sleeve 2 was welded to the external surface of Sleeve 1. At the right hand side of Wrinkle 2 as shown in Figure 4.30a, split collars were used to fit in the gap between the internal surface of the sleeve and the external surface of the pipe. The procedures for installing Sleeve 2 and the new collar are the same as those when installing Sleeve 1 in the year of 1999.

1.) Using butt weld welds the split collars together to form a whole collar.

2.) Then using fillet weld welds the collar to the external surface of the pipe.

3.) Using butt weld welds the split sleeve together to form a whole sleeve.

4.) Using fillet weld welds Sleeve 2 to the external surface of Sleeve 1 at one end and to the external of the collar at the other end.

It is the purpose of this stage, Stage Three, to try to predict the possible behavior of the pipe segment under the DSRS using the FE method and hypothetical rotations ate the two ends of the pipe model, provided that the loading conditions in the pipeline field do not have significant change. The welding processes of the new collar and the new sleeve (Sleeve 2) are not simulated in Stage Three. But, similar to that in Stage Two, the residual stresses due to the welding of the collar and the sleeve were modeled by using the technique as described in Section 4.4.5.2.

In Stage Three, the third collar and the 2nd sleeve (Sleeve 2) were put onto the wrinkled sleeved pipe model under the current stress state and configuration. The final deformed configuration of the numerical model at the end of Stage Two, which is shown in Figure 4.30b, becomes the initial configuration of the numerical model in Stage Three. The double sleeve repair system (DSRS) including three collars and two sleeves together with the pipe segment is further loaded with combined internal pressure, axial and further increased rotation values at the two

ends of the pipe model so that the possible behavior of the pipe model under the DSRS could be predicted. Similar to that in Stage Two, the main consideration of the numerical analysis in this stage is to put the new collar (the third collar) and the new sleeve (Sleeve 2) onto the SSRS under the current stress state and configuration in order to represent the actual situation occurred in the field. As before, the results transfer technique in ABAQUS/Standard is used here in carrying out the numerical analysis.

As the yearly based GEOPIG run has not been carried out yet at the time the report is being written, the updated information of the change in curvature along the wrinkled pipe segment, i.e., the change in the rotations at the two ends of the wrinkled pipe segment under the DSRS, is not known. Consequently, hypothetical rotation values were used in Stage Three to study the response of the pipe segment under the DSRS for predictive purposes. A new wrinkle (i.e., the third wrinkle), which corresponds to a rotation value of 0.12 radians at the left end and a rotation value of 0.09 radians at the right end, is shown in Figure 4.31.

4.8 DISCUSSION OF THE RE-ENACTMENT OF THE DSRS

The purpose of the re-enactment of the DSRS at KP 311 of Norman Wells to Zama pipeline is to try to trace back the possible loading history this pipe segment might experience by using the finite element method based on a large amount of valuable data information accumulated through the yearly based GEOPIG tool run along the line. The available database provides significant input in building the numerical model and in processing the data for carrying out this study. In addition, the criteria for the re-enactment of the DSRS at KP 311 were set up based on the field GEOPIG measurements, against which the FEA results are compared. The sequential activities that occurred in the field for the pipe wrinkle sleeve repair process are closely simulated through the numerical analyses. Excellent match between the field GEOPIG measurements and the FEA results was obtained at the first two stages of the re-enactment of the DSRS by using the FEA package ABAQUS/Standard.

As one of the primary loads, internal pressure plays a vital role in the wrinkling behavior of the pipelines. The effect of the internal pressure on the formation of the local wrinkle was also observed during the pipe full scale laboratory tests (see, for example, Mohareb (1994), Yoosef-Ghodsi (1994), Dorey et al (2001)) and was discussed in Section 3.2.4 of Chapter 3. Due to the fluctuating nature of the internal pressure during the pipeline operations, different loading regimes of the internal pressure are tested in this project along with the secondary axial force (SAF) due to soil movement in order to determine the possible loading combinations that provides the best match to the shape and the magnitude of Wrinkle 1 as measured by the 1999 GEOPIG run. In total, 6 internal pressure values were tested in this study based on the information provided by Enbridge. The variations of pipe internal diameter due to the formation of the local wrinkle from the numerical analysis are compared with those measured by the field GEOPIG tool run as shown in Figures 4.24, 4.25 and 4.26, respectively. It can be seen from the above three figures that the solution based on the loading regime P4.8C4.3 gives the closest match to the 1999 GEOPIG measurements. Consequently, the final configuration of the pipe numerical model from solution P4.8C4.3 is used as the initial configuration of the numerical model in conducting the numerical simulations for the SSRS in Stage Two. Similarly, the final configuration of the numerical model of Stage Two forms the initial configuration of Stage Three for the re-enactment of the DSRS.

Comparing the screen shot from 1999 GEOPIG measurements at KP 311 in Figure 4.18 and the screen shot from 2005 GEOPIG measurements shows that the magnitude of the first wrinkle did not change after it was encased by the sleeve. The same observations can also be seen from Figure 4.28, the comparison of the variation of the pipe internal diameter between the FEA results and the 1999 GEOPIG measurements, and from Figure 4.29, the comparison of the pipe internal diameter between the FEA results and the 2005 GEOPIG field measurements. These provide strong support of the effectiveness of the repairing sleeve in inhibiting the increase of the wrinkle magnitude.

The formation of a wrinkle in the pipe segment indicates the yielding of the pipe material. The collars and sleeves were installed under stress free states. Consequently, any further loading applied to the collar, sleeve and the wrinkled pipe assembly will be mainly carried by the sleeve as the sleeve is in the elastic state. Another observation is that a new wrinkle is always developed offset from the end of the collar after certain increase of rotations at the two ends of the pipe segment, which represent the further soil movements.

Because the pipe wrinkle sleeve repair process is a sequential activity, several ABAQUS runs by three stages are required in order to complete the re-enactment of the DSRS at KP 311. The moment vs. curvature curves are correlated between different stages. The final configuration of the pipe numerical model at the end of one stage becomes the initial configuration of the numerical model for the next stage. Figure 4.32 shows the complete path of the moment vs. curvature curve from Stage One, i.e., the formation of Wrinkle 1, to Stage Two, the formation of Wrinkle 2 and to Stage Three, i.e., the formation of possible Wrinkle 3 assuming that the loading combinations will not change significantly.

After reaching the first peak value in Figure 4.32, the moment carrying capacity of the pipe segment starts to drop with increased curvatures due to the formation of a local wrinkle. Point A in Figure 4.32 is the point at which Sleeve 1 was installed. This corresponds to the end of Stage One, the creation of the SSRS (single sleeve repair system). The moment carrying capacity of the pipe segment under the SSRS starts to increase with increased curvature values as the plastically deformed portion of the pipe segment is encased by the sleeve, which was installed in the elastic state. At certain curvature value, the moment carrying capacity of the pipe segment under the SSRS reaches the second peak. Further increasing the curvature initiates a new wrinkle in the pipe segment, i.e., the moment capacity starts to drop again. Point B in Figure 4.32 is the point at which the second sleeve was installed. This corresponds to the end of Stage Two, the generation of the

DSRS (double sleeve repair system). The moment carrying capacity of the pipe segment under the DSRS starts to increase again with increased curvature values because of the installation of Sleeve 2. At the time of carrying out this project, no new information is available about the field pipe configuration. Hypothetical curvature values are assumed based on field GEOPIG data records for the continuing increased curvatures and applied to the pipe model until the third peak in the moment vs. curvature curve is reached and passed. A new wrinkle (i.e., the third wrinkle) could be developed with the further increased curvature values. By the end of Stage Three of the numerical analysis, the rotational capacity of the pipe segment could be doubled from the initiation of the first wrinkle to the initiation of the third wrinkle as shown in Figure 4.32. Consequently, the residual life of the original pipeline after the formation of the first wrinkle at KP 311, the wrinkle site, is extended significantly by using the sleeve repairing method.
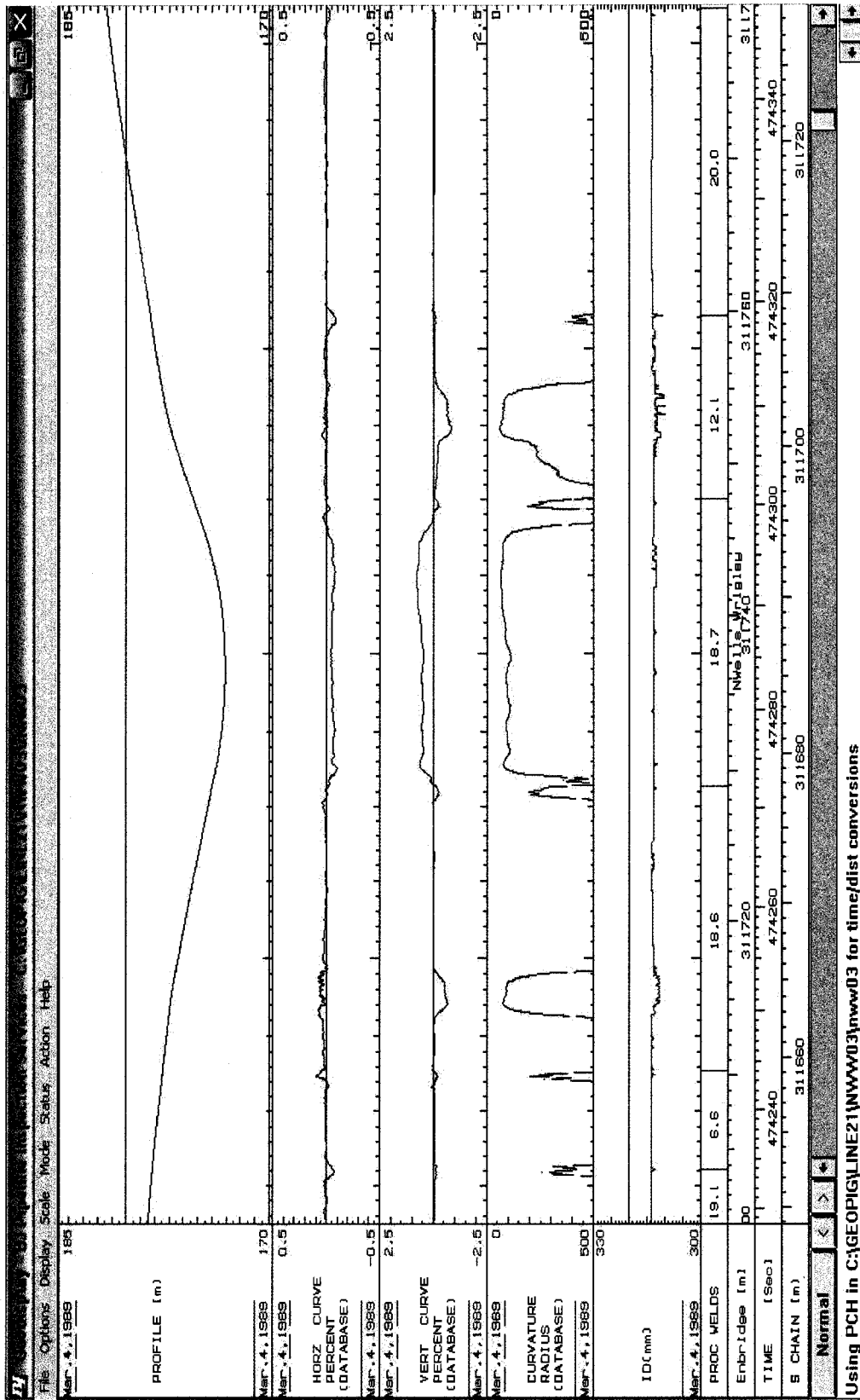
Figure 4.1 1989 GEOPIG Plot at the Wrinkle Location

Figure 4.2 1998 GEOPIG Plot at the Wrinkle Location
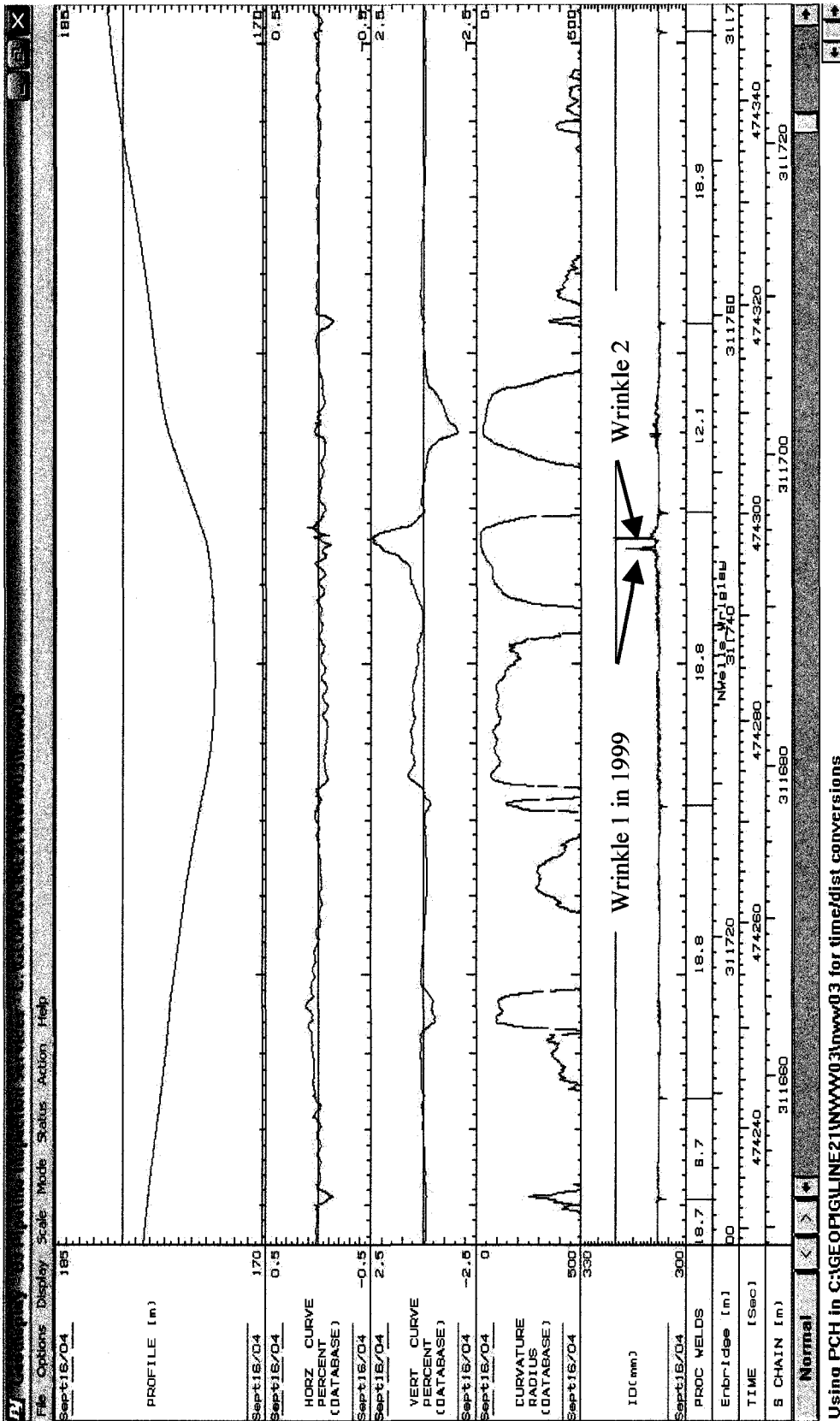
Figure 4.3 2004 GEOPIG Plot at the Wrinkle Location
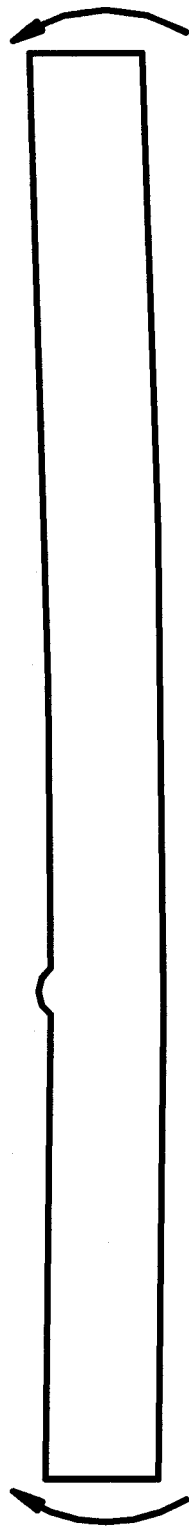
(a) Schematic of Stage One (Simulation of 1999 Wrinkle)
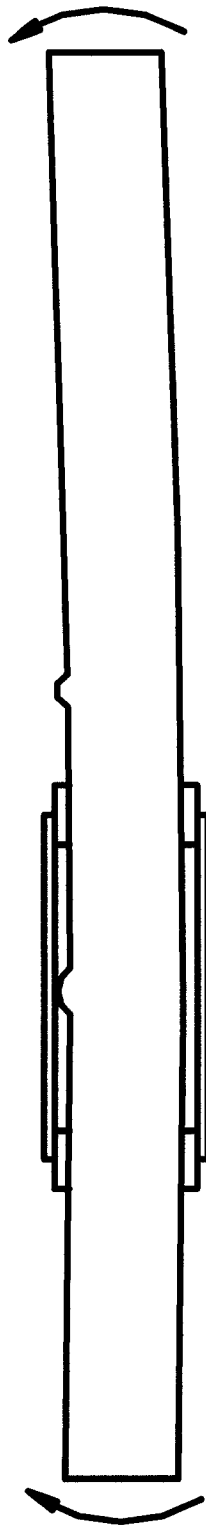
(b) Schematic of Stage Two (Simulation of 2005 Wrinkle)
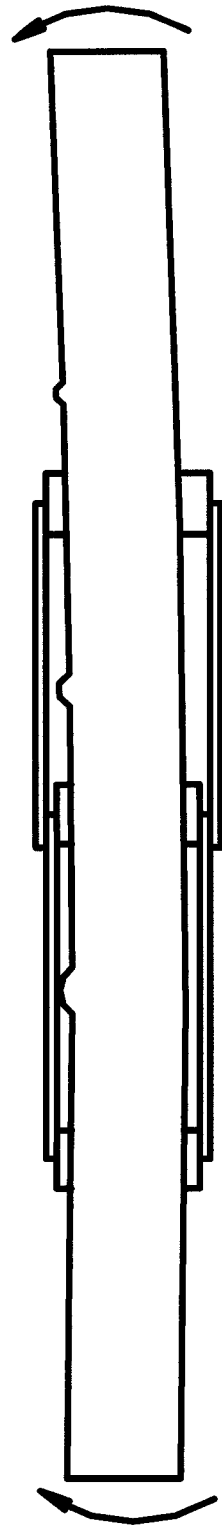
(c) Schematic of Stage Three (Prediction of Possible the Third Wrinkle)

Figure 4.4 Schematics of the Stages Used in Doing the "Re-enactment" of the DARS
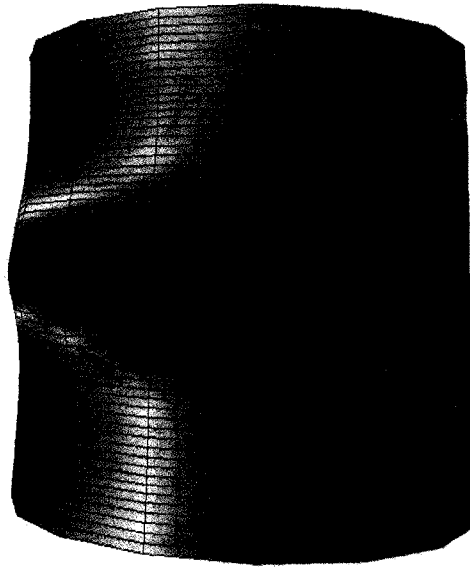
Figure 4.5 Wrinkle 1 from GEOPIG Record

97

Figure 4.6 Picture of Wrinkle 2 Taken from Pipeline Field
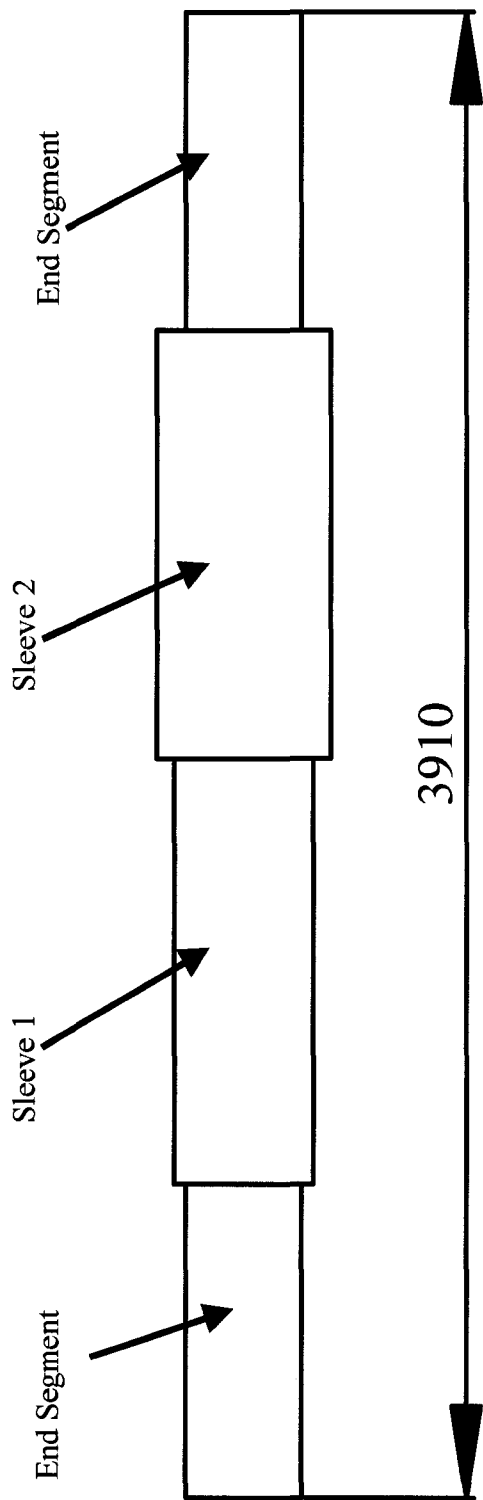
Figure 4.7 Schematic of the Principal Components of the DSRS
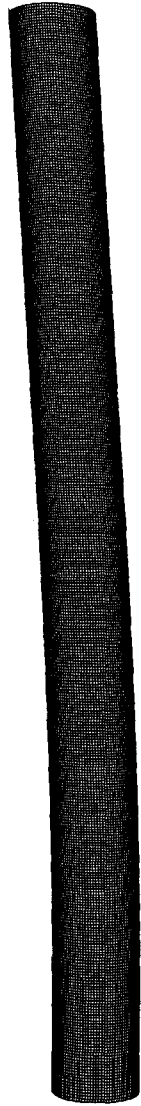
Figure 4.8 Mesh for the Pipe Used in This Study
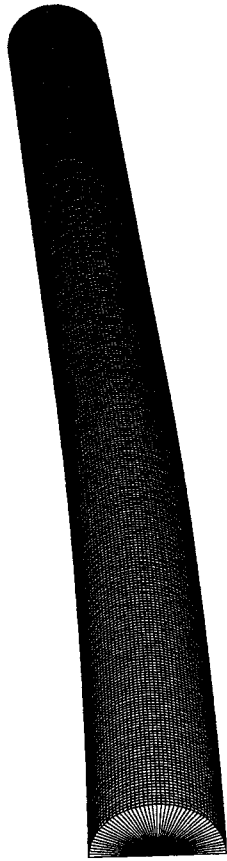
Figure 4.9 3D view of the Pipe Model
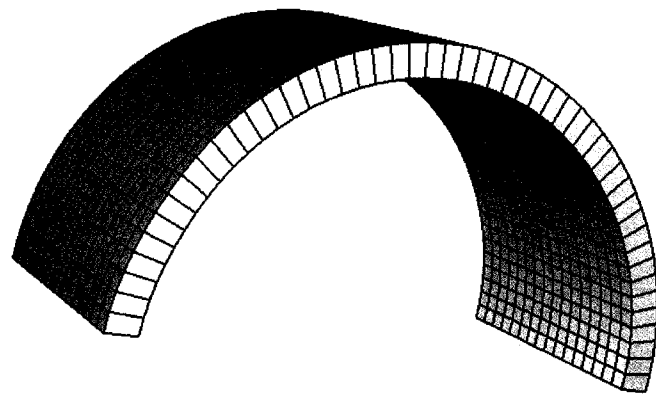
Figure 4.10 Mesh of the Collar for the First Sleeve
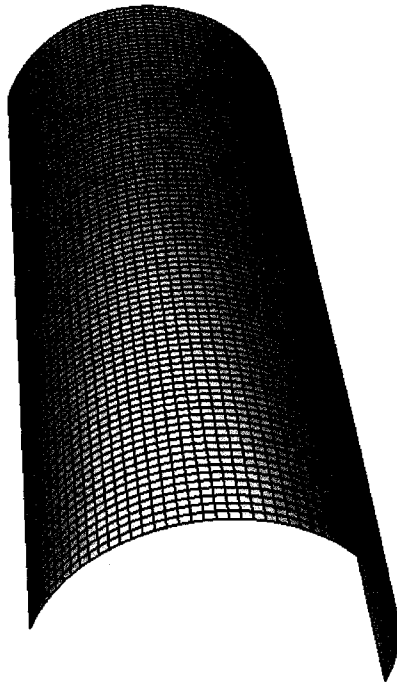
Figure 4.11 Mesh of the First Sleeve Used in This Study
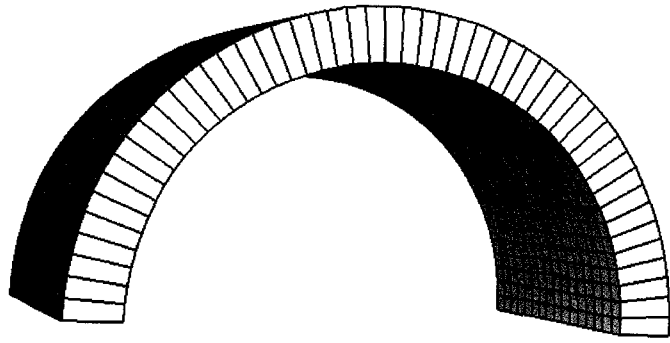
Figure 4.12 mesh of the Collar Used for the Second Sleeve
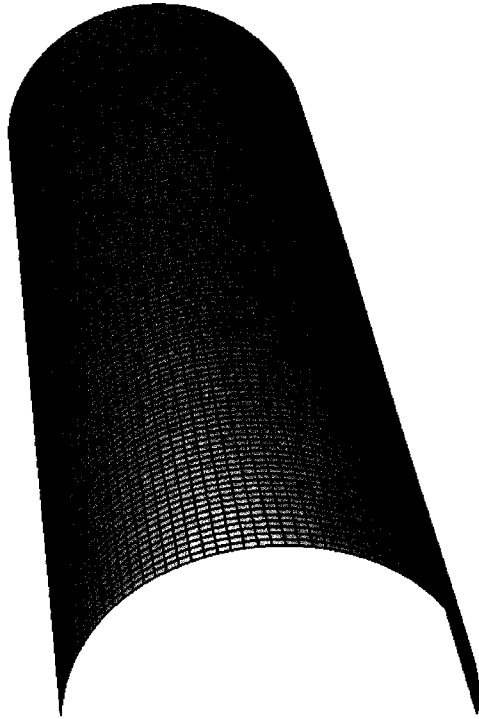
Figure 4.13 Mesh for the Second Sleeve Used in This Study
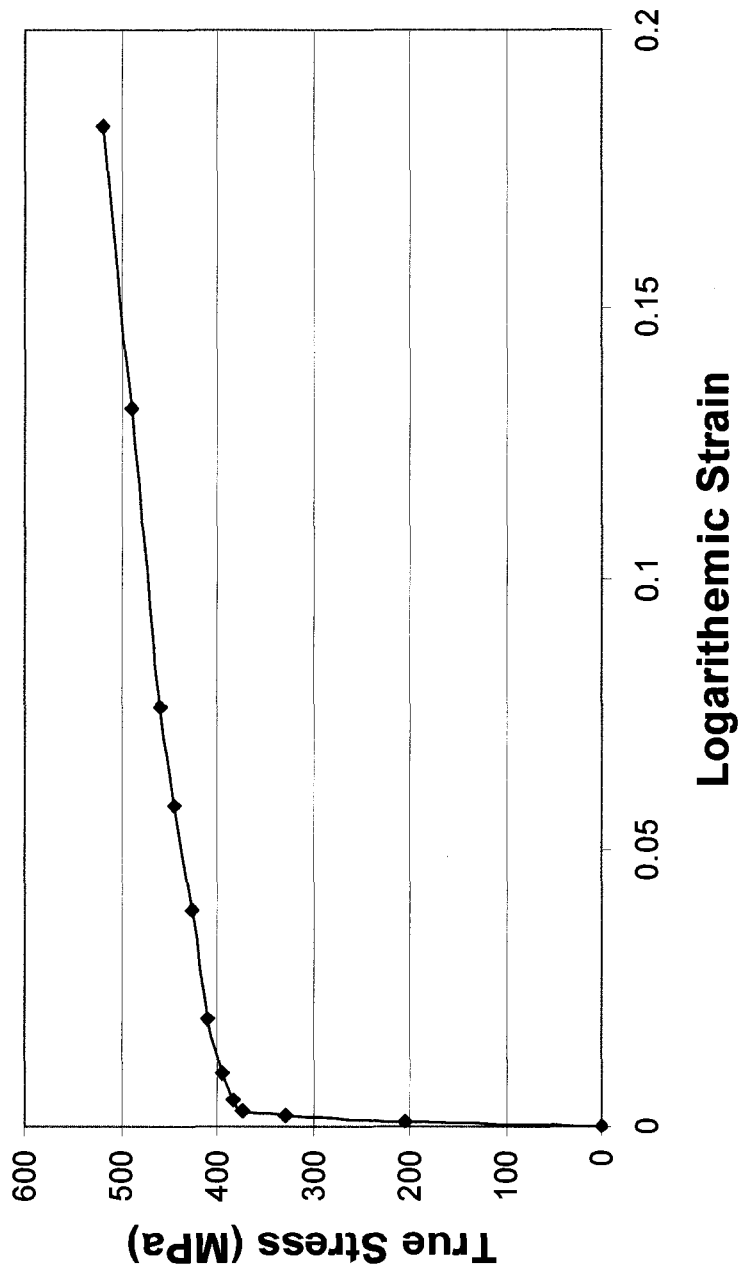
Figure 4.14 The True Stress vs. True Strain Curve for Pipe Steel and Sleeve Steel
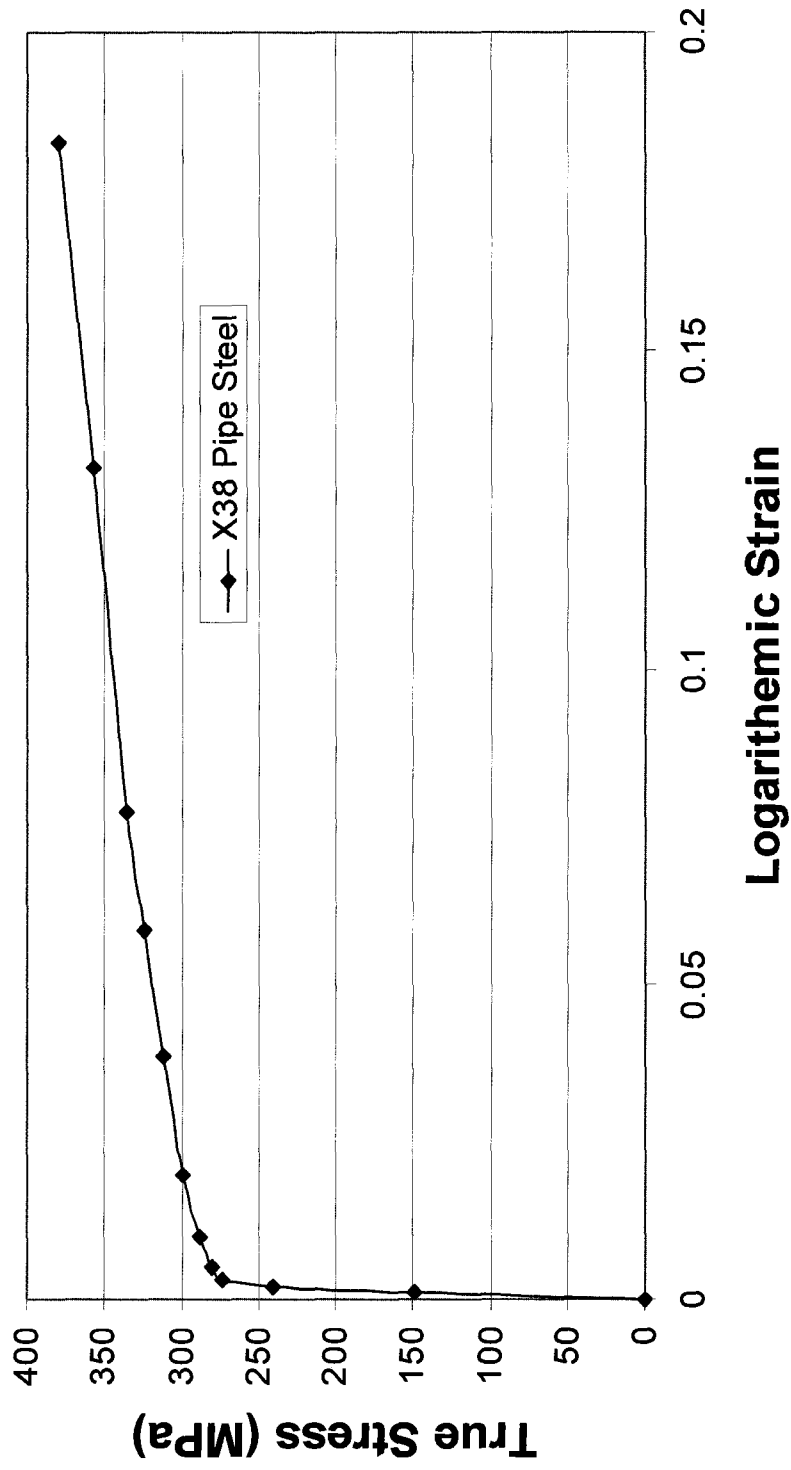
Figure 4.15 Assumed True Stress vs. True Strain Curve for Collar Steel
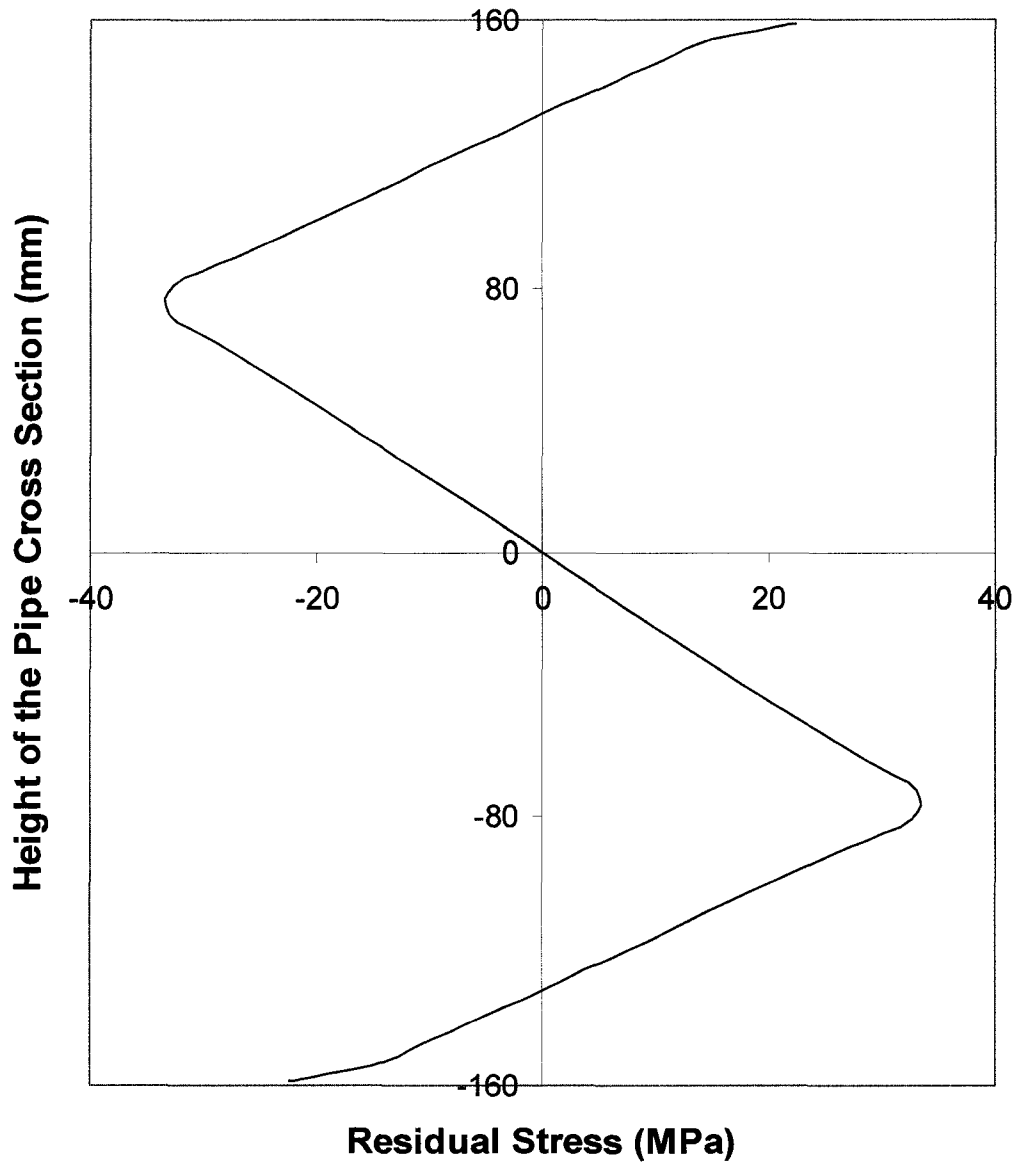
Figure 4.16 Typical Distribution Pattern of the Longitudinal Residual Stresses along Pipe Cross Section for a Curvature Value
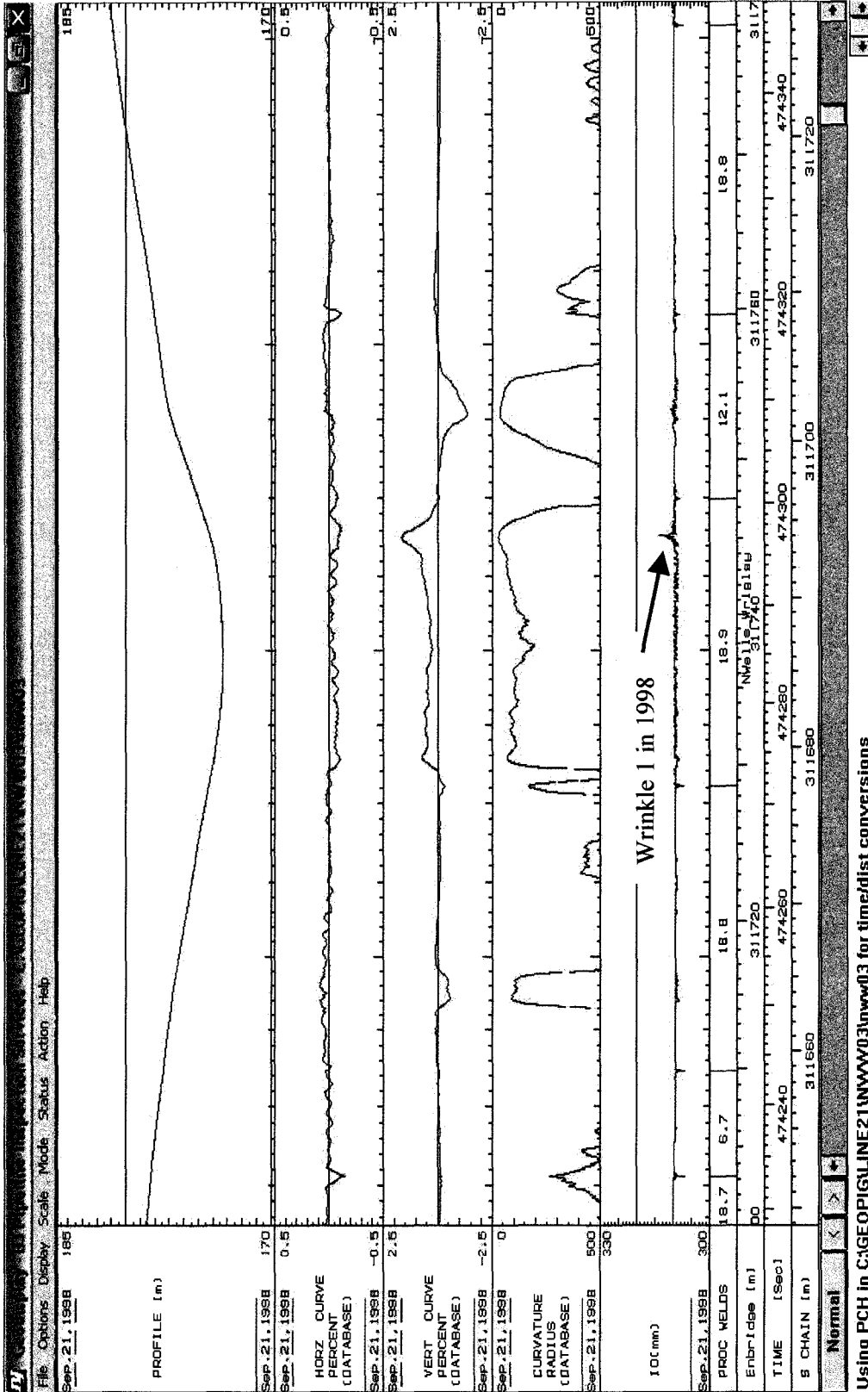
Figure 4.17 1998 GEOPIG Plot for Wrinkle 1
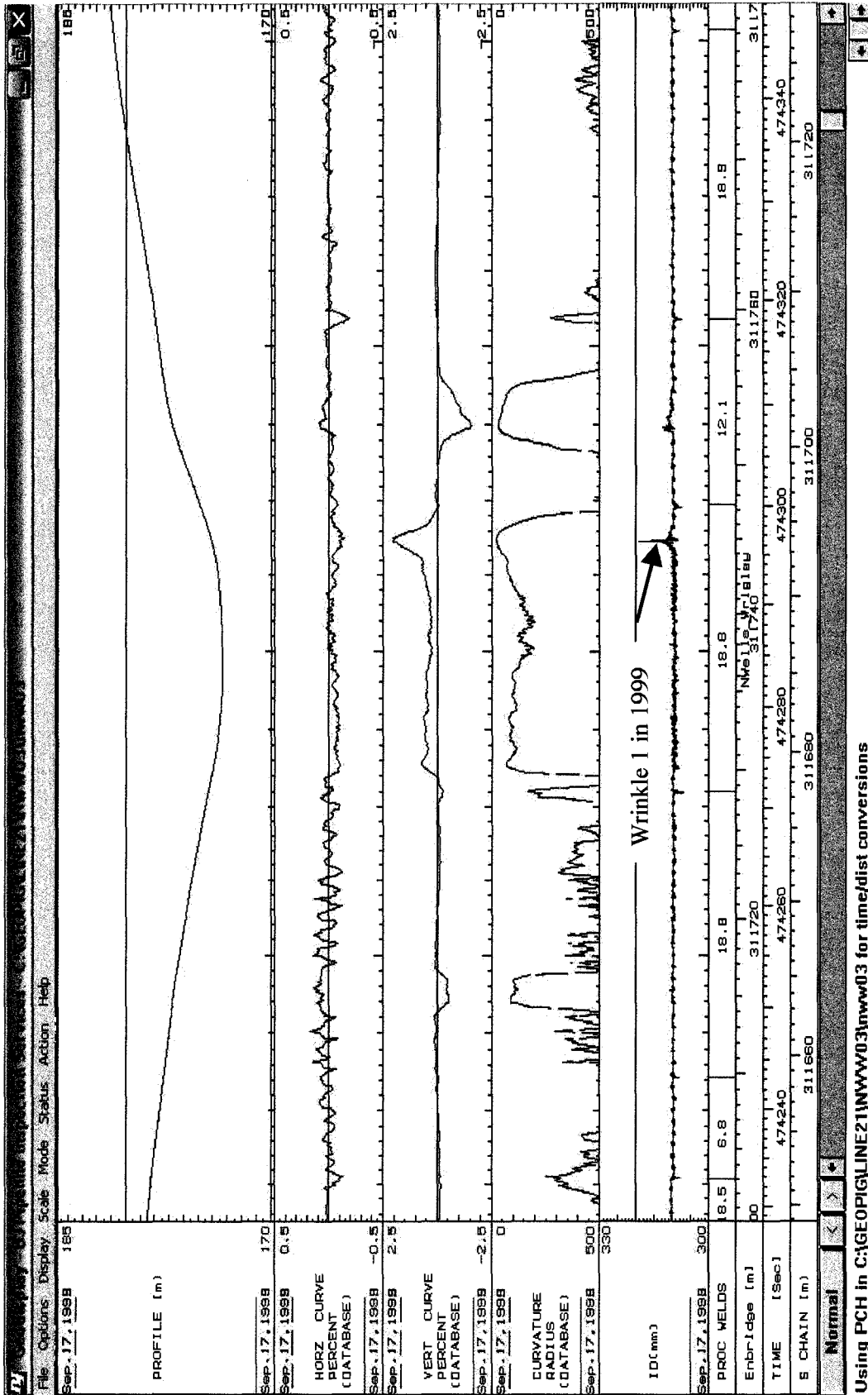
Figure 4.18 1999 GEOPIG Plot for Wrinkle 1
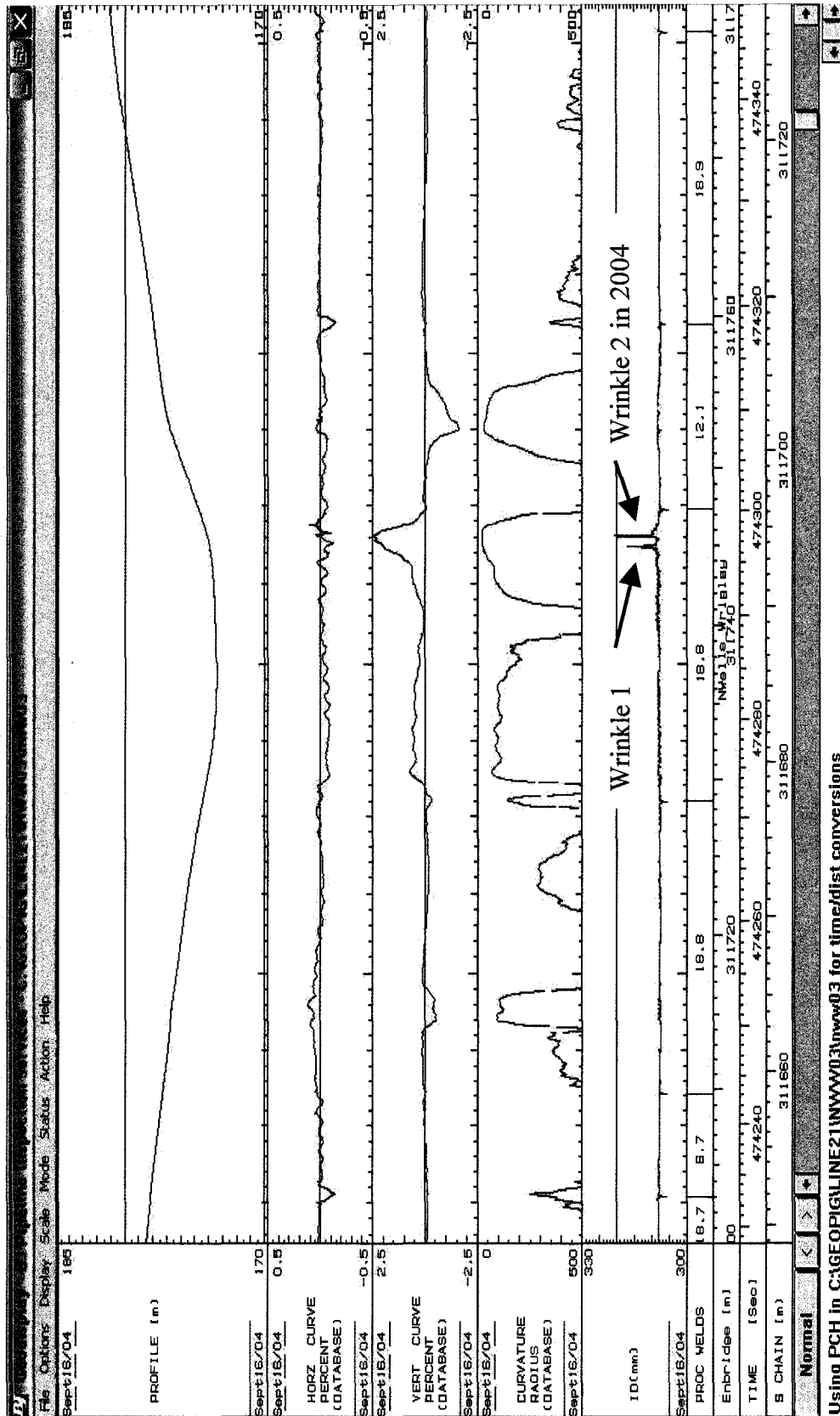
Figure 4.19 2004 GEOPIG Plot for Wrinkle 1 and Wrinkle 2

111
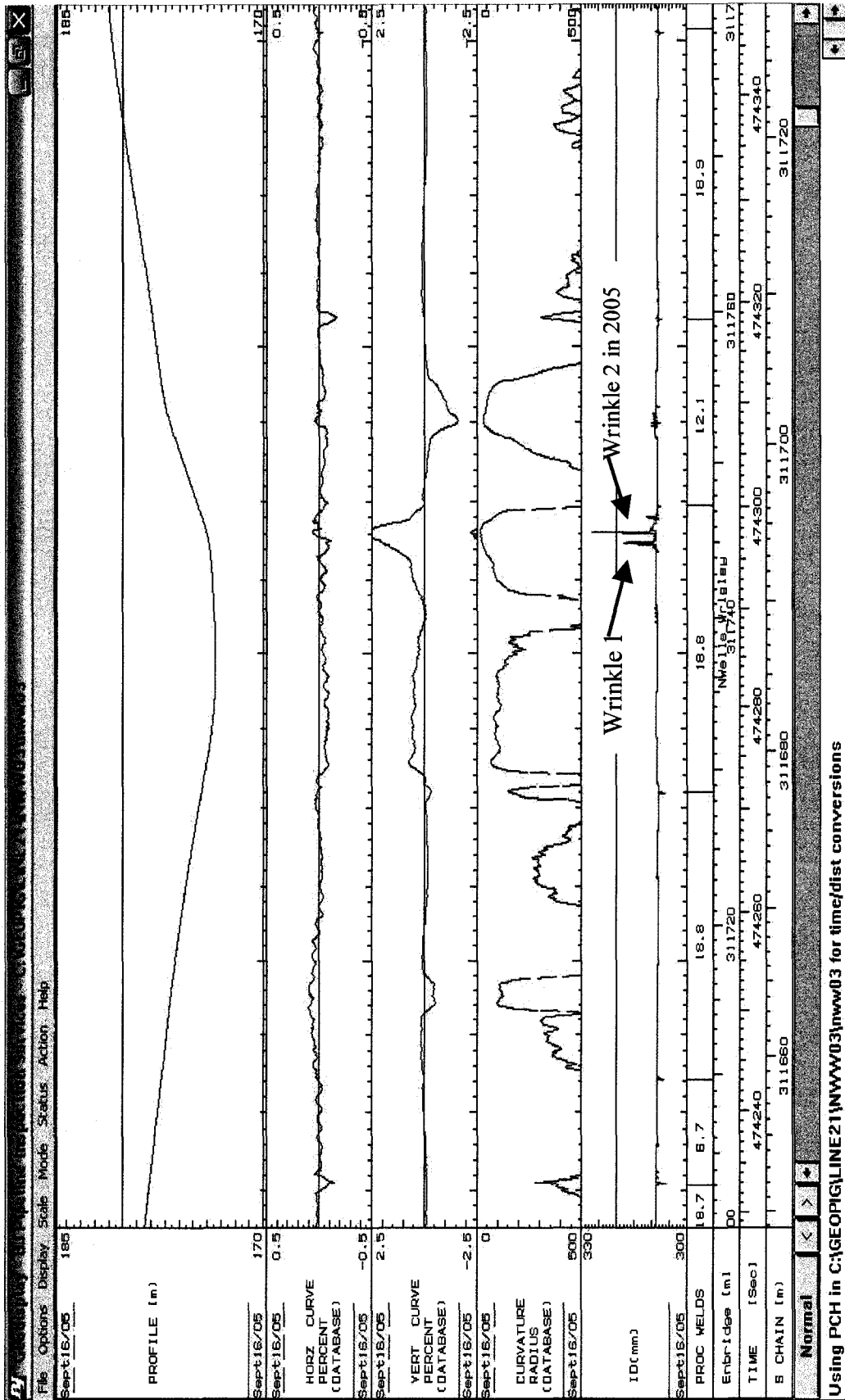
Figure 4.20 2005 GEOPIG Plot for Wrinkle 1 and Wrinkle 2

112
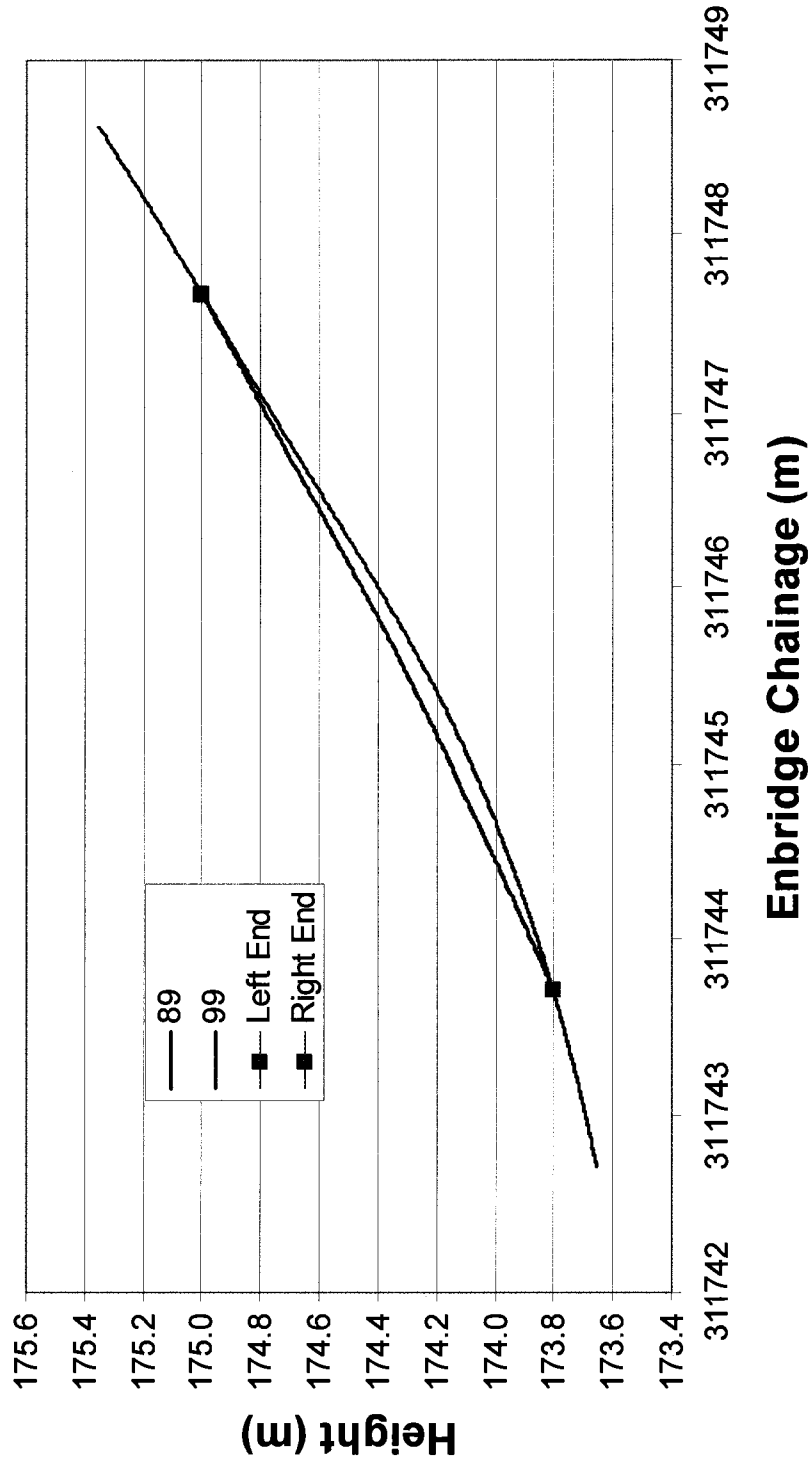
Figure 4.21 1999 Pipe Configuration with Respect to 1989 Pipe Configuration (Original Configuration)
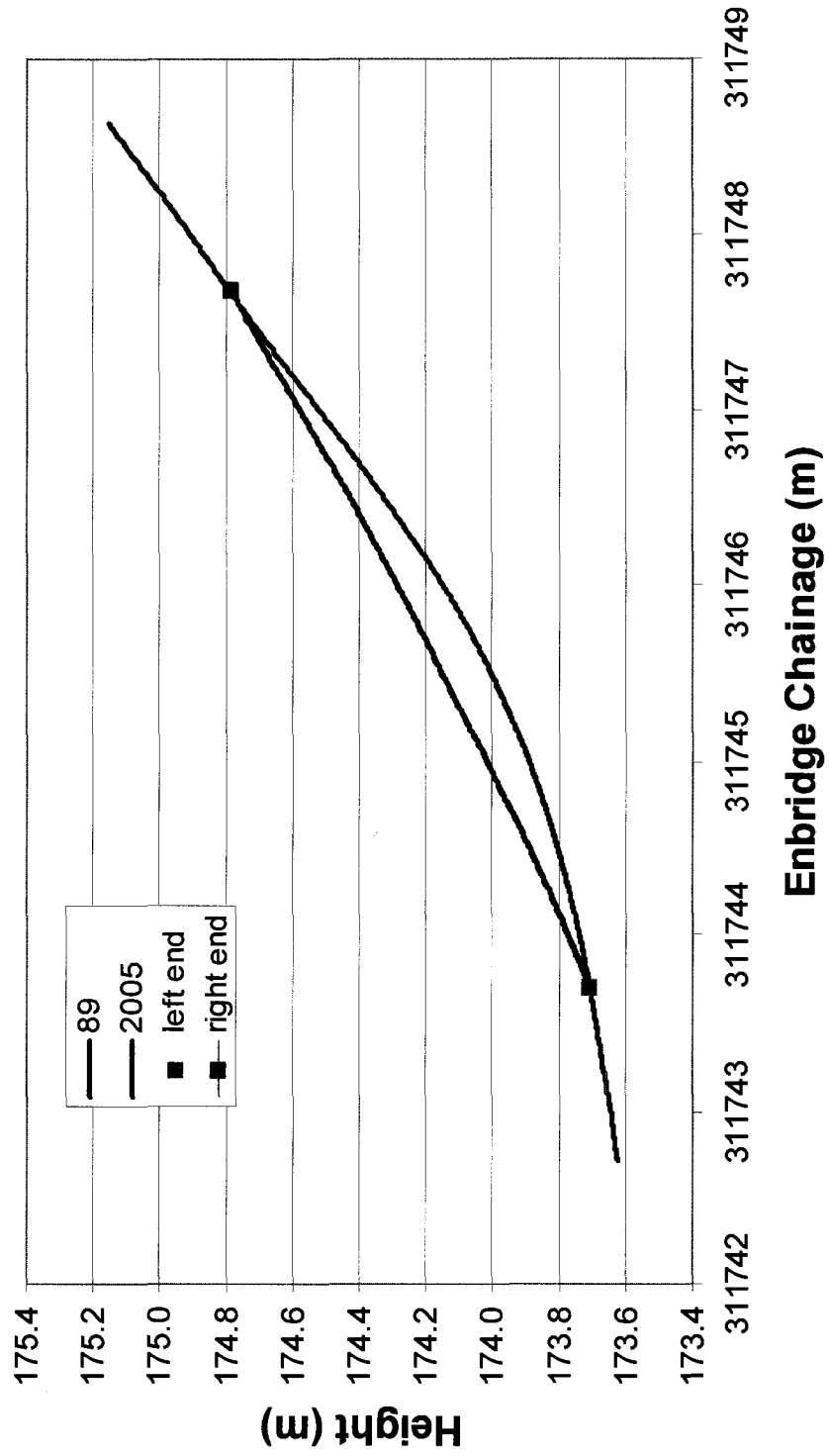
Figure 4.22 2005 Pipe Configuration with Respect to 1989 Pipe Configuration (Original Configuration)

Figure 4.23 Secondary Axial Force (SAF) vs. Axial Displacement Curve from Pipe Model in This Study

Comparison of Pipe Internal Diameter Variation between GEOPIG Measurement and FEA results
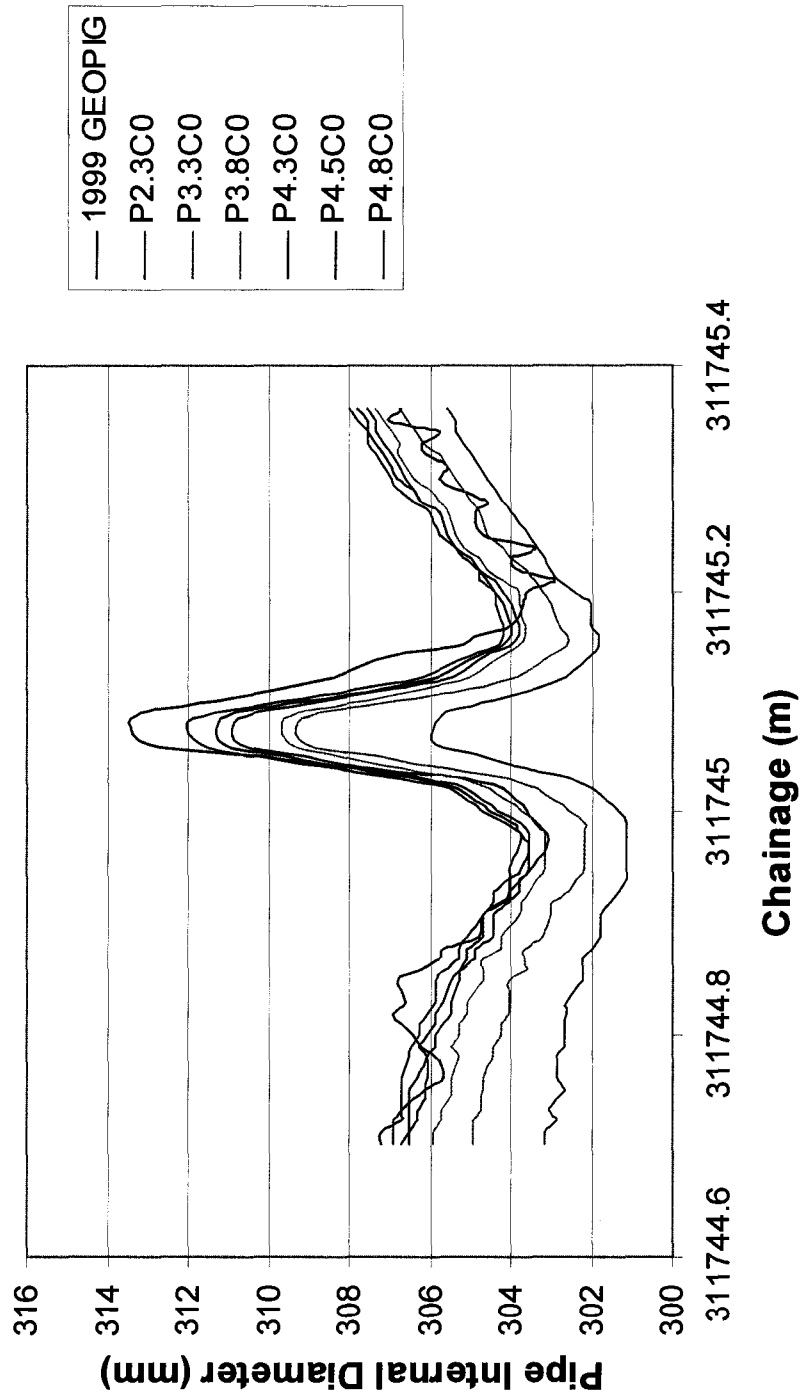
Figure 4.24 Comparison of GEOPIG Measurement and FEA Results with Different Internal Pressure values and Zero SAF

Comparison of Pipe Internal Diameter Variation Between GEOPIG Measurement and FEA Results
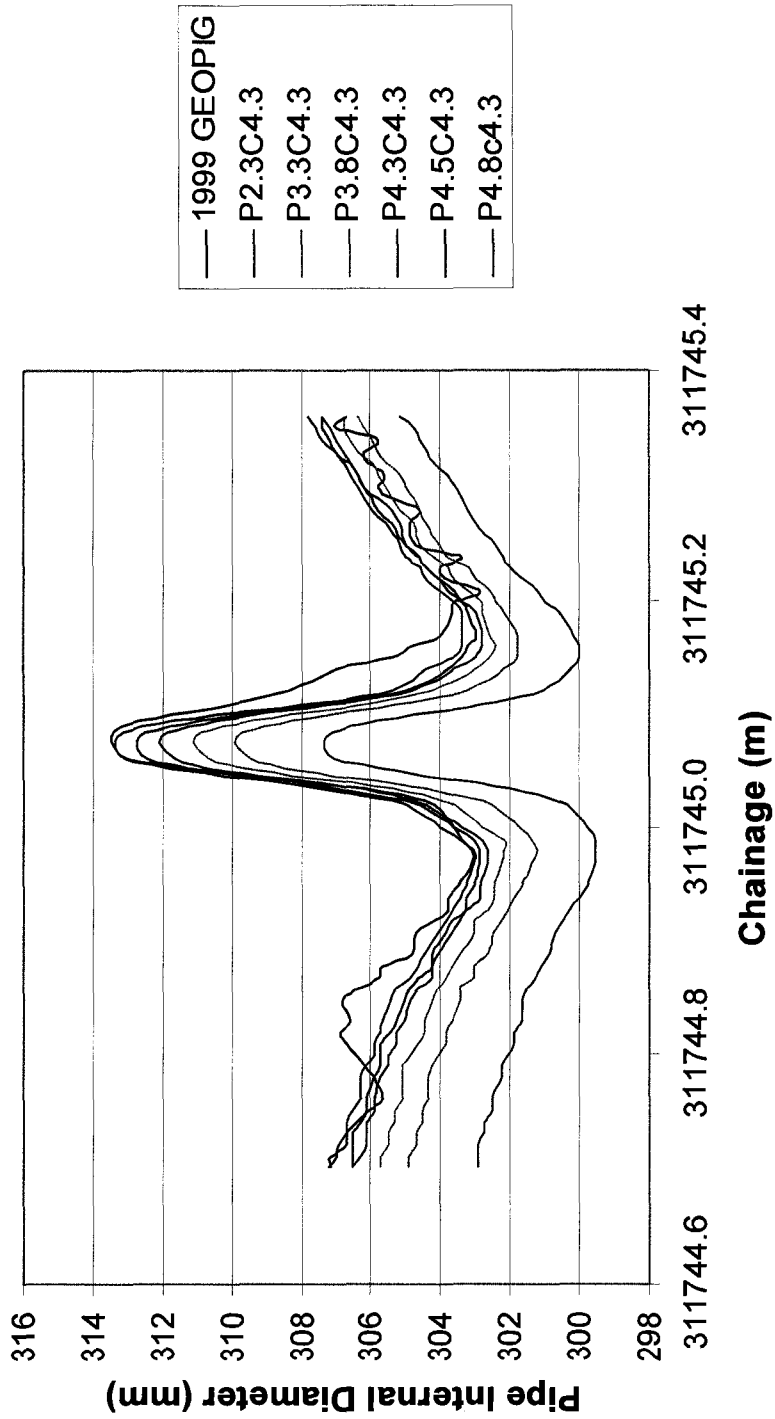
Figure 4.25 Comparison of GEOPIG Measurement and FEA Results with Different Internal Pressure values and 4.3% of SAF

117
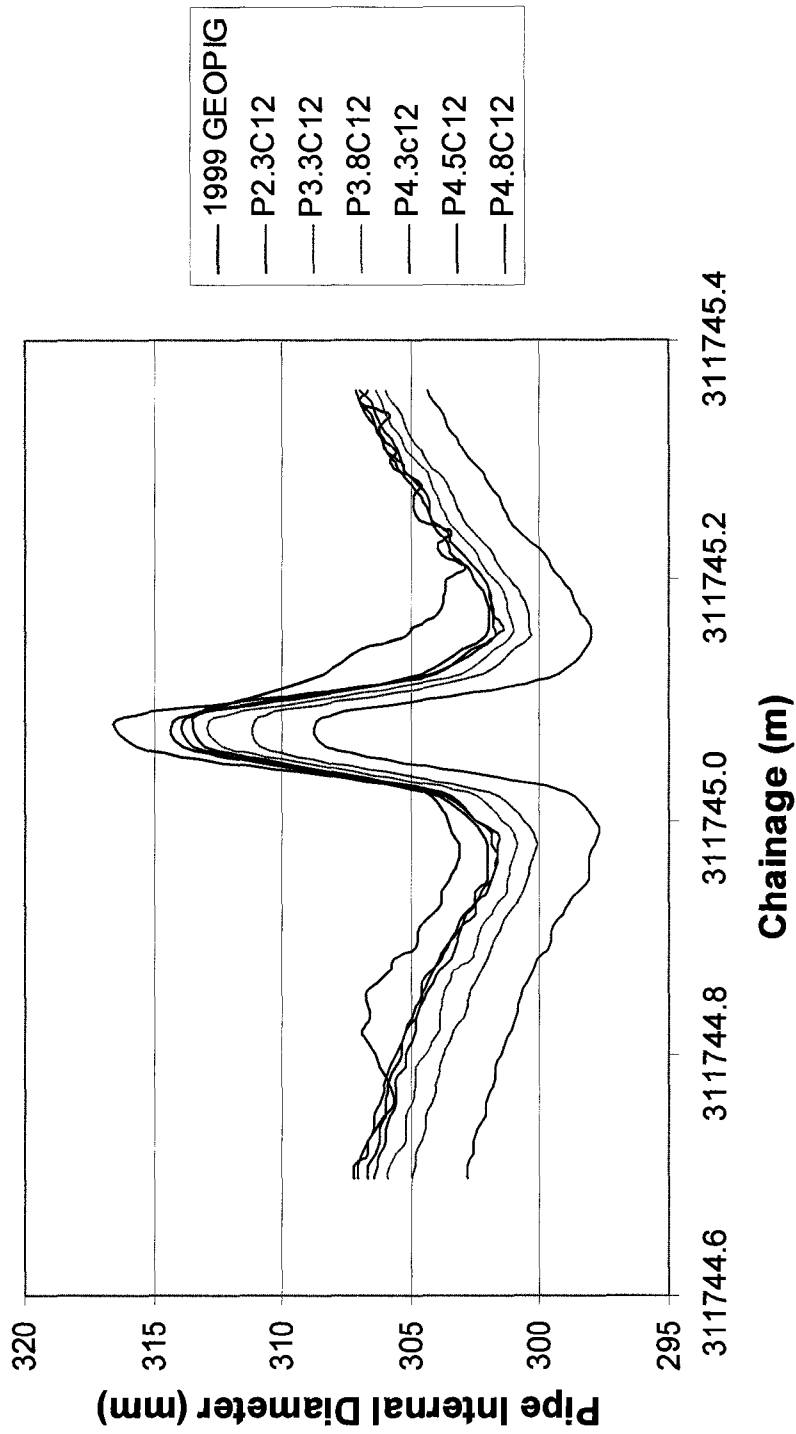
Figure 4.26 Comparison of GEOPIG Measurement and FEA Results with Different Internal Pressure values and 12% of SAF

118
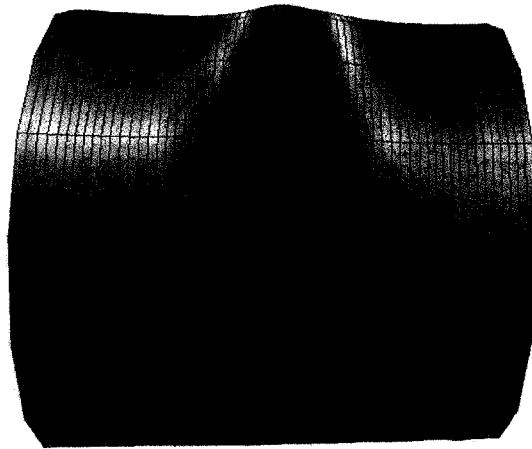
(a) Wrinkle 1 from GEOPIG Run
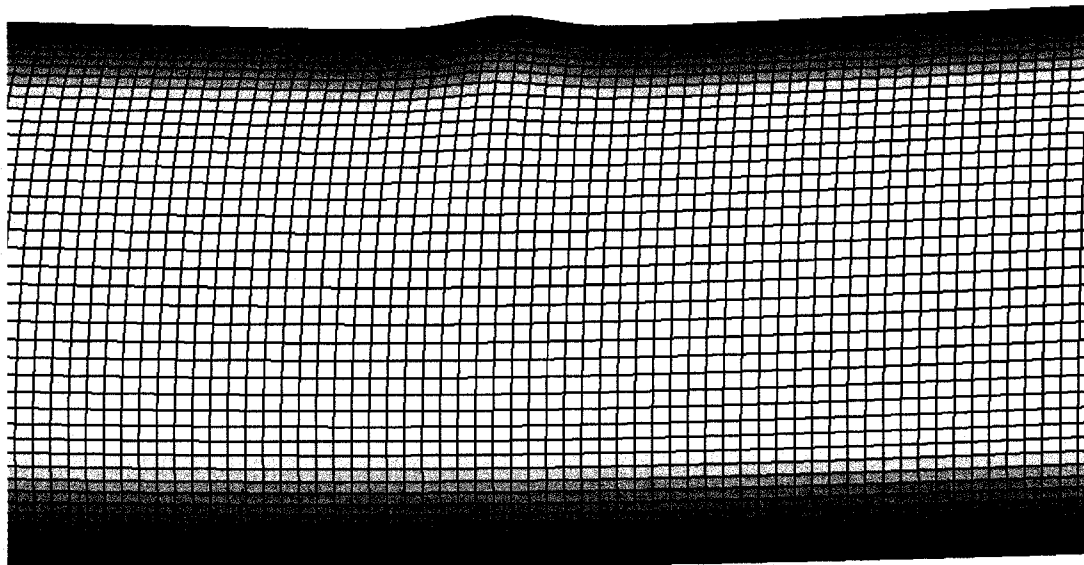
(b) Wrinkle 1 from FEA

Figure 4.27 Comparison of Wrinkle 1 from GEOPIG Record and FEA Result

119
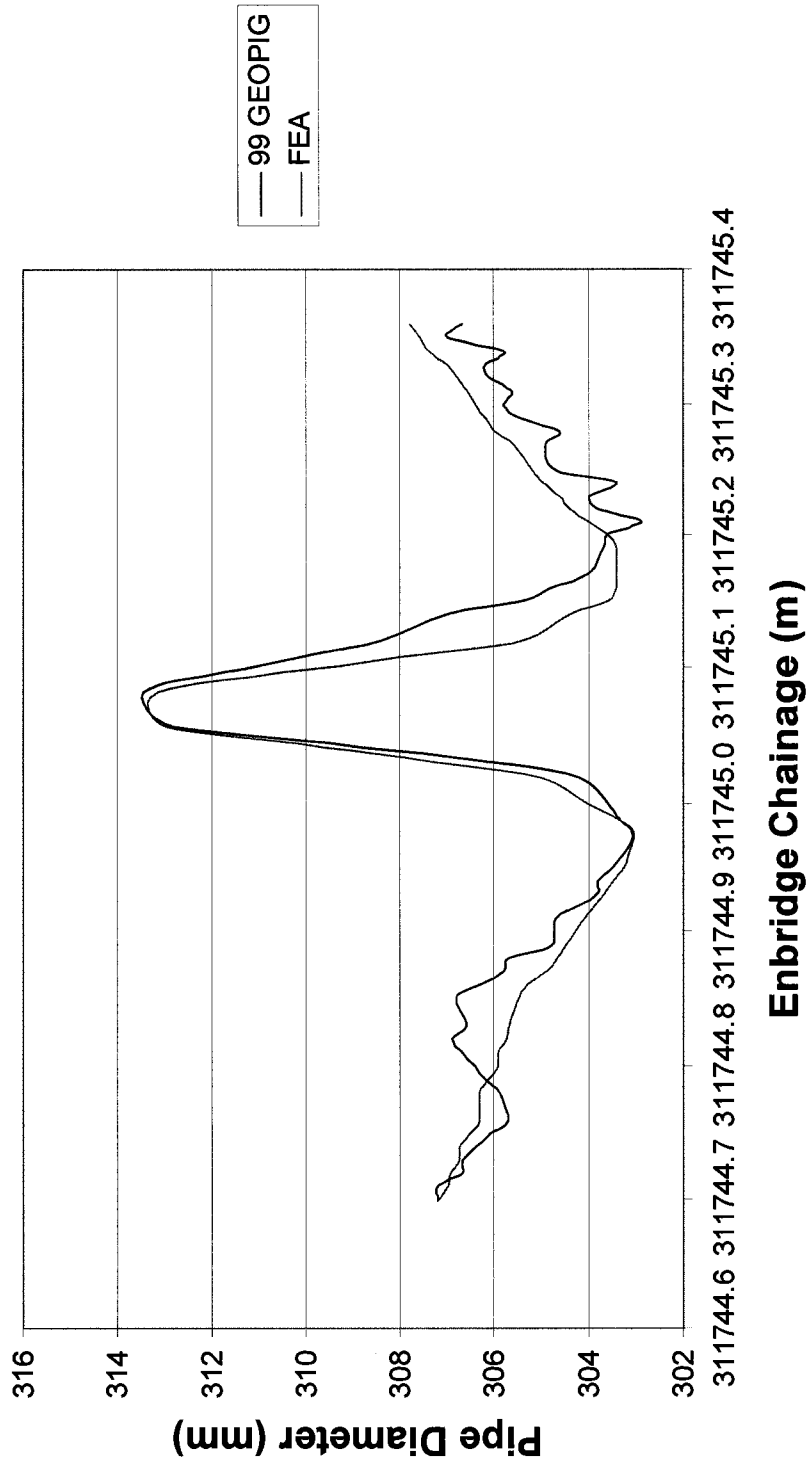
Figure 4.28 Comparison of Variation of Pipe Internal Diameter From FEA and GEOPIG Measurement

Comparison of the Variation of Pipe Internal Diameter between FEA and GEOPIG measurement
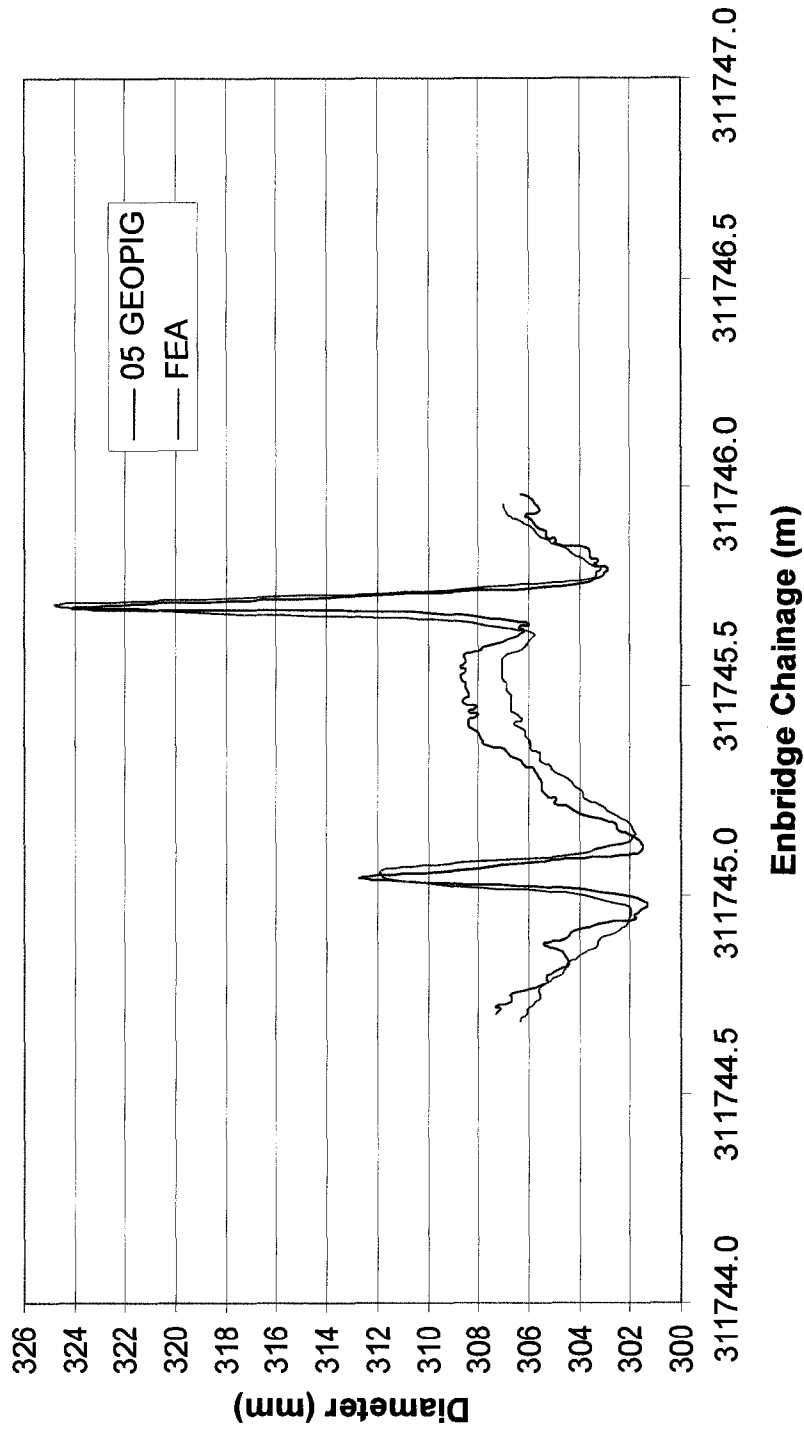
Figure 4.29 Comparison of the Variation of Pipe Internal Diameter between FEA Result and GEOPIG Measurement
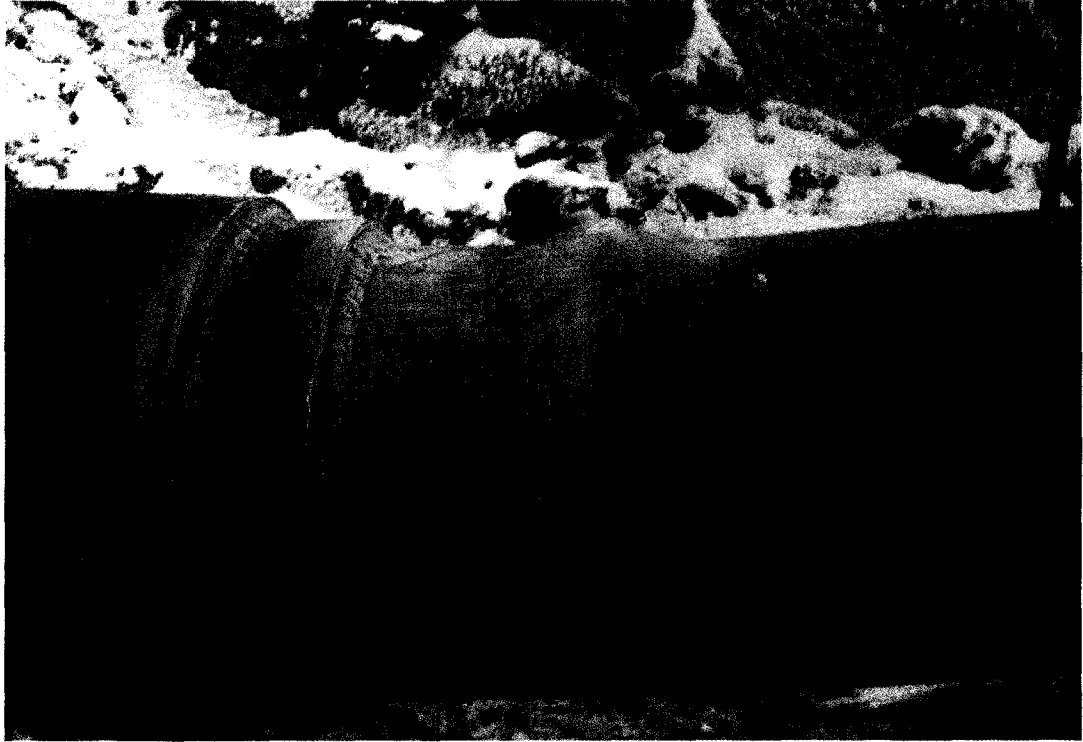
(a) Picture of Wrinkle 2 Taken from Pipeline Field
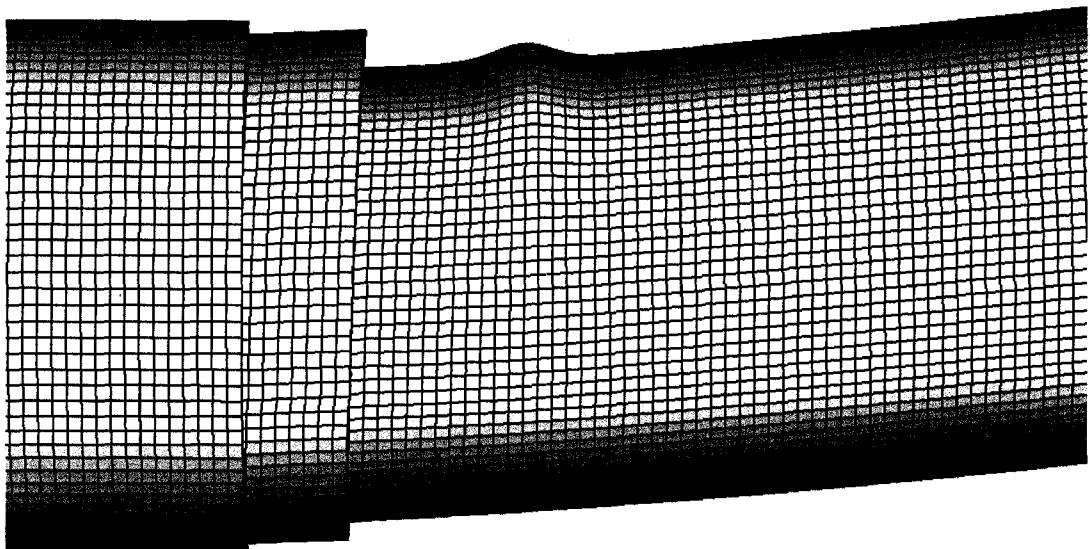
(b) Wrinkle 2 from Finite Element Simulation

Figure 4.30 Comparison Between GEOPIG Measurement and FEA Results
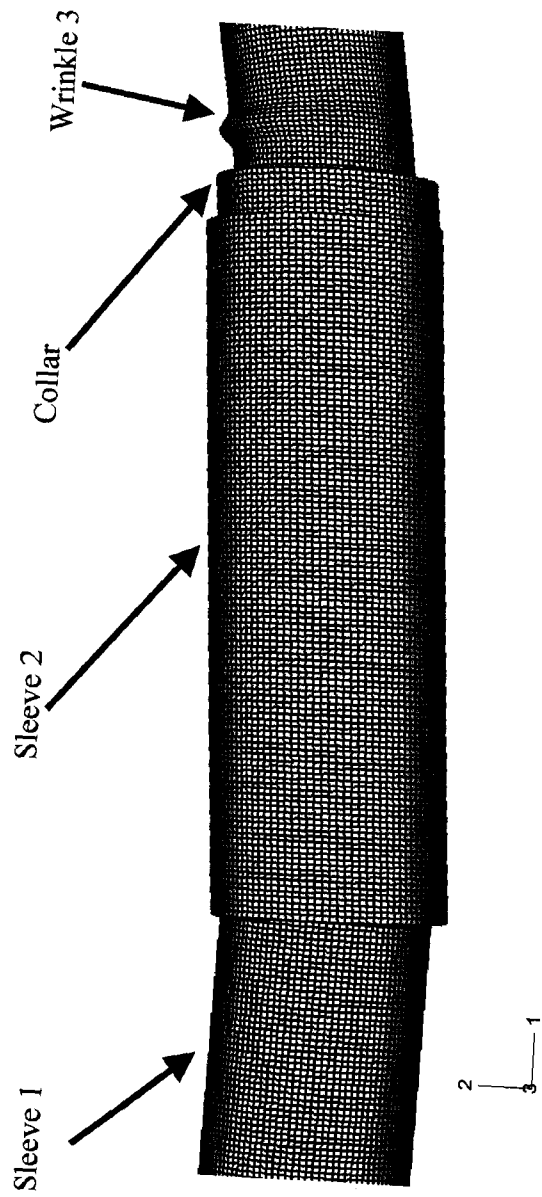
Figure 4.31 Close View of Wrinkle 3 with Collar and Sleeve Components

Figure 4.32 Bending Moment vs. Curvature Curve from Stage One ("Pipe Only" Model) to Stage Two (SSRS) to Stage Three (DSRS)

124

CHAPTER 5 PARAMETRIC STUDY

5.1 INTRODUCTION

From the case history study of the wrinkle sleeve repair which was conducted in a pipeline field as presented in Chapter 4, it can be seen that using the sleeves to repair the wrinkles in the pipeline field is an effective and economical method to deal with pipeline field local wrinkles. On the other hand, by referring to Figure 4.35 of the moment vs. curvature curve for the response of the pipe wrinkle sleeve repair system, one may ask the question "Can the wrinkle sleeve repair technique perform better? In other words, Can the rotational capacity of the sleeved wrinkled pipe segment be further improved so that the time intervals between the repairing sleeve installations can be further extended?" In addition, only the behavior of pipe wrinkling under sleeve repair for NPS12 pipe with D/t = 51 has been studied so far. It would be beneficial to expand the study results to pipes of other diameters with different D/t ratios under different loading combinations, i.e., generalizing the application of the wrinkle sleeve repair study results. Therefore a full spectrum parametric study, which reflects a variety of loading conditions and geometric configurations for pipe wrinkle sleeve repairs, will be performed.

As described in Chapter 4, very fine mesh with 10 mm by 10 mm element size was used in creating the numerical model for the re-enactment of the field wrinkle sleeve repair based on field GEOPIG measurements. In order to reduce the CPU running time but with the essential behavior of the wrinkle sleeve repair system still being captured, it was decided to conduct a mesh study first. The purpose of the mesh study is to determine a suitable mesh size for use in the following parametric study. This chapter presents the mesh study first, which was conducted as part of the project, then presents the details of the parametric study of pipe wrinkle sleeve repair system carried out thereafter. For simplification and generalization purposes, a straight pipe model is used as the initial pipe configuration in doing the mesh study and the parametric study. Because using the sleeves to repair wrinkles in the

pipeline field is not a widely used practice in the pipeline industry and this technique has not been specified or accepted in the pipeline code such as CAN/CSA-Z662, no attempt was made to develop a design equation for use in quantitively determining the parameters of the sleeve and the collar used in wrinkle repair in this project. But general guidelines are given in selection of the parameters of the sleeve and the collar based on the results of the parametric study.

5.2 MESH STUDY

Mesh size selection is an integral part of the numerical analysis using FEA software as the size of the mesh determines not only the accuracy of the analytical results but also the cost of the numerical analysis. A numerical model using too large an element size (i.e., coarse mesh) will have difficulty in convergence and in predicting the actual behavior of the structure. A numerical model using too small an element size (i.e., fine mesh) will take a much longer time in running the numerical analysis. This was observed in conducting the re-enactment of the field wrinkle sleeve repair as described in Chapter 4. Fine mesh with 10 mm by 10 mm element size was used in creating the models at that time. Consequently, there is a significant increase in the cost per ABAQUS job run. In order to choose a suitable element size, which provides essential prediction of the behavior of the pipe wrinkling and wrinkle sleeve repair but with reduced CPU processing time, it was decided to carry out a new mesh study as part of the parametric study.

5.2.1 Pipe Parameters Used in the Mesh Study

The pipe parameters used in the mesh study are the same as those mentioned in Chapters 3 and 4. To reiterate here, pipe outside diameter OD = 323.85 mm, pipe wall thickness t = 6.35 mm and pipe steel grade X52 with SMYS = 359 MPa were used here. In addition, the stress vs. strain curve obtained by Mohareb et al (1994) is still used when conducting the mesh study. Based on the consideration that a long enough sleeve will be added to the pipe model during the parametric study, the length of the pipe model is determined to be around 3660 mm, which accommodates a 5D long sleeve in the middle and two 3D long end segments.

5.2.2 The Criteria Used in the Selection of the Mesh Sizes

Two criteria are used in the selection of the size of the different meshes for the numerical models. The "first criterion" in selecting the element size for the FE model is the element aspect ratio. The aspect ratio of the element is defined as the ratio of the larger dimension of the element to the smaller dimension of the element. The common practice of the element aspect ratio used by the pipeline researchers at the University of Alberta in doing the FE analysis is between 1.0 and 2.0, for example, Dorey at al (2001). Consequently, in conducting the mesh study, the element sizes are selected in such a way that the elements tested have an aspect ratio between 1.0 and 2.0.

The "second criterion" in selecting the element size is based on the element size used in creating the pipe model for the field wrinkle sleeve repair simulations as presented in Chapter 4. In creating the pipe model for the re-enactment of the field wrinkle sleeve repair in Chapter 4, 10 mm by 10 mm elements were used in creating the numerical model, which displays a nice smooth wrinkle profile when compared with the picture of the wrinkle taken from the field and that from the GEOPIG measurements. The element sizes selected through the mesh study would also show similar smooth wrinkle profiles. Another important consideration in selecting the element size is that the difference between the load vs. displacement response obtained using 10 mm by 10 mm element size and that obtained using the would-be element size should be small

5.2.3 Results of the Mesh Study

Four different element sizes are tested in doing the mesh study, i.e., 50 × 366, 50 × 184, 30 × 230, 18 × 144. The element sizes are expressed in such a way that the first number means the number of elements in the circumferential direction and the second number means the number of elements in the pipe longitudinal direction. The above mentioned four different element sizes tested in the mesh study correspond to the element size of 10 mm by 10 mm, 10 mm by 20mm, 16.6 mm by 15.8 mm and 27.7 mm by 25.4 mm, respectively.

As for the loading conditions applied to the models, an average value of the internal pressure values from the pipeline field is used for the internal pressure. An axial load due to a temperature differential of 40 °C between the pipeline construction and pipeline operation is used here. Monotonically increased curvature values are applied at the two ends of the pipe numerical model until the wrinkle reaches a significant magnitude.

The moment vs. curvature response for different mesh sizes is shown in Figure 5.1. The points to which the arrows are pointing in Figure 5.1 correspond to the initiation of the wrinkles for different meshes. It can be observed from Figure 5.1 that the pipe segment shows quite similar moment capacity even using different meshes. Prior to the initiation of the wrinkle, the moment vs. curvature curves from different mesh sizes are essentially the same. However, the moment vs. curvature response in the post buckling region is significantly different for the 4 different mesh sizes used. That is, the 18 × 144 mesh (coarse mesh) shows the highest rotational capacity when comparing with other meshes tested. The slope of the moment vs. curvature curve in the post buckling region using the 18 × 144 mesh (coarse mesh) is gentler. The 50 × 366 mesh (finest mesh, used in field wrinkle sleeve repair simulations) has the lowest rotational capacity, which means that the wrinkle initiates at a lower curvature value than the models using larger element sizes. Table 5.1 lists the curvature difference when using the finest mesh (50 × 366 mesh) and the other 3 mesh sizes.

Table 5.1 Comparison of the Curvature Difference at the Initiation of Wrinkle

Mesh Comparison	Curvature Difference (%)
30 × 230 vs. 50 × 366	4.9
50 × 184 vs. 50 × 366	4.8
18 × 144 vs. 50 × 366	10.0

Because the curvature difference at the on-set of the wrinkle between the 50 × 366 mesh and the 30 × 230 mesh is small, and because the model using 30 × 230 mesh requires dramatically reduced CPU running time plus the fact that the element aspect ratio for the 30 × 230 mesh is approximately equal to 1.0, the 30 × 230 mesh is selected in the following parametric study to create the pipe numerical models.

5.3 THE PARAMETRIC STUDY

Following the mesh study as described above, the parametric study was carried out in this project and is presented in the following sections. As mentioned in Section 5.2.3, the 30 × 230 mesh is used for the numerical models in the parametric study, which has the element size of approximately 16.6 mm by 15.8 mm.

5.3.1 Determination of the Representative Model Parameters to Be Investigated

To carry out the parametric study for pipe wrinkle sleeve repair system, it is necessary to select a set of parameters representative of and essential to the engineering practice and having major influence on the buckling behavior of the wrinkle sleeve repair system. Based on the projects conducted in the University of Alberta, such as those by DiBattista (2000) and Dorey (2001), the following parameters are judged to be the variables that govern the buckling behavior of a wrinkle sleeve repair system:

(1) Pipe diameter, D

(2) Pipe wall thickness, t

(3) Pipe material properties, σ_y

(4) Modulus of elasticity, E

(5) Internal pressure, p_i

(6) Sleeve length, L_{SLV}

(7) Sleeve thickness, t_{SLV}

(8) Sleeve material properties, σ_{ySLV}

(9) Collar thickness, t_C

One thing that should be mentioned is that the length of the collar is not included in the set of parameters listed above. By referring to the schematic of the pipe wrinkle sleeve repair system as shown in Figure 5.2, the collars are supplementary to the sleeve repair and are used to fit in the gap between the internal surface of the sleeve and the outside surface of the pipe. This means that the thicknesses of the collars do influence the geometric compatibility when installing the sleeve onto the wrinkled pipe segment. As in the pipe longitudinal direction, it can be seen, from Figure 5.2, that C_L and C_R are much shorter than L_{SLV}. Consequently, the effect of the length of the collars was not studied separately. When the length of the sleeve is mentioned, the collar length is included indicatively.

Loading functions, except for the internal pressure, are not included in the list of the parameters. However, the axial force is a function of the pipe diameter, pipe wall thickness and the internal pressure, and is proportional to the three parameters above. The end rotations are applied monotonically at the two ends of the numerical model. Consequently, they are omitted from the parameter list above. For the wrinkle sleeve repair system, the collars are supplemental to the sleeve, which plays a major role in the wrinkle repair work and the length of the collars form part of the sleeve length, L_{SLV}. Consequently, only the effect of the collar thickness is studied separately here in the parametric study.

5.3.2 Dimensional Analysis

Based on the discussion in Section 5.3.1, in total, nine variables were considered in the parametric study of the pipe wrinkle sleeve repair system, i.e., D, t, σ_y, E, p_i, L_{SLV}, t_{SLV}, σ_{ySLV}, t_C.

To carry out the parametric study on the combinations of these nine variables, it would require that a large number of analyses be conducted. Therefore,

dimensional analysis, a process for eliminating extraneous information from relations between quantities (Taylor, 1974), is used to carry out the parametric study. The details of the dimensional analysis will not be presented here and can be readily found in Langhaar (1951) and Taylor (1974). A brief description of the dimensional analysis was also made by DiBattista (2000). The essential concept of the dimensional analysis is to "reduce the number of parameters to be investigated based on Buckingham's Pi theorem", namely, *if an equation is dimensionally homogeneous, it can be reduced to a relationship among a complete set of dimensionless products*. The number of dimensionless products in a complete set is equal to the total number of variables used to form a dimensional matrix minus the highest rank of the dimensional matrix (Langhaar, 1951).

Using the fundamental units of mass (M), length (L) and time (T), the dimensional matrix for the nine variables in the pipe wrinkle sleeve repair has the following form:

	D	t	σ_y	E	p_i	L_{SLV}	t_{SLV}	σ_{ySLV}	t_C
M	0	0	1	1	1	0	0	1	0
L	1	1	−1	−1	−1	1	1	−1	1
T	0	0	−2	−2	−2	0	0	−2	0

The number of variables in the above matrix is nine and the rank of the matrix is two. Consequently, there are seven independent non-dimensional π-terms based on the Buckingham pi theorem for use in the parametric study. Choosing terms commonly used in the pipeline industry such as D/t, the non-dimensional parameters can be expressed as:

$$\pi_1 = \frac{D}{t}$$

$$\pi_2 = \frac{\sigma_y}{E} = \varepsilon_y$$

$$\pi_3 = \frac{\sigma_h}{\sigma_y} = \frac{p}{p_y} = \frac{p}{\dfrac{2 \times \sigma_y \times t}{D}} \tag{5.1}$$

$$\pi_4 = \frac{L_{SLV}}{D}$$

$$\pi_5 = \frac{t_{SLV}}{t}$$

$$\pi_6 = \frac{\sigma_{ySLV}}{E}$$

$$\pi_7 = \frac{t_C}{t}$$

where,

p_y = Pressure at which the hoop stress induced equals the yield strength of pipe steel

ε_y = strain value at which yielding begins

As for the output from the FEA software ABAQUS/Standard, the moment capacity, M, and the rotational capacity or curvature values are the main concerns. For consistency purposes, they are also non-dimensionalized using the following method. For a simply supported beam of hollow cylindrical (i.e., pipe) cross section under pure bending with single curvature, the yield moment, i.e., moment under which yielding just initiates at the extreme fiber of the beam, and the corresponding curvature, ϕ_y, can be expressed as (Beer and Johnston, 1992):

$$M_y = \frac{I}{\left(\dfrac{D_o}{2}\right)} \sigma_y \tag{5.2}$$

and

$$\phi_y = \frac{M_y}{EI} \tag{5.3}$$

where,

I = moment of inertia for a hollow cylindrical pipe cross section,

$$\frac{1}{64}\pi\left(D_o^4 - D_i^4\right)$$

D_o = outside diameter of the pipe

σ_y = yield strength of the pipe steel

E = Modulus of Elasticity

5.3.3 Range of the π - Parameters Investigated

In current practice in the petroleum pipeline industry, the typical values of SMYS (Specified Minimum Yield Strength) of the commonly used pipe steel materials range from 359 MPa (X52) to 550 MPa (X80). According to Clause 4.3.3.1.4 of CAN/CSA-Z662-03, the design pressure shall be determined by the following formula:

$$p = \frac{2St}{D} \times F \times L \times J \times T \qquad (5.4)$$

where,

p = design pressure

S = Specified Minimum Yield Strength

t = design wall thickness

D = outside diameter of the pipe

F = design factor, 0.8

L = location factor

J = joint factor, 1.0 for seamless, electric welded and submerged arc welded pipes

T = temperature factor, 1.0 for operating temperature below 120°C

For pipes typically used in the oil and gas pipeline industry, the value for the joint factor, J, and the temperature factor, T, is 1. For pipelines in the remote regions, location factor L is taken as 1.0. The above formula can be rewritten as:

$$\frac{D}{t} = \frac{1.6}{p}S \qquad (5.5)$$

133

For pipelines with a typical SMYS of 550 MPa and typical operating pressure around 9.5 MPa, the D/t ratio would be 92 (Dorey et al, 2001). On the other hand, the D/t ratio of the pipeline studied in Chapter 4 has a value of 50. Consequently, the values for the π_1 parameter, i.e., the D/t ratio, which will be considered in the parametric study, are 50, 70 and 90, typical range of the currently used values in the pipeline industry.

The second π-parameter is the yield strain, ε_y, of the material. Because E is essentially constant at 207000 MPa for steel material, this parameter varies with the SMYS, σ_y, of the material. Three values are studied in the parametric study, which correspond to the lower bound of the pipe steel of 359 MPa, the upper bound of the pipe steel of 550 MPa in and about half way value of 448 MPa. It should be noted that the selection of the range of the material properties were also referred to Dorey et al (2001).

As the pipeline studied in Chapter 4 was installed at a time when the maximum value for the hoop stress was set to be $0.72\sigma_y$, the upper limit for the third π-parameter, p/p_y, is set to be equal to 0.72 in the parametric study. As described in Section 3.2.4 and Section 3.4, there exist two types of buckling modes, i.e., the "bulge" buckle and the "diamond-shape" buckle, which correspond to different internal pressure values applied to the pipeline. As mentioned earlier, the formation of the "diamond-shape" buckles, forming at a relatively low internal pressure, blocks the passage of the in-line-inspection tools. They must be removed from the mainline system. This means that the wrinkle sleeve repair technique is best suitable for the "bulge" buckles, which form at a relative high internal pressure. As currently the transition internal pressure at which the pipe buckling mode changes from "diamond-shape" buckle to "bulge" buckle is unclear and in order to ensure the formation of a "bulge" buckle, the lower limit for the third π-parameter, p/p_y, is set to be 0.5.

134

The length of the repairing sleeve used in the common practice by the pipeline operating company is 3D. In addition, the wrinkle region is highly stressed region where plastic deformation occurred. The preference of the wrinkle sleeve repair technique is that the material in the vicinity of the highly stressed wrinkle region should not to further disturbed when carrying out welding of the collars and sleeve during the repair. Consequently, longer sleeve lengths of 4D and 5D are considered in the parametric study for the fourth π-parameter. It should be noted that in determining the upper limit of the sleeve investigated, the following consideration is also taken into: because of the curvature induced into the pipe segment, if too long sleeve that is still straight is used, the internal surface of the sleeve will be interacting at the apex of the external surface of the pipe in the middle and angles will be formed at the two ends of the sleeve between the sleeve and the pipe segment. Consequently, 5D long sleeve is used as the upper limit in doing the parametric study.

The sleeve thickness is described by the fifth π-parameter. Because the sleeve that is used for the wrinkle repair is pressure-containment sleeve, the design of the sleeve should meet the requirement for the operating pressure in the pipeline. Based on Barlow's equation

$$\sigma_h = \frac{pD_i}{2t} \qquad (5.6)$$

The thickness of the sleeve is determined by the following expression

$$t = \frac{pD_i}{2\sigma_h} \qquad (5.7)$$

The current practice of the sleeve thickness by the pipeline operating company is 12.7 mm (1/2 in). Two other values for the sleeve thickness, 9.5 mm (0.375 in) and

19.05 mm (0.75 in), both of which meet the pressure-containment requirement, will be investigated in the parametric study.

The value of the SMYS of a material plays an important role in determining the load carrying capacity of the pipe segment as shown in Equation (5.2). In general, the material properties of the repairing sleeve used for the wrinkle repair are the same as those of the carrying pipe, i.e., the same steel grade. In order to study the effect of the SMYS of the sleeve (i.e., the sixth π-parameter) to the performance of the wrinkle sleeve repair system, three different SMYS values of the sleeve materials, i.e., 359 MPa, 448 MPa and 550 MPa, will be investigated, which are in the same range as those of the material properties for the pipe studied in the parametric study.

The last π-parameter describes the thickness of the collar. As mentioned in Section 5.3.1 and shown in Figure 5.2, the thickness of the collar does influence the geometric compatibility when installing the sleeve onto the wrinkled pipe segment. The inside surface of the sleeve should not interact with the apex of the pipe segment, which was formed due to the curvature of the pipe segment. The gap between the internal surface of the sleeve and the external surface of the pipe is determined by the thickness of the collars. In current practice of the pipeline operating company, the thickness of the collar is 19.05 mm (3/4 in). Two other values for the collar thickness, i.e., 25.4 mm (1 in) and 31.75 mm (1.25 in), will be studied in the parametric study.

5.3.4 Suitability Check of the Non-dimensionalized Parameters in the Parametric Study

As mentioned in Section 5.3.2, Buckingham's Pi theorem in dimensional analysis is used in conducting the parametric study. One of the necessary conditions in applying the Buckingham's Pi theorem is that the set of variables used in the study must be a complete set of the variables describing the mechanics of the problem (Langhaar, 1951). As presented in Section 5.3.2, the identified variables in

the set for the wrinkle sleeve repair problem include the pipe outside diameter D, the pipe wall thickness t, the pipe material properties σ_y, the modulus of elasticity E, the internal pressure p_i, the sleeve length L_{SLV}, the sleeve thickness t_{SLV}, the sleeve material properties σ_{ySLV} and the collar thickness t_C. To evaluate whether all the essential variables, which play important roles in the buckling behavior of the wrinkle sleeve repair system, are included in the variable set, an investigation is conducted.

In the investigation that was carried out, identical π-parameters were used. But the scales of the parameters were different. For example, if the following parameters are in one variable set: OD = 323.85 mm, t = 6.35 mm, σ_y = 359 MPa, E = 203500 MPa, p_i = 7.33 MPa, L_{SLV} = 971 mm, t_{SLV} = 12.7 mm, σ_{ySLV} = 359 MPa, t_C = 19.05 mm and the following parameters in another variable set: OD = 762 mm, t = 14.94 mm, σ_y = 359 MPa, E = 203500 MPa, p_i = 7.33 MPa, L_{SLV} = 2286 mm, t_{SLV} = 29.88 mm, σ_{ySLV} = 359 MPa, t_C = 44.82 mm, they have identical π-parameters but different scales, i.e., $\pi_1 = D/t = 51$, $\pi_2 = \sigma_y/E = 1.76 \times 10^{-3}$, $\pi_3 = \sigma_h/\sigma_y = 0.52$, $\pi_4 = L_{SLV}/D = 3$, $\pi_5 = t_{SLV}/t = 2$, $\pi_6 = \sigma_{ySLV}/E = 1.76 \times 10^{-3}$ and $\pi_7 = t_C/t = 3$. If all the essential variables in determining the buckling behavior of the wrinkle sleeve repair system are included in the two variable sets, the analytical results obtained, i.e., the non-dimensionalized moment vs. non-dimensionalized curvature curve as described in Section 5.3.2, should be identical, i.e., the results not affected by changes of the scales of the variables. One obvious advantage based on this investigation is that the diameter of the pipe does not need to vary from model to model in doing the parametric study. What need to be changed are the π-parameters because the behavior of the numerical models with any other scales is essentially the same. This means that by keeping D constant and only varying the other eight parameters, i.e., t, σ_y, E, p_i, L_{SLV}, t_{SLV}, σ_{ySLV} and t_C, the purpose of the parametric study will be achieved. This will reduce the number of the models that need to be studied dramatically in the parametric study.

In conducting the above mentioned investigation, six numerical analyses are carried out, which have identical π-parameters of $D/t = 50$, $\varepsilon_y = 1.76 \times 10^{-3}$, $p/p_y = 0.5$, $L_{SLV}/D = 3$, $t_{SLV}/t = 2$, $\varepsilon_{ySLV} = 1.76 \times 10^{-3}$ and $t_C/t = 3$. Table 5.2 on the following page lists the parameters used in the six numerical analyses, which have the typical values commonly encountered in the pipeline industry. In determining the parameters in Table 5.2, the values for D and σ_y are first selected to be the representative values that are most commonly used in the pipeline industry. Then, the values for t, E, p_i, L_{SLV}, t_{SLV}, σ_{ySLV}, t_C are chosen in such a way that all the seven π-parameters are kept to be constant. The designations of the parameters listed in Column 1 of Table 5.2 have the form of D–SMYS (for simplification purpose in expressing the numbers, the unit used for D and SMYS in imperial units). For example, a designation of 12-X52 means 323.85 mm diameter pipe with SMYS of 359 MPa. It should be noted that some values of an individual variable are not the true values used in the pipeline industry. They are selected only for demonstration purpose for the investigation of the effect from different scales of the pipe parameters. If identical non-dimensionalized moment vs. non-dimensionalized curvature response is obtained from these six numerical analyses, it could be concluded that all the variables that play a vital role in determining the buckling behavior of the wrinkle sleeve repair system have been identified.

The non-dimensionalized moment vs. curvature curves for the models based on the parameters listed in Table 5.2 are shown in Figure 5.3. It can be seen from Figure 5.3 that the moment vs. curvature response from these six numerical analyses are identical. This means that the scale change of the pipe, the sleeve and the collar parameters does not affect the buckling behavior of wrinkled sleeved pipe segments. Consequently, it can be concluded that all the variables that govern the mechanics of the pipe wrinkle sleeve repair problem have been included in the set of seven π-parameters as shown in Equation (5.1).

Table 5.2 Parameters Used in the Investigation of Evaluating the Essential Variables for Pipe Wrinkle Sleeve Repair System

Designations	D (mm)	t (mm)	σ_y (MPa)	L_{SLV} (mm)	t_{SLV} (mm)	σ_{ySLV} (mm)	t_C (mm)	P_i (MPa)	E (MPa)
12-X52	323.85	6.35	359	970	12.7	359	19.05	7.33	203500
12-X65	323.85	6.35	448	970	12.7	448	19.05	9.14	253950
16-X52	406.4	7.97	359	1218	15.94	359	23.91	7.33	203500
20-X65	508	9.96	448	1524	19.92	448	29.88	9.14	253950
30-X65	762	14.94	448	2286	29.88	448	44.82	9.14	253950
30-X52	762	14.94	359	2286	29.88	359	44.82	7.33	203500

Note: for the designations listed in the table, the seven π-parameters $\dfrac{D}{t} - \varepsilon_y - \dfrac{p}{p_y} - \dfrac{L_{SLV}}{D} - \dfrac{t_{SLV}}{t} - \varepsilon_{ySLV} - \dfrac{t_C}{t}$ have the same

corresponding values of 50-1.76-0.5-3-2-1.76-3.

139

5.3.5 The Layout of the Parametric Study

From the investigation that was described in Section 5.3.4, it can be concluded that all essential variables that play a major role in the buckling behavior of the pipe wrinkle sleeve repair system have been identified. Based on the discussion presented in Section 5.3.3, the following matrix is set up for all the parameters that govern the behavior of the pipe wrinkle sleeve repair system. It should be noted that all the parameters are within the range as specified in Section 5.3.3:

D/t Ratio	ε_y	p/p_y	L_{SLV}/D	t_{SLV}/t	ε_{ySLV}	t_C/t
50	1.76×10^{-3}	0.5	3	1.5	1.76×10^{-3}	3
70	2.20×10^{-3}		4	2	2.20×10^{-3}	4
90	2.70×10^{-3}	0.72	5	3	2.70×10^{-3}	5

Based on the matrix for the parameters given above, the required ABAQUS numerical job runs would be 1458 if all the cases and combinations were considered. As discussed in Section 5.1, no attempt was made to develop a design equation for use in quantitively determining the parameters for the sleeve and the collar in this project. Consequently, the following strategy is used in carrying out the parametric study.

(i) Phase I: identify the parameter that plays the most important role in determining the behavior of the wrinkled pipe segment under sleeve repair. It is believed that this parameter is the fourth π-parameter, L_{SLV}/D, i.e., the length of the sleeve. The detailed discussion will be presented in Section 5.3.7. Investigate the way this parameter affects the behavior of the pipe wrinkle sleeve repair system through a number of numerical analyses using FEA package ABAQUS;

(ii) Phase II: after identifying the parameter that plays the most important role in determining the behavior of the pipe wrinkle sleeve repair system, using the value of this parameter that provides the best performance to study the effects of other parameters for the pipe, the sleeve and the collar.

The two phases mentioned above are described in Figures 5.4, 5.5 and 5.6, respectively.

5.3.6 Results of the Parametric Study

5.3.6.1 Results of Phase I Analyses of the Parametric Study

In carrying out the Phase I analyses of the parametric study for $D/t = 50$ case as shown in Figure 5.4, two groups are divided based on the third π-parameter, p/p_y, one for 0.5 and one for 0.72. In total, for $p/p_y = 0.5$ case, 3 different cases for the fourth π-parameter, L_{SLV}/D, are studied, including 9 ABAQUS job runs, to investigate the effect due to the length of the sleeve. The non-dimensionalized moment vs. non-dimensionalized curvature curves are shown in Figures 5.7, 5.8 and 5.9, respectively.

It can be seen, from the Figures 5.7, 5.8 and 5.9, that the moment vs. curvature curves display the characteristic behavior of the pipe wrinkle sleeve repair sequence as described before (Section 3.6 and Section 4.7.2)

- In the pre-buckling region, with the increase of the curvature, the moment increases until it reaches a peak value

- Further increasing the curvature causes the moment to start to drop due to the formation of a local wrinkle

- With the installation of the repairing sleeve to encase the local wrinkle, the moment carrying capacity of the wrinkled sleeved pipe segment increases again with further increasing the curvature until reaching the second peak

- Further increasing the curvature causes the moment to drop again due to the formation of the second wrinkle

One additional observation from Figures 5.7, 5.8 and 5.9 is that the peak moment capacities for the three sleeve lengths used are very similar. But with the increase of the sleeve length which is used to encase the local wrinkle, the rotational capacity (or the curvature value) of the wrinkled sleeved pipe segment also increases. In another word, the longer the repairing sleeve is used, the larger the rotational capacity of the sleeved pipe segment will be. This is very important for pipeline in the field. If it is assumed that the yearly pipe settlement is constant, the increased rotational capacity of the wrinkle sleeve repair system means the extended wrinkle repair time span between the installations of the sleeves.

Based on the results for $p/p_y = 0.5$ case study, one case (Case 4 in Figure 5.4, i.e., $\varepsilon_y = 1.76 \times 10^{-3}$) for $p/p_y = 0.72$ is investigated to see if similar phenomenon can be observed, i.e., increasing the repairing sleeve length increases the rotational capacity of the wrinkled sleeved pipe segment. The non-dimensionalized moment vs. non-dimensionalized curvature curve for Case 4 in Figure 5.4 is shown in Figure 5.10. As shown in Figure 5.10, similar observations as those in Case 1, Case 2 and Case 3 studies are also obtained for Case 4, i.e., the peak moment capacity for three sleeve lengths tested are very similar before and after the installation of the sleeve; with the increase of the repairing sleeve length, the rotational capacity of the wrinkled sleeved pipe segment also increases. It is believed that the above mentioned observations will also be obtained for the other cases of $p/p_y = 0.7$, i.e., $\varepsilon_y = 2.20 \times 10^{-3}$ and $\varepsilon_y = 2.70 \times 10^{-3}$. Consequently, no further attempt is made to conduct the investigations for the cases of $\varepsilon_y = 2.20 \times 10^{-3}$ and $\varepsilon_y = 2.70 \times 10^{-3}$ of $p/p_y = 0.72$.

Studies for D/t = 70 and D/t = 90 cases were also carried out as shown in Figures 5.5 and 5.6. Similar procedures and cases as those for D/t = 50 are also used and investigated in D/t = 70 and D/t =90 studies. The non-dimensionalized moment vs. non-dimensionalized curvature curves obtained for the 4 cases for D/t = 70 pipes are shown in Figures 5.11, 5.12, 5.13 and 5.14, respectively. The non-dimensionalized moment vs. non-dimensionalized curvature curves for the 4 cases for D/t =90 pipes are shown in Figures 5.15, 5.16, 5.17 and 5.18, respectively. It can be seen through Figures 5.11 to 5.18 that similar observations as those for D/t = 50 case studies are also obtained for D/t = 70 and D/t = 90 cases:

- Increasing the length of the repairing sleeve increases the rotational capacity of the sleeved pipe segment

- The first and second moment peaks (before and after the installation of the repairing sleeve) are quite similar

5.3.6.2 The Effect of the Length of the Pipe End Segment

It can be seen, through Figure 5.7 to Figure 5.18 for all the cases studied, that the longer sleeve provides larger rotational capacity for the pipe wrinkle sleeve repair system. When modeling the pipe wrinkle sleeve repair using different lengths of sleeves (3D, 4D or 5D), the same pipe model was used. Shown in Figure 5.19 (a) is the schematic of a pipe model with a 3D long repairing sleeve. Shown in Figure 5.19 (b) is the schematic of a pipe model with a 5D long repairing sleeve (for comparison purpose, only 3D long sleeve and 5D long sleeve was investigated). One speculation, which could be arisen, is that the observation described in Section 5.3.6.1 could be induced by the length difference of the end segment for the 3D long sleeve and the 5D long sleeve, i.e., from the edge of the collar to the closest end of the pipe segment, as shown in Figures 5.19 (a) and (b). In order to check whether the above mentioned speculation is correct or wrong and to justify the effect of the length of the repairing sleeve, the following two investigations are carried out:

(i) Use decreased pipe model length so that the length from the edge of the collar to the closest end of the pipe when using 3D long repairing sleeve is the same as that when using 5D long sleeve,

(ii) Use increased pipe model length so that the length from the edge of the collar to the closest end of the pipe when using 5D long repairing sleeve is the same as that when using 3D long sleeve.

The moment vs. curvature curves for the above two investigations are shown in Figures 5.20 and 5.21, respectively. The distinct observations from Figures 5.20 and 5.21 are as follows.

(i) The second peak moment, which is due to the installation of the repairing sleeve after the pipe wrinkling, always displays a plateau with increased curvature values when using 5D long sleeve. The second wrinkle forms at a larger curvature value.

(ii) The second peak moment starts to decrease immediately after the peak moment value is reached with increased curvature values when using 3D long sleeve. The formation of the second wrinkle is at a smaller curvature value.

The two observations obtained above are consistent with those that were obtained through the investigations presented in Section 5.3.6.1 as shown through Figure 5.7 to Figure 5.18. Accordingly, it can be concluded that the length of the end segment (from the edge of the collar to the closest end of the pipe) is not the factor that causes the rotational capacity difference of the pipe wrinkle sleeve repair system. In other words, the increase in the rotational capacity of the wrinkled sleeved pipe segment after the installation of the sleeve is due to the length of the repairing sleeve used, not due to the length difference of the pipe end segment. Longer repairing sleeve length does provide larger rotational capacity to the pipe wrinkle sleeve system.

5.3.6.3 Results of Phase II of the Parametric Study

Based on the numerical analyses carried out in Phase I, presented in Section 5.3.6.1 and the investigative study described in Section 5.3.6.2, it can be concluded that the longer sleeve does display a better performance for the pipe wrinkle sleeve repair system. Consequently, the focus of the numerical analyses to investigate the other three parameters, i.e., the fifth π-parameter, t_{SLV}/t, the sixth π-parameter, ε_{ySLV}/E, and the seventh π-parameter, t_C/t, in Phase II is given to the longest sleeve length studied, i.e., $L_{SLV}/D = 5$. If recalling the Phase I studies as shown in Figures 5.4, 5.5 and 5.6, the above mentioned three parameters were kept unchanged in studying the effect of the length of the repairing sleeve to the behavior of the pipe wrinkle sleeve repair system as described in Section 5.3.6.1. It is the purpose of the numerical studies in Phase II to investigate the effect of these three above mentioned parameters, i.e., the thickness of the sleeve, t_{SLV}, the material properties of the sleeve, ε_{ySLV} and the thickness of the collar, t_C. The layouts of the numerical investigations carried out in Phase II study are shown in Figures 5.22, 5.23 and 5.24, respectively. Similar strategy as that used in the Phase I study is utilized here: Studying one parameter at a time by keeping other parameters unchanged.

For $D/t = 50$ pipe cases, shown in Figures 5.25, 5.26 and 5.27 are the analytical results of the non-dimensionalized moment vs. non-dimensionalized curvature curves, which correspond to Case A, Case B and Case C as listed in Figure 5.22, respectively. It can be seen from Figures 5.25, 5.26 and 5.27 that different sleeve thicknesses, t_{SLV}, different sleeve material properties, σ_{ySLV} and different collar thicknesses, t_C, provide almost identical moment vs. curvature response. In other words, the change of sleeve thickness, the change of the sleeve material properties or the change of the collar thickness does not affect the moment vs. curvature response of the pipe wrinkle sleeve repair system. This means that the behavior of the wrinkled pipe segment under sleeve repair is not affected by the three parameters studied.

145

The non-dimensionalized moment vs. non-dimensionalized curvature responses for D/t = 70 pipes are shown in Figures 5.28, 5.29 and 5.30, which correspond to Case A, Case B and Case C as listed in Figure 5.23, respectively. The results for D/t = 90 pipes are shown in Figures 5.31, 5.32 and 5.33, which correspond to Case A, Case B and Case C as listed in Figure 5.24, respectively. It can be seen through Figure 5.25 to Figure 5.33 that almost identical moment vs. curvature responses are obtained for the pipe wrinkle sleeve repair system even using different sleeve thickness, different sleeve material properties or different collar thickness when keeping the length of the repairing sleeve unchanged. These observations apply to pipes with D/t = 50 cases, as well as to pipes with D/t = 70 cases and D/t = 90 cases.

5.3.7 Discussion of the Results of the Parametric Study

As presented in Section 5.3.6, two phases of the parametric studies are carried out to investigate the effect of four parameters to the buckling behavior of the pipe wrinkle sleeve repair system for pipes with different D/t ratios under different internal pressures and combined axial load and bending moment. These four parameters that were investigated are: the length of the sleeve, L_{SLV}, the thickness of the sleeve, t_{SLV}, the material properties of the sleeve, ε_{ySLV} and the thickness of the collars, t_C. The effect of the length of the repairing sleeve, L_{SLV}, to the buckling behavior of the pipe wrinkle sleeve repair system was investigated in the Phase I study as it is believed that this parameter, L_{SLV}, plays the most important role among all the parameters investigated. It was found that the longer the sleeve is used in the wrinkle repair, the larger the rotational capacity of the pipe wrinkle sleeve repair system can be obtained, i.e., the better the performance of the wrinkle sleeve repair system. The change of the thickness of the repairing sleeve, the change of the material properties of the repairing sleeve and the change of the thickness of the collars do not affect the performance of the wrinkle sleeve repair system.

The above mentioned observations can be explained, to some extent, through the studies of the plastic buckling of inelastic beam column by Chakrabarty (2000). The general deformational behavior of the internally pressurized pipe segment under combined axial load and bending moment, i.e., the structure studied in this project, is somewhat similar to that of eccentrically loaded beam column that was studied by Chakrabarty (2000). According to Chakrabarty (2000), for a column under combined effect of bending and axial compression, in the initial stage of the deformation, a plastic zone in simple compression exists on the concave side, until the bending stress becomes large enough to cause yielding in tension on the convex side. The plastic zones formed on the concave side and on the convex side are referred to as the primary and the secondary plastic zones, respectively. These two plastic zones coexist in the later stages of the elastic/plastic deformation, as shown in Figure 5.34, the schematic of the structure studied by Chakrabarty (2000). As mentioned earlier, the primary plastic zone always forms first and the secondary plastic zone forms second. Further increasing the loads will cause the plastic zones to expand, longitudinally and transversely. It is believed that the internally pressurized pipe segment under combined axial load and bending moment behaves in a similar way.

The formation of the local wrinkle due to yielding of the pipe material at the midspan of the pipe segment means the formation of the plastic zone in the pipe segment. The collars and the repairing sleeve are still in the elastic state when they are installed on the external surface of the pipe segment to encase the local wrinkle and the adjacent pipe segment. Any further applied loads to the pipe wrinkle sleeve repair system will be carried by the repairing sleeve and the pipe segment together. The length of the sleeve determines the size of the plastic zone that is covered underneath the repairing sleeve. By referring to Figure 5.35, the schematic of the pipe wrinkle sleeve repair system, the longer the repairing sleeve is used, the larger the plastic zone is encased by the sleeve, i.e., the less the plastic zone is left uncovered. When further increasing the loads, the one with more plastic zone encased by the sleeve need to deform more in order for the second wrinkle to fully

develop than the one with less plastic zone encased. This was shown in Figures 5.7 through 5.18 by the larger rotational capacity of the wrinkle sleeve repair system where longer sleeve was used. This also explains the observations as shown in Figures 5.20 and 5.21 where a plateau in the moment vs. curvature curve is always obtained when using longer sleeve, i.e., the second wrinkle forms at a larger rotation value. When repairing the pipe local wrinkle using a shorter sleeve, the moment capacity drops immediately after the second moment peak is reached, i.e., the second wrinkle forms at a smaller rotation value.
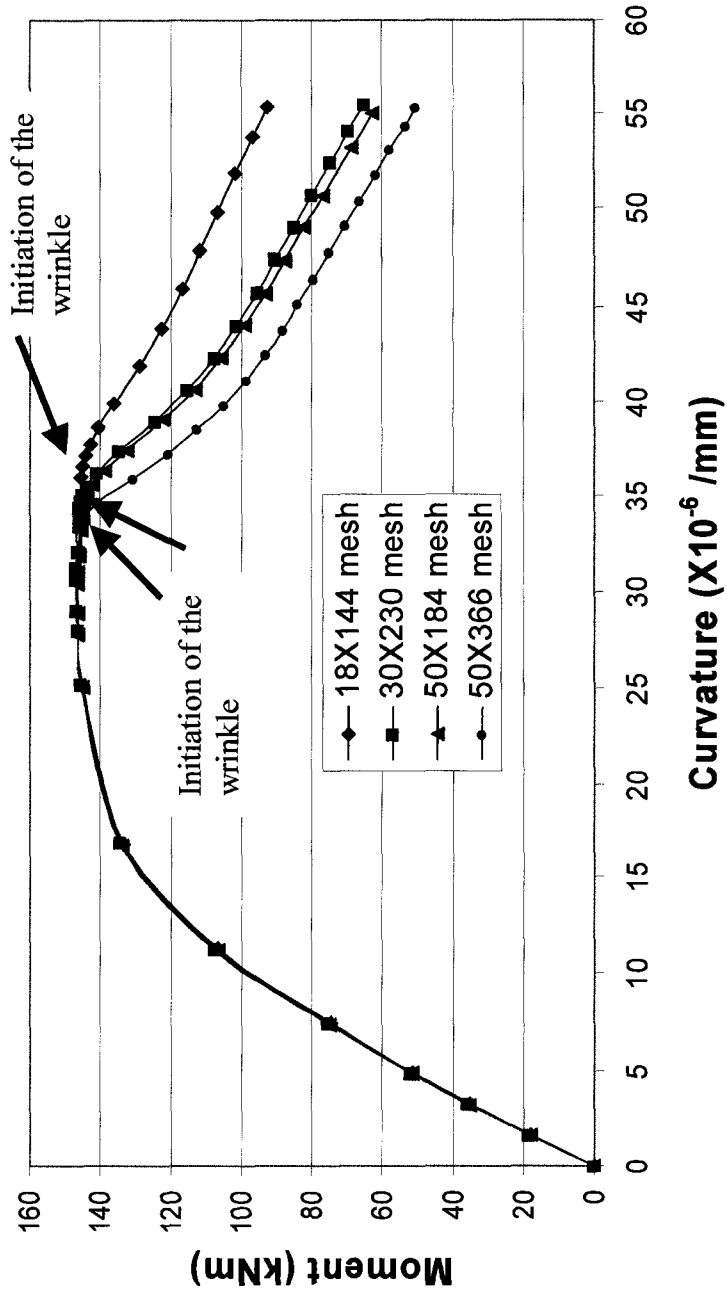
Figure 5.1 Moment *vs.* Curvature Response for Different Mesh Sizes
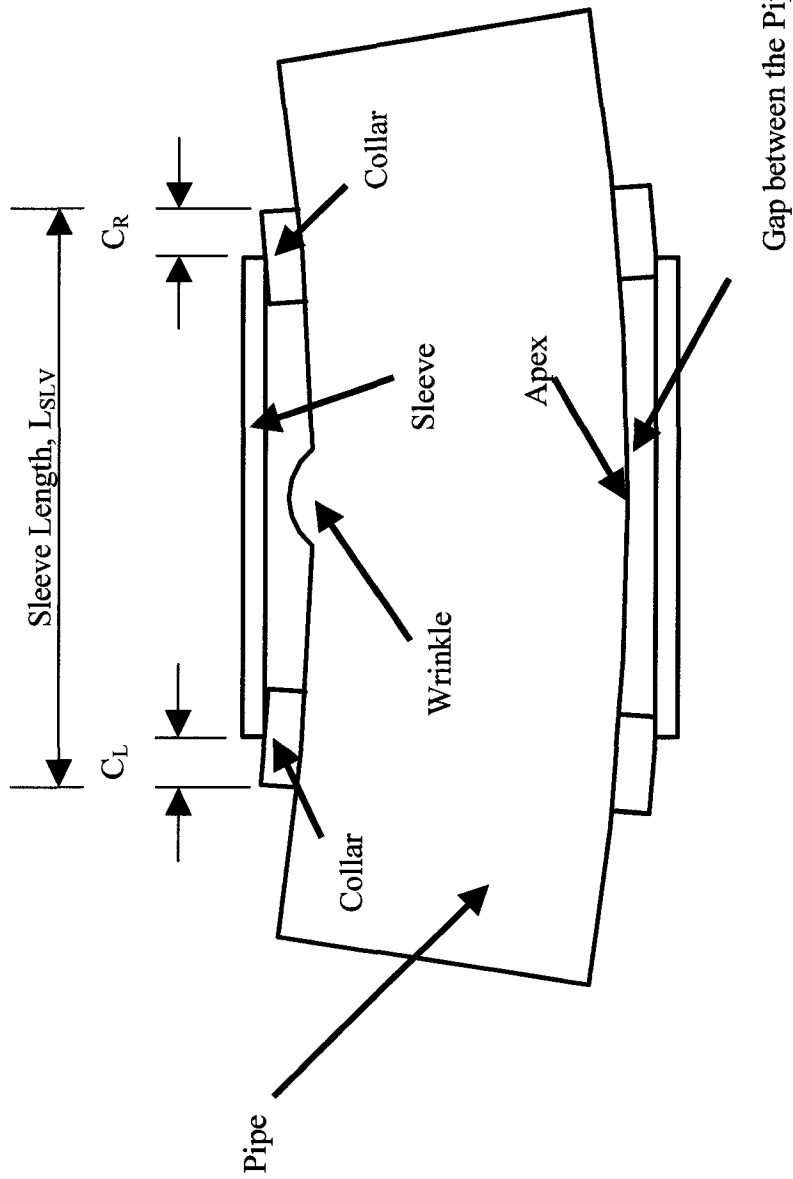
Figure 5.2 Schematic of the Geometric Compatibility of the Wrinkle Sleeve Repair System

Figure 5.3 Non-dimensionalized Moment vs. Curvature Response for Models of Different Scales with Constant π-parameters
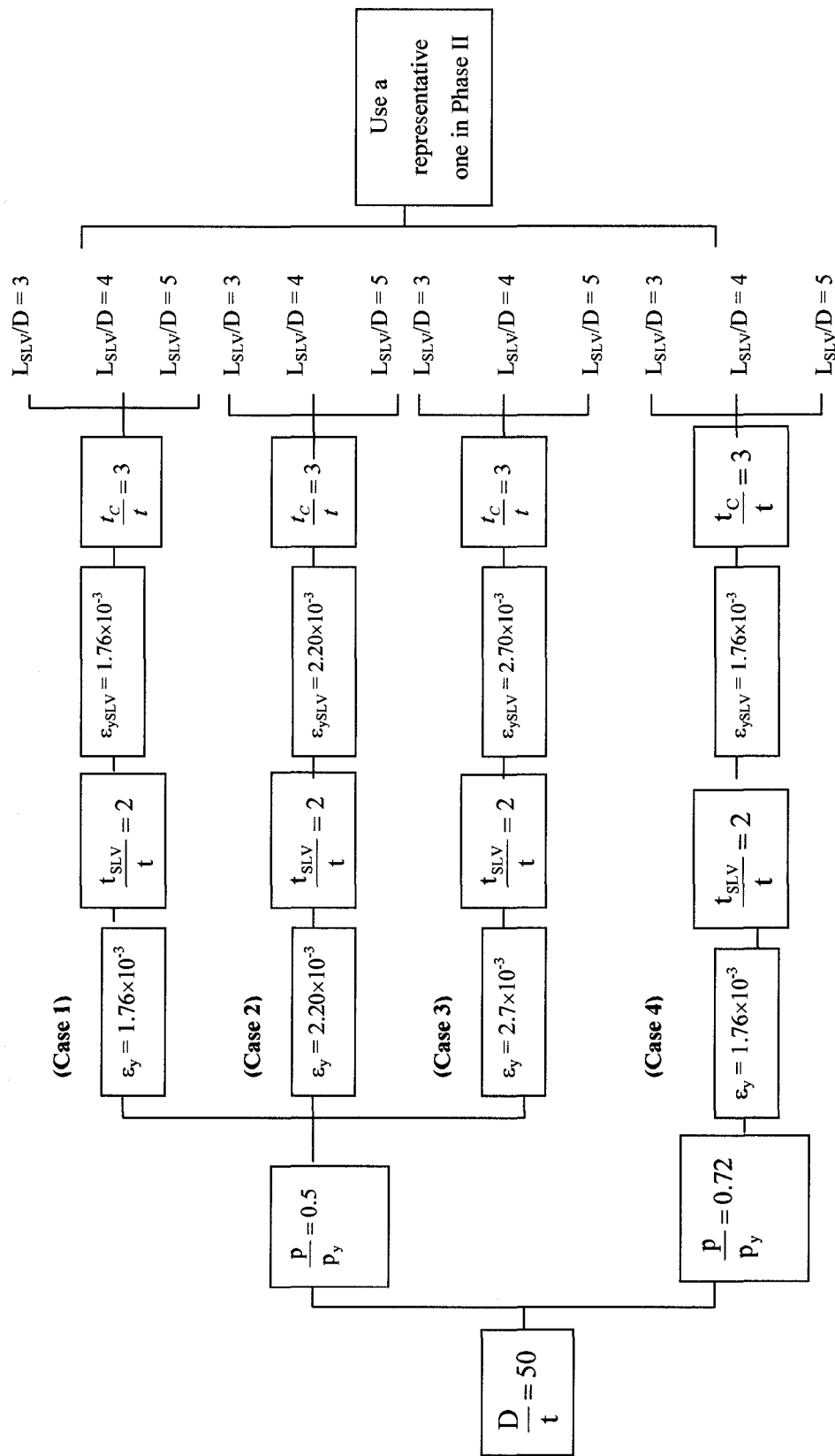
Figure 5.4 Layout of the Numerical Analyses in Phase I for D/t = 50 Pipe
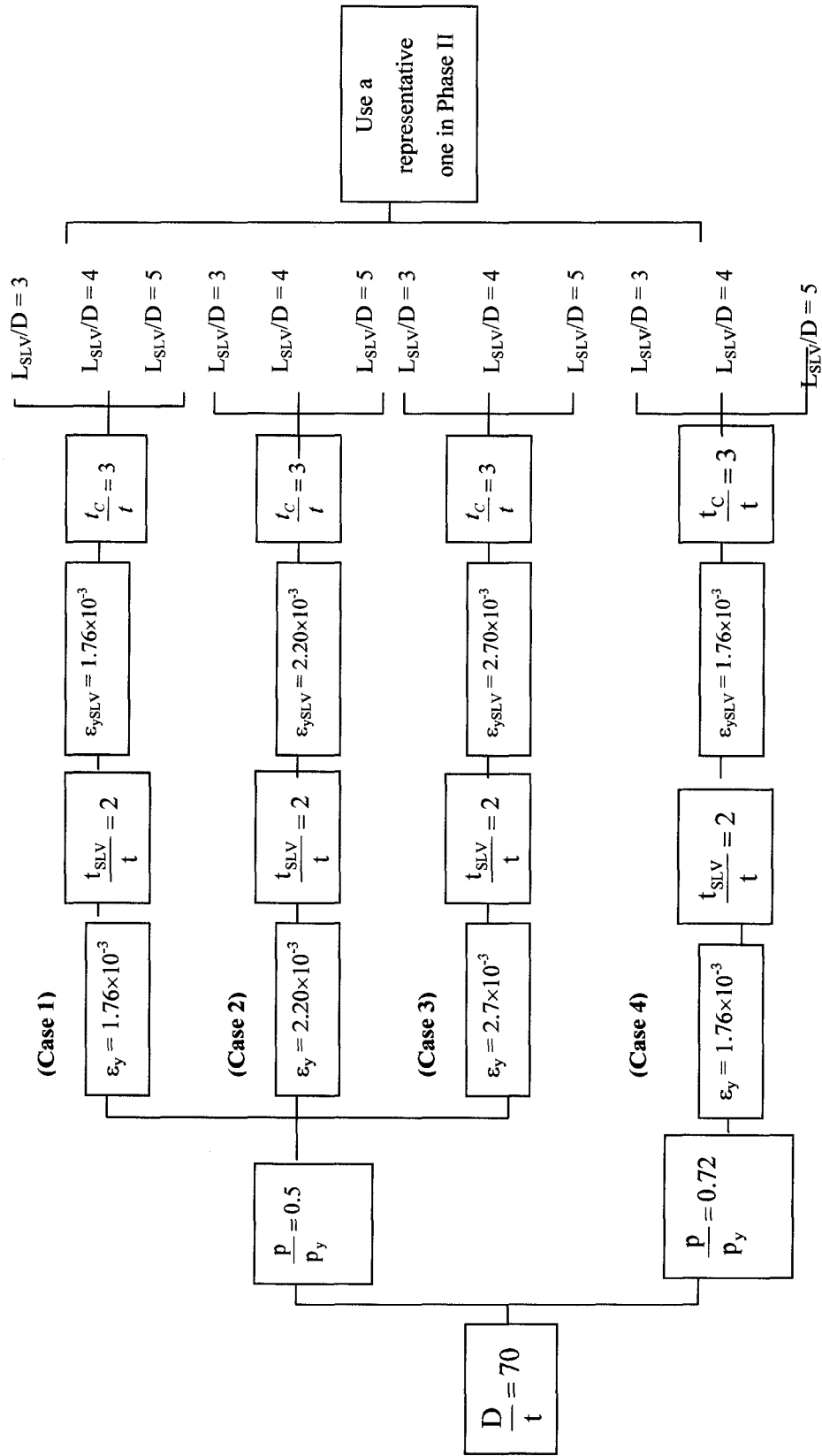
Figure 5.5 Layout of the Numerical Analyses in Phase I for D/t = 70 Pipe

153
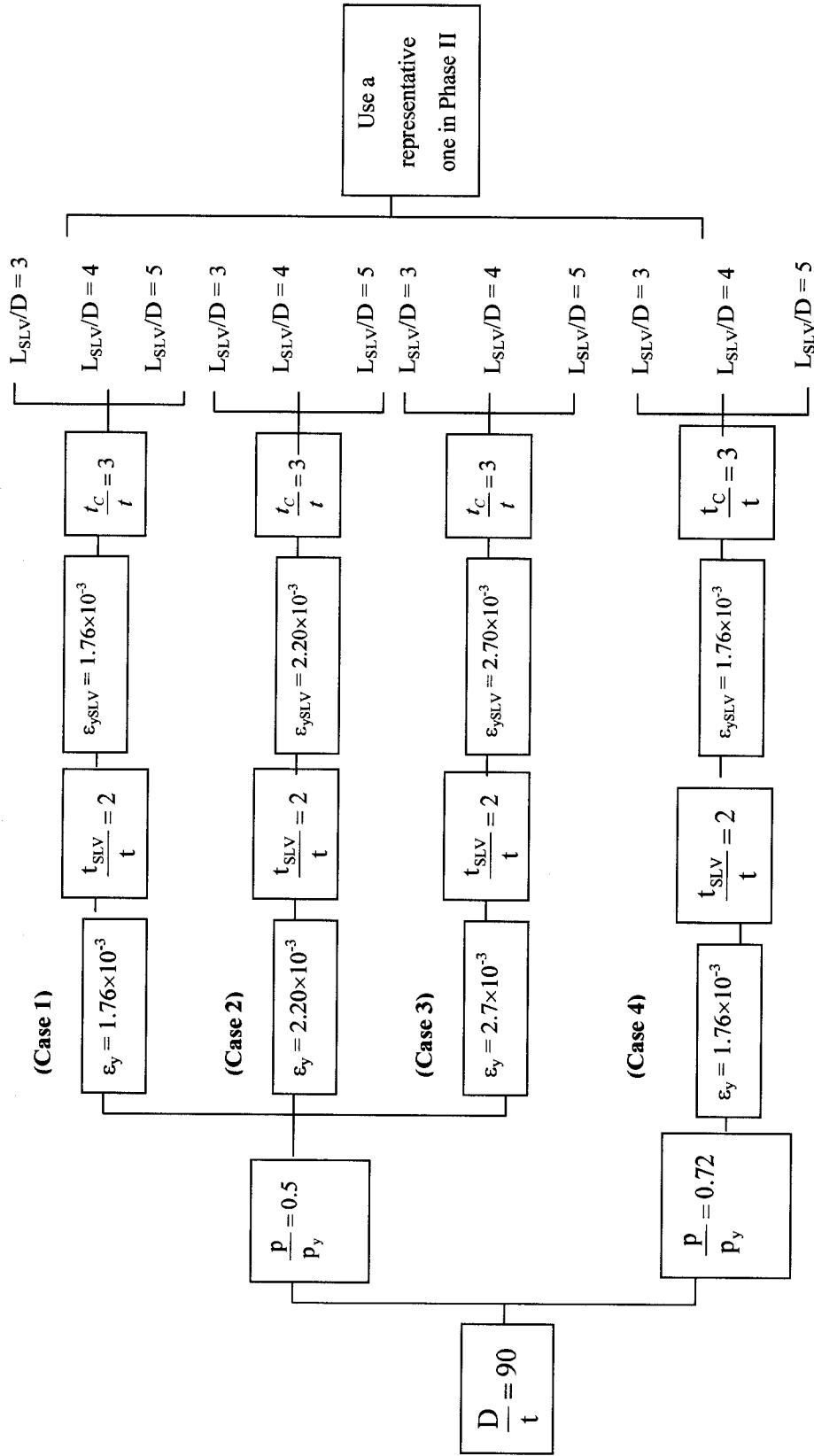
Figure 5.6 Layout of the Numerical Analyses in Phase I for D/t = 90 Pipe

Sleeve Length Effect for Case 1 of D/t=50 Pipe
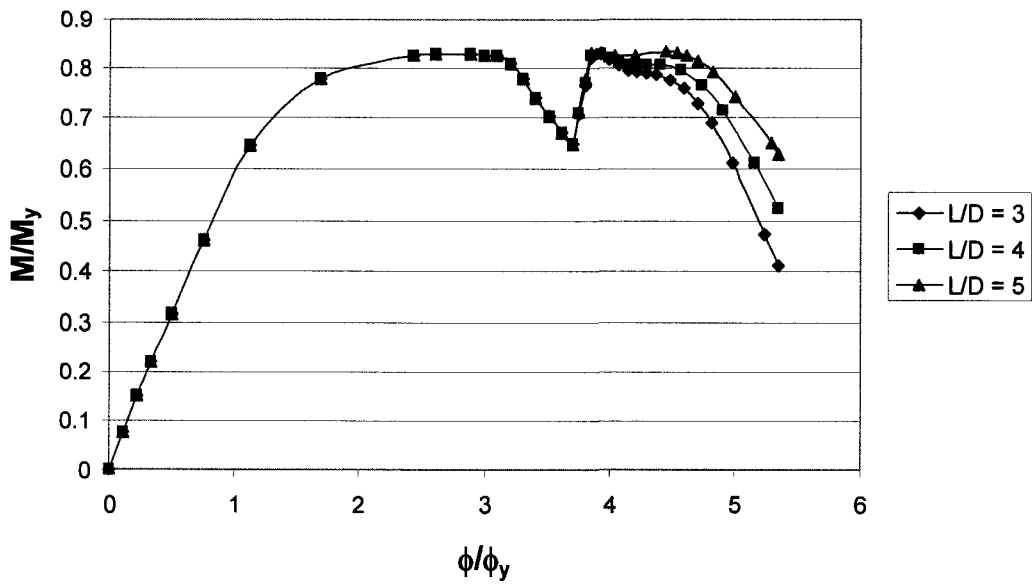
Figure 5.7 Sleeve Length Effect for Case 1 of D/t = 50

Sleeve Length Effect for Case 2 of D/t=50 Pipe
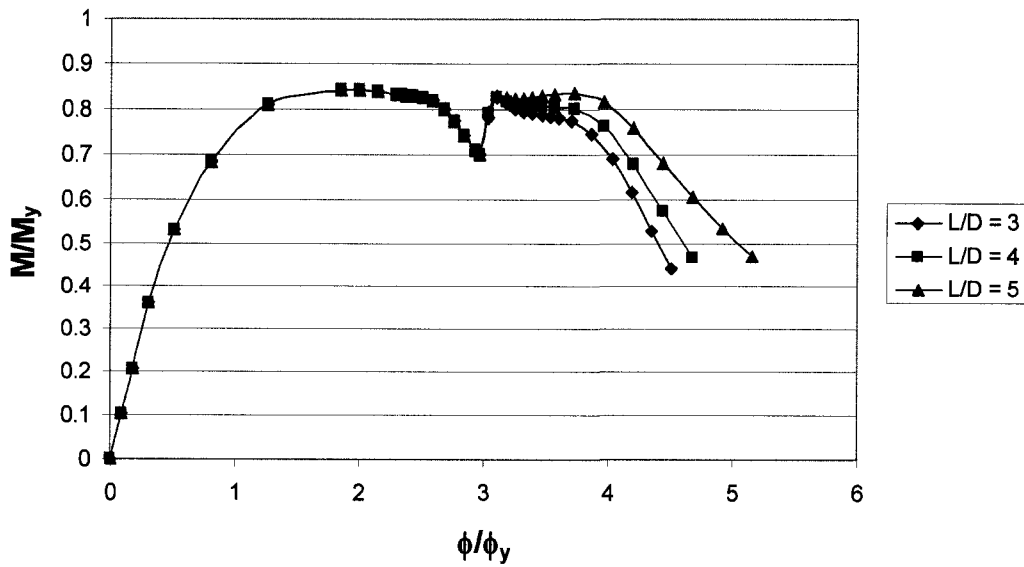
Figure 5.8 Sleeve Length Effect for Case 2 of D/t = 50

Sleeve Length Effect for Case 3 of D/t=50 Pipe
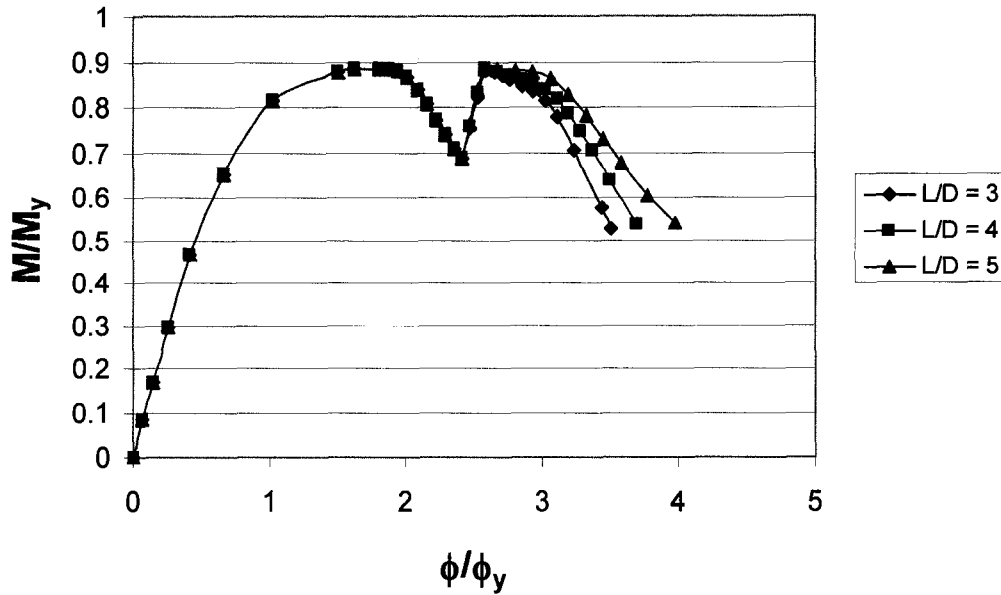
Figure 5.9 Sleeve Length Effect for Case 3 of D/t = 50

Sleeve Length Effect for Case 4 for D/t=50 Pipe
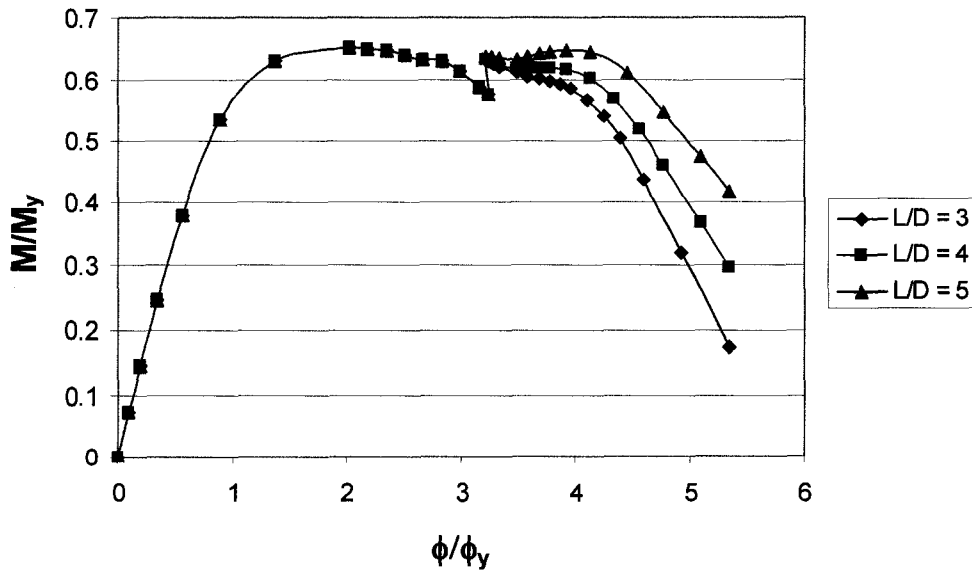
Figure 5.10 Sleeve Length Effect for Case 4 of D/t = 50

Sleeve Length Effect for Case 1 of D/t=70 Pipe
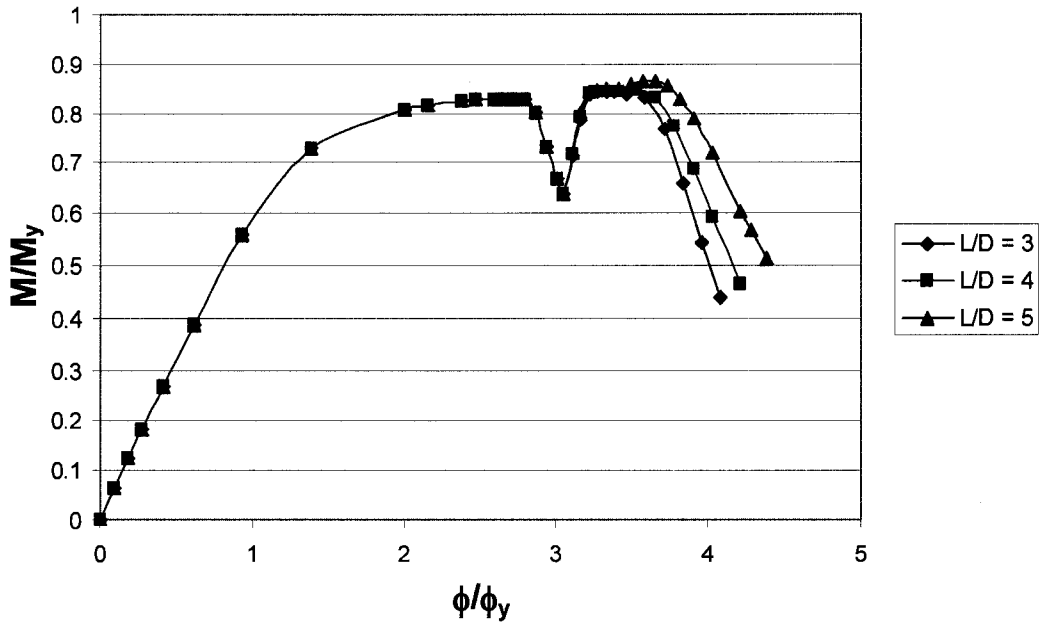
Figure 5.11 Sleeve Length Effect for Case 1 of D/t = 70

Sleeve length Effect for Case 2 of D/t=70 Pipe
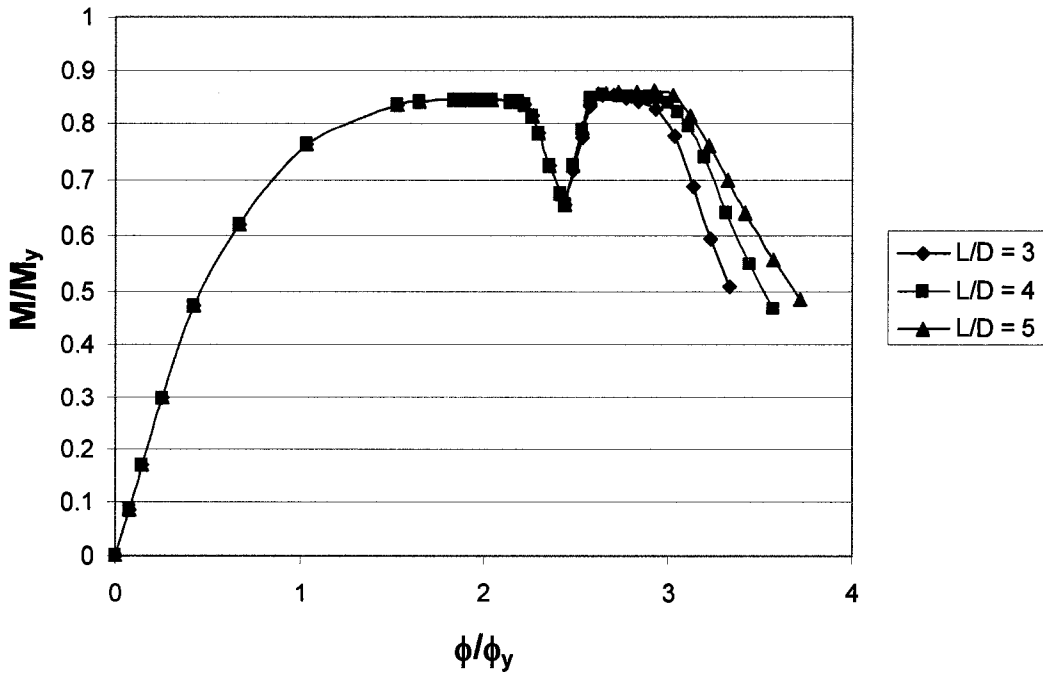
Figure 5.12 Sleeve Length Effect for Case 2 of D/t = 70

Sleeve Length Effect for Case 3 of D/t=70 Pipe
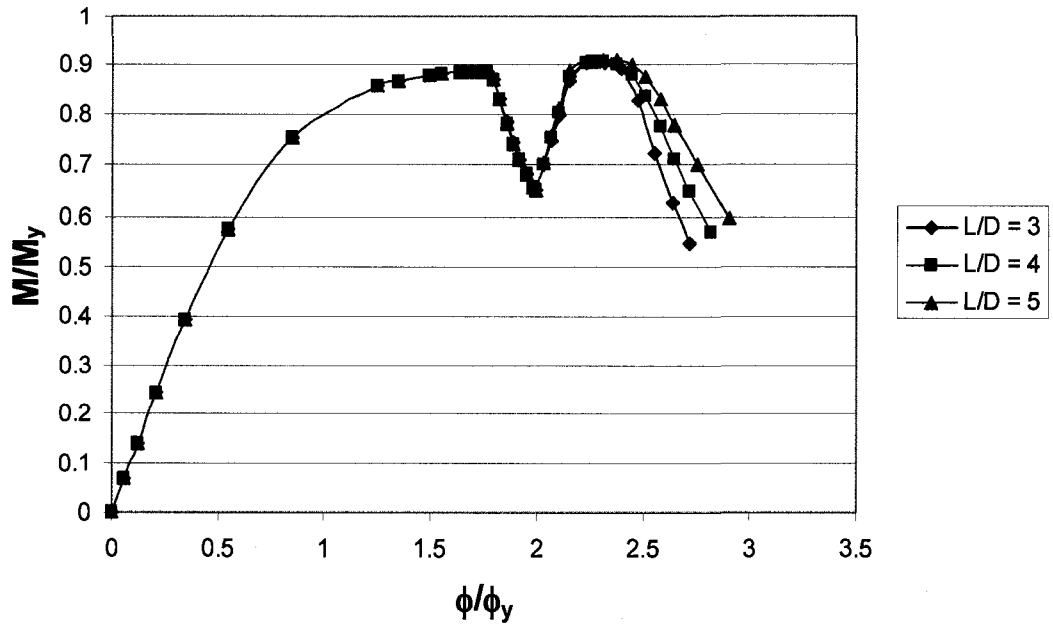
Figure 5.13 Sleeve Length Effect for Case 3 of D/t = 70

Sleeve Length Effect for Case 4 of D/t=70 Pipe
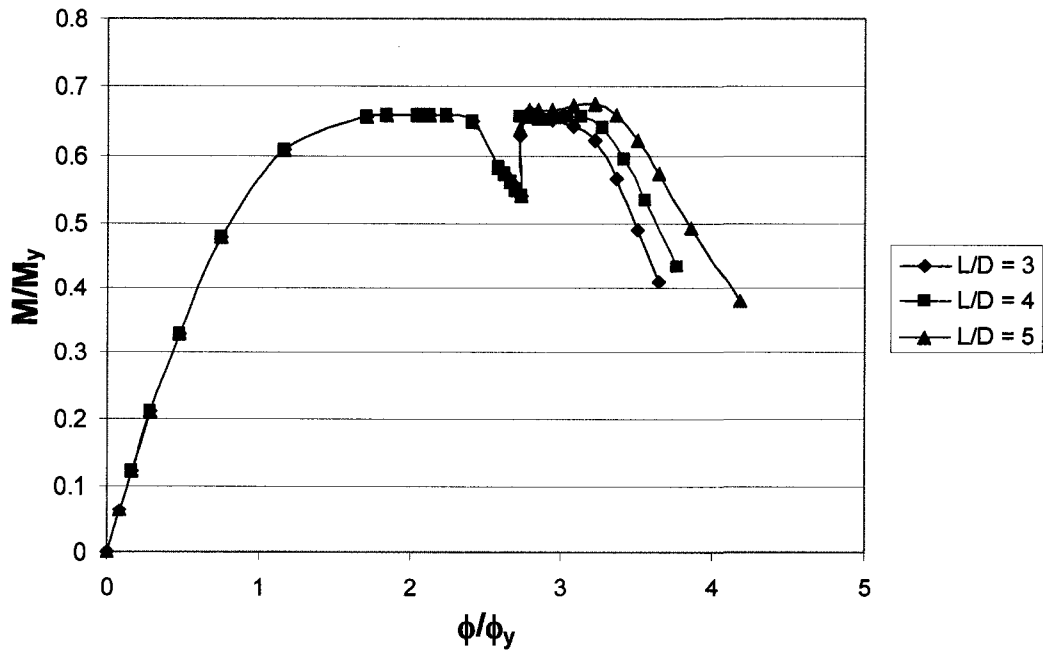
Figure 5.14 Sleeve Length Effect for Case 4 of D/t = 70

Sleeve Length Effect for Case 1 of D/t=90 Pipe
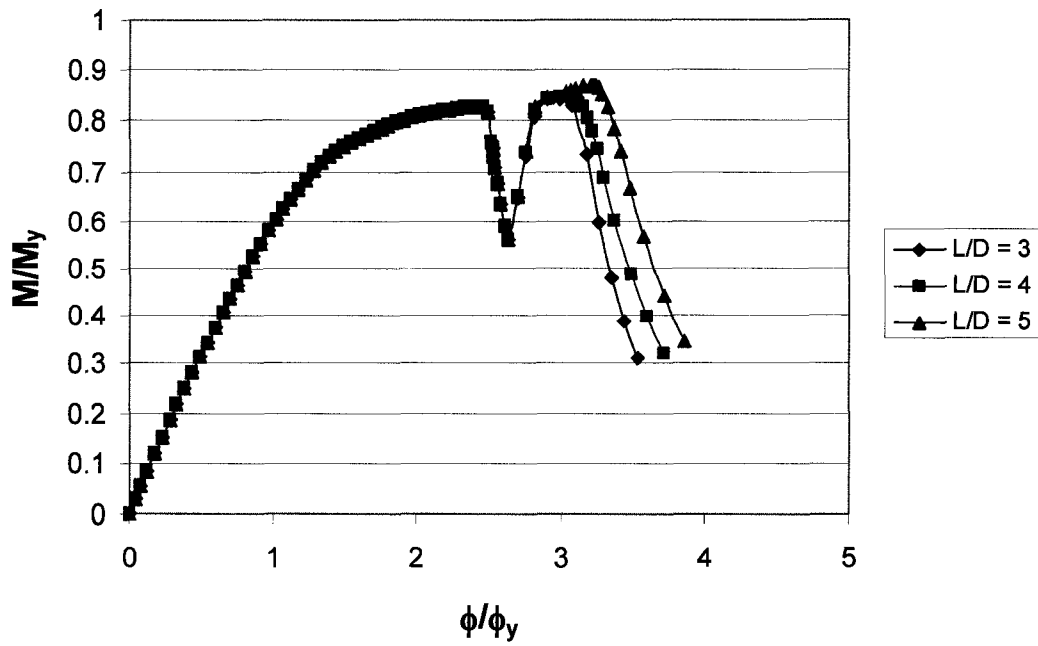
Figure 5.15 Sleeve Length Effect for Case 1 of D/t = 90

Sleeve Length Effect for Case 2 of D/t=90 Pipe
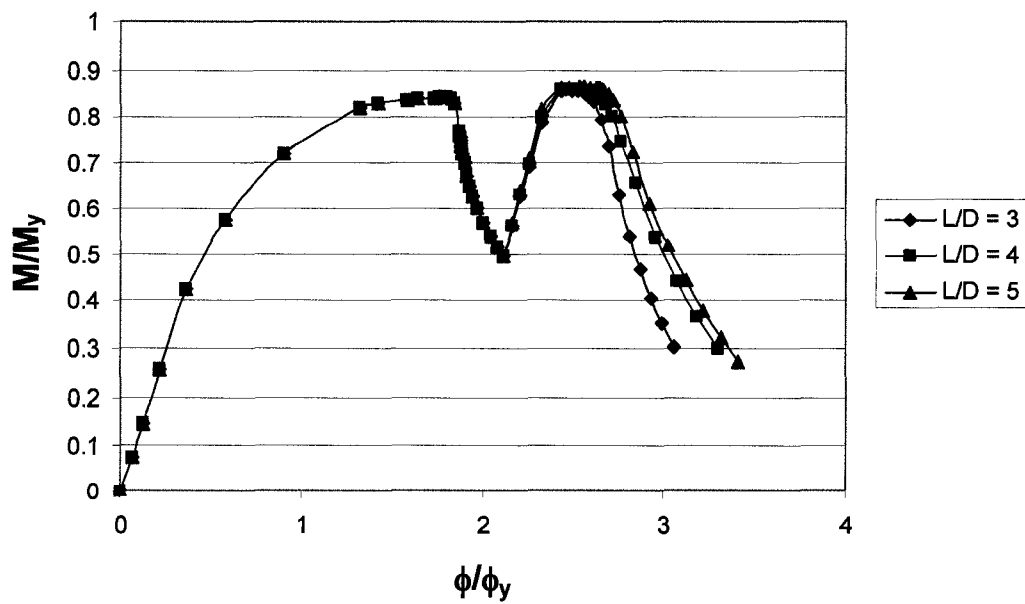
Figure 5.16 Sleeve Length Effect for Case 2 of D/t = 90

Sleeve Length Effect for Case 3 of D/t=90 Pipe
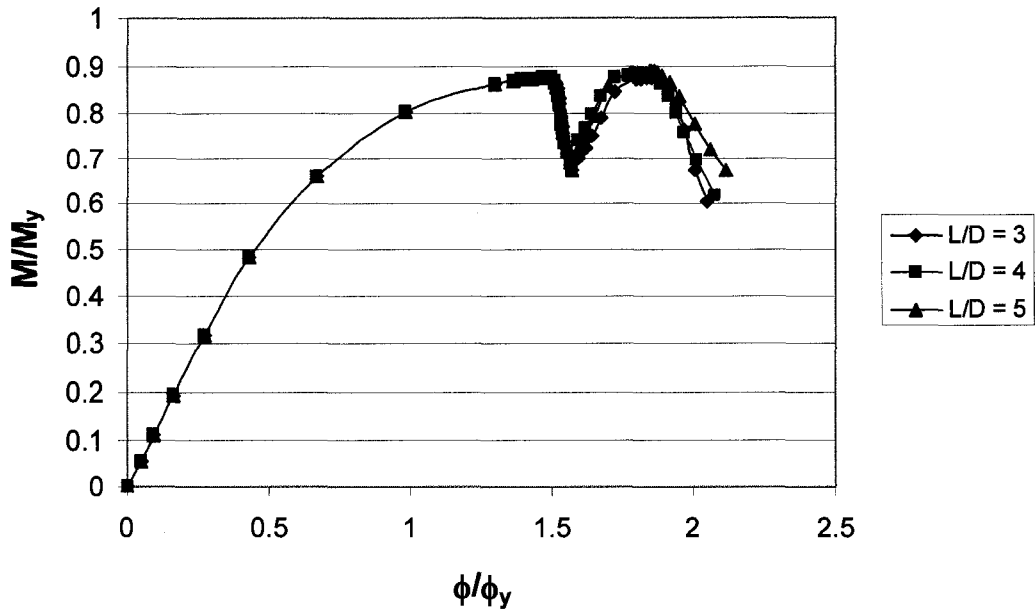
Figure 5.17 Sleeve Length Effect for Case 3 of D/t = 90

Sleeve Length Effect for Case 4 of D/t=90 Pipe
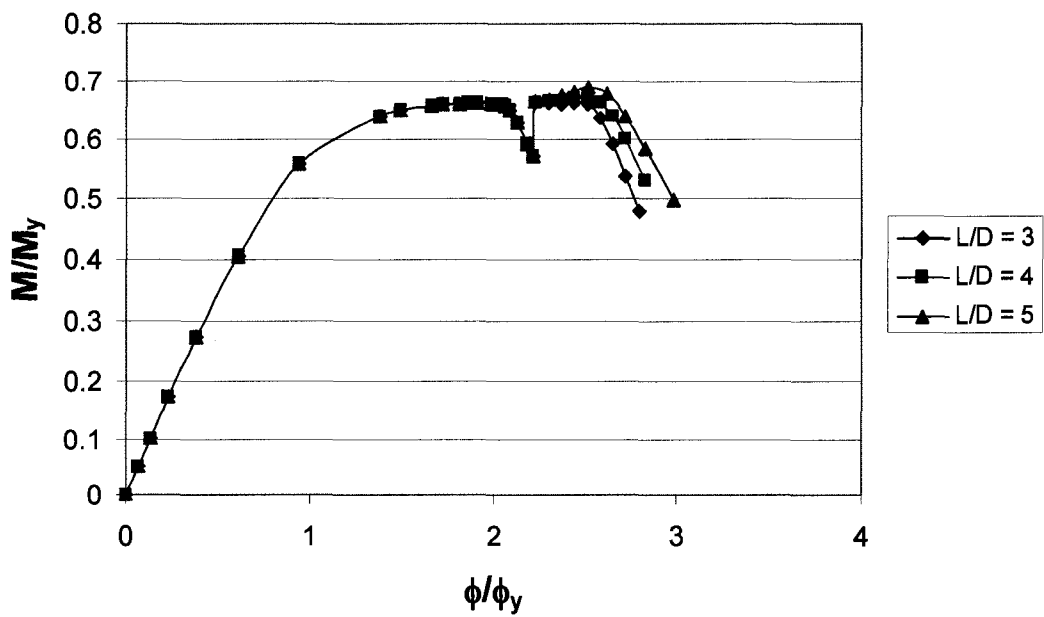
Figure 5.18 Sleeve Length Effect for Case 4 of D/t = 90

(a) Sleeve Length of 3D Long

(b) Sleeve Length of 5D Long
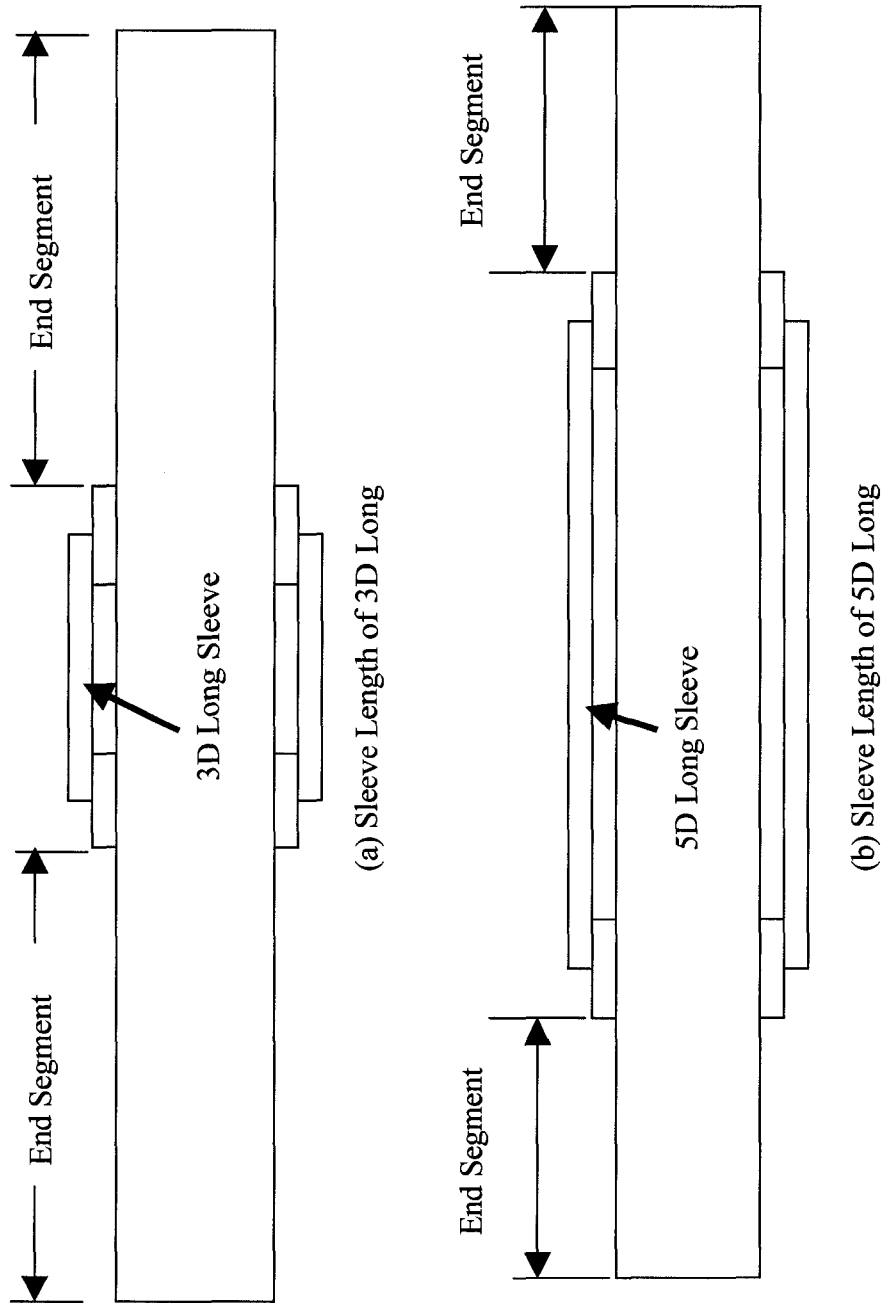
Figure 5.19 Schematic of the Pipe, Collar and Sleeve Assembly

161

3D Long Sleeve with Shorter End Segments
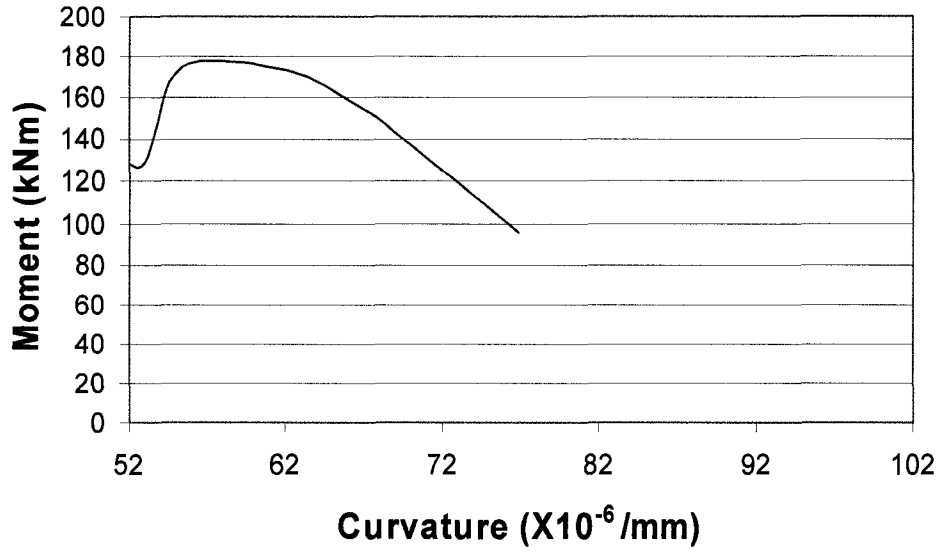
Figure 20 Moment vs. Curvature Response for 3D Sleeve with Shorter End Segment

5D Sleeve with Longer End Segments
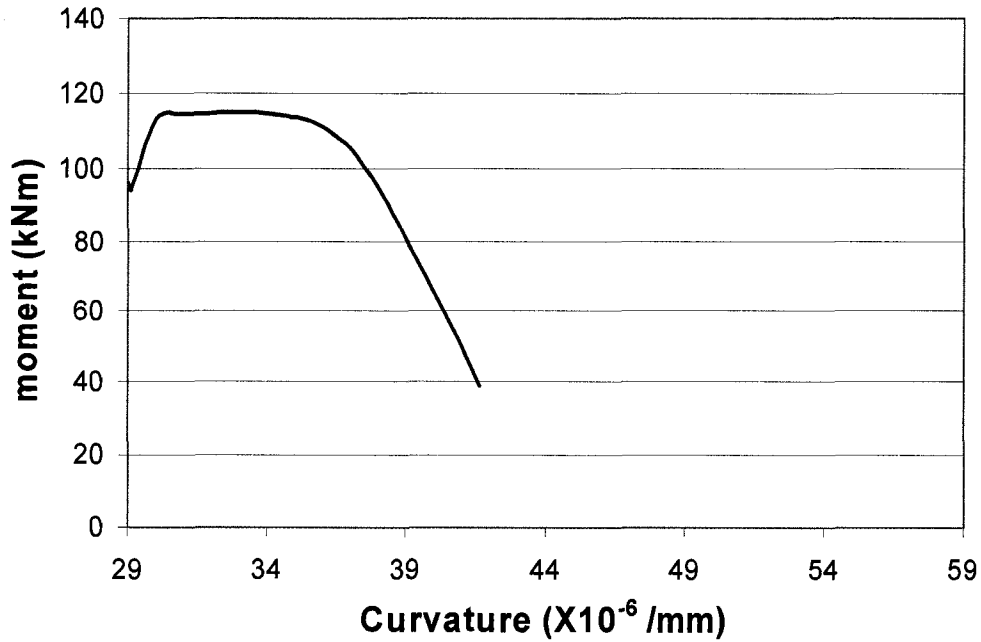
Figure 21 Moment vs. Curvature Response for 5D Sleeve with Longer End Segment

(Case A)

$$\frac{D}{t} = 50 \quad \frac{p}{p_y} = 0.5 \quad \varepsilon_y = 1.76 \times 10^{-3}$$

$t_{SLV}/t = 1.5$
$t_{SLV}/t = 2$
$t_{SLV}/t = 3$

$$\varepsilon_{ySLV} = 1.76 \times 10^{-3} \quad \frac{t_c}{t} = 3 \quad \frac{L_{SLV}}{D} = 5$$

(Case B)

$$\frac{D}{t} = 50 \quad \frac{p}{p_y} = 0.5 \quad \varepsilon_y = 1.76 \times 10^{-3} \quad t_{SLV}/t = 2$$

$\varepsilon_{ySLV} = 1.76 \times 10^{-3}$
$\varepsilon_{ySLV} = 2.20 \times 10^{-3}$
$\varepsilon_{ySLV} = 2.70 \times 10^{-3}$

$$\frac{t_c}{t} = 3 \quad \frac{L_{SLV}}{D} = 5$$

(Case C)

$$\frac{D}{t} = 50 \quad \frac{p}{p_y} = 0.5 \quad \varepsilon_y = 1.76 \times 10^{-3} \quad t_{SLV}/t = 2 \quad \varepsilon_{ySLV} = 1.76 \times 10^{-3}$$

$t_C/t = 3$
$t_C/t = 4$
$t_C/t = 5$

$$\frac{L_{SLV}}{D} = 5$$
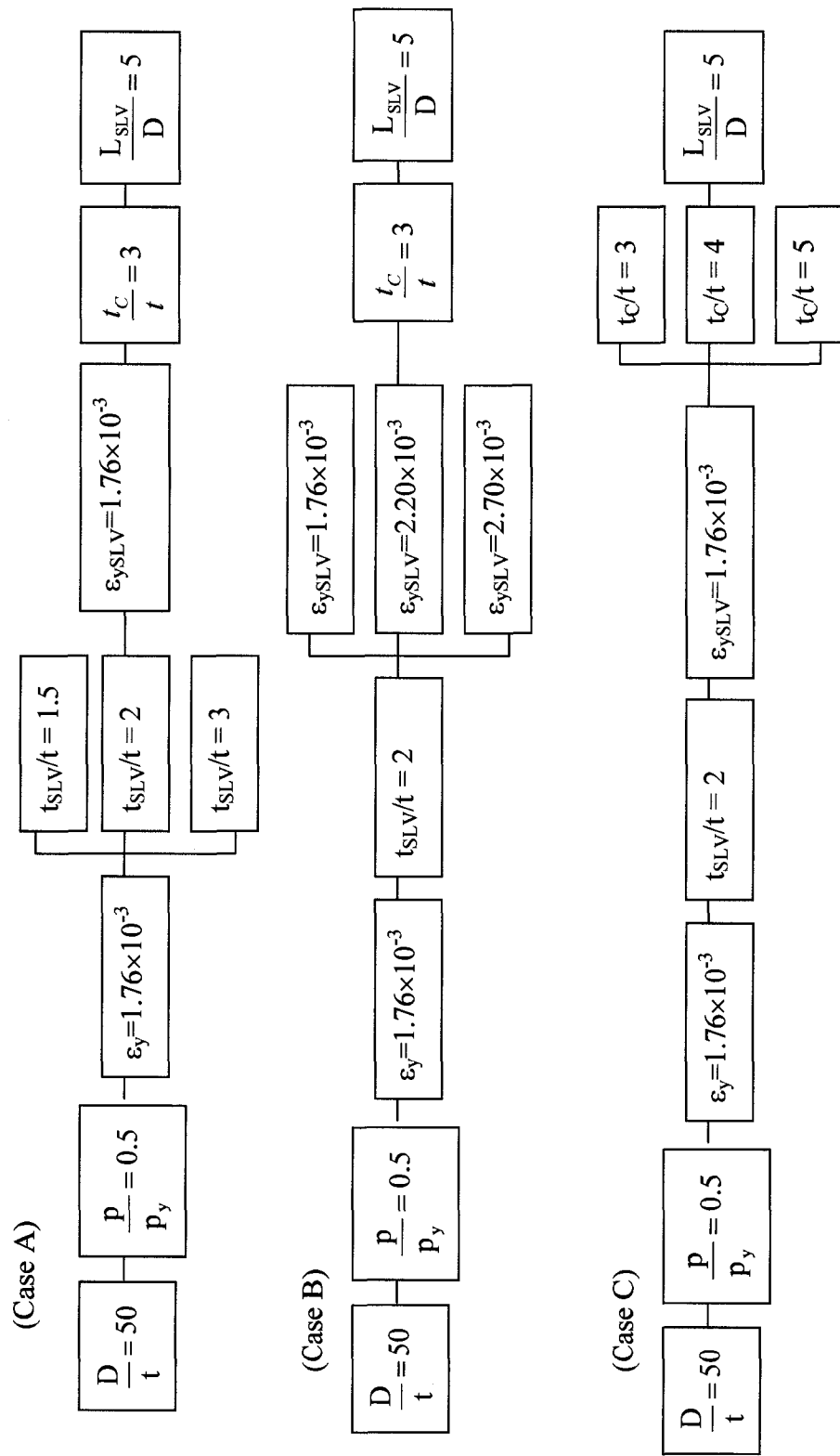
Figure 5.22 Layout of Phase II Study for D/t = 50 Pipe

163

(Case A)

$\dfrac{D}{t} = 70$ — $\dfrac{p}{p_y} = 0.5$ — $\varepsilon_y = 1.76 \times 10^{-3}$ — $t_{SLV}/t = 1.5$ / $t_{SLV}/t = 2$ / $t_{SLV}/t = 3$ — $\varepsilon_{ySLV} = 1.76 \times 10^{-3}$ — $\dfrac{t_C}{t} = 3$ — $\dfrac{L_{SLV}}{D} = 5$

(Case B)

$\dfrac{D}{t} = 70$ — $\dfrac{p}{p_y} = 0.5$ — $\varepsilon_y = 1.76 \times 10^{-3}$ — $t_{SLV}/t = 2$ — $\varepsilon_{ySLV} = 1.76 \times 10^{-3}$ / $\varepsilon_{ySLV} = 2.20 \times 10^{-3}$ / $\varepsilon_{ySLV} = 2.70 \times 10^{-3}$ — $\dfrac{t_C}{t} = 3$ — $\dfrac{L_{SLV}}{D} = 5$

(Case C)

$\dfrac{D}{t} = 70$ — $\dfrac{p}{p_y} = 0.5$ — $\varepsilon_y = 1.76 \times 10^{-3}$ — $t_{SLV}/t = 2$ — $\varepsilon_{ySLV} = 1.76 \times 10^{-3}$ — $t_C/t = 3$ / $t_C/t = 4$ / $t_C/t = 5$ — $\dfrac{L_{SLV}}{D} = 5$
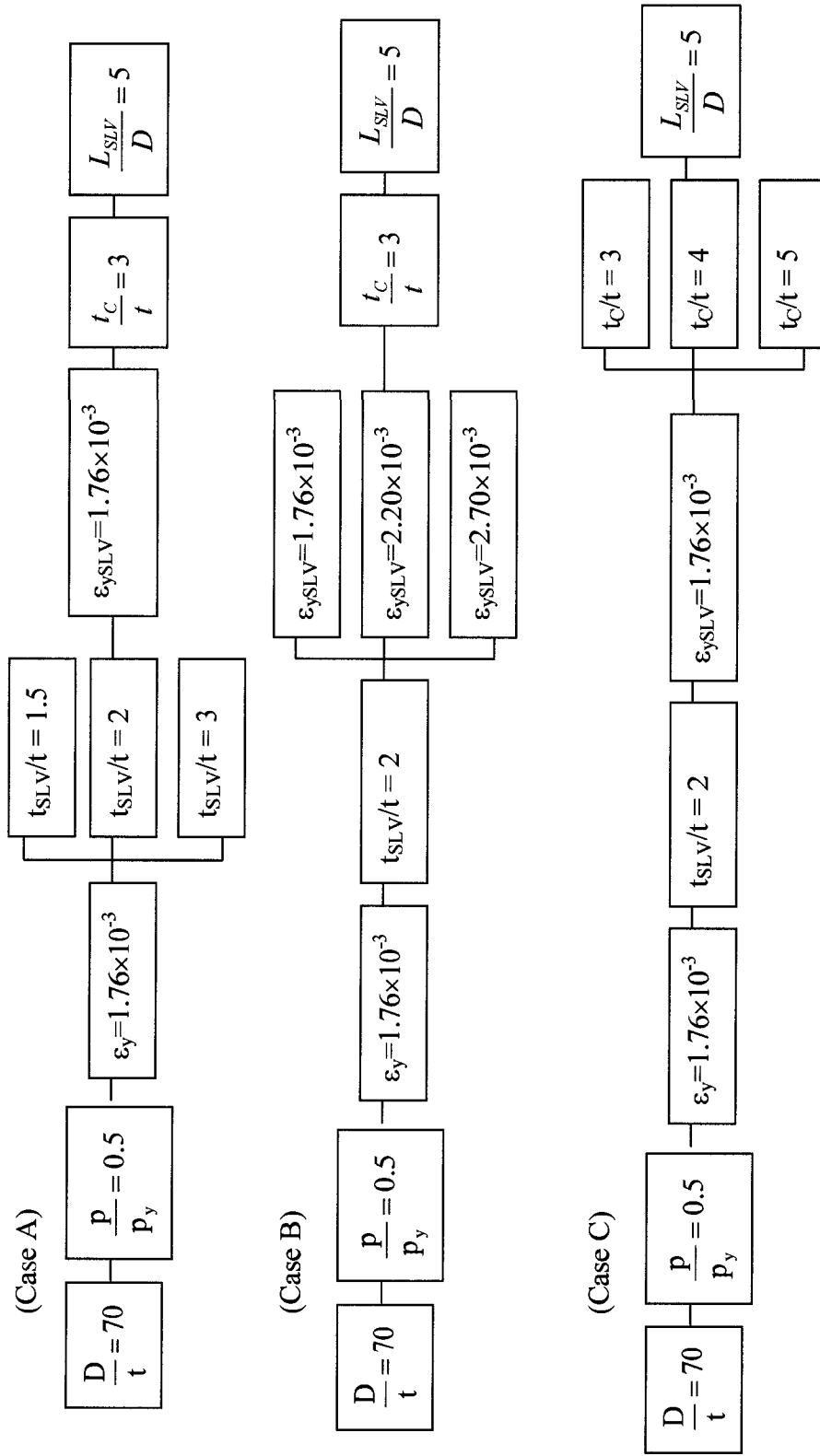
Figure 5.23 Layout of Phase II Study for D/t = 70 Pipe

(Case A)

$$\frac{D}{t} = 90$$ — $$\frac{p}{p_y} = 0.5$$ — $\varepsilon_y = 1.76 \times 10^{-3}$ — [$t_{SLV}/t = 1.5$ | $t_{SLV}/t = 2$ | $t_{SLV}/t = 3$] — $\varepsilon_{ySLV} = 1.76 \times 10^{-3}$ — $$\frac{t_C}{t} = 3$$ — $$\frac{L_{SLV}}{D} = 5$$

(Case B)

$$\frac{D}{t} = 90$$ — $$\frac{p}{p_y} = 0.5$$ — $\varepsilon_y = 1.76 \times 10^{-3}$ — $t_{SLV}/t = 2$ — [$\varepsilon_{ySLV} = 1.76 \times 10^{-3}$ | $\varepsilon_{ySLV} = 2.20 \times 10^{-3}$ | $\varepsilon_{ySLV} = 2.70 \times 10^{-3}$] — $$\frac{t_C}{t} = 3$$ — $$\frac{L_{SLV}}{D} = 5$$

(Case C)

$$\frac{D}{t} = 90$$ — $$\frac{p}{p_y} = 0.5$$ — $\varepsilon_y = 1.76 \times 10^{-3}$ — $t_{SLV}/t = 2$ — $\varepsilon_{ySLV} = 1.76 \times 10^{-3}$ — [$t_C/t = 3$ | $t_C/t = 4$ | $t_C/t = 5$] — $$\frac{L_{SLV}}{D} = 5$$
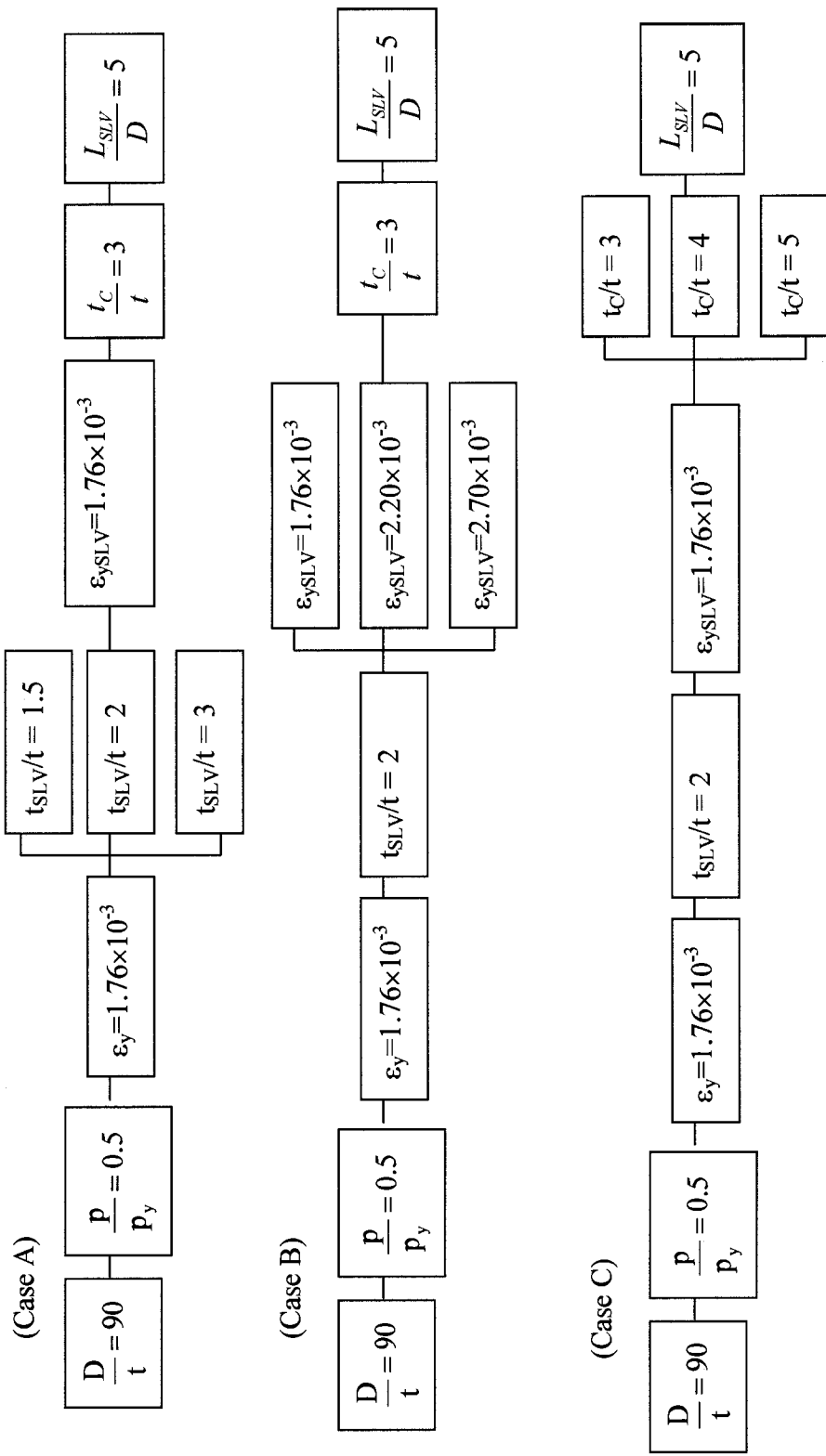
Figure 5.24 Layout of Phase II Study for D/t = 90 Pipe

165

Sleeve Thickness Effect for D/t=50 Pipe in Phase II Study
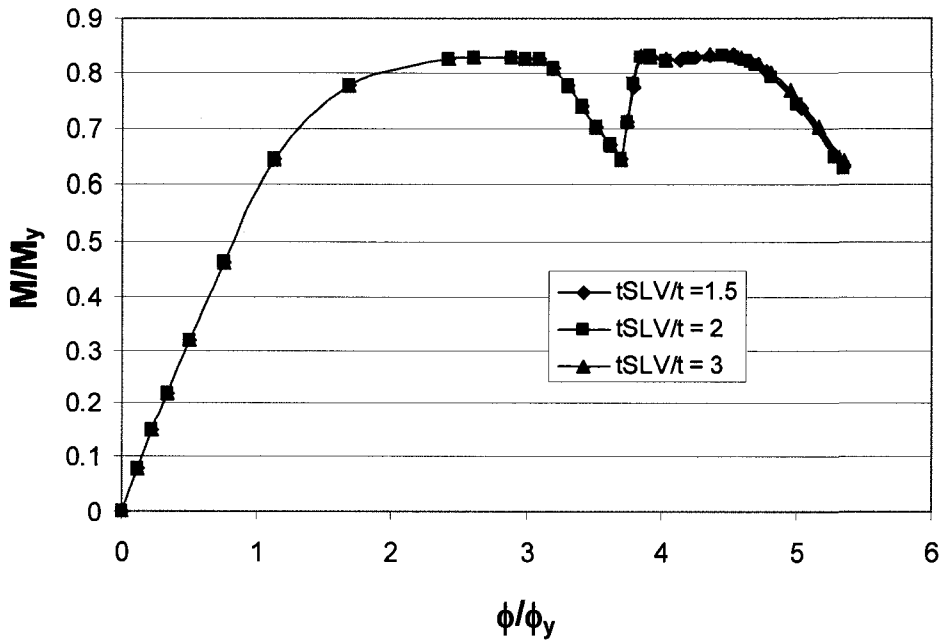
Figure 5.25 Sleeve Thickness Effect for D/t = 50 Pipe

Sleeve Material Properties Effect for D/t=50 Pipe in Phase II Study
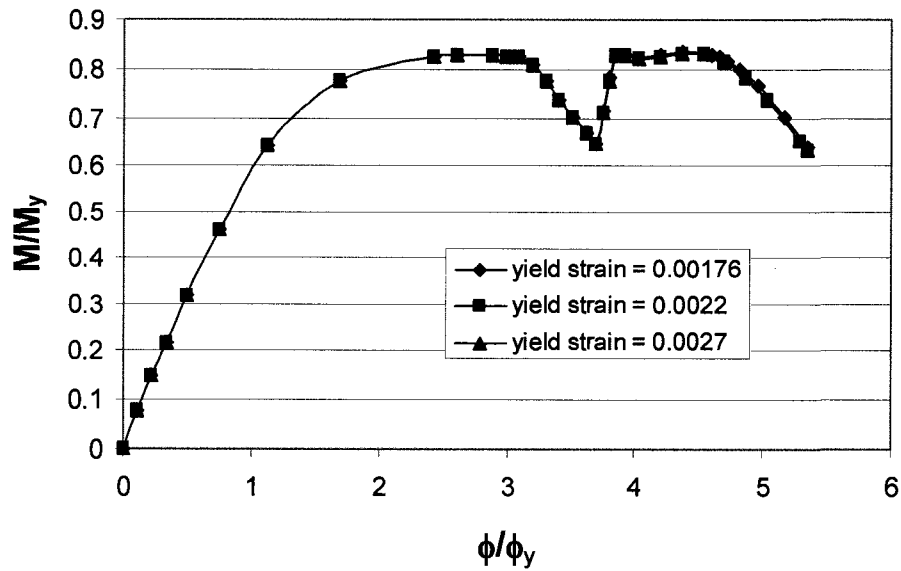
Figure 5.26 Sleeve Material Properties Effect for D/t = 50 Pipe
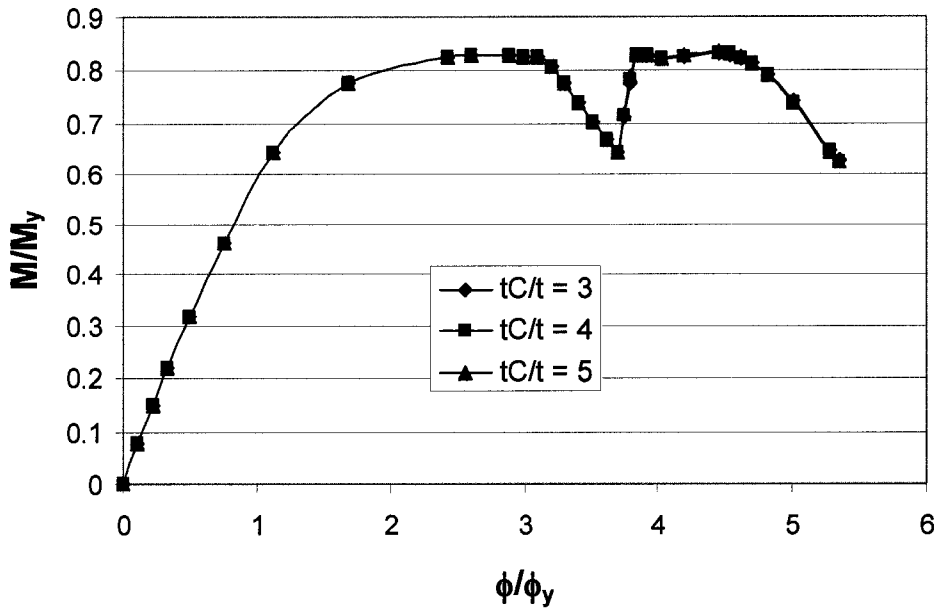
Figure 5.27 Collar Thickness Effect for D/t = 50 Pipe
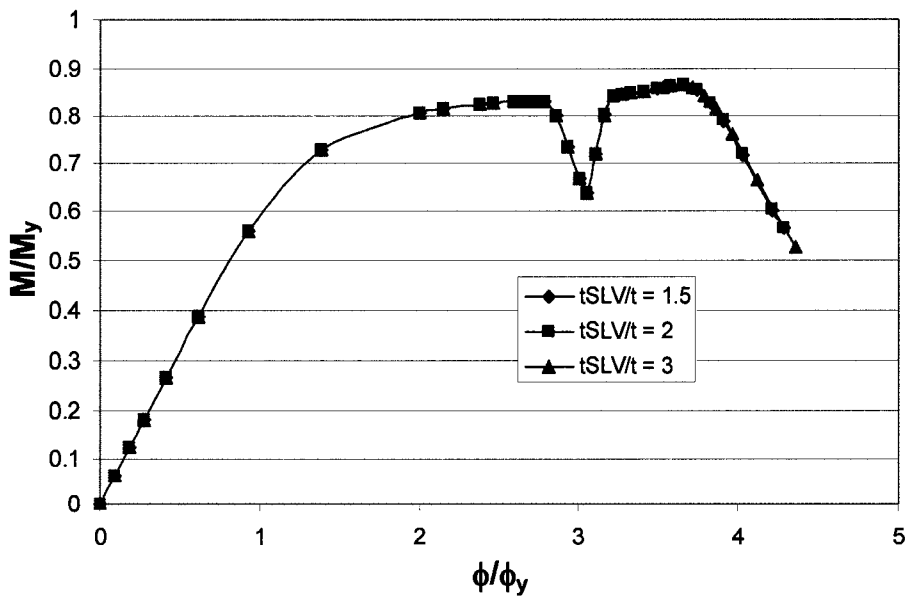
Figure 5.28 Sleeve Thickness Effect for D/t = 70 Pipe

Sleeve Material Properties Effect for D/t=70 Pipe in Phase II Study
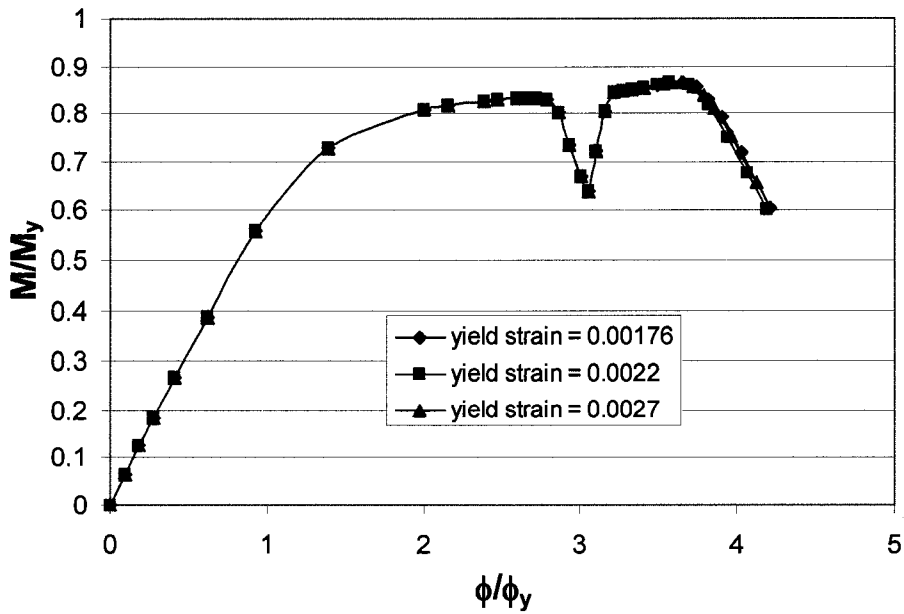
Figure 5.29 Sleeve Material Properties Effect for D/t = 70 Pipe

Collar Thickness Effect for D/t=70 Pipe in Phase II Study
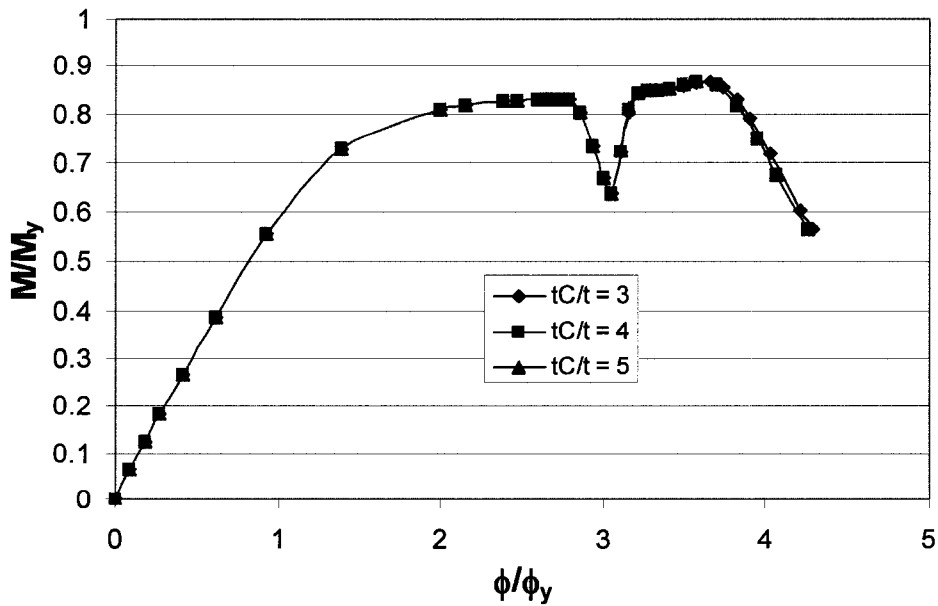
Figure 5.30 Collar Thickness Effect for D/t = 70 Pipe
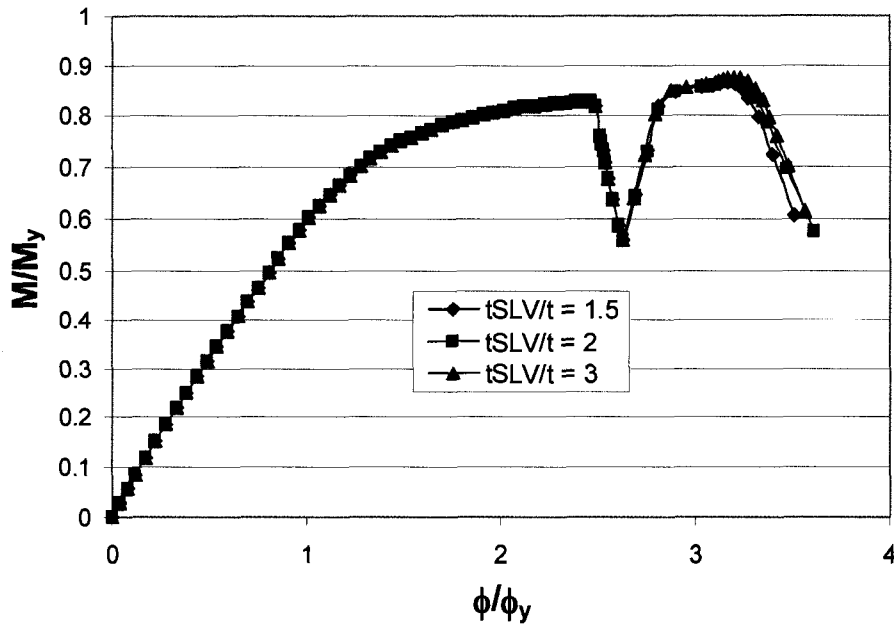
Figure 5.31 Sleeve Thickness Effect for D/t = 90 Pipe

Figure 5.32 Sleeve Material Properties Effect for D/t = 90 Pipe

169

comparison of sleeve length effect for D/t=90 X52 pipe steel
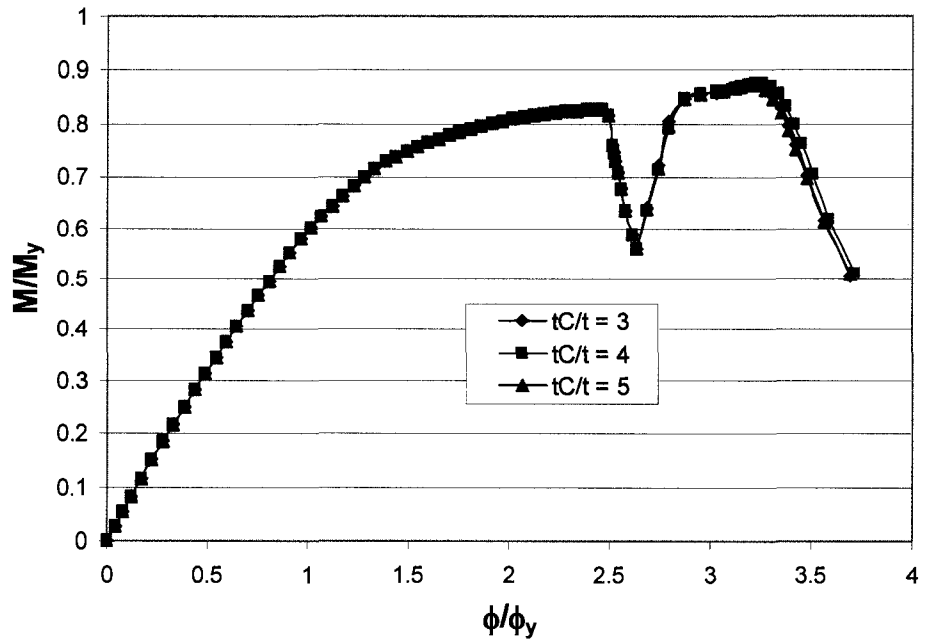
Figure 5.33 Collar Thickness Effect for D/t = 90 Pipe
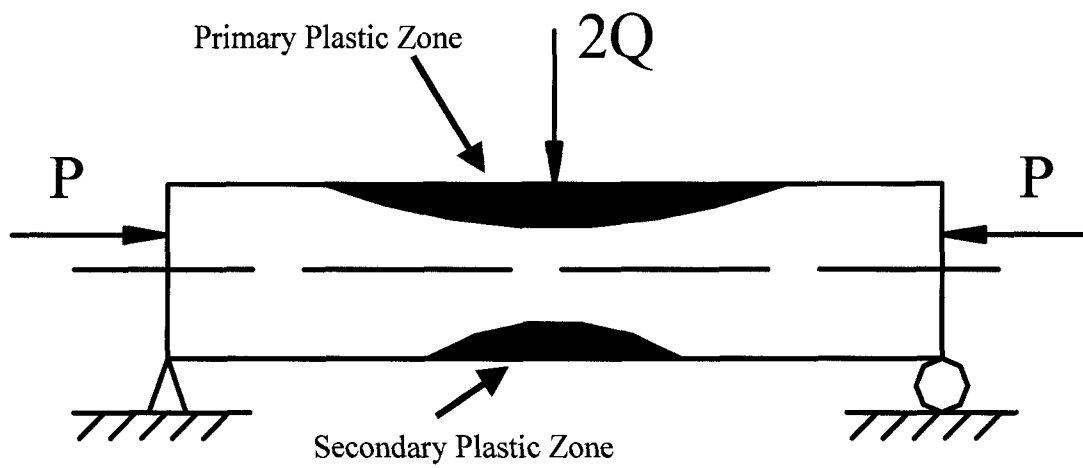
Figure 5.34 Spread of the Plastic Zone in an Elastic/Plastic Beam Column

(Chakrabarty, 2000)
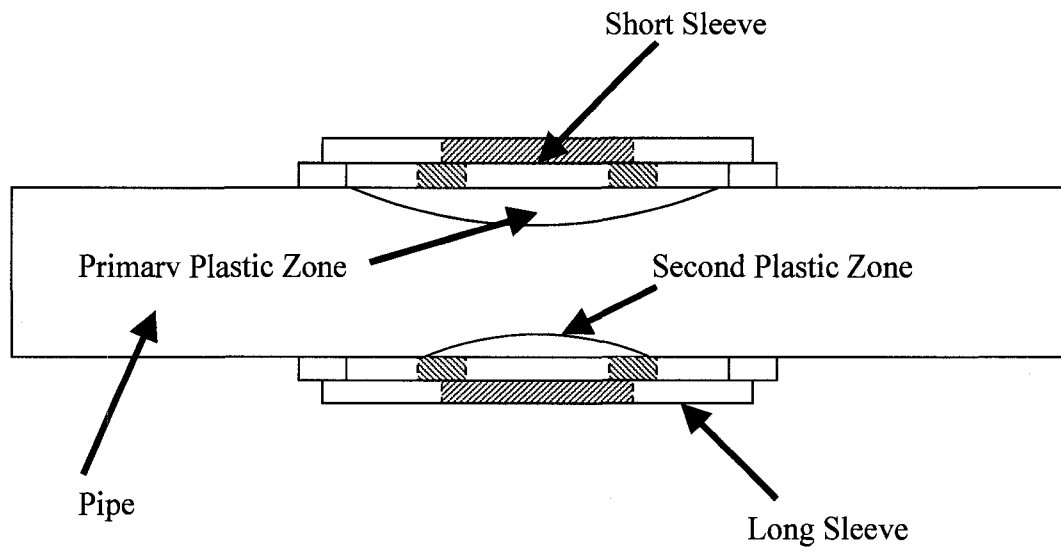
Figure 5.35 Schematic of the Long and Short Repairing Sleeve

CHAPTER 6 CONCLUSIONS AND RECOMMENDATIONS

During the past 15 years, the safety management has become the top priority of the pipeline operating companies. Numerous research projects have been carried out to study the buckling behavior of the pipes in order to ensure the safety and integrity of the pipelines. Because of the complexity of the pipeline field conditions and unpredictable events which could occur along the line, once in a while, local wrinkles are detected in the pipeline field by running a kind of pipeline defect detection tool called the GEOPIG tool. It is the pipeline operating company's interest that the wrinkles detected in the field are handled using the least cost so that the integrity of the pipeline is ensured and the revenue of the company is not significantly affected.

The traditional way to deal with local wrinkles in the pipeline industry is to cut out the wrinkled pipe segment and replace it with a new segment. The pipeline operating company has to suffer significant revenue loss due to the pipeline shut down and pipe segment cut-out replacement related costs. A promising local wrinkle repair technique is causing the pipeline operating company's attention, which involves the encasement of the local wrinkle by using steel sleeves without cutting out the wrinkled pipe segment. There are no need to shut down the pipeline and no need to replace the wrinkled pipe segment. Consequently, the residual life of the original pipeline is extended without interrupting the normal operation of the pipeline. The sleeve repair technique has been used by some pipeline operating companies as the wrinkle repair practice in the pipeline field. Up to date, few researches have been carried out to study the buckling behavior of the wrinkled pipe segment under sleeve repair. It is the purpose of this project to carry out such a study for the pipe wrinkle sleeve repair process.

A built-in technique in the FEA package ABAQUS, the Results Transfer Technique, is attempted in carrying out the numerical analysis of the pipe wrinkle sleeve repair process because of the sequential characteristics of the repairing process. The application of the Results Transfer technique to model the pipe wrinkle sleeve repair process is validated through the comparison with the results obtained by using the

Element Removal/Reactivation modeling technique in the FEA package ABAQUS and through a case history study of pipe wrinkle sleeve repair project conducted in a pipeline field. The Norman Wells to Zama pipeline of Enbridge in northern Alberta experienced wrinkling and double sleeves have been installed onto the wrinkled pipe segment in the pipeline field. The newly attempted modeling technique, i.e., the Results Transfer technique, in the ABAQUS package is used to simulate the behavior of the wrinkled sleeved pipe segment in the pipeline field and to try to trace the loading history the wrinkled pipe segment might experience. The data used for the set-up of and the input to the numerical models is from the GEOPIG measurements, which are carried out on a yearly basis for the past 17 years along this line.

After the validation of the newly attempted Results Transfer technique in the ABAQUS package and the simulations of the pipeline field case history study of the wrinkle sleeve repair process, a full spectrum parametric study, which reflects a variety of loading conditions and geometric configurations for pipe wrinkle sleeve repair process, is performed as part of the project. The purpose of the parametric study is to expand the study results of the pipe wrinkle sleeve repair process based on the pipeline field case to pipes of other diameters with different D/t ratios under different loading combinations with the values being typical in the pipeline industry.

The conclusions based on the study carried out in this project are listed below. Recommendations about the further work regarding the pipe wrinkle sleeve repair are given thereafter.

6.1 CONCLUSIONS

Based on the numerical analyses as described through Chapters 3, 4 and 5 and the numerical simulations of the pipeline field wrinkle sleeve repair, the following conclusions can be obtained in this project.

1.   Running the GEOPIG tool along the pipeline is an effective way in monitoring and detecting defects of the pipelines and in ensuring the safety

174

and integrity of the pipelines. Through the regular GEOPIG run along the pipeline, the local wrinkles occurred along the pipeline can be identified as soon as they formed and can be closely monitored. The data obtained through every GEOPIG run is compiled into database so that the history of the wrinkles can be recorded and accumulated. Decisions can be made by the engineers based on the accumulated GEOPIG data regarding how to to take care of the detected local wrinkles in the pipelines.

2.   The newly attempted Results Transfer Technique in the FEA package ABAQUS, which was initially formulated to model the forming process and assembly process in the ABAQUS, is successfully used to model the pipe wrinkle sleeve repair process because of the close similarity of these processes, i.e., the sequential characteristics of the forming process, the assembly process and the pipe wrinkle sleeve repair process. An excellent agreement is obtained between the field measurements and the numerical analysis.

3.   The sleeve repair technique is an effective and efficient method in rehabilitating the local wrinkles occurred in the pipeline field. By encasing the local wrinkle using a sleeve, the growth of the wrinkle is inhibited. There is no need to shut down the pipeline. The residual life of the original pipeline is extended. The impact to the pipeline operating company's revenue can be minimized as the pipe replacement work is replaced by pipe repair work. In addition, the work time duration is also reduced significantly.

4.   The length of the sleeve used has a significant effect to the behavior of the pipe wrinkle repair work. The longer the sleeve is used, the higher the ductility or deformational capacity of the wrinkle sleeve repair system. The deformational capacity of the pipe wrinkle sleeve repair system, when using 5D long sleeve, can be increased by as high as 15%, comparing with that using 3D long sleeve, which is the current practice in the pipeline industry.

Considering that the pipe deformation occurred in the pipeline field is a slow process, such an increase in the deformational capacity is significant.

5.   The thickness of the sleeve does not affect the performance of the pipe wrinkle sleeve repair system. Based on the considerations of the sleeve manufacture process and the sleeve welding process onto the wrinkled pipe segment in the pipeline field, the preference should give to the thinner sleeve when designing the sleeve repair system as long as the pressure containing requirement is satisfied.

6.   The material properties of the sleeve do not affect the performance of the pipe wrinkle sleeve repair system. Using higher yield strength of the sleeve will not increase the load carrying capacity and the deformational capacity of the sleeve repaired pipe segment. Therefore, the same material properties as those of the carrying pipe should be used for the repairing sleeve.

7.   Change of the thickness of the collars does not affect the buckling behavior of the wrinkled sleeved pipe segment. Thinner collar thickness should be preferred in carrying out the engineering design for the sleeve repair system as long as the geometric compatibility and pressure containment requirement are satisfied.

6.2 RECOMMENDATIONS

The results of this research project provide significant enhancement in understanding the behavior of the wrinkled pipe segment under sleeve repair. In order to gain further understanding to this pipe wrinkle repair technique and ultimately to formulate a design equation for choosing the parameters for the sleeve and the collar, the following areas are identified that require further investigation.

1.   There were no laboratory tests carried out in this project. In order to further validate the numerical model used in the wrinkle sleeve repair simulations,

conducting full scale laboratory tests of the pipe wrinkle sleeve repair work would be beneficial.

2. In conducting the field wrinkle sleeve repair simulations, relatively short segment of pipe isolated from the unstable slope was used. Using much longer pipe segment covering the whole length of the slope and considering the pipe soil interaction in future numerical simulations would be helpful in further understanding the behavior of the field wrinkle sleeve repair system.

3. In carrying out the numerical analysis of the pipe wrinkle sleeve repair process, the same material properties as those of the carrying pipe are used for the sleeve material. Tensile coupon tests for the sleeve material need to be conducted in order to understand and to truly represent the stress vs. strain response of the sleeve material.

4. In doing the parametric study of the pipe wrinkle sleeve repair work, two internal pressure values were studied. Previous full scale pipe laboratory tests carried out in University of Alberta showed that there exists a transition internal pressure under which the pipe buckling mode changes from diamond shape buckle to outward bulge shape. More laboratory tests need to be conducted to further determine the transition pressure value for different pipe D/t ratios.

5. In doing the parametric study of the pipe wrinkle sleeve repair process, straight configuration for the pipe model was used. Cold bent curved pipe model configuration need to be also considered in order to further generalize the applicability of the research results.

6. Only plain pipes (pipes without girth weld) were considered in this project. The behavior of the girth welded pipe segment under sleeve repair needs to be studied.

7. There is a need for the pipeline industry to clarify the acceptable magnitude of the local wrinkle, which they feel comfortable to leave in the pipeline field. Because the soil movement is a very slow process, it is uneconomical to repair the local wrinkle using sleeve at the incipient stage. Full scale laboratory tests of the pipe buckling have shown that the strain can be reached as high as 20% without causing rupture of the pipe specimen. To which extent for a local wrinkle to be safely left in the field needs to be determined.

8. Significant increase of the numerical models in the parametric study is needed for different pipe geometries and loading combinations. This would allow the development of a design equation for use to select the parameters for the sleeve and the collar by the pipeline operating companies.

REFERENCES

ABAQUS Inc., 2003, ABAQUS/Standard User's Manual, Version 6.4, ABAQUS Inc., Pawtucket, Rhode Island, USA

Bang et al, 2002, "Numerical Simulation of Sleeve Repair Welding of In-Service Gas Pipelines", Welding Journal, pp 273-S – 282-S

Barlow, J., 1976, "Optimal Stress Locations in Finite Element Models", International Journal for Numerical Methods in Engineering, Vol. 10, pp 243 – 251.

Bathe, K. G., 1982, "Finite Element Procedures in Engineering Analysis", Prentice Hall Inc., Englewood Cliffs, NJ, USA

Bathe, K. G., 1996, "Finite Element Procedures", Prentice Hall Inc., Upper Saddle River, NJ, USA

Baumgard, A., 2005, "Ward Road Loss Containment – Geotechnical Assessment", BGC Engineering Inc., Vancouver, British Columbia, Canada

Beer, F. P. and Johnston, E. R., 1992, "Mechanics of materials", McGraw Hill, Toronto, Ontario, Canada

Canadian Standards Association, 2003, "Z662 – 03 Oil and Gas Pipeline Systems", Canadian Standard Association, Etobicoke, Ontario

Chakrabarty, J., 2000, "Applied Plasticity", Springer-Verlay, New York, NY, USA

Chen, W. F. and Han, D. J., 1988, "Plasticity for Structural Engineers", Springer – Verlag New York Inc., NY, USA

Clough, R. W., 1960, "The Finite Element Method in Plane Stress Analysis", Proceedings, Second ASCE Conference on Electronic Computation. Pittsburgh, PA, pp 345 – 378

Crisfield, M. A., 1997, "Non-linear Finite Element Analysis of Solids and Structures", Vol. 1, John Wiley & Son Ltd., West Sussex, England, U. K.

Das, S, Cheng, J. J. R. and Murray, D. W., 2002, "Fracture of Wrinkled Energy Pipelines", Structural Engineering Report No. 247, Department of Civil and Environmental Engineering, University of Alberta, Edmonton, Alberta

Del Col, P. R., Grondin, G. Y., Cheng, J. J. R. and Murray, D. W., 1998, "Behavior of Large Diameter Line Pipe Under Combined Loads", Structural Engineering Report No. 224, Department of Civil and Environmental Engineering, University of Alberta, Edmonton, Alberta

DiBattista, J. D., Cheng, J. J. R. and Murray, D. W., 2000, "Behavior of Sleeper – Supported Line Pipe", Structural Engineering Report No. 230, Department of Civil and Environmental Engineering, University of Alberta, Edmonton, Alberta

Dorey, A. B., Cheng, J. J. R. and Murray, D. W., 2001, "Critical Buckling Strains for Energy Pipelines", Structural Engineering Report No. 237, Department of Civil and Environmental Engineering, University of Alberta, Edmonton, Alberta

Fung, Y. C., 1965, "Foundations of Solid Mechanics", Prentice Hall, Inc., Englewood Cliffs, NJ, USA

Gresnigt, A. M. et al, 2003, "Remaining Life of Buckled Pipelines", International Conference on Design, Inspection, Maintenance and Operation of Cylindrical Steel Tanks and Pipelines, Prague, Czech Republic, pp 176 - 182

Hart, James D. et al, 1995, "Experimental and Analytical Investigations of Sleeved Pipeline Configurations", Pipeline Engineering, Vol. 69, PP 47 – 78

Hibbit, H. D., Karlsson, B. I., and Sorenson, P., 1993a, ABAQUS Theory Manual, Version 5.3, Hibbit, Karlsson & Sorenson, Inc., Pawtucket, Rhode Island, USA

Hibbit, Karlsson & Sorenson, Inc., 1994, ABAQUS Theory Manual, Version 5.4, Hibbit, Karlsson & Sorenson, Inc., Pawtucket, Rhode Island, USA

Hill, R., 1950, "The Mathematical Theory of Plasticity", Oxford University Press, London

Langhaar, H. L., 1951, "Dimensional Analysis and Theory of Models", John Wiley & Son Ltd., New York, NY, USA

Lay, M. G., 1982, "Structural Steel Fundamentals – An Engineering and Metallurgical Primer", Australian Road Research Board

Matthies, H. and Strang, G., 1979, "The Solution of Nonlinear Finite Element Equations", International Journal of Numerical Methods in Engineering, Vol. 14, pp 1613 - 1626

Mohareb, M. et al, "Laboratory Testing of Line Pipe to Determine Deformational Behavior", Proceedings of the 12th International Conference on OMAE, Vol. V – Pipeline Technology, ASME pp 109 - 114

Mohareb, M. E., Elwi, A. E., Kulak, G. L. and Murray, D. W., 1994, "Deformational Behavior of Line Pipe", Structural Engineering Report No. 202, Department of Civil and Environmental Engineering, University of Alberta, Edmonton, Alberta

Mroz, Z, 1969, "An Attempt to Describe the Behavior of Metals under Cycling Loads Using a More General Work-Hardening Model", Acta Mechanica, Vol. 7, pp 199 - 212

Rice, J. R., 1975, "Continuum Mechanics and Thermodynamics of Plasticity in Relation to Microscale Deformation Mechanics", Constitutive equations in Plasticity, A. S. Argon, editor, MIT Press, Cambridge, Massachusetts

Sandovall, A., Beruvides, M. and Wiesner, T., 2001, "State of the Art Analysis of Current Research Trends in Pipeline Safety", AIChE Spring National Conference, Process Plant Safety Symposium , Transportation Safety: Safe Transportation of Hazardous Material by Pipeline, Truck, Railroad and Marine Vessel, Paper # T5a05

Schneider, Stephen P., 1998, "Flexural Capacity of Pressurized Steel Pipe", Journal of Structural Engineer, ASCE, Vol. 124, No. 3, PP330 – 340

Sen, M. and Cheng, J. J. R., 2005, "Behavior of Cold Bend Pipes Under Combined Loads", PhD Thesis, Department of Civil and Environmental Engineering, University of Alberta, Edmonton, Alberta

Song, X., Cheng, J. J. R. and Murray, D. W., 2003, "Numerical Solutions for Pipeline Wrinkling", Structural Engineering Report No. 249, Department of Civil and Environmental Engineering, University of Alberta, Edmonton, Alberta

Taylor, E. S., 1974, "Dimensional Analysis for Engineers", Oxford University Press, Ely House, London, U. K.

Westwood, S. and Hektner, D., March, 2003, "Data Integration Ensures Integrity", World Pipelines

Wilkie, S. A., Doblanko, R. M. and Fladager, S. J., 2000, "Case History of Local Wrinkle of a Pipeline", IPC 2000, Calgary, Alberta, Canada, pp 917 - 922

Wu, Z. and Grondin, G. Y., 2002, "Behavior of Steel Columns Reinforced With Welded Steel Plates", MSc Thesis, Department of Civil and Environmental Engineering, University of Alberta, Edmonton, Alberta

Yao et al, 2000, "A Numerical Study of Buckling Sleeved Pipelines", A Report to Enbridge Pipelines Inc., Department of Civil and Environmental Engineering, University of Alberta, Edmonton, Alberta

Yoosef-Ghodsi, N., Kulak, G. L. and Murray, D. W., 1994, "Behavior of Girth – Welded Line Pipe", Structural Engineering Report No. 203, Department of Civil and Environmental Engineering, University of Alberta, Edmonton, Alberta

Yoosef-Ghodsi, N. Y., Cheng, J. J., Murray, D. W., Doblanko, R., and Wilkie, S., 2000, "Analytical Simulation and Field Measurements for a Wrinkle on the Norman Wells Pipeline", IPC 2000, Calgary, Alberta, Canada

Ziegler, H., 1959, "A Modification of Prager's Hardening Rule", Quarterly of Applied Mathematics, Vol. 17, PP 55 - 65

APPENDIX A

MATHEMATICAL FORMULATIONS FOR PAPS PROGRAM

A.1 INTRODUCTION

In this Appendix A, a theoretical approach describing the moment vs. curvature response of the pipes is reported. In the numerical investigation, the strain-hardening of the material is considered, using a mixed hardening formulation. However, the change in the cross-section configuration is not considered. Therefore, ovalization and local buckling are not taken into account. In addition, the residual stresses and transverse girth welds are not taken into account in this investigation. The objective is to develop a simple model capable of predicting the behavior of pipes up to the softening point.

The mathematical formulation for computing the moment vs. curvature response of a pipe cross-section has been implemented in a computer program called Plastic Analysis of Pipe Sections (PAPS). In the following subsections, the initial elastic behavior is described. Then, various choices of stress vs. strain measures and strain-hardening rules are discussed. This is followed by the formulation of the elastic–plastic model used in this study. The analytical procedures to obtain the local and global moment vs. curvature responses of pipe are then described.

A.2 INITIAL YIELDING OF PIPES

A.2.1 General

In this section, a closed-ended pipe similar to a very short test specimen is considered. The sequence of loading is identical to that of the test specimens. Thus, it is assumed that the pipe is first pressurized to the final pressure, then it is subjected to the external axial load, and, finally, curvature is imposed. In the latter step, the very short slice of pipe is considered to be gradually subjected to the imposed curvature to some prescribed value. During this bending procedure, the moment corresponding to the increased curvature at each step is calculated by the computer program PAPS.

The behavior of the pipe is elastic from the beginning of the loading until the proportional limit is reached anywhere in the cross-section. This is the beginning of nonlinearity and plastic behavior. However, for a closed-ended pipe subjected to only internal pressure and axial load, the longitudinal stress, σ_x, and the hoop stress, σ_θ, are independent of the material properties and can be determined from statics.

In the free body diagram shown in Figure A.1, the equilibrium of the forces in the x direction yields

185

$$2 \pi R_m t \sigma_x = \pi R_i^2 p - P \qquad (A.1)$$

where t is the pipe wall thickness, R_i is the inside radius, R_m is the average of inside and outside radii, p is the internal pressure, and P is the applied axial load. The (tensile) stress σ_x can be obtained from Equation (A.1) as

$$\sigma_x = \frac{p R_i}{2 t} \left(\frac{R_i}{R_m} \right) - \frac{P}{2 \pi R_m t} \qquad (A.2)$$

The free body diagram of a half-cylindrical portion of the pipe, with an arbitrary small length l, is shown in Figure A.2. The equilibrium of the forces in the y direction gives

$$2 l t \sigma_\theta = 2 l R_i \, p \qquad (A.3)$$

Hence,

$$\sigma_\theta = \frac{p R_i}{t} \qquad (A.4)$$

The through-thickness stress in a pressurized pipe varies from zero on the outside surface of the pipe to the internal pressure on the inside surface. However, this stress is very small compared to the longitudinal and hoop stresses. Thus, for simplicity, the through-thickness stress is neglected.

The first encounter with the proportional limit could occur during any of the three stages of loading. For a given cross-section and material stress vs. strain curve, this depends on the magnitude of the final pressure and the external axial load.

Because of the biaxial state of the stress (longitudinal and hoop stress), a yield function should be adopted (here *yield* means reaching the proportional limit). There are a number of yield criteria available in the literature. In this study, the von Mises yield criterion, which is commonly used for metals, is employed. This yield criterion has been shown to be in excellent agreement with experimental results for many ductile metals, including different types of steel (Hill 1950). The form of the von Mises criterion for the biaxial state of stress, with the longitudinal and hoop stresses as the principal stresses can be expressed as

$$\sigma_x^2 + \sigma_\theta^2 - \sigma_x \sigma_\theta = \sigma_p^2 \qquad (A.5)$$

where σ_p is the yield stress (i.e., the proportional limit in a uniaxial test). The conditions for reaching the proportional limit during each of the loading stages are discussed in the following subsections.

A.2.2 Initiation of Yielding During Pressurization

Since no external axial load has been applied prior to pressurization, the value of P in Equation (A.2) is zero. Substituting Equation (A.2) and Equation (A.4) into Equation (A.5) results in

$$p_0 = \frac{\sigma_p(\frac{t}{R_i})}{\left[1 - \frac{R_i}{2R_m} + (\frac{R_i}{2R_m})^2\right]^{1/2}} \tag{5.6}$$

where p_0 is the value of the pressure at the first occurrence of the proportional limit. Thus, if the final value of the pressure is less than p_0, the pipe remains elastic during the pressurization.

A.2.3 Initiation of Yielding During Application of Axial Load

Here the pipe has remained elastic under the prescribed final pressure, p. If it is assumed that inelasticity starts during the second stage of loading (i.e., the application of axial load), then the value of axial load, P_0, required to reach the proportional limit can be determined by substituting equation (A.2) and Equation (A.4) into Equation (A.5). This yields

$$P_0 = \pi R_m p \left[R_i(\frac{R_i}{R_m} - 1) \pm \sqrt{4(\frac{\sigma_p t}{p})^2 - 3R_i^2} \right] \tag{A.7}$$

If the prescribed final axial load is less than P_0 determined by Equation (A.7), then the pipe remains elastic throughout the application of axial load. It should be noted that the use of Equation (A.7) is valid only when the pipe has remained elastic during the pressurization. This requires that the prescribed final pressure be less than p_0 obtained from Equation (A.6).

For the usual sizes of line pipes, R_i (the inside radius) is very close to R_m (the average of the inside and outside radii). Therefore, the first term in the bracket in

Equation (A.7) (i.e., $R_i (\frac{R_i}{R_m} - 1)$) is much smaller than the second term in a general case. Consequently, when the sign of the radical is positive, the solution for P_0 is positive, meaning compression. Since the tests carried out at the University of Alberta were always done for P_0 in compression, the only use herein for Equation (A.7) is for the case when that equation gives a positive answer.

A.2.4 Initiation of Yielding During Imposition of Curvature

If the pipe is still elastic at the completion of application of the axial load, then plastification must begin during imposition of the curvature. Figure A.3 illustrates the path along which the stress state proceeds during the three loading stages. As shown in Figure A.3, in the first loading stage (i.e., the pressurization) the stress state of the whole cross-section moves from point O to A on a straight line. This is because from Equations (A.2) and (A.4)

$$\frac{\sigma_\theta}{\sigma_x} = 2 \frac{R_m}{R_i} = \text{constant} \tag{A.8}$$

For a very thin-walled pipe, the inside and mid-surface radii (i.e., R_i and R_m, respectively) are almost equal to each other. Hence, the above ratio is approximately 2. Therefore, the stress state proceeds along the line Om, as shown in Figure A.3. However, the actual path of the stress state for a closed-ended pipe segment subjected to internal pressure must be to the left of the line Om because the slope of the stress path for an actual pipe, given by Equation (A.8), is always greater than 2.

The longitudinal movement of a pipeline in the field can be assumed to be restricted. This implies that the longitudinal strain be zero. Thus, while still elastic, the Poisson's effect gives the value of longitudinal stress as $\mu \sigma_\theta$. At the same time, the pipe segment ends are open and, consequently, Equation (A.2) does not apply. Therefore, the stress state proceeds along the line On shown in Figure A.3 until it reaches the yield ellipse.

For the remaining two loading stages, the hoop stress, which depends only on the internal pressure, remains constant. Therefore, the consequent movements of the stress state for every point on the cross-section occur on the horizontal line passing through A (perpendicular to the σ_θ axis), as shown by line CD in Figure A.3. This line intersects

the yield surface at C and D, and the longitudinal stress values can be determined from Equation (A.5) as

$$\sigma_x(C) = \sigma_0 - \sqrt{\sigma_p^2 - 3\sigma_0^2} \qquad (A.9)$$

$$\sigma_x(D) = \sigma_0 + \sqrt{\sigma_p^2 - 3\sigma_0^2} \qquad (A.10)$$

where $\sigma_0 = \dfrac{\sigma_\theta}{2} = \dfrac{p\,R_i}{2t}$.

It can be seen that point A is slightly to the left of the midpoint between C and D. (The midpoint of CD in Figure A.3 is the point at which Om intercepts CD.) This is because the value of σ_x for the midpoint equals

$$\frac{1}{2}[\sigma_x(C) + \sigma_x(D)] = \sigma_0 = \frac{p\,R_i}{2t} \qquad (A.11)$$

whereas from equation (A.2),

$$\sigma_x(A) = \frac{p\,R_i}{2\,t}(\frac{R_i}{R_m}) \qquad (A.12)$$

Since $\dfrac{R_i}{R_m}$ is less than one, the longitudinal stress at point A is smaller than that of the midpoint.

Applying a compressive axial force moves the stress state from point A toward C on the horizontal path. Here it is assumed that the axial compression does not initiate the plastification. Thus, the stress state of the cross-section at the completion of application of the axial load must be between A and C, the point B in Figure A.3. The value of longitudinal stress for the whole cross-section at B is obtained from Equation (A.2):

$$\sigma_x(B) = \frac{p\,R_i}{2\,t}(\frac{R_i}{R_m}) - \frac{P}{2\,\pi R_m\,t} \qquad (A.13)$$

If the cross-section remains elastic during the application of curvature, the resulting stress distribution can be determined by superposition. From elementary beam theory, the values of stress at the extreme fibers due to the imposed curvature are $\pm\dfrac{M}{S}$, where M is the moment corresponding to the imposed curvature and S is the section modulus,

$$S = \frac{\pi (D_o^4 - D_i^4)}{32 \, D_o} \qquad (A.14)$$

where D_o and D_i are the outside and inside diameters of the pipe, respectively. Therefore, for elastic conditions, the stress states of the extreme compressive and tensile fibers occur at equal distances to the left and right of point B in Figure A.3. Since BC is shorter than BD, the stress state of the extreme compressive fiber is the first to reach the yield ellipse (see Figure A.3). Thus,

$$\sigma_x(B) - \frac{M_0}{S} = \sigma_x(C) \qquad (A.15)$$

where M_0 is the moment required to initiate yielding. Equations (A.9), (A.13), and (A.15) give the value of M_0 as

$$M_0 = S \left(\sqrt{\sigma_p^2 - 3\sigma_0^2} - \sigma_0 + \frac{pR_i}{2t}\left(\frac{R_i}{R_m}\right) - \frac{P}{2\pi R_m t} \right) \qquad (A.16)$$

For the nonlinear analysis that will follow, the values of strains and stresses at the extreme fibers and the curvature corresponding to the yield moment (M_0) need to be calculated. The stress at the maximum tension fiber at the beginning of plasticity is equal to

$$\sigma_x^t = \sigma_x(C) + 2\frac{M_0}{S} \qquad (A.17)$$

Because the through-thickness stress is small, the longitudinal strains can be obtained using the plane stress formulae. Hence,

$$\varepsilon^c = \frac{1}{E}\left(\sigma_x(C) - \nu\sigma_\theta\right) \qquad (A.18)$$

$$\varepsilon^t = \frac{1}{E}\left(\sigma_x^t - \nu\sigma_\theta\right) \qquad (A.19)$$

where ε^c and ε^t are the values of the longitudinal strains at the extreme compression and tension fibers, respectively. The value of curvature at the first yield, ϕ_0, is calculated by the following equation,

$$\phi_0 = \frac{\varepsilon^t - \varepsilon^c}{D_o} \qquad (5.20)$$

Finally, from Equation (A.9) and (A.16) to (A.20),

$$\varphi_0 = \frac{2}{ED_o}\left(\sqrt{\sigma_p^2 - 3\sigma_0^2} - \sigma_0 + \frac{pR_i}{2t}\left(\frac{R_i}{R_m}\right) - \frac{P}{2\pi R_m t}\right) \qquad (A.21)$$

Using the relationship $\phi_0 = \dfrac{M_0}{EI}$ to obtain the curvature ϕ_0 gives the same result as that

given by Equation (A.21).

Note that the equations in this section are to be used only when the pipe is still elastic at the completion of the application of pressure and axial load.

A.3 INCREMENTAL STRESS VS. STRAIN FORMULATIONS

Plasticity can be accompanied by large strains and the choices of strain and stress measures become important. Some widely-used measures of stress and strain are discussed in the subsequent sections in order to determine the most appropriate ones. First, the strain-hardening of the material is examined by reviewing different theories. Then, the elastic–plastic formulation implemented in the computer program PAPS is presented.

A.3.1 Stress and Strain Measures

Among the large number of conjugate stress and strain measures in the literature, three kinematic formulations are employed effectively in elasto-plasticity (Bathe 1982):

1. Engineering Stress and Strain Formulation (ESS)

This formulation assumes infinitesimally small displacements and rotations on the basis that the strain measure is not invariant under rigid body motions (Bathe 1982). The ESS formulation is recommended only for materially-nonlinear analysis. This formulation has been chosen as one of the options in the program PAPS.

2. Total Lagrangian Formulation (TL)

This formulation employs 2nd Piola-Kirchhoff stresses and Green-Lagrange strains. This measure of strain is unaffected by rigid body motions (Bathe 1982). The kinematic assumptions for the strain measure permit large displacements and large rotations. However, this formulation is most effective only for small strains. This is because the constitutive tensor in each increment is subjected to a transformation determined by the deformation gradient with respect to the initial configuration. Nevertheless, if the strains are small, these transformations do not change the components

of the constitutive tensor (provided that the material is isotropic). This formulation without the transformation of the constitutive tensor is one of the options in the program PAPS.

3. Updated Lagrangian Formulation (UL)

This formulation employs Cauchy (true) stresses and updated Lagrangian strains. Under rigid body motion, the strain measure remains unchanged. Hence, it is applicable to general elastic–plastic analysis with large displacements and rotations and large strains. The formulation is effective in large strain analysis because the stress and strain measures used are those that describe the material response in a natural way (Bathe 1982). This strain measure is commonly used for problems in metal plasticity. One motivation for this choice is that when true stress (force per current unit area) is plotted against logarithmic strain, then tension, compression, and torsion test results coincide closely with each other (Hibbit et al. 1993a). In general, at any point of a body the updated Lagrangian longitudinal strain in the direction of an arbitrary axis attached to the body reduces to $\ln(\lambda)$, where λ is the stretch (current length divided by the original length) in that direction.

A.3.2 Elastic–Plastic Formulations

A.3.2.1 General

The elasto-plasticity formulation employed in this model, and discussed below, has been adapted from the book by Chen and Han (1988). In the subsequent derivations, σ_{ij} and ε_{ij} are general notations that could represent any of the three stress and strain measures mentioned in Section A.3.1. The fundamentals of the elastic–plastic formulation are discussed in the following subsections.

A.3.2.1.1 Yield Function

Yield function defines the elastic limit of a material under a combined state of stress. In general, the yield stress is a function of the state of stress, σ_{ij}, and can be expressed as

$$f(\sigma_{ij}, k) = 0 \qquad\qquad (A.22)$$

where k is the hardening parameter. The yield function can be best interpreted geometrically as a surface in stress space. For a perfectly-plastic material, the yield function is assumed to remain unchanged. Thus, the parameter k in Equation (A.22) is a

constant, and the yield surface is therefore fixed in stress space. However, for a work-hardening material the yield surface changes as elastic–plastic deformation occurs.

A.3.2.1.2 Hardening Rule

When an initial yield surface is known, the work hardening rule defines its modification during the process of plastic flow. A number of hardening rules have been proposed. The most widely used are those of isotropic hardening, kinematic hardening, and a combination of both, so-called mixed hardening.

The isotropic hardening rule is based on the assumption that the initial yield surface expands uniformly without distortion and translation in stress space as plastic flow occurs. The size of the yield surface is governed by the value of a parameter k, which depends upon plastic strain history.

The kinematic hardening rules assume that, during elastic–plastic deformation, the loading surface translates as a rigid body in stress space, maintaining the size, shape, and orientation of the initial surface. This rule is implemented by keeping k constant and replacing the stress tenor, σ_{ij}, in Equation (A.22) with the reduced stress tensor, $\overline{\sigma}_{ij}$. Reduced stress components are measured from the center of the yield surface.

$$\overline{\sigma}_{ij} = \sigma_{ij} - \alpha_{ij} \tag{A.23}$$

Here α_{ij} are the coordinates of the yield surface center in stress space, and they depend on the plastic strain history.

A combination of isotropic and kinematic hardening leads to the more general mixed hardening rule. In this case, the yield surface undergoes a translation defined by α_{ij} and a uniform expansion measured by k. This constitutes a more general work hardening, which contains the isotropic and kinematic hardening rules as its two limiting conditions.

Detailed formulations of the isotropic and kinematic rules, along with their contributions in the mixed hardening model, are presented in Sections A.3.2.2.1 and A.3.2.3, respectively. The applicability of the isotropic and kinematic hardening rules to different loading conditions is discussed in Section A.3.3.

A.3.2.1.3. Elastic and Plastic Strain Increment Tensors

One important assumption for elastic–plastic deformation is that the total strain increment tensor is composed of the sum of the elastic and plastic strain increment tensors:

$$d\varepsilon_{ij} = d\varepsilon_{ij}^e + d\varepsilon_{ij}^p \qquad (A.24)$$

where $d\varepsilon_{ij}^e$ and $d\varepsilon_{ij}^p$ are the elastic and plastic strain increment tensors, respectively.

Hooke's law is assumed to provide the necessary relation between the incremental changes of stress and elastic strain; hence,

$$d\sigma_{ij} = C_{ijkl}\, d\varepsilon_{kl}^e \qquad (A.25)$$

where C_{ijkl} is the tensor of elastic moduli. Substituting for $d\varepsilon_{kl}^e$ from Equation (A.24) gives

$$d\sigma_{ij} = C_{ijkl}(\, d\varepsilon_{kl} - d\varepsilon_{kl}^p\,) \qquad (A.26)$$

This is the basic equation for developing the nonlinear constitutive relations to be discussed in Section A.3.2.4.

A.3.2.1.4 Plastic Potential and Flow Rule

The flow rule is the kinematic assumption postulated for elastic–plastic deformation. It gives the ratio or the relative magnitudes of the components of the plastic strain increment tensor, $d\varepsilon_{ij}^p$. In other words, the flow rule defines the direction of the plastic strain increment vector, $d\varepsilon_{ij}^p$, in strain space. By defining a plastic potential function, $g(\sigma_{ij})$, which is a scalar function of the stresses, the plastic flow equations can be written in the form

$$d\varepsilon_{ij}^p = \frac{\partial g}{\partial \sigma_{ij}}\, d\lambda \qquad (A.27)$$

where $d\lambda$ is a positive scalar factor of proportionality, which is nonzero only when elastic–plastic deformations occur. Of great importance is the simplest case for which the yield function and the plastic potential functions coincide, i.e., $f = g$. Thus,

$$d\varepsilon_{ij}^p = \frac{\partial f}{\partial \sigma_{ij}}\, d\lambda \qquad (A.28)$$

and plastic flow develops along the normal to the yield surface. Equation (A.28) is called the associated flow rule and it has been used successfully for metals (Chen and Han 1988). This equation will be used in formulating the nonlinear constitutive relations developed in Section A.3.2.4.

A.3.2.1.5 Consistency Condition

The consistency condition requires that the state of stress remain on the yield surface during plastic flow. Thus, after a small elastic–plastic deformation, the yield condition represented by Equation (A.22) must still be satisfied. Hence,

$$f(\sigma_{ij} + d\sigma_{ij}, \ k + dk) = f(\sigma_{ij}, \ k) + df = 0 \tag{A.29}$$

This, in combination with Equation (A.22), yields

$$df = 0 \tag{A.30}$$

The scalar $d\lambda$ can be determined from this condition, as described in Section A.3.2.4.

A.3.2.2 Von Mises Yield Function

A.3.2.2.1 Generalization of Yield Function for Mixed Hardening

The Von Mises yield function for an isotropic-hardening material is expressed as

$$f(\sigma_{ij}, k) = \frac{3}{2} S_{ij} S_{ij} - k^2 = 0 \tag{A.31}$$

where S_{ij} is the deviatoric stress, defined as

$$S_{ij} = \sigma_{ij} - \frac{1}{3} \sigma_{kk} \delta_{ij} \tag{A.32}$$

In general, the hardening parameter, k, is defined as a function of either the effective plastic strain or the plastic work. Bland (1956) showed that for any yield function that is linear or quadratic (such as the von Mises yield function), using either the effective plastic strain or the plastic work as the argument for k is equivalent. Herein, the simpler choice, which is the effective plastic strain, is used as k in the Von Mises yield criterion. For a Von Mises material, the effective strain, ε_p, is defined in incremental form by

$$d\varepsilon_p = \sqrt{\frac{2}{3} d\varepsilon_{ij}^p d\varepsilon_{ij}^p} \tag{A.33}$$

In the mixed hardening formulation, the plastic strain increment tensor is assumed to be the sum of the isotropic and kinematic portions, denoted by $d\varepsilon_{ij}^i$ and $d\varepsilon_{ij}^k$, respectively:

$$d\varepsilon_{ij}^p = d\varepsilon_{ij}^i + d\varepsilon_{ij}^k \tag{A.34}$$

The isotropic strain increment, $d\varepsilon_{ij}^i$, is associated with the expansion of the yield surface, and the kinematic plastic strain increment, $d\varepsilon_{ij}^k$, is associated with the translation of the yield surface. These two strain components can be written as

$$d\varepsilon_{ij}^i = M \, d\varepsilon_{ij}^p \tag{A.35}$$

$$d\varepsilon_{ij}^k = (1 - M) \, d\varepsilon_{ij}^p \tag{A.36}$$

in which M is the parameter of mixed hardening. It has the range $0 \leq M \leq 1$.

For a mixed-hardening material, the generalized form of the Von Mises yield function is expressed as

$$f(\overline{\sigma}_{ij}, \overline{k}) = \frac{3}{2} \overline{S}_{ij} \, \overline{S}_{ij} - \overline{k}^2(\overline{\varepsilon}_p) = 0 \tag{A.37}$$

where $\overline{S}_{ij}$ is the reduced deviatoric stress, defined as

$$\overline{S}_{ij} = \overline{\sigma}_{ij} - \frac{1}{3} \overline{\sigma}_{kk} \, \delta_{ij} \tag{A.38}$$

and $\overline{\varepsilon}_p$ is the *reduced effective strain*, which is defined in incremental form as

$$d\overline{\varepsilon}_p = \sqrt{\frac{2}{3} d\varepsilon_{ij}^i \, d\varepsilon_{ij}^i} \tag{A.39}$$

From Equations (A.33), (A.35), and (A.39), the relationship between the effective stress and the reduced effective stress is obtained as

$$d\overline{\varepsilon}_p = M \, d\varepsilon_p \tag{A.40}$$

The hardening parameter for an isotropic-hardening material (i.e., k in Equation (A.31)) is called the *effective stress* because it identifies with the yield stress in a uniaxial tension test. For a Von Mises material, the effective stress, σ_e, can be expressed as

$$\sigma_e = \sqrt{\frac{3}{2} S_{ij} S_{ij}} \tag{A.41}$$

For a mixed-hardening material, the *reduced effective stress*, $\overline{\sigma}_e$, is used as the hardening parameter (i.e., $\overline{k}$ in Equation (A.37)). For a Von Mises material, the reduced effective stress can be expressed as

$$\overline{\sigma}_e = \sqrt{\frac{3}{2} \overline{S}_{ij} \, \overline{S}_{ij}}$$
(A.42)

Therefore, the von Mises yield condition for a mixed-hardening material becomes (upon redefining the arguments of the function f in Equation (A.37))

$$f(\sigma_{ij}, \alpha_{ij}, \overline{\varepsilon}_p) = \frac{3}{2} \overline{S}_{ij} \, \overline{S}_{ij} - \overline{\sigma}_e^{\,2}(\overline{\varepsilon}_p) = 0$$
(A.43)

A.3.2.2.2 Plastic Moduli

The effective stress vs. effective strain relationship, characterizing the hardening process of a material, is determined by the experimental uniaxial stress vs. strain relationship, which has the general form

$$\sigma_e = \sigma_e(\varepsilon_p)$$
(A.44)

In the incremental form it becomes

$$d\sigma_e = H_p \, d\varepsilon_p$$
(A.45)

where $H_p(\sigma_e)$ is called the *plastic modulus*. For an isotropic-hardening material, H_p is associated with the expansion of the yield surface. For a mixed-hardening material, however, the *reduced plastic modulus* defined by

$$\overline{H}_p = \frac{d\overline{\sigma}_e}{d\overline{\varepsilon}_p}$$
(A.46)

represents the expansion of the yield surface. However, note that the experimental relationship is always that expressed by Equation (A.44). In a uniaxial test, $d\sigma_e$ and $d\varepsilon_p$ are equal to $d\sigma_{11}$ and $d\varepsilon_{11}$, respectively. (Subscript 1 represents the longitudinal direction in the uniaxial test.) However, the values of the reduced effective stress and strain depend on the choice of the mixed hardening parameter, M. Moreover, the value of $d\overline{\sigma}_e$, which is equal to $d\overline{\sigma}_{11}$, cannot be determined from the test results because the value of $d\alpha_{11}$ can be obtained only from the theory. (Note that $d\overline{\sigma}_{11} = d\sigma_{11} - d\alpha_{11}$ according to Equation (A.23).)

A.3.2.3 Kinematic Hardening Rules

A.3.2.3.1 General Comment

The two kinematic hardening rules considered in the formulations herein are those of Prager and Ziegler. The hardening rule in each case relates the increments in the coordinates of the yield surface center, $d\alpha_{ij}$, to the strain increments and the current states of stress and strain. These relations are used to substitute for $d\alpha_{ij}$ in the derivation of the nonlinear constitutive equations to be described in Section A.3.2.4. The two kinematic hardening rules are discussed as follows.

A.3.2.3.2 Prager Hardening Rule

It is assumed herein that $d\alpha_{ij}$ depends linearly on $d\varepsilon_{ij}^p$. Thus,

$$d\alpha_{ij} = C\,d\varepsilon_{ij}^p \quad \text{or} \quad \alpha_{ij} = C\,\varepsilon_{ij}^p \tag{A.47}$$

where C is the work-hardening constant, characteristic for a given material. By adopting the "associated flow rule," the Prager hardening rule is equivalent to the assumption that the vector $d\alpha_{ij}$ moves in the direction parallel to the normal vector on the yield surface at the current stress state. For a mixed-hardening material, $d\varepsilon_{ij}^k$ replaces $d\varepsilon_{ij}^p$ in Equation (A.47) and it can be shown (Chen and Han 1988) that

$$\overline{H}_p = H_p = \frac{3}{2}C \tag{A.48}$$

Thus, for a mixed-hardening material with the Prager rule,

$$d\alpha_{ij} = \frac{2}{3}H_p\,d\varepsilon_{ij}^k = \frac{2}{3}H_p\,(1-M)\,d\varepsilon_{ij}^p \tag{A.49}$$

A.3.2.3.3 Ziegler Hardening Rule

Ziegler (1959) modified the Prager hardening rule to make it valid for subspaces. He assumed that the transition of the yield surface occurs in the direction of the reduced stress vector in the form

$$d\alpha_{ij} = d\mu\,(\sigma_{ij} - \alpha_{ij}) \tag{A.50}$$

where $d\mu$ is a positive proportionality factor, which depends on the history of the deformation. For simplicity, this factor can be assumed to have the form

$$d\mu = a\,d\varepsilon_p \tag{A.51}$$

in which a is a positive constant characteristic for a given material. Thus,

$$d\alpha_{ij} = a\, d\varepsilon_p\, (\sigma_{ij} - \alpha_{ij}) \qquad (A.52)$$

For a mixed-hardening material, $d\bar{\varepsilon}_p$ replaces $d\varepsilon_p$ in Equation (A.52) and it can be shown (Chen and Han 1988) that

$$\bar{H}_p = H_p = a\, \bar{\sigma}_e \qquad (A.53)$$

Thus, for a mixed-hardening material with the Ziegler rule, from Equations (A.53) and (A.36),

$$d\alpha_{ij} = \frac{H_p}{\bar{\sigma}_e}\, (1 - M)(\sigma_{ij} - \alpha_{ij}) \qquad (A.54)$$

A.3.2.4 Generalization of Kinematic Constitutive Relationships

In this section, a nonlinear constitutive relationship for a mixed-hardening material is derived. This relates the stress and strain increments during elastic–plastic deformation.

Using the consistency condition, i.e., Equation (A.30), for the yield function expressed in Equation (A.43) gives

$$df = \frac{\partial f}{\partial \sigma_{ij}} d\sigma_{ij} + \frac{\partial f}{\partial \alpha_{ij}} d\alpha_{ij} + \frac{\partial f}{\partial \varepsilon_p} d\bar{\varepsilon}_p = 0 \qquad (A.55)$$

In the following, each of the six terms in Equation (A.55) is expressed in terms of the current stress and strain states, strain increments, and the scalar $d\lambda$. After the appropriate substitutions, Equation (5.55) is solved for the scalar $d\lambda$. The constitutive relationship is then obtained by using the expression for $d\lambda$.

i) *Expression for* $\dfrac{\partial f}{\partial \sigma_{ij}}$

It can be shown that (Chen and Han 1988) that

$$\frac{\partial f}{\partial \sigma_{ij}} = 3\,\bar{S}_{ij} \qquad (A.56)$$

ii) *Expression for* $d\bar{\varepsilon}_p$

In order to determine $d\bar{\varepsilon}_p$, the term $d\varepsilon_{ij}^p$ is first obtained from Equation (A.28) (i.e., the flow rule) and Equation (A.56) as

$$d\varepsilon_{ij}^p = 3\,\overline{S}_{ij}\,d\lambda \qquad\qquad (A.57)$$

Equations (A.33), (A.40), and (A.57) yield $d\bar{\varepsilon}_p$ as

$$d\bar{\varepsilon}_p = 2\,M\,\overline{\sigma}_e\,d\lambda \qquad\qquad (A.58)$$

iii) Expression for $\dfrac{\partial f}{\partial \bar{\varepsilon}_p}$

To determine $\dfrac{\partial f}{\partial \bar{\varepsilon}_p}$, Equation (A.43) is differentiated with respect to $\bar{\varepsilon}_p$.

$$\frac{\partial f}{\partial \bar{\varepsilon}_p} = -2\,\overline{\sigma}_e\,\frac{\partial \overline{\sigma}_e}{\partial \bar{\varepsilon}_p} = -2\,\overline{\sigma}_e\,\overline{H}_p \qquad\qquad (A.59)$$

From either Equation (A.48) for the Prager kinematic hardening rule or Equation (A.53) for the Ziegler kinematic hardening rule, $\overline{H}_p$ equals H_p. Hence,

$$\frac{\partial f}{\partial \bar{\varepsilon}_p} = -2\,\overline{\sigma}_e\,H_p \qquad\qquad (A.60)$$

iv) Expression for $\dfrac{\partial f}{\partial \alpha_{ij}}$

The chain rule can be used to derive $\dfrac{\partial f}{\partial \alpha_{ij}}$, and, with the use of Equations (A.23) and (A.56), as

$$\frac{\partial f}{\partial \alpha_{ij}} = \frac{\partial f}{\partial \overline{\sigma}_{kl}}\,\frac{\partial \overline{\sigma}_{kl}}{\partial \alpha_{ij}} = 3\,\overline{S}_{kl}\,(-\overline{S}_{ik}\,\delta_{jl}) \qquad\qquad (A.61)$$

where δ_{jl} is the Kronecker delta. Hence,

$$\frac{\partial f}{\partial \alpha_{ij}} = -3\,\overline{S}_{ij} \qquad\qquad (A.62)$$

v) Expression for $d\alpha_{ij}$

The term $d\alpha_{ij}$ for the Prager rule can be obtained from Equations (A.49) and (A.57) as

$$d\alpha_{ij} = 2\,H_p\,(1-M)\,\overline{S}_{ij}\,d\lambda \qquad\qquad (A.63)$$

For the Ziegler rule, $d\alpha_{ij}$ can be obtained from Equations (A.54) and (A.58) as

$$dα_{ij} = 2 H_p (1 - M) \overline{σ}_{ij} dλ \qquad (A.64)$$

vi) Expression for $dσ_{ij}$

Finally, $dσ_{ij}$ is obtained from Equations (A.26) and (A.57) as

$$dσ_{ij} = C_{ijkl} (dε_{kl} - 3 \overline{S}_{kl} dλ) \qquad (A.65)$$

Substituting Equations (A.56), (A.58), (A.60), (A.62), (A.63), and (A.65) into Equation (A.55) and solving it for $dλ$ results in the following equation for a mixed-hardening material with the Prager rule as the kinematic hardening part.

$$dλ = \frac{3 \overline{S}_{ij} C_{ijkl} dε_{kl}}{9 \overline{S}_{ij} C_{ijkl} \overline{S}_{kl} + 4 H_p \overline{σ}_e^2} \qquad (A.66)$$

In order to obtain the result for a mixed-hardening material with the Ziegler rule as the kinematic hardening part, the same substitutions are to be made except that Equation (A.64) is used instead of Equation (A.63). This reduces to the same expression for $dλ$ as in Equation (A.66).

Substituting Equation (A.66) back into Equation (A.65) gives

$$dσ_{ij} = (C_{ijpq} - \frac{9 C_{ijkl} \overline{S}_{kl} \overline{S}_{mn} C_{mnpq}}{9 \overline{S}_{ij} C_{ijkl} \overline{S}_{kl} + 4 H_p \overline{σ}_e^2}) dε_{pq} \qquad (A.67)$$

This is the constitutive relationship between the stress and strain increments in an elastic–plastic deformation.

By defining C_{ijpq}^* as the term in the brackets in Equation (A.67), that is,

$$C_{ijpq}^* = C_{ijpq} - \frac{9 C_{ijkl} \overline{S}_{kl} \overline{S}_{mn} C_{mnpq}}{9 \overline{S}_{ij} C_{ijkl} \overline{S}_{kl} + 4 H_p \overline{σ}_e^2} \qquad (A.68)$$

Equation (A.67) becomes

$$dσ_{ij} = C_{ijpq}^* dε_{pq} \qquad (A.69)$$

in which, C_{ijpq}^* is called the *elastic–plastic constitutive tensor*.

A.3.2.5 Matrix Representation

The objective is to simplify the constitutive relationship, expressed by Equation (A.67), for the special conditions of the problem under study. The result, expressed in

matrix notation, has been implemented in the program PAPS, as discussed in Section A.4.1.

It is taken herein that the subscripts 1, 2, and 3 are representative of longitudinal, circumferential, and through-thickness directions, respectively. These are also the principal axes for the stress and strain tensors at any point on the cross-section. Therefore, the stress and strain tensors are each represented by their three principal values. Thus, in matrix notation, the stress and stress tensors could be represented by 3x1 vectors and the elastic constitutive tensor could be represented by a 3x3 matrix, $[E]$. Equation (A.66) is expressed in matrix notation as

$$d\lambda = \frac{3\{\overline{S}\}^T[E]\{d\epsilon\}}{9\{\overline{S}\}^T[E]\{\overline{S}\} + 4H_p\overline{\sigma}_e^{\;2}} \tag{A.70}$$

and Equation (A.67) as

$$\{d\sigma\} = \left([E] - \frac{9[E]\{\overline{S}\}\{\overline{S}\}^T[E]}{9\{\overline{S}\}^T[E]\{\overline{S}\} + 4H_p\overline{\sigma}_e^{\;2}}\right)\{d\epsilon\} \tag{A.71}$$

where

$$\{d\sigma\} = \begin{Bmatrix} d\sigma_1 \\ d\sigma_2 \\ d\sigma_3 \end{Bmatrix} \qquad \{\overline{S}\} = \begin{Bmatrix} \overline{S}_1 \\ \overline{S}_2 \\ \overline{S}_3 \end{Bmatrix} \qquad \{d\epsilon\} = \begin{Bmatrix} d\epsilon_1 \\ d\epsilon_2 \\ d\epsilon_3 \end{Bmatrix} \tag{A.72}$$

Here, the principal stresses or strains are noted by a single subscript (e.g., $\overline{S}_2 = \overline{S}_{22}$ is the reduced deviatoric stress in circumferential direction). The elastic constitutive matrix, $[E]$, can be expressed as (Chen and Han 1988)

$$[E] = \begin{bmatrix} 2G + \lambda_E & \lambda_E & \lambda_E \\ \lambda_E & 2G + \lambda_E & \lambda_E \\ \lambda_E & \lambda_E & 2G + \lambda_E \end{bmatrix} \tag{A.73}$$

in which

$$G = \frac{E}{2(1+\mu)} \qquad \text{and} \qquad \lambda_E = \frac{\mu E}{(1+\mu)(1-2\mu)} \tag{A.74}$$

where E is the modulus of elasticity and μ is Poisson's ratio.

A.3.2.6 Two-Dimensional Analysis

As mentioned in Section A.2.1, the through-thickness stress is neglected in the numerical model. This means that $d\sigma_3$ always equals zero. However, to be able to carry out the above calculations in two dimensions (i.e., longitudinal and circumferential directions), the yield function needs to be reduced to a two-dimensional form. The yield function in terms of the reduced stresses, rather than the reduced deviatoric stresses, can be expressed as

$$f = \frac{1}{2}\left[(\overline{\sigma}_1 - \overline{\sigma}_2)^2 + (\overline{\sigma}_2 - \overline{\sigma}_3)^2 + (\overline{\sigma}_3 - \overline{\sigma}_1)^2\right] - \overline{\sigma}_e^2 \qquad (A.75)$$

Recall from Equation (A.23) that $\overline{\sigma}_i = \sigma_i - \alpha_i$. Thus, in order for Equations (A.70) and (A.71) to be two-dimensional and since σ_3 always equals zero, the value of α_3 should remain zero during plastification. (Note that the α_i terms are zero at the beginning of plastification.)

For the Prager kinematic hardening rule, $d\alpha_3$ is obtained from Equation (A.63) as

$$d\alpha_3 = 2\,H_p\,(1-M)\,\overline{S}_3\,d\lambda \qquad (A.76)$$

where $\overline{S}_3$ is, in general, nonzero. For the Ziegler kinematic hardening rule, $d\alpha_3$ is obtained from Equation (A.64) as

$$d\alpha_3 = 2\,H_p\,(1-M)\,(\sigma_3 - \alpha_3)\,d\lambda \qquad (A.77)$$

in which σ_3 is always equal to zero and α_3 is initially zero. Therefore, α_3 remains zero throughout the elastic–plastic deformation. Thus, for a mixed-hardening material using the Ziegler rule the yield function becomes two-dimensional. However, when the Prager rule is used, the yield function remains three-dimensional. Note that in the case of the isotropic-hardening material (i.e., M = 1), the yield function is two-dimensional because all α_i terms (including α_3) are zero.

In order to carry out the calculations in Section A.3.2.5 in two dimensions, the constitutive matrix, $[E]$, must be that for a plane stress situation ($\sigma_3 = 0$). Thus, in this case (Chen and Han 1988),

$$[E] = \begin{bmatrix} 2G + \lambda_E - Q & \lambda_E - Q \\ \lambda_E - Q & 2G + \lambda_E - Q \end{bmatrix} \qquad (A.78)$$

where

$$Q = \frac{\lambda_E^2}{2G + \lambda_E} \qquad (A.79)$$

A.3.2.7 Loading Criterion

The objective is to determine the loading criterion to be used during the bending process. It is assumed that the stress state of an arbitrary point on the cross-section is on the yield surface, i.e., $f = 0$. A subsequent curvature increment in the numerical procedure increases the longitudinal strain at the point by an amount $\Delta\varepsilon_x$.

One possible state of deformation due to the longitudinal strain increment is elastic unloading. In this case, the longitudinal stress increment can be large enough to produce an elastic–plastic loading subsequent to the elastic unloading (i.e., by meeting the yield surface at a new point across from the initial stress state). Therefore, the criterion to be used herein must be able to detect the immediate state of deformation. This is carried out by assuming an infinitesimal increment in the longitudinal strain, $d\varepsilon_x$, in the same direction as the original longitudinal strain increment, $\Delta\varepsilon_x$. (Note that ε_x and ε_1 are used interchangeably herein.) This is accomplished if $\Delta\varepsilon_x$ and $d\varepsilon_x$ have the same sign. In addition, it is assumed tentatively that the deformation due to $d\varepsilon_x$ is elastic (i.e., either unloading or neutral loading).

If the actual deformation is elastic, the increment in yield function, df, due to the assumed elastic deformation will be non-positive. This is because, in an elastic deformation (loading or neutral loading), the stress state either moves inside or slides on the yield surface. This implies that $df \leq 0$.

However, if the actual deformation is elastic–plastic, df, which is due to the assumed elastic deformation, must be positive. This is because the yield surface is unchanged during the assumed elastic deformation. Thus, the resultant stress state ends up outside the original yield surface. This implies that $df > 0$.

Hence, the loading criterion can be expressed as

$$df \begin{cases} > 0, & \text{loading} \\ = 0, & \text{neutral loading} \\ < 0, & \text{unloading} \end{cases} \tag{A.80}$$

Equation (A.55) is used to evaluate df. As mentioned, the assumed deformation is elastic; thus, the plastic parameters such as α_{ij}, ε_{ij}^p, and $\bar{\varepsilon}_p$ remain unchanged. Therefore, $d\alpha_{ij}$ and $d\bar{\varepsilon}_p$ are zero in Equation (A.55). Hence,

$$df = \frac{\partial f}{\partial \sigma_{ij}} d\sigma_{ij} \tag{A.81}$$

The through-thickness stress (σ_3) is small and can be neglected in this study. In addition, during bending the hoop stress (σ_2), which depends only on internal pressure, remains constant. Consequently, $d\sigma_1$ $(= d\sigma_x)$ is the only nonzero stress component in Equation (A.81). Thus,

$$df = \frac{\partial f}{\partial \sigma_1} d\sigma_1 \tag{A.82}$$

The term $d\sigma_1$ $(= d\sigma_x)$ is the stress increment due to the assumed elastic deformation. Therefore, it can be obtained by the use of elastic stress vs. strain relationships

$$\begin{Bmatrix} d\sigma_1 \\ 0 \\ 0 \end{Bmatrix} = [E] \begin{Bmatrix} d\varepsilon_1 \\ d\varepsilon_2 \\ d\varepsilon_3 \end{Bmatrix} \tag{A.83}$$

where $[E]$ is given by Equation (A.73). Solving Equation (A.83) for $d\sigma_1$ yields

$$d\sigma_1 = \zeta \, d\varepsilon_1 \quad \text{or} \quad d\sigma_x = \zeta \, d\varepsilon_x \tag{A.84}$$

in which

$$\zeta = \frac{4G(G + \lambda_E - Q)}{2G + \lambda_E - Q} > 0 \tag{A.85}$$

The terms $\dfrac{\partial f}{\partial \sigma_1}$ and $d\sigma_1$ are substituted into Equation (A.82) from Equations (A.56) and (A.84), respectively, to give

$$df = 3\zeta \, \overline{S}_1 \, d\varepsilon_1 = 3\zeta \, \overline{S}_x \, d\varepsilon_x \tag{A.86}$$

Here only the sign of df is of interest. Since ζ is a positive constant and $d\varepsilon_x$ has the same sign as $\Delta\varepsilon_x$, the criterion expressed in Equation (A.80) can be rewritten as

$$\overline{S}_x \Delta\varepsilon_x \begin{cases} > 0, & \text{loading} \\ = 0, & \text{neutral loading} \\ < 0, & \text{unloading} \end{cases} \tag{A.87}$$

205

Note that the result of the expression in Equation (A.87) never comes exactly to zero in an actual calculation by computer. Therefore, in practical terms there are only two cases, loading and unloading.

In the case of loading, the entire deformation increment is elastic–plastic. In the case of unloading, however, it must be checked whether there is an elastic–plastic deformation following the initial elastic deformation. This is done by comparing the longitudinal strain increment, $\Delta\varepsilon_x$, with the strain increment value, $\Delta\varepsilon_x^*$, that moves the stress state onto the yield surface (onto a new point on the yield surface across from the initial stress state). If $\left|\Delta\varepsilon_x\right|$ exceeds $\left|\Delta\varepsilon_x^*\right|$, then there will be an elastic–plastic deformation subsequent to the elastic deformation with a longitudinal strain increment of $\Delta\varepsilon_x - \Delta\varepsilon_x^*$.

A.3.2.8 Forcing Increments to Satisfy Consistency Condition

The consistency condition of Equation (A.55), df = 0, must be met in an elastic–plastic loading process. However, since many approximations are made in the numerical implementation of the incremental constitutive relation, the consistency condition is often only approximately satisfied. In other words, the stress does not stay on the subsequent yield surface. A correction to the stress vector is required to meet the yield condition and to prevent error accumulation. This can be achieved by adding a correction to the stress vector in the direction normal to the yield surface. The correction vector, $\{\delta\sigma\}$, can be expressed as (Chen and Han 1988)

$$\{\delta\sigma\} = \gamma\left\{\frac{\partial f}{\partial\sigma}\right\} \tag{A.88}$$

where

$$\gamma = \frac{-f(\{\sigma\},\varepsilon_p)}{\left\{\dfrac{\partial f}{\partial\sigma}\right\}^T\left\{\dfrac{\partial f}{\partial\sigma}\right\}} \tag{A.89}$$

By substituting for $\left\{\dfrac{\partial f}{\partial\sigma}\right\}$ from Equation (A.56), the correction vector becomes

$$\{\delta\sigma\} = \frac{-f\{\overline{S}\}}{3\{\overline{S}\}^T\{\overline{S}\}} \tag{A.90}$$

This can be further simplified by using the yield condition Equation (A.43) as

206

$$\{\delta\sigma\} = \frac{-f}{2\overline{\sigma}_e^{\,2}}\{\overline{S}\}$$

(A.91)

A.3.3 Evaluation of Strain-Hardening Rules

Isotropic hardening is generally considered to be a suitable model for problems in which the plastic straining goes well beyond the incipient yield state where the Bauschinger effect is noticeable (Rice 1975). This hardening is therefore used for such applications as large motion dynamic problems and manufacturing process involving large plastic strain, and where the plastic strain rate does not reverse direction sharply (Hibbit et al. 1993a).

In cases involved low-amplitude strain cycling, it is important to model the Bauschinger effect. Kinematic hardening is the simplest theory that does this. The basic concept is that the yield surface shifts in the stress space so that straining in one direction reduces the yield stress in the opposite direction. Various levels of sophistication in the kinematic hardening model have been reported in the literature (Hibbit et al. 1993a). Two of these kinematic hardening models, namely, the Prager and the Ziegler models have been used in this investigation as alternatives to isotropic hardening.

Since a nonlinear stress vs. strain curve from a coupon test will be passed on to the program, the hardening is nonlinear (more precisely, multilinear). In addition, large strains form in the process of bending the pipe. The kinematic hardening theory, however, is not a good material model for nonlinear work hardening and it is not recommended for large strain problems (Hibbit et al. 1993b). This gives rise to some disadvantages in the use of kinematic hardening as the work hardening model in this study.

In many problems, when the applied loads or displacements do not increase in proportion but vary in a more complex manner (for instance, oscillating between fixed or variable limits), the simple hypotheses of work hardening models are not sufficient to describe the plastic behavior. Thus, more general work hardening models have been introduced for these cases (Mroz 1969). However, since the loading procedure for the pipe under study is rather simple and non-cyclic, only the isotropic and kinematic hardening models have been used in this investigation. These hardening models are combined in a mixed hardening model that is described subsequently.

A.4 ANALYTICAL PROCEDURES

A.4.1 Procedure to Obtain Local Moment vs. Curvature Response

The numerical model developed herein is based on the assumptions and formulation described in the preceding sections of this chapter. This formulation has been implemented in the computer program PAPS (Section A.1). The output of PAPS consists of the local moment vs. curvature response and the stress and strain values around the cross-section of the pipe throughout the loading. The loading sequence is similar to that for the test specimens: pressure is applied first, axial load is applied next, and finally the bending moment is applied. In the first and second stages of loading, the entire cross-section has uniform states of stress and strain. Upon bending, however, the cross-section is discretized into a number of elements to represent the variation in the stress and strain values around the section, as shown in **Figure A.4**. Only one-half of the cross-section needs to be considered because of the symmetry about the plane of bending.

The following steps are carried out in order to obtain the local moment vs. curvature response of the pipe.

1. *Find the stage at which plastification begins.* This is done using the criteria developed in Section A.2. If the initiation of plasticity occurs during the pressurization, *go to Step 1a.* If plastification begins during the application of axial load, *go to Step 1b.* If the initiation of plasticity occurs during bending, *go to Step 1c.*

   1a. When the initiation of plasticity occurs during the pressurization, the values of longitudinal and hoop stress upon yielding are obtained from Equations (A.2) and (A.4), where the pressure, p, is determined from equation (A.6) $(p = p_0)$ and the axial load, P, equals zero. The values of strains are simply calculated by the plane stress formulae. *Go to Step 2 of the algorithm.*

   1b. When plastification begins during the application of axial load, the longitudinal and hoop stresses upon yielding are obtained from Equations (A.2) and (A.4), in which the pressure, p, is at the prescribed (final) value and the axial load, P_0, is determined from equation (A.7). The strain values are calculated by the plane stress formulae. *Go to Step 3 with* $\overline{P} = P_0$. Note that $\overline{P}$ is the initial axial load used in Step 3 of the algorithm.

1c. When the initiation of plasticity occurs during bending, the values of internal pressure and axial load are at their prescribed values (final values). The longitudinal stresses at the extreme compressive and tensile fibers upon yielding are obtained from equations (A.15) and (A.17), respectively. The corresponding strain values are obtained from Equations (A.18) and (A.19), respectively. The assumption that the cross-section remains planar after deformation results in linear variations of stresses and strains with the depth. By interpolation of the stress and strain values at the extreme tensile and compressive fibers, the stress and strain values for each element of the cross-section are determined. The moment at first yield, M_0, and the corresponding curvature, ϕ_0, are obtained from equations (A.16) and (A.21), respectively. *Go to Step 4 with* $\overline{M} = M_0$ *and* $\overline{\phi} = \phi_0$. Note that $\overline{M}$ and $\overline{\phi}$ are the initial values of moment and curvature used in Step 4 of the algorithm.

2. *Increase the pressure from p_0 to the final value (prescribed).* The pressurization is carried out in a prescribed number of equal pressure increments. From Equations (A.2) and (A.4), the longitudinal and hoop stress increments can be expressed as

$$\Delta\sigma_x = \frac{\Delta p\, R_i}{2\,t}(\frac{R_i}{R_m}) \tag{A.92}$$

$$\Delta\sigma_\theta = \frac{\Delta p\, R_i}{t} \tag{A.93}$$

where Δp is the pressure increment. For each pressure increment, the increment in strain values are calculated from equation (A.71), and all the stress and strain values as well as the effective plastic strain and the coordinates of the yield surface center are updated. These updated values are used for the next increment; thus, the constitutive equation (equation (A.71)) is updated at each increment. *Go to Step 3 with* $\overline{P} = 0$ *and* $\overline{\phi} = 0$.

3. *Increase the axial load from $\overline{P}$ to the final value (prescribed).* The compression of the pipe is carried out in a prescribed number of equal increments of axial load. Since the pressure has already been applied, it is constant (at its final value) from the beginning. Therefore, the hoop stress increment is zero. Thus, the only stress increment is the longitudinal one, determined from Equation (A.2) as

$$\Delta\sigma_x = -\frac{\Delta P}{2\pi R_m t} \tag{A.94}$$

where ΔP is the axial load increment. *Go to Step 4 with* $\overline{M} = 0$ *and* $\overline{\phi} = 0$.

4. *Increase the curvature from* $\overline{\phi}$ *to the prescribed value,* ϕ^*. Bending of the pipe is carried out in a prescribed number of equal curvature increments:

$$\Delta\phi = \frac{\phi^* - \overline{\phi}}{N_C} \qquad (A.95)$$

where $\Delta\phi$ is the curvature increment and N_C is the prescribed number of curvature increments.

Note 1: Up to Step 4, all the calculations have been for the entire cross-section. At this step, however, because of the variation in stress and strain values due to bending, the cross-section is discretized into a prescribed number of elements (see Figure A.4). Each element will have a separate set of stresses, strains, effective plastic strain, and coordinates of the center of the yield surface. Also, up to bending, because the strains remain small, the three stress vs. strain measures lead to almost identical results. Therefore, prior to bending engineering stress vs. strain measures are used for convenience. In the process of bending, however, large membrane strains are produced. Therefore, all the calculations in Step 4 are carried out using the stress vs. strain formulation chosen for the analysis.

Note 2: Because the axial force of the pipe remains constant throughout bending, the neutral axis of bending (i.e., the axis with zero longitudinal bending strain) stays within the cross-section (see Figure A.4). However, the position of the bending neutral axis varies with increasing curvature and this requires an iterative procedure to locate the bending neutral axis. As shown in Figure A.4, the position of the bending neutral axis is located by the angle ψ_0. This angle is set to zero at the beginning of the iterations for the first curvature increment. Thereafter, the current position of the neutral axis is taken as the initial value for the next curvature increment. Each curvature increment is carried out according to the following procedure.

Go to Step 4.a

4a. *Set the position of the bending neutral axis.* As described above, if this is the first curvature increment, set the angle ψ_0 to zero; otherwise, set ψ_0 to the last position of the bending neutral axis. *Go to Step 4b.*

4b. *Calculate the engineering longitudinal strain of each element,* e, for the increased curvature by the following formula (see Appendix B, equation (B.32)).

$$e = e_0 + y\,(\phi + \Delta\phi)\,(1 + e_0) \qquad\qquad (A.96)$$

where e_0 is the engineering longitudinal strain of the cross-section at the start of bending and y is the depth of the center of the element from the bending neutral axis, as shown in Figure A.4. This engineering strain is converted to logarithmic strain or Lagrangian strain, respectively, depending upon whether the UL or TL formulation has been selected. The conversion is carried out using the conversion formulae derived in Appendix B (Equations (B.8) and (B.9)). Next, the increment of the longitudinal strain of the element, $\Delta\varepsilon_x$, is obtained by subtracting the initial value of the strain (known at the beginning of the iteration) from the increased one. *Go to Step 4c.*

4c. *Examine the stress state of the element with respect to the yield surface.* The stress state at the beginning of the increment is known from the previous increment. If the initial stress state is plastic (i.e., on the yield surface), *go to Step 4c.1.* If the initial stress state is elastic (i.e., inside the yield surface), *go to Step 4c.2.*

4c.1. The loading criterion for an initial state of stress that is on the yield surface has been discussed in Section A.3.2.7. The loading criterion expressed by Equation (A.87) determines whether there is a loading or unloading condition due to the longitudinal strain increment, $\Delta\varepsilon_x$. In the case of loading, *go to Step 4d.1.* In the case of unloading, *go to Step 4d.2.*

4c.2. When the stress state is initially elastic, the deformation may be large enough to entail an elastic–plastic loading after the elastic loading. This is checked by comparing the longitudinal strain increment with the strain increment value that moves the stress state onto the yield surface in the same direction as the strain increment. Note that there are two possible directions, opposite to each other, that can be taken to reach the yield surface. The direction in

which the stress state moves is determined by the sign of the longitudinal strain increment. *Go to step 4d.3.*

4d. *Solve the constitutive equations.*

4d.1. In the case of loading, Equation (A.71) is solved for the three unknowns which are the longitudinal stress increment (the other two stress increments are zero), the hoop strain increment, and the through-thickness strain increment. If two-dimensional analysis is selected, the two unknowns are the longitudinal stress increment and the circumferential strain increment. *Go to Step 4e.*

4d.2. In the case of unloading, a check is carried out to determine whether an elastic–plastic loading follows the initial elastic deformation (as described in Section A.3.2.7). The elastic part of the deformation is evaluated by the plane stress formulation and the elastic–plastic part, if any, is evaluated as described in Step 4d.1. *Go to Step 4e.*

4d.3. The elastic part of the deformation is evaluated by the plane stress formulation and the elastic–plastic part, if any, is evaluated as described in Step 4d.1. *Go to Step 4e.*

4e. *Calculate the axial force for the trial position of the bending neutral axis.* When Step 4d is carried out for all the elements, the axial force of the cross-section is calculated by integrating the longitudinal stress over the area of the cross-section.

If the difference between the calculated axial force, P_{cal}, and the prescribed axial force, P^*, is small enough to satisfy the following criterion

$$\frac{P^* - P_{cal}}{P^*} < \beta \tag{A.97}$$

where β is a prescribed tolerance, *then go to step 4e.1*. Otherwise, *go to step 4e.2.*

4e.1. When P_{cal} satisfies the criterion in Equation (A.97), the trial position of the bending neutral axis is satisfactory. Thus, all the variables associated with each element (i.e., stress and strain components, effective plastic strain, and

212

coordinates of the yield surface center) are updated using the last results. The loading moment is also calculated by integration to obtain the moment corresponding to the current curvature. At this point, the increment is complete. *Begin the next increment from Step 4a.*

4e.2. When P_{cal} does not satisfy the criterion in Equation (A.97), the position of the presumed bending neutral axis is moved in a way that depends on the magnitude of P_{cal} compared with P^*. If P_{cal} is less than P^*, the actual bending neutral axis is located below the position assumed. Thus, the presumed bending neutral axis is shifted downward by adding a prescribed fraction of $\delta\psi$ to ψ_0 (see Figure A.4) and the Steps 4b to 4e are repeated. Similarly, if P_{cal} is greater than P^*, the presumed bending neutral axis will be moved upward by the angle $\delta\psi$. This procedure continues until the actual bending neutral axis is located within the current angle increment $\delta\psi$. This happens when the inequality in Equation (A.97) changes direction (e.g., $P_{cal} < P^*$ but after adding $\delta\psi$ to ψ_0, $P_{cal} > P^*$). When the bending neutral axis is located within the angle $\delta\psi$, the bisection method is employed to close in on the actual bending neutral axis position until the criterion in equation (A.97) is satisfied. Upon satisfying this criterion, the calculations for the curvature increment are final and the variables associated with each element can be updated and the bending moment corresponding to the current curvature calculated. *Go to Step 4a for the next curvature increment.*
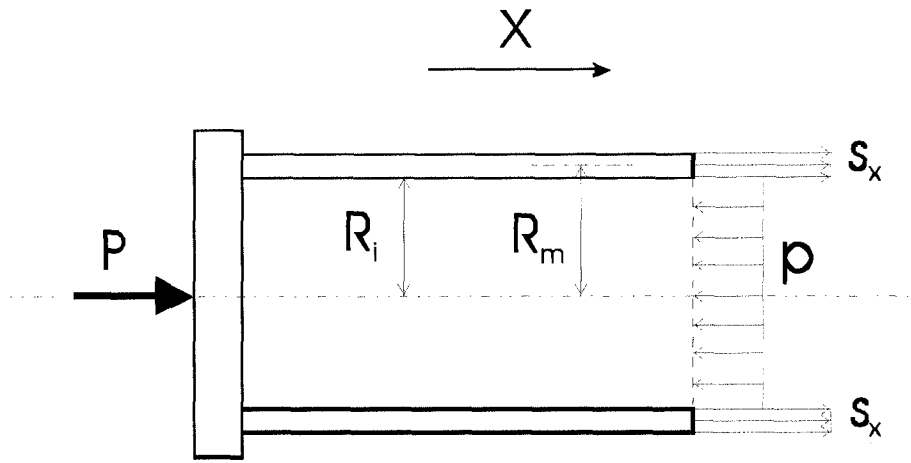
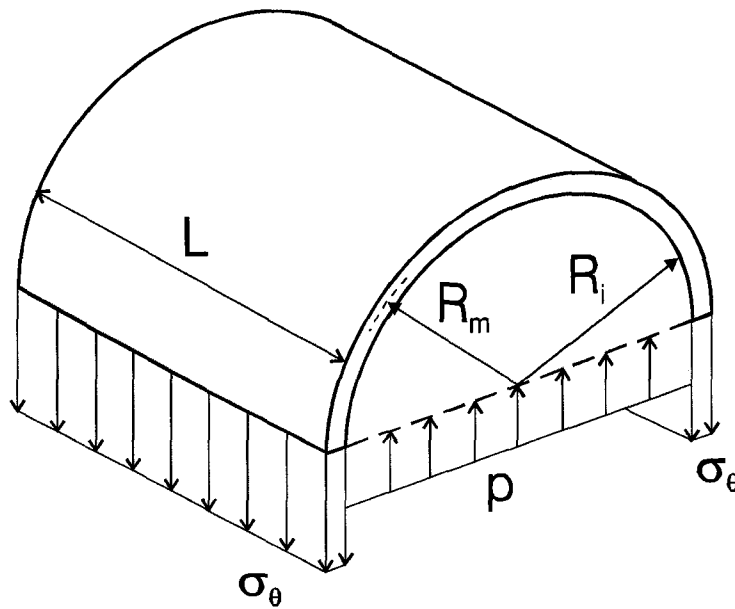Figure A.1 Free Body Diagram of The Pipe End Segment

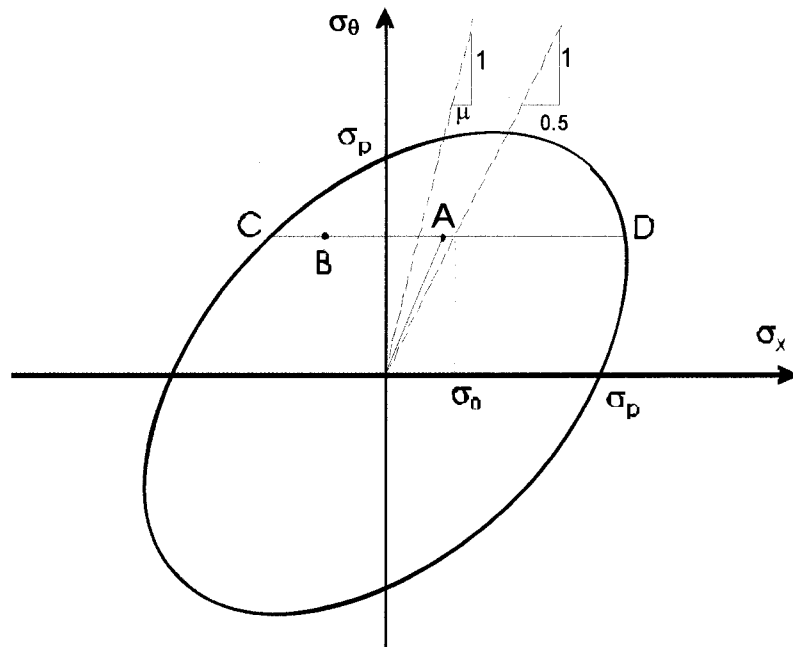Figure A.2 Free Body of A Half-Cylindrical Portion of the Pipe

214

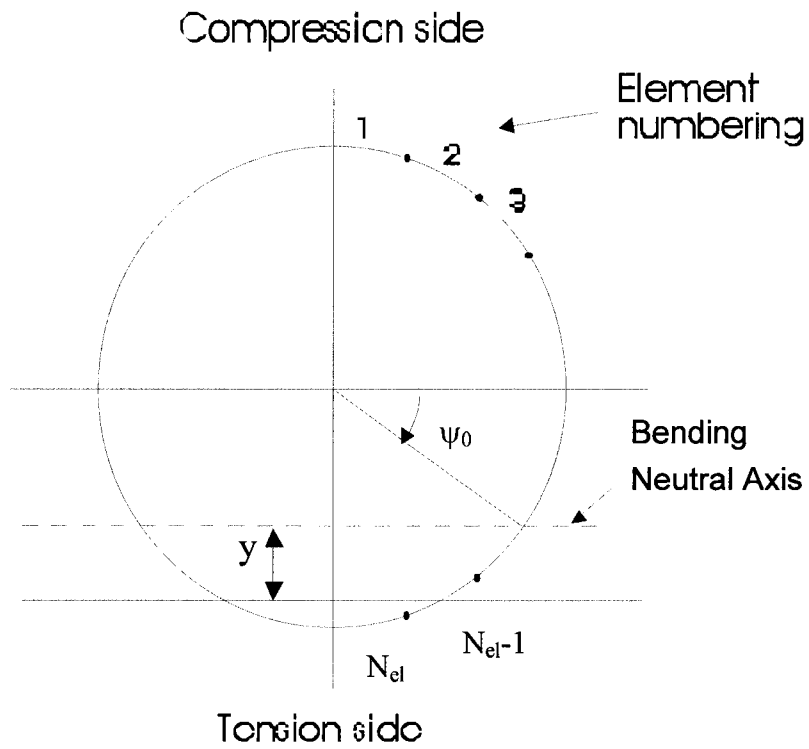Figure A.3 Von Mises Yield Criterion in Two Dimensions

Figure A.4 Cross-Section Lay-out in PAPS Program

215

APPENDIX B

STRAIN, STRESS AND CURVATURE FORMULATION

B.1 Strain Measures

In the program PAPS, at each curvature increment, the longitudinal strains for the elements around the cross-section are calculated in engineering strain measure. If any formulation other than ESS is chosen (i.e., UL or TL), the engineering strains need to be converted into a different type of strain (see Section A.2.2.1). The definition and conversion formulas for different strain measures are discussed in the following.

a. Lagrangian Strain

Figure B.1 shows the original and deformed configuration of an infinitesimal element of the pipe. The directions in the figure are as defined in Section A.2.2.3.3 (i.e., subscripts 1, 2, and 3 correspond to the longitudinal, circumferential and through-thickness directions, respectively). In the program PAPS, an infinitesimally short pipe is considered to undergo symmetric bending. Therefore, the deformation of each element of the pipe is only straining with no rigid body motion. As a result, the three principal directions remain fixed throughout the deformation.

As Figure B.1 shows, a_i and x_i are the i_{th} coordinates of a body point in the original and deformed configurations, respectively. The Lagrangian strain (or Green's strain in the longitudinal direction, E_x is expressed as (Fung, 1965)

$$E_x = E_1 = \frac{\partial u_1}{\partial a_1} + \frac{1}{2}\left[\left(\frac{\partial u_1}{\partial a_1}\right)^2 + \left(\frac{\partial u_2}{\partial a_1}\right)^2 + \left(\frac{\partial u_3}{\partial a_1}\right)^2\right] \tag{B.1}$$

Where u_i is the displacement in the ith direction defined by

$$u_i = x_i - a_i \tag{B.2}$$

Hence in differential form,

$$du_i = dx_i - da_i \tag{B.3}$$

Since the direction 1, 2 and 3 are the principal axes and always remain fixed,

$$\frac{\partial u_2}{\partial a_1} = \frac{\partial u_3}{\partial a_1} = 0 \tag{B.4}$$

Thus, Equation B.1 becomes

$$E_x = E_1 = \frac{\partial u_1}{\partial a_1} + \frac{1}{2}\left(\frac{\partial u_1}{\partial a_1}\right)^2 \qquad (B.5)$$

Where $\frac{\partial u_1}{\partial a_1}$ is, by definition, the engineering strain, e_1.

$$e_x = e_1 = \frac{\partial u_1}{\partial a_1} \qquad (B.6)$$

Hence,

$$E_x = e_x + \frac{e_x^2}{2} \qquad (B.7)$$

Similarly, for the ith direction,

$$E_i = e_i + \frac{e_i^2}{2} \qquad (B.8)$$

b. Logarithmic (true) strain

The updated Lagrangian strains can be reduced to the logarithmic strains when the principal axes remain fixed during deformation. The logarithmic strain in the ith direction, ε_i, can be expressed in terms of the engineering strain, e_i, as (Hill, 1950)

$$\varepsilon_i = \ln(1 + e_i) \qquad (B.9)$$

B.2 Area

Two measures of the area are used in the formulations herein. They are the original and deformed areas, shown by dA_0 and dA in Figure B.1, respectively. Assuming the volume of the element in Figure B.1 remains constant during the deformation (This is a direct result of the flow rule for a plastic deformation, and is approximately valid for an elastic deformation),

$$dA\, dx_1 = dA_0\, da_1 \qquad (B.10)$$

By substituting dx1 from Equation B.3,

$$dA\left(1 + \frac{du_1}{da_1}\right) = dA_0 \qquad (B.11)$$

Where $\dfrac{du_1}{da_1}$ is the engineering longitudinal strain, e_1. Hence,

$$dA = \frac{dA_0}{1 + e_1} \qquad (B.12)$$

B.3 Stress Measures

a. Engineering stress

Engineering stress is defined by the force per unit of the original area. Thus, the engineering longitudinal stress in Figure B.1b can be expressed as

$$\sigma_1 = \frac{dT_1}{dA_0} \qquad (B.13)$$

where dT_1 is the longitudinal component of the infinitesimal force vector acting on the area perpendicular to the longitudinal direction (part of the cross-section area). Here the longitudinal direction is a principal direction, therefore, dT1 is the total force acting on the element surface.

b. True (Cauchy) stress

True stress is defined by the force per unit of the current area. Thus, the true longitudinal stress in Figure B.1b can be written as

$$\tau_1 = \frac{dT_1}{dA} \qquad (B.14)$$

From Equations B.12, B.13 and B.14, the true stress is expressed in terms of the engineering stress as

$$\tau_1 = \sigma_1 (1 + e_1) \qquad (B.15)$$

219

Similarly, in general,

$$\tau_i = \sigma_i (1+e_i) \qquad (B.16)$$

c. 2nd Poila-Kirchhoff stress

Virtual force $dT_i^{(k)}$, used to define 2nd Poila-Kirchhoff stress, are defined by (Fung, 1965)

$$dT_i^{(k)} = \frac{\partial a_i}{\partial x_j} dT_j \qquad (B.17)$$

Substituting for x_j from Equation B.2 and summing on j in Equation B.17 gives

$$dT_i^{(k)} = \frac{da_i}{da_i + du_i} dT_i = \frac{dT_i}{1 + e_i} \qquad \text{(no sum)} \qquad (B.18)$$

The 2nd Poila-Kirchhoff stress in the ith direction, s_i, (for the element shown in Figure B.1) is defined by

$$s_i = \frac{dT_i^{(k)}}{(dA_0)_i} \qquad \text{(no sum)} \qquad (B.19)$$

where $(dA_0)_i$ is the original area perpendicular to the ith direction. Thus, for the longitudinal direction (note that $(dA_0)_1 = dA_0$)

$$s_1 = \frac{dT_1^{(k)}}{dA_0} \qquad (B.20)$$

Substituting $dT_1^{(k)}$ from Equation B.18 yields

$$s_1 = \frac{1}{1 + e_1} \frac{dT_1}{dA_0} = \frac{\sigma_1}{1 + e_1} \qquad (B.21)$$

Similarly, in the ith direction,

$$s_i = \frac{\sigma_i}{1+e_i} \qquad \text{(no sum)} \qquad \text{(B.22)}$$

B.4 Calculation of Force in Different Formulations

The longitudinal force for each element, dT_1, is used to calculate the axial force and bending moment of the cross-section. The longitudinal force, dT_1, is obtained for different formulations as follows.

a. Engineering stress and strain (SEE)

From Equation B.13,

$$dT_1 = \sigma_1 \, dA_0 \qquad \text{(B.23)}$$

b. Updated Lagrangian formulation (TL)

From Equations B. 12 and B. 14,

$$dT_i = \tau_1 \frac{dA_0}{1+e_1} \qquad \text{(B.24)}$$

c. Total Lagrangian formulation (TL)

Equations B.18, B.20 and B.21 yield

$$dT_1 = s_1 \, (1 + e_1) \, dA_0 \qquad \text{(B.25)}$$

B.5 Curvature Formulation

For the infinitesimally short slice of the pipe shown in Figure B.2,

$$\overline{da} = Rd\alpha \qquad \text{(B.26)}$$

where $\overline{da}$ is the length of the slice after the application of the internal pressure and axial load, R is the radius of the bending neutral axis, and $d\alpha$ is the angle made by the end surfaces of the slice due to bending. By assuming that e0 is the engineering strain of the cross-section at the start of the bending, $\overline{da}$ can be expressed as

$$\overline{da} = da \, (1 + e_0) \qquad \text{(B.27)}$$

221

where da is the original length of the slice prior to any loading (see Figure B.2).

Curvature in this study is defined as the inverse of the radius of the bending neutral axis. Thus, from Equations B.26 and B.27, the curvature, ϕ, can be written as

$$\phi = \frac{1}{R} = \frac{d\alpha}{da(1+e_0)} \tag{B.28}$$

Hence,

$$d\alpha = \phi \, da \, (1 + e_0) \tag{B.29}$$

From the geometry of the deformed configuration in Figure B.2,

$$d\alpha = \frac{dx - da(1+e_0)}{y} \tag{B.30}$$

where dx is the length of the slice at the ordinate y, measured from the bending neutral axis (Figure B.2). Eliminating $d\alpha$ from Equations B.29 and B.30 gives
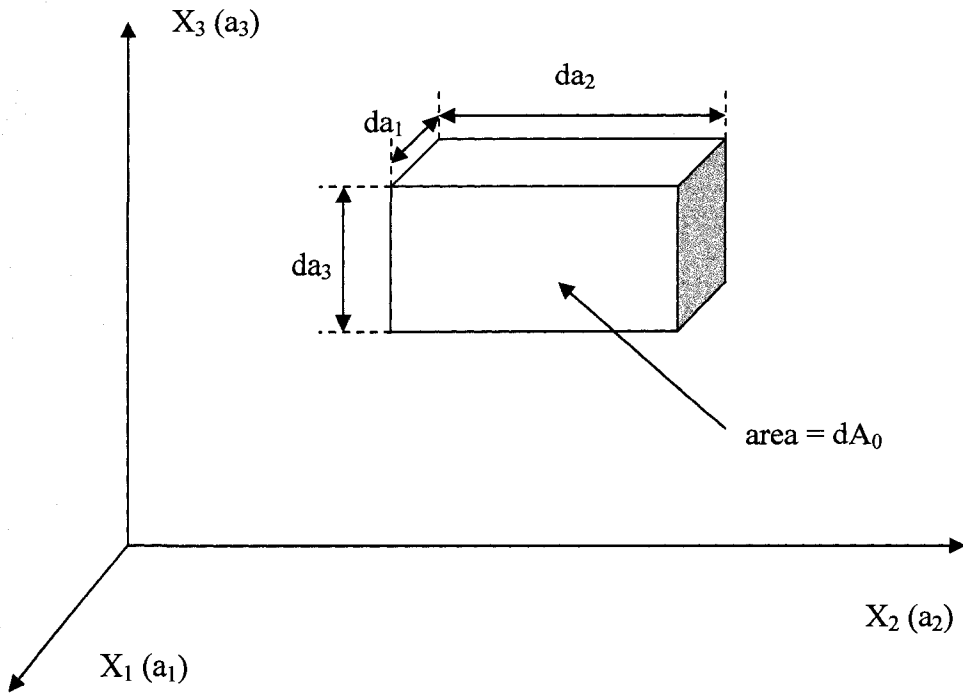
$$\frac{dx - da}{da} - e_0 = \phi \, y \, (1 + e_0) \tag{B.31}$$

Here, $\dfrac{dx - da}{da}$ is, by definition, the engineering strain (e) at the ordinate y. hence,

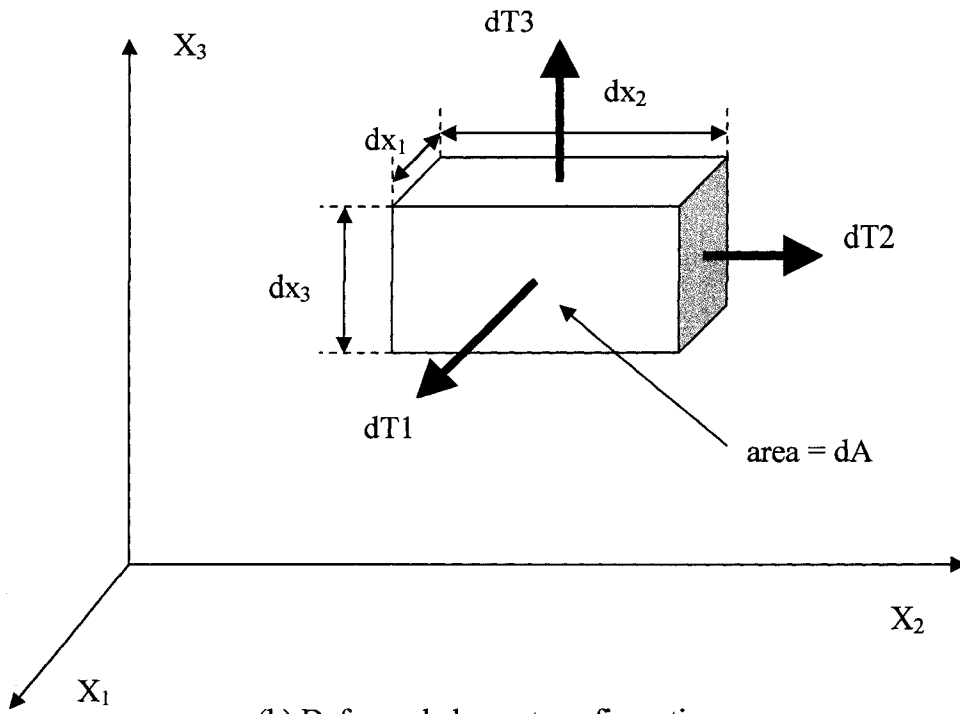$$e = e_0 + \phi \, y \, (1 + e_0) \tag{B.32}$$

or

$$\phi = \frac{e - e_0}{y(1+e_0)} \tag{B.33}$$

(a) Original element configuiration

(b) Deformed element configuration

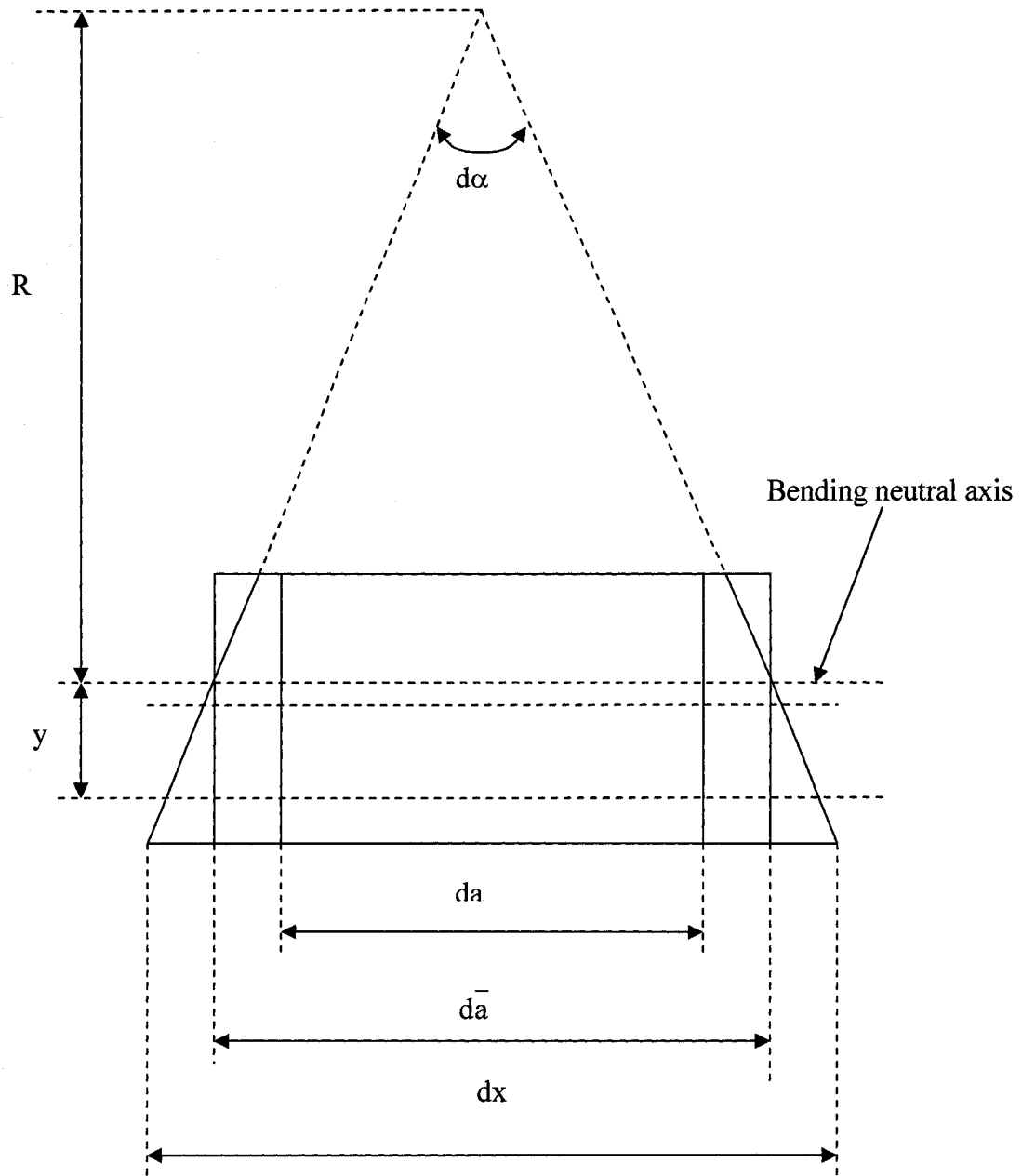Figure B.1 Original and Deformed Configurations of An Element of Pipe Slice

223

Figure B.2 Original and Deformed Configurations of Pipe Slice